Technical Report 32-1526

Volume IV

The Deep Space Network

Progress Report For May and June 1971

JET PROPULSION LABORATORY
CALIFORNIA INSTITUTE OF TECHNOLOGY
PASADENA, CALIFORNIA

August 15, 1971

Acc. No.: N71 33163 / N71 33168

TECHNICAL REPORT STANDARD TITLE PAGE

1. Report No. 32-1526, Vol. IV	2. Government Accession No.	3. Recipient's Catalog No.
4. Title and Subtitle THE DEEP SPACE NETWORK PROGRESS REPORT FOR MAY AND JUNE 1971		5. Report Date August 15, 1971 6. Performing Organization Code
7. Author(s) JPL Staff		8. Performing Organization Report No.
9. Performing Organization Name and Address JET PROPULSION LABORATORY California Institute of Technology 4800 Oak Grove Drive Pasadena, California 91103		10. Work Unit No. 11. Contract or Grant No. NAS 7-100 CR 121378 13. Type of Report and Period Covered Technical Report
12. Sponsoring Agency Name and Address NATIONAL AERONAUTICS AND SPACE ADMINISTRATION Washington, D.C. 20546		14. Sponsoring Agency Code

15. Supplementary Notes

16. Abstract

This report describes work performed for the JPL/NASA Deep Space Network (DSN). Progress is presented on DSN supporting research and technology, advanced development and engineering, and implementation, and DSN operations which pertain to mission-independent or multiple-mission development as well as to support of flight projects. Each issue contains a description of the functions and facilities of the DSN.

17. Key Words (Selected by Author(s))	18. Distribution Statement
Antennas and Transmission Lines Information Theory Telemetry and Command Tracking	Unclassified -- Unlimited

19. Security Classif. (of this report)	20. Security Classif. (of this page)	21. No. of Pages	22. Price
Unclassified	Unclassified	217	

HOW TO FILL OUT THE TECHNICAL REPORT STANDARD TITLE PAGE

Make items 1, 4, 5, 9, 12, and 13 agree with the corresponding information on the report cover. Use all capital letters for title (item 4). Leave items 2, 6, and 14 blank. Complete the remaining items as follows:

3. Recipient's Catalog No. Reserved for use by report recipients.

7. Author(s). Include corresponding information from the report cover. In addition, list the affiliation of an author if it differs from that of the performing organization.

8. Performing Organization Report No. Insert if performing organization wishes to assign this number.

10. Work Unit No. Use the agency-wide code (for example, 923-50-10-06-72), which uniquely identifies the work unit under which the work was authorized. Non-NASA performing organizations will leave this blank.

11. Insert the number of the contract or grant under which the report was prepared.

15. Supplementary Notes. Enter information not included elsewhere but useful, such as: Prepared in cooperation with... Translation of (or by)... Presented at conference of... To be published in...

16. Abstract. Include a brief (not to exceed 200 words) factual summary of the most significant information contained in the report. If possible, the abstract of a classified report should be unclassified. If the report contains a significant bibliography or literature survey, mention it here.

17. Key Words. Insert terms or short phrases selected by the author that identify the principal subjects covered in the report, and that are sufficiently specific and precise to be used for cataloging.

18. Distribution Statement. Enter one of the authorized statements used to denote releasability to the public or a limitation on dissemination for reasons other than security of defense information. Authorized statements are "Unclassified—Unlimited," "U. S. Government and Contractors only," "U. S. Government Agencies only," and "NASA and NASA Contractors only."

19. Security Classification (of report). NOTE: Reports carrying a security classification will require additional markings giving security and downgrading information as specified by the Security Requirements Checklist and the DoD Industrial Security Manual (DoD 5220.22-M).

20. Security Classification (of this page). NOTE: Because this page may be used in preparing announcements, bibliographies, and data banks, it should be unclassified if possible. If a classification is required, indicate separately the classification of the title and the abstract by following these items with either "(U)" for unclassified, or "(C)" or "(S)" as applicable for classified items.

21. No. of Pages. Insert the number of pages.

22. Price. Insert the price set by the Clearinghouse for Federal Scientific and Technical Information or the Government Printing Office, if known.

NATIONAL AERONAUTICS AND SPACE ADMINISTRATION

Technical Report 32-1526

Volume IV

The Deep Space Network

Progress Report
For May and June 1971

JET PROPULSION LABORATORY
CALIFORNIA INSTITUTE OF TECHNOLOGY
PASADENA, CALIFORNIA

August 15, 1971

Prepared Under Contract No. NAS 7-100
National Aeronautics and Space Administration

Preface

This report series presents progress on DSN supporting research and technology, advanced development and engineering, and implementation, and DSN operations which pertain to mission-independent or multiple-mission development as well as to support of flight projects. Each issue presents material in some, but not all, of the following categories in the order indicated.

Description of the DSN

Mission Support
- Interplanetary Flight Projects
- Planetary Flight Projects
- Manned Space Flight Project
- Radio Science Experiments
- Advanced Flight Projects

Advanced Engineering
- Tracking and Navigational Accuracy Analysis
- Communications Systems Research
- Communications Elements Research
- Supporting Research and Technology

Development and Implementation
- Space Flight Operations Facility Development
- Ground Communications Facility Development
- Deep Space Instrumentation Facility Development
- DSN Projects and Systems Development

Operations and Facilities
- DSN Operations
- Space Flight Operations Facility Operations
- Ground Communications Facility Operations
- Deep Space Instrumentation Facility Operations
- Facility Engineering

In each issue, the part entitled "Description of the DSN" describes the functions and facilities of the DSN and may report the current configuration of one of the six DSN systems (tracking, telemetry, command, monitoring, simulation, and operations control).

The work described in this report series is either performed or managed by the Tracking and Data Acquisition organization of JPL for NASA.

Contents

Contents (contd)

Communications Systems Research

Communications Elements Research

Supporting Research and Technology

Contents (contd)

DEVELOPMENT AND IMPLEMENTATION

SFOF Development

GCF Development

DSIF Development

Contents (contd)

OPERATIONS AND FACILITIES

DSN Operations

DSIF Operations

DSN Functions and Facilities

N. A. Renzetti
Mission Support Office

The objectives, functions, and organization of the Deep Space Network are summarized. The Deep Space Instrumentation Facility, the Ground Communications Facility, and the Space Flight Operations Facility are described.

The Deep Space Network (DSN), established by the NASA Office of Tracking and Data Acquisition under the system management and technical direction of JPL, is designed for two-way communications with unmanned spacecraft traveling approximately 16,000 km (10,000 mi) from earth to planetary distances. It supports, or has supported, the following NASA deep space exploration projects: *Ranger, Surveyor, Mariner* Venus 1962, *Mariner* Mars 1964, *Mariner* Venus 67, *Mariner* Mars 1969, *Mariner* Mars 1971 (JPL); *Lunar Orbiter* and *Viking* (Langley Research Center); *Pioneer* (Ames Research Center); *Helios* (West Germany); and *Apollo* (Manned Spacecraft Center), to supplement the Manned Space Flight Network (MSFN).

The DSN is distinct from other NASA networks such as the MSFN, which has primary responsibility for tracking the manned spacecraft of the *Apollo* Project, and the Space Tracking and Data Acquisition Network (STADAN), which tracks earth-orbiting scientific and communications satellites. With no future unmanned lunar spacecraft presently planned, the primary objective of the DSN is to continue its support of planetary and interplanetary flight projects.

To support flight projects, the DSN simultaneously performs advanced engineering on components and systems, integrates proven equipment and methods into the network,[1] and provides direct support of each project through that project's Tracking and Data System. This management element and the project's Mission Operations personnel are responsible for the design and operation of the data, software, and operations systems required for the conduct of flight operations. The organization and procedures necessary to carry out these activities are described in Ref. 1.

[1]When a new piece of equipment or new method has been accepted for integration into the network, it is classed as Goldstone duplicate standard (GSDS), thus standardizing the design and operation of identical items throughout the network.

By tracking the spacecraft, the DSN is involved in the following data types:

(1) *Radio Metric:* generate angles, one- and two-way doppler, and range.

(2) *Telemetry:* receive, record, and retransmit engineering and scientific data.

(3) *Command:* send coded signals to the spacecraft to activate equipment to initiate spacecraft functions.

The DSN operation is characterized by six DSN systems: (1) tracking, (2) telemetry, (3) command, (4) monitoring, (5) simulation, and (6) operations control.

The DSN can be characterized as being comprised of three facilities: the Deep Space Instrumentation Facility (DSIF), the Ground Communications Facility (GCF), and the Space Flight Operations Facility (SFOF).

I. Deep Space Instrumentation Facility

A. Tracking and Data Acquisition Facilities

A world-wide set of deep space stations (DSSs) with large antennas, low-noise phase-lock receiving systems, and high-power transmitters provide radio communications with spacecraft. The DSSs and the deep space communications complexes (DSCCs) they comprise are given in Table 1.

Radio contact with a spacecraft usually begins when the spacecraft is on the launch vehicle at Cape Kennedy, and it is maintained throughout the mission. The early part of the trajectory is covered by selected network stations of the Air Force Eastern Test Range (AFETR) and the MSFN of the Goddard Space Flight Center.[2] Normally, two-way communications are established between the spacecraft and the DSN within 30 min after the spacecraft has been injected into lunar, planetary, or interplanetary flight. A compatibility test station at Cape Kennedy (discussed later) monitors the spacecraft continuously during the launch phase until it passes over the local horizon. The deep space phase begins with acquisition by either DSS 51, 41, or 42. These and the remaining DSSs given in Table 1 provide radio communications to the end of the flight.

To enable continuous radio contact with spacecraft, the DSSs are located approximately 120 deg apart in longitude; thus, a spacecraft in deep space flight is always

[2]The 9-m (30-ft) diam antenna station established by the DSN on Ascension Island during 1965 to act in conjunction with the MSFN orbital support 9-m (30-ft) diam antenna station was transferred to the MSFN in July 1968.

Table 1. Tracking and data acquisition stations of the DSN

DSCC	Location	DSS	DSS serial designation	Antenna		Year of initial operation
				Diameter, m (ft)	Type of mounting	
Goldstone	California	Pioneer	11	26 (85)	Polar	1958
		Echo	12	26 (85)	Polar	1962
		(Venus)[a]	13	26 (85)	Az–El	1962
		Mars	14	64 (210)	Az–El	1966
—	Australia	Woomera[b]	41	26 (85)	Polar	1960
Tidbinbilla	Australia	Weemala (formerly Tidbinbilla)[b]	42	26 (85)	Polar	1965
		Ballima[b] (formerly Booroomba)	43	64 (210)	Az–El	Under construction
—	South Africa	Johannesburg[b]	51	26 (85)	Polar	1961
Madrid	Spain	Robledo[b]	61	26 (85)	Polar	1965
		Cebreros[b]	62	26 (85)	Polar	1967
		Robledo	63	64 (210)	Az–El	Under construction

[a]A research-and-development facility used to demonstrate the feasibility of new equipment and methods to be integrated into the operational network. Besides the 26-m (85-ft) diam az–el-mounted antenna, DSS 13 has a 9-m (30-ft) diam az–el-mounted antenna that is used for testing the design of new equipment and support of ground-based radio science.

[b]Normally staffed and operated by government agencies of the respective countries (except for a temporary staff of the Madrid DSCC), with some assistance of U.S. support personnel.

within the field-of-view of at least one DSS, and for several hours each day may be seen by two DSSs. Furthermore, since most spacecraft on deep space missions travel within 30 deg of the equatorial plane, the DSSs are located within latitudes of 45 deg north or south of the equator. All DSSs operate at S-band frequencies: 2110–2120 MHz for earth-to-spacecraft transmission and 2290–2300 MHz for spacecraft-to-earth transmission.

To provide sufficient tracking capability to enable useful data returns from around the planets and from the edge of the solar system, a 64-m (210-ft) diam antenna network will be required. Two additional 64-m (210-ft) diam antenna DSSs are under construction at Madrid and Canberra, which will operate in conjunction with DSS 14 to provide this capability. These stations are scheduled to be operational by the middle of 1973.

B. Compatibility Test Facilities

In 1959, a mobile L-band compatibility test station was established at Cape Kennedy to verify flight–spacecraft–DSN compatibility prior to the launch of the *Ranger* and *Mariner* Venus 1962 spacecraft. Experience revealed the need for a permanent facility at Cape Kennedy for this function. An S-band compatibility test station with a 1.2-m (4-ft) diam antenna became operational in 1965. In addition to supporting the preflight compatibility tests, this station monitors the spacecraft continuously during the launch phase until it passes over the local horizon.

Spacecraft telecommunications compatibility in the design and prototype development phases was formerly verified by tests at the Goldstone DSCC. To provide a more economical means for conducting such work and because of the increasing use of multiple-mission telemetry and command equipment by the DSN, a compatibility test area (CTA) was established at JPL in 1968. In all essential characteristics, the configuration of this facility is identical to that of the 26-m (85-ft) and 64-m (210-ft) diam antenna stations.

The JPL CTA is used during spacecraft system tests to establish the compatibility with the DSN of the proof test model and development models of spacecraft, and the Cape Kennedy compatibility test station is used for final flight spacecraft compatibility validation testing prior to launch.

II. Ground Communications Facility

The GCF provides voice, high-speed data, wideband data, and teletype communications between the SFOF and the DSSs. In providing these capabilities, the GCF uses the facilities of the worldwide NASA Communications Network (NASCOM)[3] for all long distance circuits, except those between the SFOF and the Goldstone DSCC. Communications between the Goldstone DSCC and the SFOF are provided by a microwave link directly leased by the DSN from a common carrier.

Early missions were supported by voice and teletype circuits only, but increased data rates necessitated the use of high-speed circuits for all DSSs, plus wideband circuits for some stations.

III. Space Flight Operations Facility

Network and mission control functions are performed at the SFOF at JPL. The SFOF receives data from all DSSs and processes that information required by the flight project to conduct mission operations. The following functions are carried out: (1) real-time processing and display of radio metric data; (2) real-time and non-real-time processing and display of telemetry data; (3) simulation of flight operations; (4) near-real-time evaluation of DSN performance; (5) operations control, and status and operational data display; and (6) general support such as internal communications by telephone, intercom, public address, closed-circuit TV, documentation, and reproduction of data packages. Master data records of science data received from spacecraft are generated. Technical areas are provided for flight project personnel who analyze spacecraft performance, trajectories, and generation of commands.

[3]Managed and directed by the Goddard Space Flight Center.

Reference

1. *The Deep Space Network*, Space Programs Summary 37-50, Vol. II, pp. 15–17. Jet Propulsion Laboratory, Pasadena, Calif., Mar. 31, 1968.

DSN Telemetry System

E. S. Burke and C. W. Harris
DSN Engineering and Operations Office

The Telemetry System Analysis Group is responsible for analyzing the total performance of the DSN telemetry system. The group's tasks include both real time and non-real time functions. By combining these two functions, the telemetry system can be analyzed for short- and long-term performance. This can be illustrated by the results of the data which was accumulated during real-time operations for the solar occultation of Pioneer 9, and compiled and analyzed during non-real time periods.

I. Introduction

The Telemetry System Analysis Group evaluates the telemetry system performance, reports status and anomalies to the operations chief, generates telemetry predicts, establishes and monitors standards and limits, provides performance data to various engineering organizations, and will supervise the generation of telemetry master data records.

II. Real-Time Operations and Analysis

During real-time operations, the quality of incoming telemetry data is assessed to ascertain that it is within limits of the predicted values and various parameters are recorded for further analysis. If anomalies create degradation within the system, corrective actions are recommended to the operations chief.

III. Non-Real Time Analysis

Operations for non-real time include the generation of telemetry signal-to-noise ratio and the signal level predicts. These are generated by use of station and spacecraft parameters, and by the range of the spacecraft from the station. Also standards and limits are established for various parameters, which if not met are cause for corrective action to be taken by the real-time analyst.

Analysis in non-real time is performed to determine long-term trends of station parameters and residuals, and to provide this data to various engineering organizations.

IV. Illustration

An example of the data, which was obtained during the superior conjunction of the sun and *Pioneer 9* spacecraft, collected by the real-time analysts, and examined and compiled by the non-real-time analysts, is shown in Figs. 1 through 4.

Figure 1 shows the degradation of the system temperature T_S from approximately ± 9 deg of the sun-earth-probe (SEP) angle related to the day of year (DOY). There are two actual curves and two predicted curves. The dual curves are due to the effect of the quadripod structure on the 64-m (210-ft) antenna at DSS 14 as can be seen in

Fig. 3. After approximately 6 or 7 deg of SEP angle, the effect of the quadripod structure is minimal.

Figure 2a shows the degradation of the telemetry data by actual and predicted residual signal-to-noise ratio (SNR) curves up to ±9 deg of SEP angle. The predicted curve data was compiled from system temperatures taken during this period.

Figure 2b is a continuation of Fig. 2a which shows the degradation continuing past 15 deg prior to syzygy.

Figure 3 is an actual reproduction of the T_S strip chart recording for Pass 760 on December 7, 1970. This graph shows the high peaks due to the effect of the quadripod structure.[1]

Figure 4 shows the fixed sun–earth line trajectory for *Pioneer* 9 giving the dates and angles concerned.[2]

The data in Fig. 2b is discontinuous from approximately 15 to 18 deg of SEP angle due to DSS 14 not tracking during this period. After 18 deg the data is within ±0.5 dB tolerance.

---

[1]DSN Doc. 810-5 Rev. A, Oct. 1, 1970 (Fig. 2-5).

[2]IBM 7094 Trajectory Program Tapes 12309 and 12856.

Due to a retrograde motion of PN9, as can be seen in Fig. 4, the SEP angle has been less than 8.78 deg since 15 March 1971. This will continue until June 30, 1971 when the angle will increase until the next retrograde. A maximum range was reached on April 30, 1971. Since March 15, the SNR residuals have maintained predictions within ±0.5 dB.

The compiled data in Figs. 1 and 2a show that the change in system temperature created most of the degradation in the telemetry. Figures 1 and 2b indicate that the degradation continued past the time when the system temperature was at its predicted value. Figure 4 shows that from less than 18 deg prior to syzygy, and greater than 9 deg after syzygy, the only difference is the distance from the sun. Therefore, other solar effects have influenced the signal besides the change in system temperature.

V. Summary

In order to have an efficient telemetry system which can operate at maximum performance, the system has to be monitored, analyzed, and corrected for degradations. These tasks are the responsibility of the DSN Telemetry System Analysis Group. The group plans to continue to provide engineering results, as described in *Subsection IV* above, for all Projects and to provide real-time support of spacecraft missions as required.

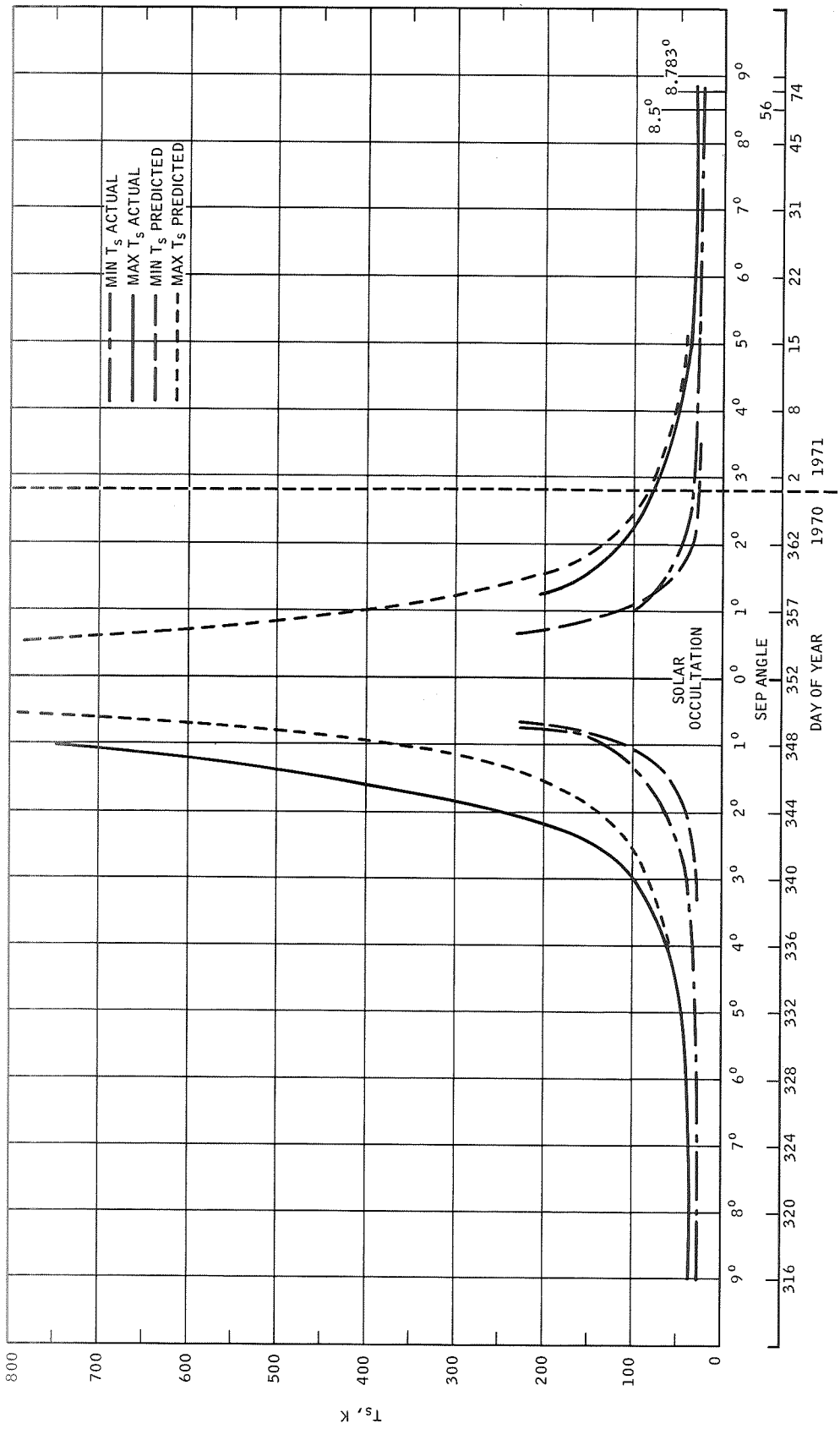

Fig. 1. DSS 14 Actual and predicted system temperature T_N versus sun–earth–probe (SEP) angle and day of year (DOY) for *Pioneer 9* occultation

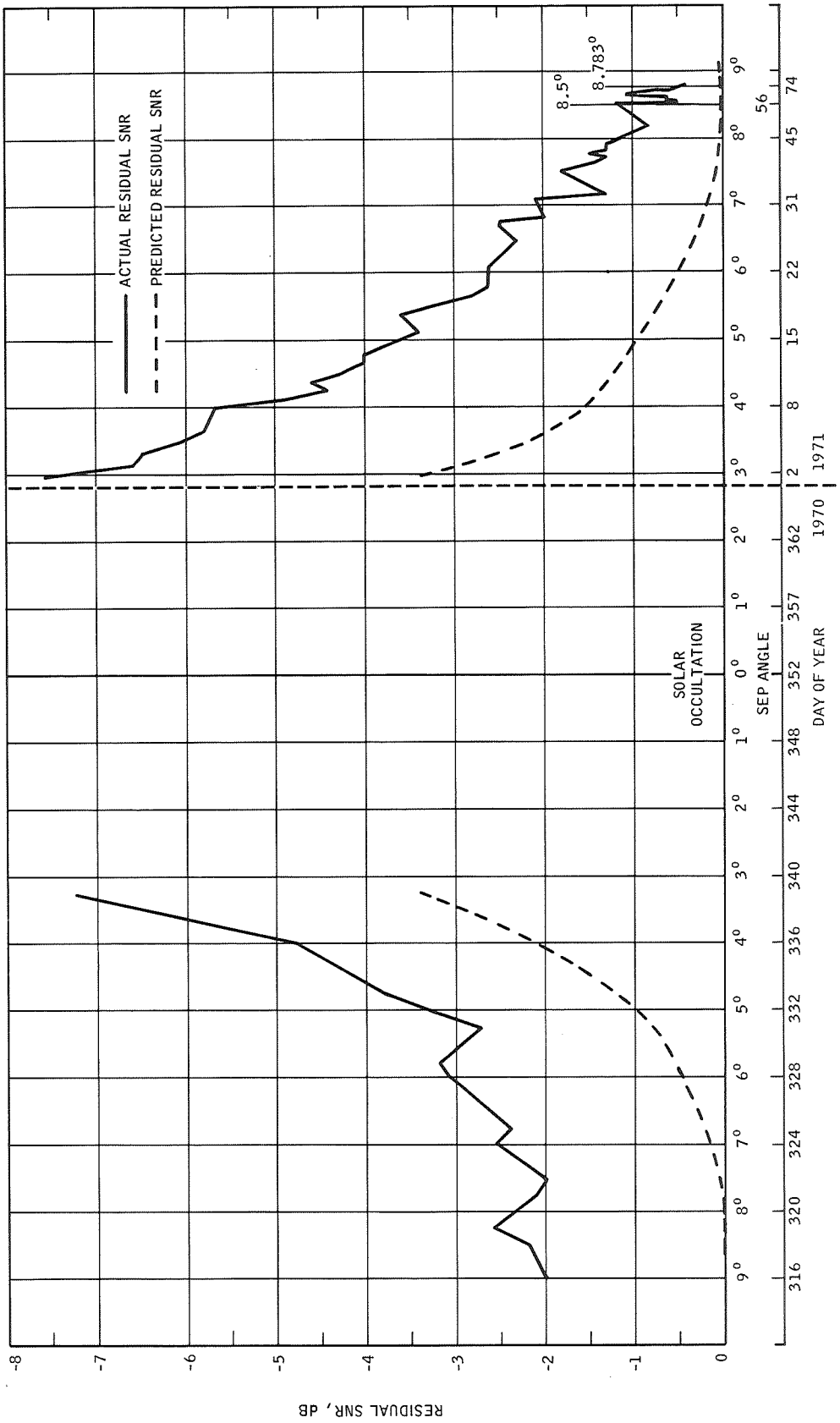

Fig. 2a. DSS 14 Actual and predicted residual signal-to-noise ratio (SNR) versus sun–earth–probe (SEP) angle and day of year (DOY) for *Pioneer 9* occultation

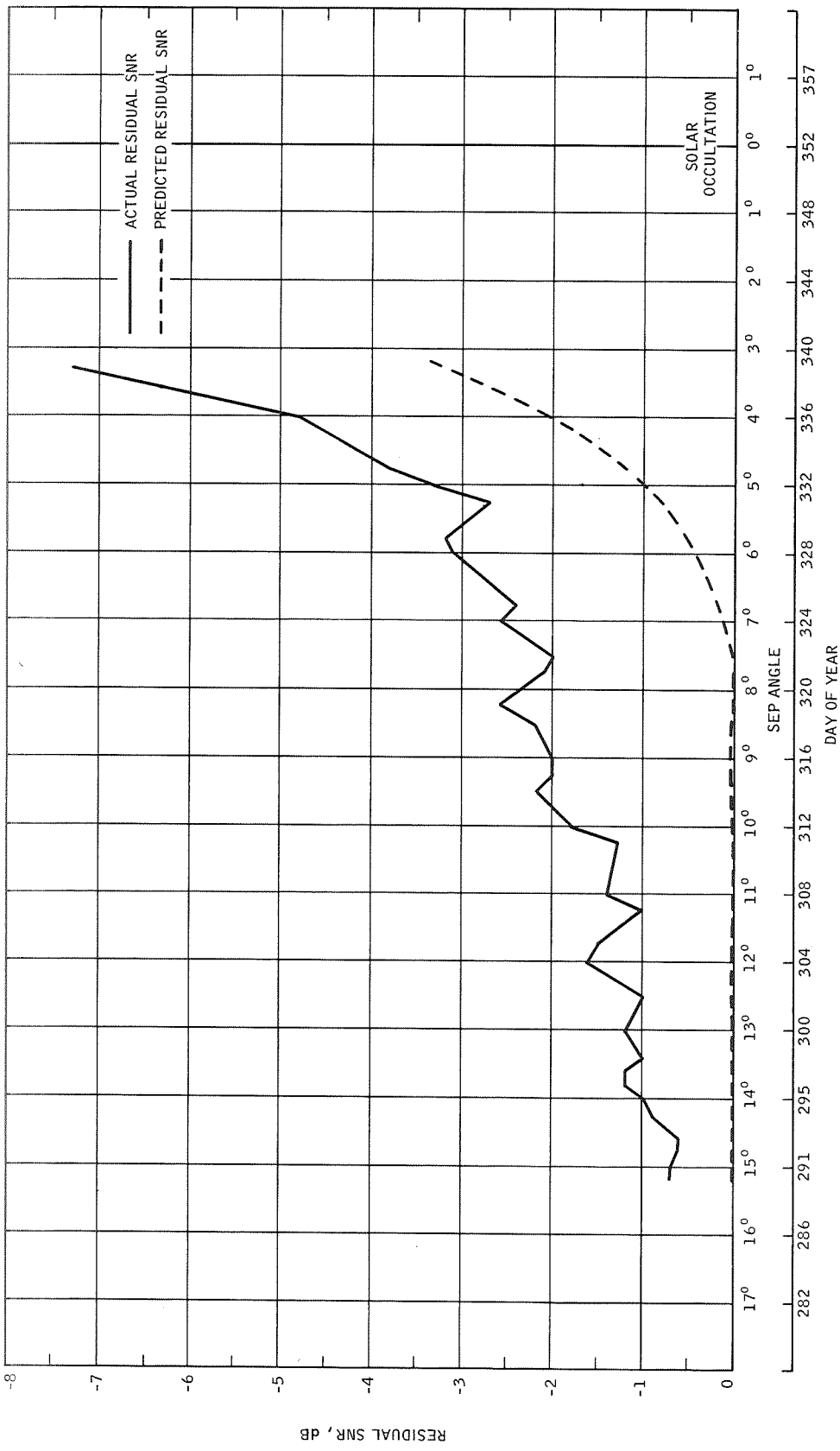

Fig. 2b. DSS 14 Actual and predicted residual signal-to-noise ratio (SNR) versus extended sun–earth–probe (SEP) angle and day of year (DOY) for *Pioneer 9* occultation

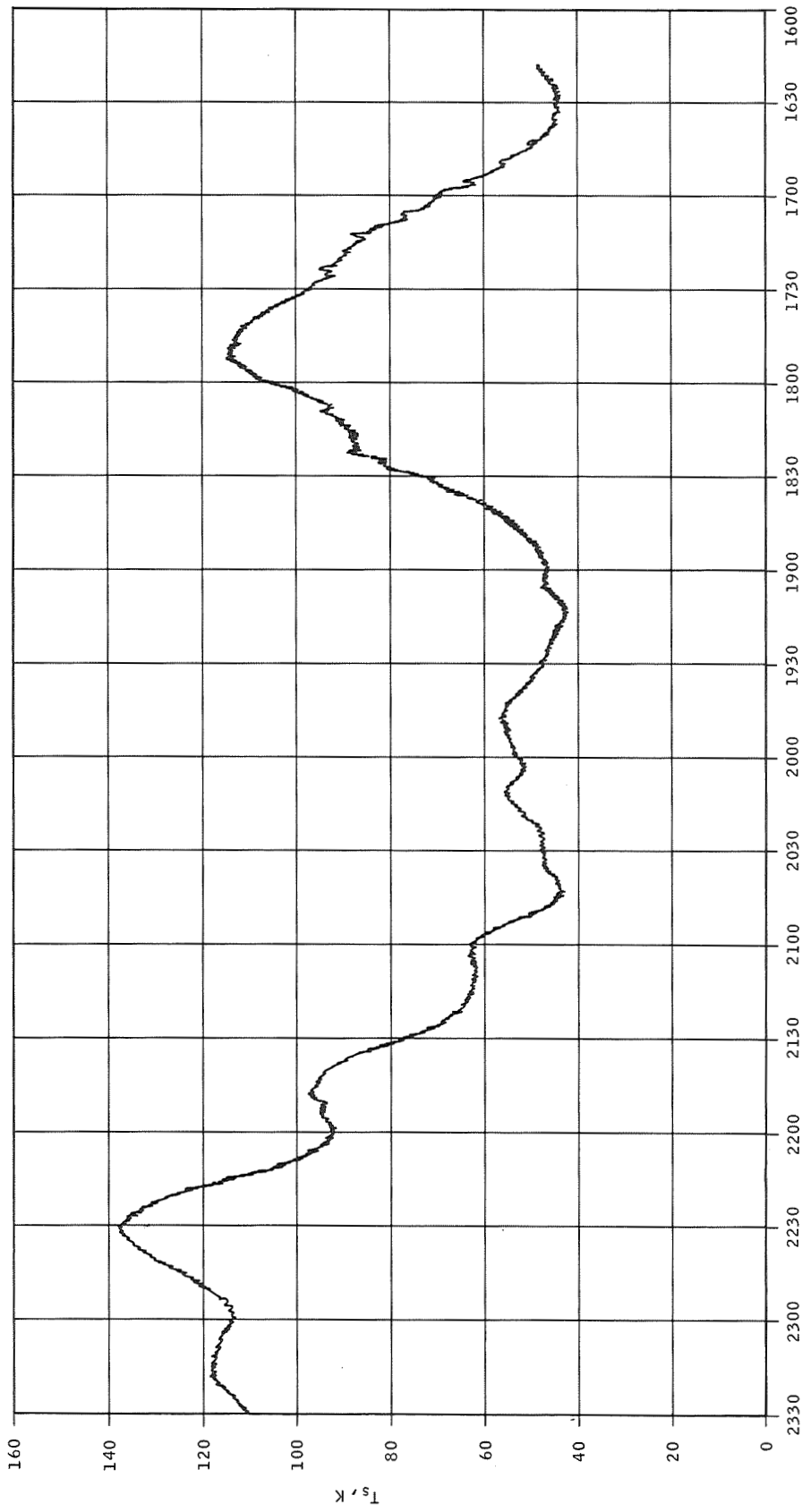

Fig. 3. Normal system temperature T_S versus GMT plot at DSS 14 during *Pioneer 9* occultation period pass 760, Day 341

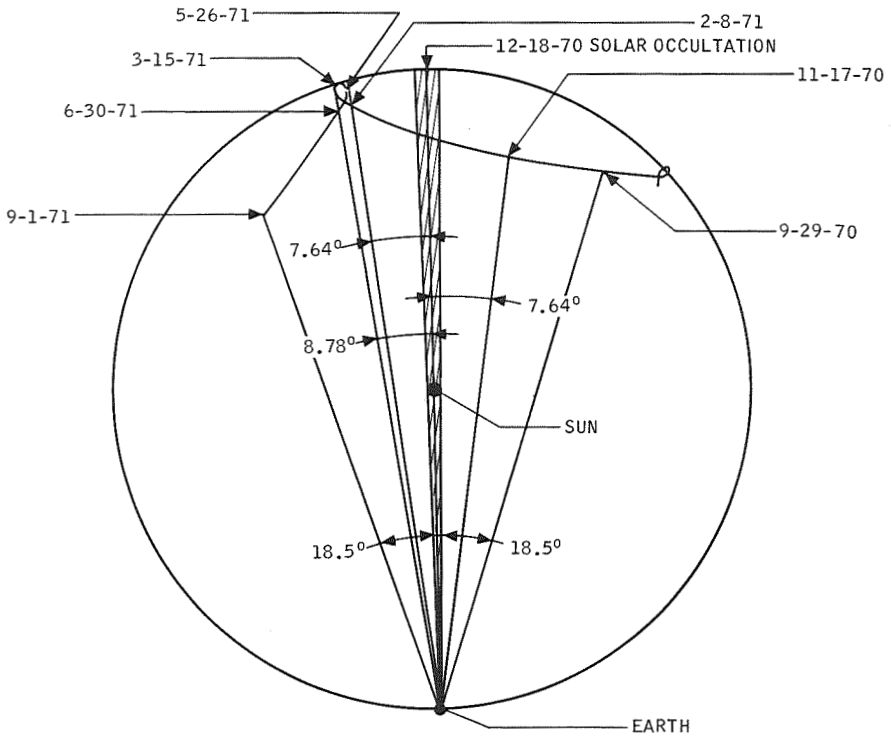

Fig. 4. Sun–earth–probe (SEP) angles for *Pioneer 9* near superior conjunction

DSN Monitor System

J. E. Maclay
DSN Engineering and Operations Office

The Deep Space Network (DSN) Monitor System is now operational. The system has been significantly changed during the process of moving into the Space Flight Operations Facility (SFOF) IBM 360/75 computers. The display capability is much greater than that available in the previous monitor system design. Additionally, SFOF and Ground Communications Facility monitoring provisions are augmented over the previous design.

I. Introduction

The purpose of the DSN Monitor System is to gather, process, and display data relative to the configuration and status of the ground data system, i.e., the DSN. DSN personnel use this monitor data to enhance the performance of the other systems (Telemetry, Tracking, and Command) by continual monitoring of conditions throughout the network.

The DSN Monitor System that has been implemented for support of *Mariner* Mars 1971 and *Pioneer F* basically differs in two ways from earlier designs: (1) the display capability has been greatly expanded, and (2) SFOF and GCF monitoring provisions have been augmented.

II. Displays

An earlier article (Ref. 1) described the DTV display formats defined as of that date. Since then, most of the 11 DTV formats described have undergone extensive redesign and some have been deleted. The changes have come as a direct result of the "learning process" attendant to implementing the changeover from the 7044/7094 to the 360/75. Nearly all users of monitor data now have a summary format of higher-level parameters backed up by several specialty formats that display monitor parameters at a detail level. When alarms occur on a summary format, the user selects the appropriate specialty format for troubleshooting. Twenty-five formats have been implemented to date, with a final count of 34 expected.

Two additional display mediums are now in use; alarms generated in the DSN monitor processor are printed out on a TTY character printer, and incoming high-speed data blocks can be printed on an IBM 1443 line printer.

Each alarm is a time-tagged mnemonic. The TTY printer is located in the monitor operations area, and will also be distributed building-wide via CCTV. Thus, this display is a form of backup in the event of the loss of DTV. Alarms are generated by the comparison of real versus predicted configuration and tolerances as defined

in a monitor criteria data set. Currently, only DSIF monitor data are processed against the predicted data.

The printing of incoming HSD blocks is initiated by the monitor chief. The print may be selected for octal, hex, or binary. The HSD block header is printed in readable form for all print options. Because of limited printer speed, the print request times out before a large queue can form. Such prints are used extensively by monitor, telemetry, and command in troubleshooting.

III. SFOF Monitor

Two of the SFOF displays described in Ref. 1 are now implemented: (1) HSD input/output status, and (2) 360/75 user device status.

The HSD input/output status identifies incoming data by source, mission, and type of data. Alarms for data stoppages, GCF error flags, and HSD block serial number skips are displayed. An indication of whether each incoming data stream is being processed or not is included. The monitoring of output HSD is limited to configuration information.

The user device display shows all 360/75 peripheral devices and identifies their current usage. An alarm, by device, is displayed for any device malfunctions or misusage (e.g., a printer with the motor turned off causes an alarm). This information requires four separate display formats due to the large number of devices:

(1) All devices in the data processing control center.

(2) All devices in the computer area.

(3) All 2260 I/O devices in the DSN and project areas.

(4) All card readers and line printers in the DSN and project areas.

IV. GCF Monitor

In addition to monitoring of the GCF HSD terminal equipment in the SFOF, a capability which has existed for several years, data from the station communications terminal are now also available. This information is returned via DSIF monitor. It is comparable to the SCT data: configuration, line, and error detection encoder–decoder (EDED) status. Comparison of status data from both ends of a high-speed data line (HSDL) is valuable in maintaining good service.

V. Conclusion

The progress described above typifies past and planned activities in the monitor system designs: improvement of existing capabilities, and expansion of monitoring functions in the SFOF and GCF to bring them on a par with the DSIF monitor.

Reference

1. Maclay, J. E., "Mission-Independent Computer-Driven Volatile Data Displays," in *The Deep Space Network*, Space Programs Summary 37-61, Vol. II, pp. 147–150. Jet Propulsion Laboratory, Pasadena, Calif., Jan. 31, 1970.

Pioneer Mission Support

A. J. Siegmeth
Mission Support Office

The Deep Space Network (DSN) is preparing for the tracking and data acquisition support of Pioneers F and G. The major objective is to produce an effective data return capability from the vicinity of Jupiter. This report describes the spacecraft's internal data flow design and identifies the interfaces between the spacecraft and the DSN data system. This report is a continuation of two previous papers which delineated the mission profiles and spacecraft design.

I. Introduction

The Deep Space Network is preparing for the tracking and data acquisition support of the *Pioneer F/G* missions. *Pioneer F* will be launched at the end of February, 1972, and *Pioneer G* 14 months later. Both missions are designed to investigate the interplanetary medium, to explore the hazards on the asteroid belt and increase our knowledge of the solar system's largest planet, Jupiter.

The first two parts of this report were published in Refs. 1 and 2. The first part described the *Pioneer F/G* mission profile, spacecraft system, electrical power supply, thermal control and attitude control. The characteristics of these missions which interface with the tracking and data acquisition functions were delineated. The second part described the telecommunications, antenna and Conscan subsystems. The objective of this report is to provide the reader some insight into the spacecraft internal data flow design by presenting a description of the data handling and command subsystems.

II. *Pioneer F/G* Data Handling Subsystem

The spacecraft's data handling subsystem processes data originating from two major data sources: The first group of data is obtained from the outputs of the eleven onboard scientific instruments which provide data on the scientific measurements, configuration status, and operational health. The second group of data is composed of engineering data collected from sensors and transducers furnishing information necessary to determine spacecraft configuration status, operational characteristics, and operational health.

The data handling subsystem has special capabilities of formatting and time-division multiplexing the data into a coded or uncoded serial type of data stream suitable for modulating the spacecraft's telemetry transmitter. Timing and operational signals are also provided to be included in the science and engineering data blocks. The data-handling subsystem can store and provide time-delayed readout of formatted data upon command request. The data handling subsystem consists of

a digital telemetry unit, a data storage unit, and a convolutional coder which is an integral part of the digital telemetry unit (Fig. 1). The data-handling subsystem has three operational modes, eight commandable bit rates from 16 to 2048 bits per second in binary increments and eleven data formats with 23 format combinations.

The three operational modes are: (1) real-time, (2) telemetry store, and (3) memory readout. In the *real-time mode* the data are transmitted directly without interim storage. In the *telemetry storage mode* the data are stored and transmitted simultaneously until the data storage unit is full. Then, at this time, the mode reverts automatically to a real-time mode at the last commanded format and bit rate. In this mode, it is possible to sample and store data at a more rapid rate than can be received on the ground. Then, the stored data can be transmitted later at the prevailing bit rate. The *memory readout mode* consists of transmitting the data stored in the memory at any selected bit rate. Figure 2 shows the interrelationship between the real-time and the telemetry storage modes and the flow of the controlling commands necessary to operate the spacecraft in these modes.

The data handling subsystem processes 88 analog, 76 digital, and 168 bilevel data input channels originating from science and engineering type data sources. The telemetry formats generated by the data-handling subsystem are divided into science and engineering groups. The science group includes two basic science formats and three special-purpose science formats for science main frame data, and two science formats that are subcommutated in the main frame. The basic science format contains 192 bits which includes 144 bits assigned to the scientific instruments, 6 bits to subcommutate the engineering formats, 6 bits to subcommutate the science subframe, 18 bits for frame synchronization and the remainder for identification of subcommutated data, telemetry mode, bit rate, and format. The basic science format word length is three bits. If higher resolution is required, two or three of these words are assigned. All of the basic science formats will be arranged for use primarily during interplanetary flight and the other during Jupiter encounter. In addition, three special-purpose science formats each contain 192 bits of digital data from only one or two scientific instruments, and are transmitted only in conjunction with one of the basic science formats alternating every 192 bits. These special formats provide the capability to sample data from certain scientific instruments at the high rate at the expense of reducing the amount of data from other instruments by one half. This feature will be particularly useful when the spacecraft is in the vicinity of Jupiter.

The typical *Pioneer F/G* formats are: A, B, C-1 through 4, A/D-1 through 8, B/D-1 through 8.

Telemetry Format A is the first science format that is arranged to meet the scientific requirements during interplanetary cruising. Figure 3 describes briefly these typical formats. All forty-three 3-bit words available are assigned to the scientific instruments for the *Pioneer F* mission. Seven scientific experiments share this format. The first 3 bits of each main frame contain the mode identification information. These words indicate whether the spacecraft is operating in the real-time, memory readout, or telemetry store modes. Bits 4 to 6 identify the spacecraft bit rate of 16 to 2048 bits per second in binary increments. Bits 8 through 24 comprise an 18-bit-long frame synchronization word. This word is standard in all *Pioneer* telemetry frames and is used by the ground data processing equipment to synchronize the received telemetry frames and words. Bits 97 through 101 are used for format identification. The subcommutation identification is represented by a 7 bit-word, bits 102 through 108 of each main frame. Bit 102 is the most significant bit for the 128-word engineering subcommutator with the most significant bit first. The subcommutated engineering words are contained in bits 109 through 114.

These 6-bit words appear in 128 successive formats and are obtained from various spacecraft engineering instrumentation such as voltage and current monitors, and switch positions. Analog, digital and status information are also included in the engineering subcommutator words. The same engineering subcommutator is also used to telemeter the time necessary for correlating the attitude of the roll index reference line with science and engineering data. The command number and the stored execute delay time of five stored commands are also made available for ground validation and analysis purposes. The sequence status of the spacecraft's attitude-control system and the roll reference source and scientific instruments roll index pulse are also identified and telemetered. Additional engineering subcommutator words are available to transmit information on the star location, on the pulse length of the hydrazine thruster impulses, on the spin period sector generator modes, and on the power status of the control electronics assembly. The science subcommutator is also provided in each main frame consisting of sixty-four 6-bit words. The science subcommutator appears in bits 115 through 120 of the main frame. Analog, digital, and status informa-

tion is accepted by the digital telemetry unit (DTU) from the scientific instruments for telemetering in the science subcommutator.

The format B is a second science format and is arranged to meet the scientific requirements during Jupiter encounter. It consists of an engineering subcommutator accelerated at the main frame-rate, resulting in a 32:1 sampling increase of the measurements. This high-time resolution engineering format will be used to investigate the engineering performance of the spacecraft or determine the source and cause of any detected anomaly. Format C has four basic types providing information on the four major engineering subsystems. C-1 is used for power, C-2 for the communications, C-3 for the electrical distribution/propulsion and C-4 for the attitude control subsystems. Formats D-1 through D-8 are special formats with the main frame of 192 bits. These mainframes are assigned to a single instrument with the exception of format D-2, in which two instruments share the format. A format-D can be telemetered only by alternating it with the frame of formats A or B.

The digital telemetry unit is the heart of the data-handling system and converts the time-multiplexed science and engineering data into a single data stream which modulates the spacecraft's transmitter. Nearly all elements of this unit are redundant. A stable, crystal-controlled 65.536 kHz clock and countdown chain will generate the timing signals needed throughout the spacecraft, and will transfer data to the digital telemetry unit. The roll index pulse generated by the attitude-control system referenced to the timing signals is used to produce accurate roll position signals. This determines the roll position of the on-board instruments in relation to both the data and the spin rate. The digital telemetry unit drives the transmitter with a serial bit stream in the NRZ-L form. This is by-phase modulated on a 32.768 kHz squarewave subcarrier.

The data storage unit (DSU) of the data-handling subsystem consists of a core stack containing 49,152 bits (or 256 streams of data) and associated logic. This unit, which is not redundant, has a read/restore type memory making possible the retransmission of stored spacecraft generated data. It is not necessary to clear the unit before starting a recording cycle. The storage and read-out of data need not be continuous, since they may be interrupted and continued later by command, if required.

The convolutional coder unit codes the format of the data from the digital telemetry unit or the data storage unit to increase the overall efficiency of the telemetry system. The telemetry data can be either coded or uncoded by command. Figure 4 shows the functional configuration of the coder. The main element of this device is a multiple-bit shift register in which the data are shifted in and out of the register at the data bit rate. The encoder replaces each data bit generated by the digital telemetry unit by two symbols, P and Q. The value of each symbol is based on the values of 32 selected data bits previously generated. Each PQ is a logical "1" if there are an odd number "1's" in the selected data bits; otherwise it is a logical "0". The encoding cycle begins at the end of the last bit of each frame synchronization word at which time each stage of the shift register containing the value of the previously transmitted 32 data bits and the 33rd flip-flop used to generate the code are reset to a logical "0". The output symbol rate of the encoder is double that of the input data rate. In error-free data, the bits of a pair provide an unambiguous representation of the original data bit. With errors in the data, the decoding process performed at the deep space stations utilizing the sequence of PQ will provide reconstructed error-free data for transmission conditions well beyond normal acceptable limits without the coding. An overall coding gain of between 3.5 to 4 dB is expected.

III. *Pioneer F/G* Command Subsystem

The spacecraft's command subsystem provides the capability of controlling the operating modes of the spacecraft equipment and scientific instruments from information received from the RF transmissions of the deep space stations and from signals generated on board at discrete events. The command subsystem consists of two command decoders and a command distribution unit (Fig. 5).

The commands are transmitted to the spacecraft by the DSN station having a PCM/FSK/PM modulation of the uplink S-band carrier signal and employing a rate of 1 bit/sec. Twenty-two bits are transmitted from the ground for a single command message. Table 1 illustrates the twenty-two command bits. After a 4-bit preamble and a 1-bit sync pulse, 2 bits are used for selecting a decoder, 3 bits are used for command routing within the spacecraft, and 8 bits contain the command information. The last 4 bits comprise a priority check word. The code used is an optimal Hamming-type linear block code capable of detecting all possible 1- and 2-bit error patterns. The modulo-2 summation of the selected routing and data bits results in even parity for each case.

The bit error rate of the ground system is 10^{-5}. By applying the described command block code, the combined spacecraft/DSN system word error rate has been increased to 10^{-9}. The activated spacecraft receiver demodulates the S-band carrier and provides the frequency shift key tones (FSK) to the command decoders. The 128 Hz represents a "0" and 204.8 Hz represents a "1". The addressed decoder converts the FSK tones to digital data and performs a verification operation with the command message to reduce the probability of executing wrong commands. The decoder forwards the routing address, command message, and if the command is properly verified, an execute pulse to the command distribution unit. If the command is not properly verified by the decoder, the execute pulse is inhibited and the command distribution unit does not act upon the command message.

The command distribution unit processes and distributes all commands to the spacecraft equipment and scientific instruments. Two basic types of output are provided by the command distribution unit: The first is a serial data output to a specific user; the routing portion of the command message identifies the user, and the 8 bits of command information provide the serial data. The second output is a signal applied to any one of the 255 discrete lines for initiating specific functions. The routing portion of the message signifies this discrete type of output and the 8-bit command information identifies the particular one of the possible 255 discrete commands. The command distribution unit also has the capability of being programmed by the routing and command messages to store up to 5 discrete commands for sequential execution at a later time and to store the time delay between sequence enable and sequence execution, and between each command of the sequence. This feature permits the command to be sent and verified by telemetry before execution and will be particularly useful when the communication round-trip time is great. In addition, the command distribution unit will provide a sequence of commands that will be activated at preset intervals by a sequencer which will be initiated automatically by separation of the spacecraft from the launch vehicle.

For redundancy, two decoders are provided for selective operation by an address in the transmitted command message. Redundant paths are provided throughout the logic of the command distribution unit. The discrete outputs are wired to prevent single-part failures from activating other outputs.

The spacecraft is capable of receiving continuous strings of commands by receiving one or more zeros between each adjacent command. Thus, it is possible to reduce the command word lengths to 19 bits for all except the first command.

IV. *Pioneer F/G* Scientific Investigations

Eleven of the scientific investigations that will be conducted by the *Pioneer F/G* program utilize specialized scientific instruments on the spacecraft. However, two investigations use only Earth-based equipment and the S-band communication signal between the spacecraft and the stations of the DSN.

Table 2 shows a listing of the scientific objectives of the thirteen scientific investigations.

References

1. Siegmeth, A. J., "*Pioneer* Mission Support," in *The Deep Space Network Progress Report*, Technical Report 32-1526, Vol. II, pp. 6–17. Jet Propulsion Laboratory, Pasadena, Calif., Apr. 15, 1971.
2. Siegmeth, A. J., "*Pioneer* Mission Support," in *The Deep Space Network Progress Report*, Technical Report 32-1526, Vol. III, pp. 7–19. Jet Propulsion Laboratory, Pasadena, Calif., June 15, 1971.

Table 1. *Pioneer F* and G command word

Bit numbers	Bits	Function
1—4	0 0 0 0	Preamble
5	1	Sync
6, 7	A_1	Decoder address
	A_2	
8—10	R_1 R_2 R_3	Routing address
11—18	C_1 C_2 C_3 C_4	Command message
	C_5 C_6 C_7 C_8	
19—22	P_1 P_2 P_3 P_4	Parity checks

Decoder addresses are 01 or 10 only.

Parity bits are generated as follows:

$P_1 = R_1 + R_2 + R_3 + C_1 + C_2 + C_3 + C_4$

$P_2 = R_1 + R_2 + R_3 + C_1 + C_6 + C_7 + C_8$

$P_3 = R_1 + R_2 + C_2 + C_3 + C_5 + C_6 + C_7$

$P_4 = R_1 + R_3 + C_2 + C_4 + C_5 + C_6 + C_8$

Table 2. *Pioneer F* and G experiments

Scientific objectives	Instrument or function (principal investigator)												
	Three-axis magnetometer (E. J. Smith)	Plasma analyzer (J. H. Wolfe)	Charged particle telescope and detector (J. A. Simpson)	Geiger-Muller telescope system (J. A. Van Allen)	Cosmic-ray telescope (F. S. McDonald)	Trapped radiation detector (R. W. Fillius)	Ultraviolet photometer (D. L. Judge)	Imaging photopolarimeter (T. Gehrels)	Two-channel infrared radiometer (G. Munch)	Asteroid/meteoroid nonimaging telescope (R. K. Soberman)	Meteoroid detector (W. H. Kinard)	S-band occultation (A. J. Kliore)	Celestial mechanics (J. D. Anderson)
Interplanetary													
Solar plasma		√			√								
Solar and galactic cosmic rays			√	√	√								
Shock waves			√										
Neutral hydrogen							√						
Magnetic fields	√												
Particulate matter								√		√	√		
Asteroid belt													
Solid particle flux								√		√	√		
Asteroid surface properties								√					
Mass properties and velocities										√			
Particle size										√	√		
Particle distribution								√		√	√		
Particle surface properties								√					
Jupiter													
Bow shock and magnetosphere boundary	√	√	√	√	√	√							
Electr. prot. in magnetosphere	√	√	√	√	√	√							
Mag. field & source charact.	√	√	√	√	√	√							
Trapped radiation belts	√		√	√	√	√							
Origins of radio emissions	√		√	√	√	√							
Location of dayside aurora							√						
Gross structure of ionosphere												√	
Temperature of upper atmosphere							√						
Atmos. hydrogen-helium ratio							√		√			√	
Temp. distrib. in outer layers of atmos.									√				
Gross structure of atmosphere												√	
Comp. variations in clouds								√	√				
Cloud structure								√	√				
Bright. temp. of dark hemisphere									√				
Jovian polar ice cap									√				
Inter. emergy rad. from Jupiter									√				
Jupiter mass & grav. field harm.									√				
Heliocentric orbit of Jupiter													√
Jovian satellites													
Gross surface characteristics								√					
Mass and orbits													√
Solar galactic boundary													
Magnetic structure	√												
Particle characteristics		√			√		√						
Interstellar space													
Cosmic-ray density			√	√	√	√							

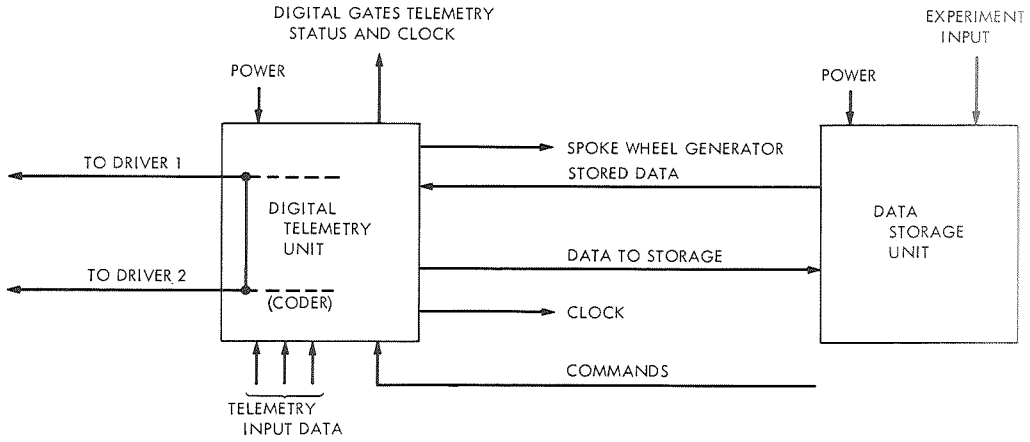

Fig. 1. *Pioneers F and G* data-handling subsystem

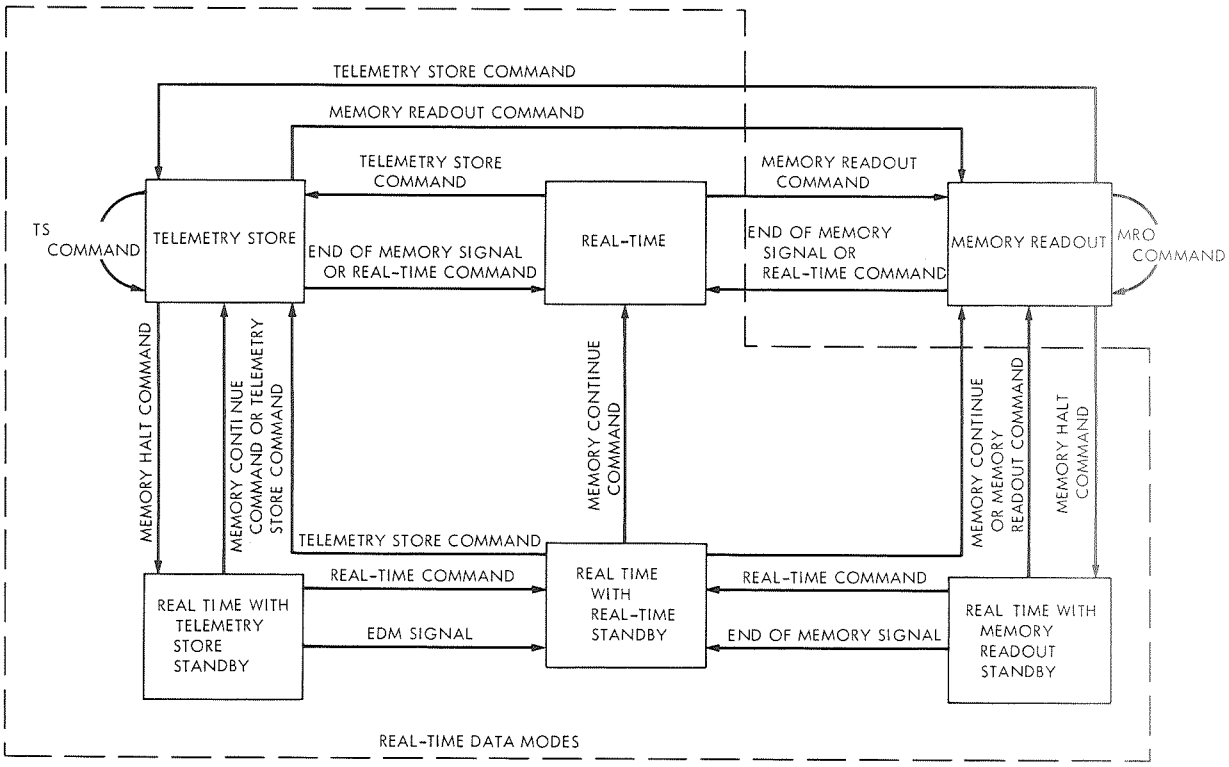

Fig. 2. *Pioneers F and G* spacecraft data system modes

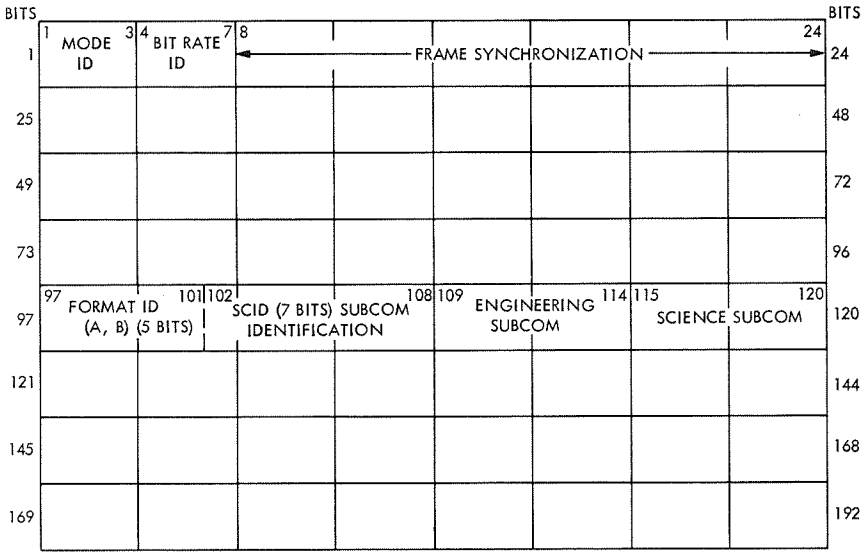

Fig. 3. *Pioneers F and G* telemetry format A

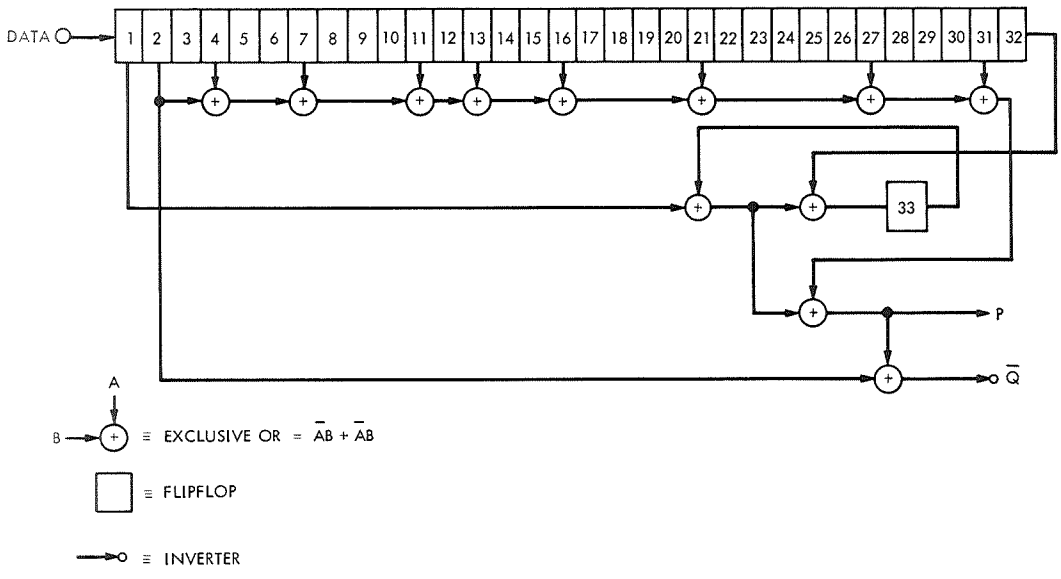

Fig. 4. *Pioneers F and G* convolutional coder

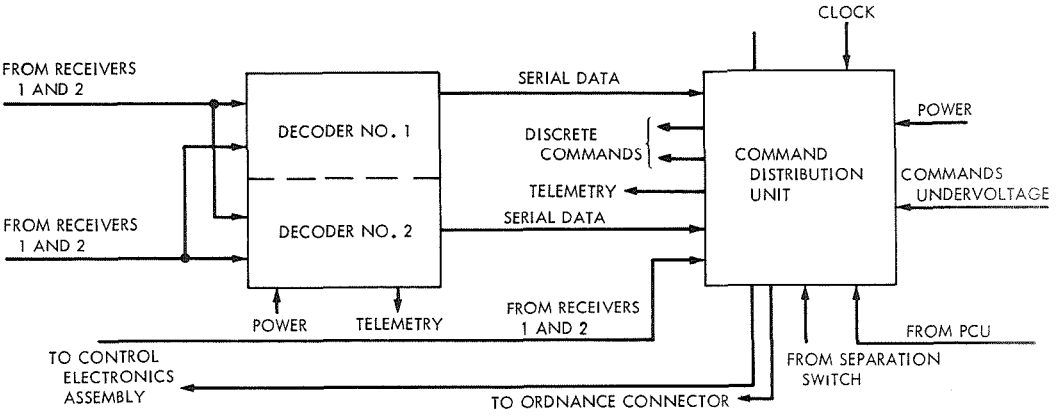

Fig. 5. *Pioneers F and G* command subsystem

Helios Mission Support

P. S. Goodwin
Mission Support Office

Project Helios, named after the ancient Greek Goddess of the Sun, is a joint space venture being undertaken by the Federal Republic of West Germany and the United States of America. Two unmanned scientific satellites will be placed into heliocentric orbits: the first during mid-1974, and the second in late 1975. The history of this Project, its mission objectives, and a general description of the spacecraft were given in previous articles. This article initiates a more detailed description of the spacecraft's radio subsystem in order that the reader may more thoroughly understand the interrelationships between spacecraft design and the planned capabilities of the Deep Space Network (DSN). Specifically, this article provides a functional description of the Helios Telemetry System.

I. Introduction

This is the third of a series of articles pertaining to Project *Helios*. The first two articles (Refs. 1 and 2) provided an overview of the Project organization, the spacecraft physical configuration and radio system design, the spacecraft trajectory to within 0.25 AU of the Sun, and the support requirements placed upon the Deep Space Network. This article will treat some of the significant highlights reported during the Fourth *Helios* Joint Working Group Meeting (held at the Goddard Space Flight Center April 28 through May 4, 1971) and will initiate a series of detailed descriptions of the spacecraft radio system and its interface with the Deep Space Network.

II. Significant Developments at the Fourth *Helios* Joint Working Group Meeting

A complete description of the proceedings of the Fourth *Helios* Joint Working Group Meeting are contained in its minutes (Ref. 3). However, it is appropriate to highlight some of the more significant developments resulting from this meeting—particularly with respect to the interface between the *Helios* spacecraft and the Deep Space Network.

A. *Helios* Spacecraft Radio System Design Review

The *Helios* Project Office provided the various working subgroups with the first comprehensive description of the contemplated spacecraft radio system design and, in turn, requested that the working group membership respond with a technical critique. It was the general reaction of the TDS Subgroup (see Fig. 1, p. 20, Ref. 1) that the Project Office had made considerable progress in developing the spacecraft radio system design since the Third *Helios* Joint Working Group Meeting. Particularly notable was the maturity of the design as depicted in the level of detail and the thoroughness with which it was presented. While few, if any, major difficulties were detected in the tech-

nical review, several features were disclosed which will be of interest to the reader.

1. Block diagram changes. Two design changes were introduced which will slightly modify the block diagram depicted in Fig. 3, p. 24, Ref. 1. It is suggested that the reader pencil the following changes into his copy: First, the two solid-state 1-watt amplifiers have been replaced by one 0.5-watt, low-power amplifier which will still have a capability of being coupled directly to the diplexer/antenna system. This single 0.5-watt amplifier will provide the spacecraft low-power mode. Second, the 20-watt Traveling-Wave-Tube (TWT) amplifiers have been replaced by a combination 10/20-watt TWT amplifier to provide either the medium-power or high-power mode of transmission from the spacecraft to the Earth. The connection between the combination medium/high-power TWT amplifiers and the diplexer/antenna system remains as shown in Fig. 3 of Ref. 1.

2. Two-way, non-coherent mode. The second significant design change in the spacecraft radio system relates to the two-way, non-coherent mode of operation of the transponder. In previous flight projects supported by the DSN, the establishment of an uplink to the spacecraft has caused an automatic switching of the transponder from a one-way (non-coherent) mode into a two-way coherent mode, while the loss of an uplink would cause the automatic reversal of the process. While the latter feature is incorporated into the present *Helios* transponder design, the establishment or re-establishment of the uplink does not automatically create a coherent mode—rather, a command must be sent to the spacecraft to cause it to change from the two-way, non-coherent mode into a two-way coherent mode, as depicted in Fig. 1 of this article. This was done for operational considerations since, during the Step I and Step II maneuvers (see previous articles, Refs. 1 and 2), there is a reasonably high probability of momentary uplink and/or downlink dropouts due to antenna pattern nulls. To avoid sudden jumps in downlink frequency caused by repetitive switching between the voltage-controlled oscillator (VCO) and the onboard very stable oscillator (VSO), the transponder is maintained in the two-way, non-coherent mode during maneuvers and other critical events such as boom deployment, etc. While the foregoing feature is advantageous insofar as the mission operations design is concerned, it does present a new and novel acquisition procedure to the Deep Space Network. A preliminary concept of the new DSN acquisition technique is shown in Fig. 2; however, the time associated with the major steps is only an initial estimate which, hopefully, will foreshorten with further study and experience with this new situation. The time from spacecraft rise to the establishment of two-way, non-coherent operation (shaded diamond of Fig. 2) is dependent upon flight conditions and is apt to be the greatest for the initial DSN acquisition where the tracking rates and other uncertainties are the greatest, and a minimum later on when the trajectory and hence station predicts are well known. However, it will always take several telemetry frames to establish frame synchronization in the DSS Sequential Decoder.

The minimum time between two-way, non-coherent operation and two-way coherent operation (shaded circle in Fig. 2) is a function of three independent factors: (1) the two-way light time for the signal to reach the spacecraft and return, (2) the time required for the spacecraft bit synchronizer to lock-up to the command idle stream prior to initiating actual commands (which is still undergoing study by the Project Office), and (3) the time it takes to re-establish downlink lock at the DSS after loss of the spacecraft's non-coherent signal.

3. Command system. While the details of the *Helios* spacecraft command system will be treated in the next article, it is significant to note that with the present design concept it is necessary to enter an idle stream of 001's into the spacecraft command bit synchronizer for several minutes prior to transmitting the command sync word and command instruction into the spacecraft. This has several operational implications:

(1) The initial DSN acquisition during the Near-Earth Phase must take this time delay into account.

(2) This time delay will also be a factor during handovers between DSSs during the cruise phase of the mission.

(3) During routine tracking operations, it may be necessary for each DSS to continuously transmit the 001 idle stream to the spacecraft in order to ensure rapid command access should the need arise.

(4) Any inadvertent interruption of the uplink will necessitate the re-establishment of bit synchronization aboard the spacecraft. Inadvertent uplink dropouts could be caused by a DSS transmitter overload trip or an unexpectedly deep null in the spacecraft antenna pattern. Known loss of uplink will occur during solar occultations where re-establishment of the command bit synchronization may be further delayed due to solar corona effects.

The foregoing factors do not impair the basic compatibility between the *Helios* spacecraft and the Deep Space Network; however, they must be considered in designing the mission sequence.

B. Telecommunication Milestone Schedule

Another significant Fourth *Helios* Joint Working Group Meeting item was the distribution of the Working Schedule for the Spacecraft Telecommunications Subsystem. This is shown in Fig. 3. Even though *Helios-A* is scheduled for launch in mid-1974, it is noted that Spacecraft Telecommunications Subsystem hardware activity commences early in 1972. One of the first activities will be compatibility tests between the Engineering Model of the spacecraft radio system and the Deep Space Network, conducted at JPL's CTA 21 facility. This test, which will span approximately two weeks, will establish the basic compatibility between the spacecraft radio subsystem hardware and the DSN. It is scheduled for this early date in order to allow time to make design changes in the spacecraft hardware should any significant incompatibilities be detected during these first compatibility tests. Following this, the Prototype Model spacecraft will be constructed. The Prototype Model will be a complete spacecraft in every detail, including the use of flight-qualified components. Because of this, the Prototype Spacecraft is scheduled to be shipped to California where it will undergo match-mate tests with the launch vehicle at San Diego, and thence undergo environmental and compatibility testing and calibration at the Jet Propulsion Laboratory, using operational software in the SFOF computers. The prototype tests are scheduled for the fall of 1973. The Flight Spacecraft are not scheduled to be processed through JPL, but rather to be shipped directly from Germany to Cape Kennedy. As a consequence, compatibility testing and spacecraft calibration for the Flight Spacecraft will be conducted at Cape Kennedy using DSS 71. Since Cape Kennedy does not have environmental test facilities comparable to JPL, it will not be possible to conduct all of the tests performed on the Prototype Spacecraft; however, all hardware and software compatibility tests performed on the prototype will be repeated using the Flight Spacecraft under the ambient conditions existing at the Cape. Considering budget and schedule constraints, this appears to be a reasonable compromise.

C. Near-Earth Phase Study Group Meeting

Following the Fourth *Helios* Joint Working Group Meeting, the second and final meeting of the Near-Earth Phase Study Group was conducted at the Goddard Space Flight Center during May 5–7, 1971. The principal objective of this latter meeting was to establish whether or not a viable near-Earth sequence of events could be established which would permit the activation of selected science instruments aboard the spacecraft in time to make magnetopause measurements in the region from 13 Earth radii to lunar distance. To accomplish this, the Study Group selected one typical trajectory (i.e., a 60-degree launch azimuth using a *Titan/Centaur* launch vehicle) and the latest available information generated by the Study Group membership together with information received during the Fourth *Helios* Joint Working Group Meeting. The Study Group succeeded in generating such a sequence of events for the selected Near-Earth Phase Mission Profile, and the results of this effort are presented in Ref. 4. Included in the list of constraints used by the Study Group was the acquisition procedure described above in *Section II-A-2*. This constraint, together with the need for the Mission Operations Team to carefully monitor and possibly send over-ride commands to the spacecraft during boom deployment, delayed the planned initiation of the two-way, coherent transponder mode of operation until spacecraft separation plus 70 minutes. This, in turn, will delay somewhat the DSN's ability to generate an early spacecraft trajectory for the purpose of computing station predicts and for use by the Mission Operations Team during the Step II manuever. The full impact of such a delayed start in the two-way, coherent mode of operation is still under study by the DSN; however, the situation is not considered serious provided ETR radar metric data are available from the C-band transponder aboard the TE-364-4 third stage. The results of the DSN study will be published when they become available.

III. *Helios* Spacecraft Telemetry Subsystem

A detailed description of the entire *Helios* Telemetry Subsystem is too involved for treatment in a single article, so it will be presented in logical or associated segments in several future articles. The present discussion is intended to acquaint the reader with the functional structure of the *Helios* Telemetry System and its major interfaces with other portions of the spacecraft. This description, together with a similar one covering the Spacecraft Command Subsystem in the next issue, should then permit a meaningful discussion of the various *Helios* telecommunications modes and their performances analyses.

A. General

The *Helios* spacecraft employs one telemetry channel to transmit both science and engineering data back to Earth. Both data types are convolutionally encoded[1] and modulated onto a single 32,768-Hz telemetry subcarrier, which, in turn, is phase-modulated onto the S-band downlink carrier. The combined science and engineering information data rate may be varied from 8 bps to 4096 bps,[2] in

[1] An uncoded mode is available for use during the Near-Earth Phase.

[2] At the present time, the DSN is limited to 2048 bps convolutionally coded telemetry processing in real time.

steps of a factor of two. The onboard science requirements dictate that the telemetry bit error rate (BER) not exceed 10^{-5}, with a maximum frame deletion rate of 10^{-4}. To accomplish this, the telemetry is convolutionally encoded at rate ½, using a Massey code with a constraint length of 32.

In addition to the foregoing real-time requirements, there is a mission requirement to be able to store telemetry onboard the spacecraft during blackout periods caused by solar occultation and/or during periods of particularly high solar activity. The latter is known as the Shock mode of operation which may be employed whenever it is desirable to obtain spacecraft science data with a higher time resolution than that permitted by the information bit rate being telemetered to Earth in real time at that particular moment. Under these circumstances, the Shock data (only) from the onboard science experiments are routed to the 5×10^5-bit core memory at a 4- to 16-kbps rate for storage, with provision for a later playback at a bit rate compatible with the telecommunications signal margins available at the time.

B. Functional Block Diagram

The method employed by the *Helios* spacecraft to meet the foregoing real-time and non-real-time telemetry requirements is depicted in Fig. 4. The real-time science and engineering data (lower lefthand corner) may be in either digital or analog form. The first step is, therefore, to digitally encode it in a manner that will permit further processing. The data is then fed to the Distribution Unit which formats it according to the telemetry mode selected, thence it is fed to the Convolutional Encoder. The output of the Convolutional Encoder, which is a symbol stream running at twice the rate of the original information bit stream, is then modulated onto the 32,768-Hz telemetry subcarrier (lower righthand corner of Fig. 4), which, in turn, is routed to the S-band phase modulator for transmission to Earth. The timing and synchronization of all of these operations is controlled by a single crystal oscillator within the telemetry control unit. This crystal oscillator also generates the 32,768-Hz telemetry subcarrier frequency. Because of this, all bit rates (or symbol rates) in the *Helios* Telemetry System are coherent with the telemetry subcarrier frequency. This coherent relationship, while advantageous from a spacecraft radio system design viewpoint, may produce interference when the data are processed through the Subcarrier Demodulator Assembly (SDA) at the DSS. Therefore, this will be one of the areas receiving particular attention when the *Helios* Engineering Model telecommunications subsystem undergoes compatibility tests in CTA 21 in early 1972.

Science and engineering blackout data enter the *Helios* Telemetry System in much the same manner as real-time data except, in this case, the Distribution Unit routes the data to Core Storage instead of to the Convolutional Encoder. This change in routing is activated by the Mode Registers when so instructed by ground command. Following the blackout period, another ground command can be sent which causes the Mode Registers to retrieve the science and/or engineering data from Storage by returning it to the Distribution Unit, which, in turn, presents it to the Convolutional Encoder for processing to Earth in a manner similar to that for real-time telemetry.

Shock data, which is defined as a sudden change in solar activity, can occur at any time throughout the spacecraft's heliocentric orbit. When the presence of a shock is detected by the science instruments, a *Shock Identification Pulse* is sent to the "Encoder Control Unit," which, in turn, enables the parallel entry of shock data into the Telemetry System. Like real-time data, the shock data is first digitally encoded but at a much higher rate (4 to 16 kbps). The digitally encoded shock data is sent by the Distribution Unit into Core Storage. As previously implied, this can be done in parallel with the spacecraft sending real-time telemetry data to Earth. The shock data so accumulated in Core Storage may or may not be recalled for playback to Earth—depending upon the particular circumstances involved. If the shock data has not been recalled for playback to Earth, the data will continue to accumulate until the 5×10^5-bit core memory is full. At this time, the entry of further shock data may be inhibited unless the shock-front magnitude exceeds that of the data already in storage. In the latter case, the new data would over-write the old data in storage—thereby establishing a new threshold for entry of further shock data into storage. The system can, therefore, be made self-adjusting so that only the most significant shock data is retained in storage between memory readouts. By monitoring the level of solar activity in the real-time science telemetry stream, the *Helios* Mission Operations Team can make real-time decisions on the frequency with which they need to command a replay of shock data from storage.

C. *Helios* Telemetry Formats

As mentioned previously, all *Helios* telemetry data, whether they be science, engineering, blackout, or shock data, are digitally encoded and routed to the Distribution Unit. The Distribution Unit has seven modes of operation. These seven distribution modes may be conveniently grouped into five functional categories as depicted in the lefthand column of Table 1. Within any one distribution mode, one of several telemetry formats is available for

selection in accordance with the second column of Table 1. In addition, each telemetry format has a range of information bit rates available in steps of a factor of two according to the listing provided in the third column of Table 1. The selection of a particular data mode, telemetry format, and bit rate for real-time transmission is done by ground command. Similar statements may be made for the Storage modes shown in Columns 4 and 5 of Table 1. With this in mind, it is appropriate to discuss the five functional distribution modes.

1. Distribution mode 0: real-time telemetry without memory read-in. This mode will usually be used when format 1 (high rate) or format 5 (very high rate) has been selected. It may be used during certain prelaunch tests, before experiment turn-on after launch, or when ascertaining the spacecraft's state of health after blackout—before all the blackout data that are in the memory have been transmitted back to Earth. However, it can be used at other times, and with any of the formats 1 through 5.

2. Distribution modes 1, 2 and 3: real-time telemetry with memory read-in. Scientific and engineering data, or engineering data alone, are combined in a selected format and sent to the RF subsystem for real-time transmission to Earth. At the same time, shock data are formatted and stored in the spacecraft core memory.

There are three real-time science formats[3] which can be selected, each associated with a different range of bit rates. These are the High, Normal and Reduced Rate Formats (Nos. 1, 2, and 3). Also, it is possible to use the engineering format (No. 4) and transmit to Earth only engineering data.

Simultaneously, the shock data are formatted (No. 6) and fed as a serial bit stream to the memory. The read-in address at the memory can be continually cycled, so that shock data may be held in storage for a fixed amount of time and then over-written by new data.

3. Distribution mode 4: real-time telemetry with memory read-in. This is a special case associated with *Subsection C-2*, above, wherein *engineering-only* data are transmitted to Earth and simultaneously read in to storage—both at a rate of 128 bps. Principal applications of this mode occur during the launch and initial DSN acquisition phases of the mission, and again during the Step I and Step II spacecraft maneuvers, i.e., times during which there is a reasonable probability of telemetry dropouts due to either lack of near-Earth station coverage or spacecraft antenna pattern nulls.

4. Distribution mode 5: blackout. The blackout mode is used whenever the spacecraft is occulted by the Sun. Both scientific and engineering data are formatted using format 3, and fed to the Core Memory for storage. The bit rate of the encoder is set very low, such that the memory will be efficiently used during the expected duration of the blackout. When the memory becomes full, the read-in process will be automatically stopped so that there will be no erasure or over-writing of the memory in this mode. This is in contrast to the shock mode memory which will permit an over-writing of the data.

5. Distribution mode 7: memory read-out. This mode is used whenever it is desired to read out science, engineering, shock, or blackout data that have been previously stored aboard the spacecraft. In this mode, the contents of the bulk memory are read out and transmitted to Earth without the addition of any real-time science or engineering data. Since the Core Memory data had been stored in digital form, it is unnecessary to use the Data Encoder, so the Core Memory data are fed directly to the Distribution Unit for processing to Earth. The read-out of the Core Memory is non-destructive, and after the memory has been completely read out, there is an automatic change of mode to the real-time telemetry *without* memory read-in mode. Thus, as little time as possible is spent in the memory read-out mode—however, if the transmission of the memory contents is unsatisfactory for any reason, the data are still available in memory for a second attempt. In addition, the memory read-out mode may be interrupted at any time by ground command without loss of the stored information. This latter feature was incorporated to allow the immediate return to the real-time telemetry mode in case of a suspected problem aboard the spacecraft, or to permit periodic sampling of real-time engineering data when the memory read-out process would consume considerable time due to very low bit rates.

D. Data Encoding System

A detailed description of the *Helios* telemetry data encoding and formatting system, including the bit-by-bit allocations within the 1152-bit *Helios* telemetry frame for each of the six formats, will be left to future articles. Of present importance to the reader is the fact that *Helios* has two separate encoding functions within the Telemetry System. The first is the Data Encoder that translates the raw science or engineering data into a digital structure

[3]These science formats also contain essential engineering data needed for proper conduct of the mission.

that is suitable for further processing within the telemetry subsystem. The second is the Convolutional Encoder that processes the data only after it has been formatted for transmission to Earth. Since confusion may otherwise result, it is important to keep in mind the foregoing adjectives since they will be used in the future articles.

IV. Conclusion

This article has presented several significant highlights resulting from the Fourth *Helios* Joint Working Group Meeting and its subsequent second meeting of the *Helios* Near-Earth Phase Study Group. It has also provided the reader with a functional description of the *Helios* Spacecraft Telemetry Subsystem. It is intended that the next article will treat the *Helios* Spacecraft Command System. Thus, this and the next article will provide a basis for discussing the mechanism and performance of the numerous uplink and downlink modes of operation of the spacecraft radio system in a subsequent article.

References

1. Goodwin, P. S., "*Helios* Mission Support," in *The Deep Space Network Progress Report*, Technical Report 32-1526, Vol. II, pp. 18–27. Jet Propulsion Laboratory, Pasadena, Calif., Apr. 15, 1971.
2. Goodwin, P. S., "*Helios* Mission Support," in *The Deep Space Network Progress Report*, Technical Report 32-1526, Vol. III, pp. 20–28. Jet Propulsion Laboratory, Pasadena, Calif., June 15, 1971.
3. *Project Helios Minutes of the Fourth Joint Working Group Meeting Held at the Goddard Space Flight Center, Greenbelt, Maryland, Apr. 28–May 4, 1971.* Goddard Space Flight Center, Greenbelt, Md.
4. *Project Helios Minutes of the Second Near-Earth Study Group Meeting Held at the Goddard Space Flight Center, Greenbelt, Maryland, May 5–7, 1971.* Goddard Space Flight Center, Greenbelt, Md.

Table 1. *Helios* telemetry: modes of operation

Distribution mode (DM)	Data conditioning for real-time transmission		Data conditioning for onboard storage	
	Format FM	Bit rate BM, bps	Format FM	Bit rate BM, bps
DM 0 Real time without memory read-in	FM 1 High rate FM 2 Normal rate FM 3 Reduced rate FM 4 Engineering FM 5 Very high rate	512–2048 64–512 8–64 8–4096 4096		
DM 1, 2, 3 Real time with memory read-in	FM 1 High rate FM 2 Normal rate FM 3 Reduced rate FM 4 Engineering	512–2048 64–512 8–64 8–4096	FM 6 Shock	4096 8192 16384
DM 4 Real time with memory read-in	FM 4 Engineering	128	FM 4 Engineering	128
DM 5 Black-out			FM 3 Reduced rate	8 (interrupted)
DM 7 Memory read-out	FM 3 Reduced rate FM 4 Engineering FM 6 Shock	8–4096 8–4096 8–4096		

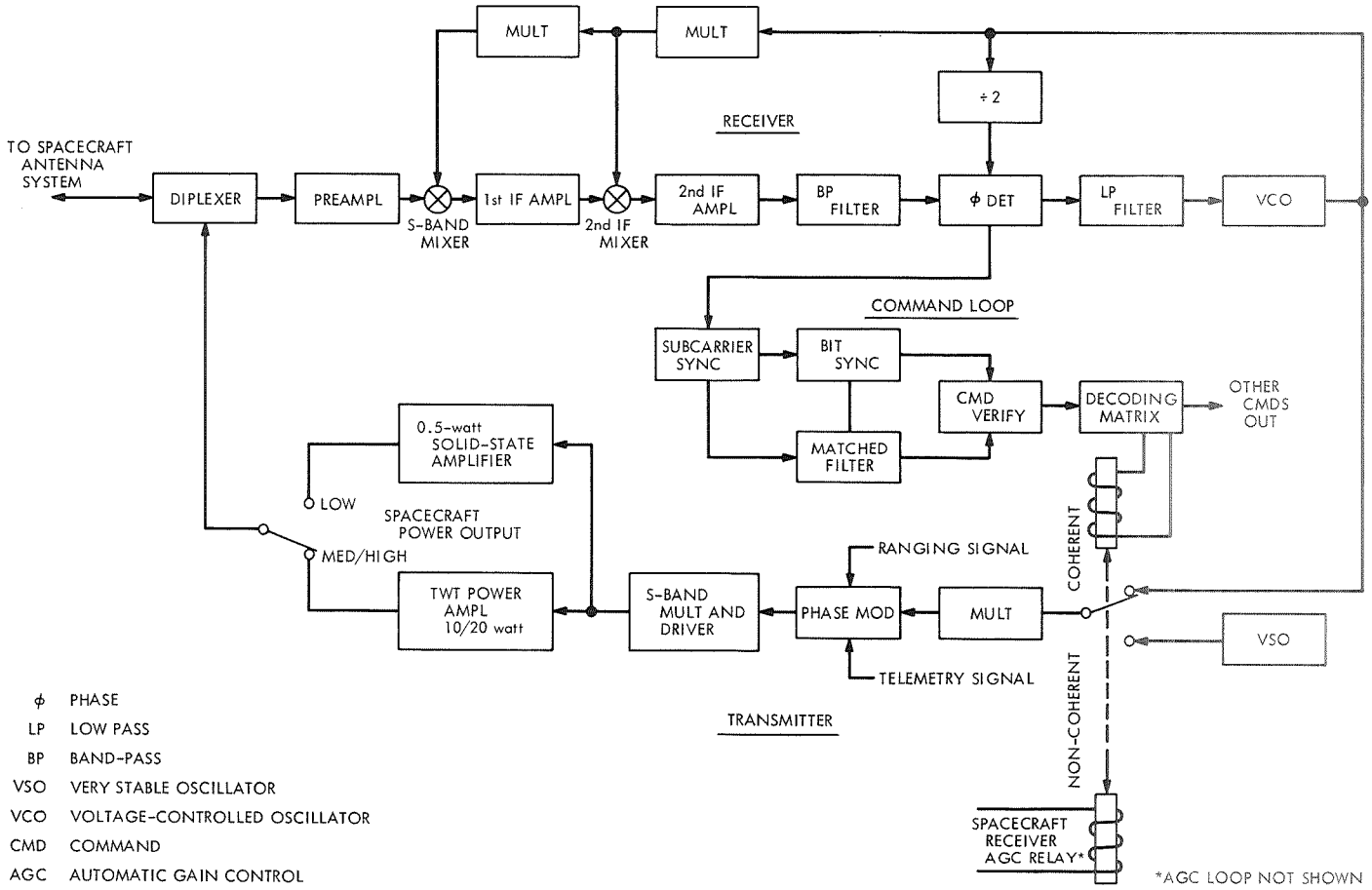

Fig. 1. Simplified diagram of *Helios* spacecraft transponder coherency mode control (only one channel shown)

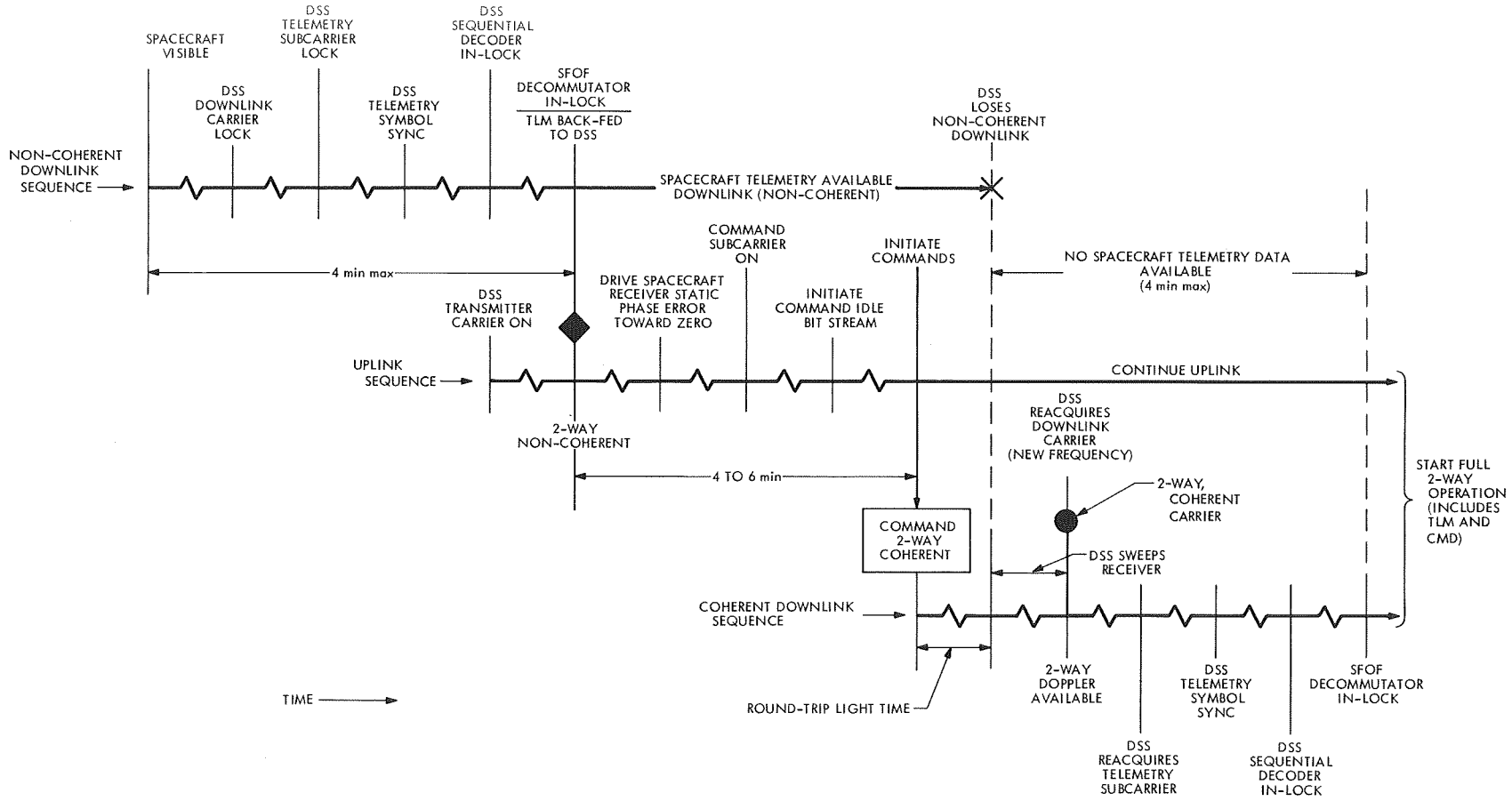

Fig. 2. DSN acquisition sequence for *Helios*

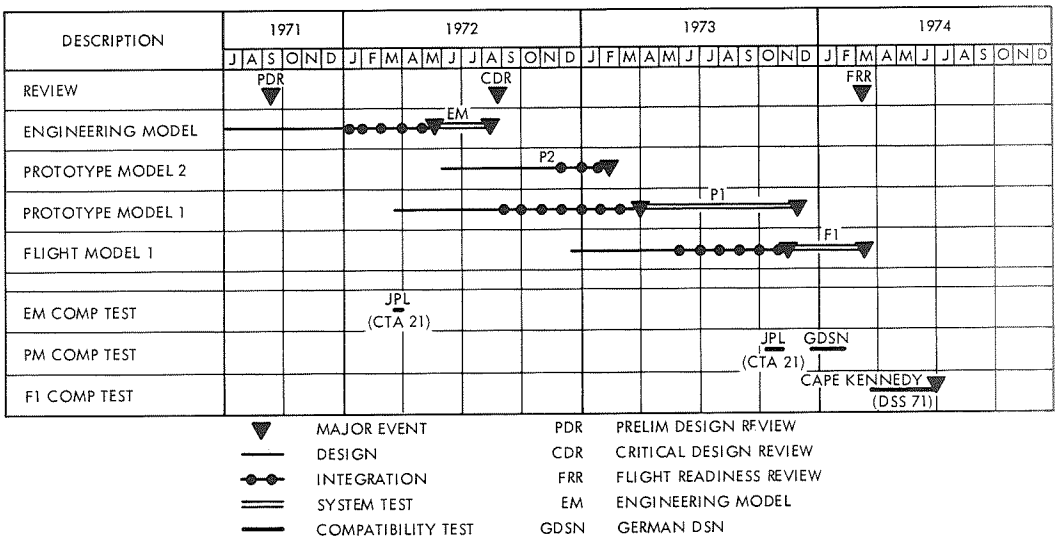

Fig. 3. Project *Helios* telecommunication subsystem: major milestones, April 1971

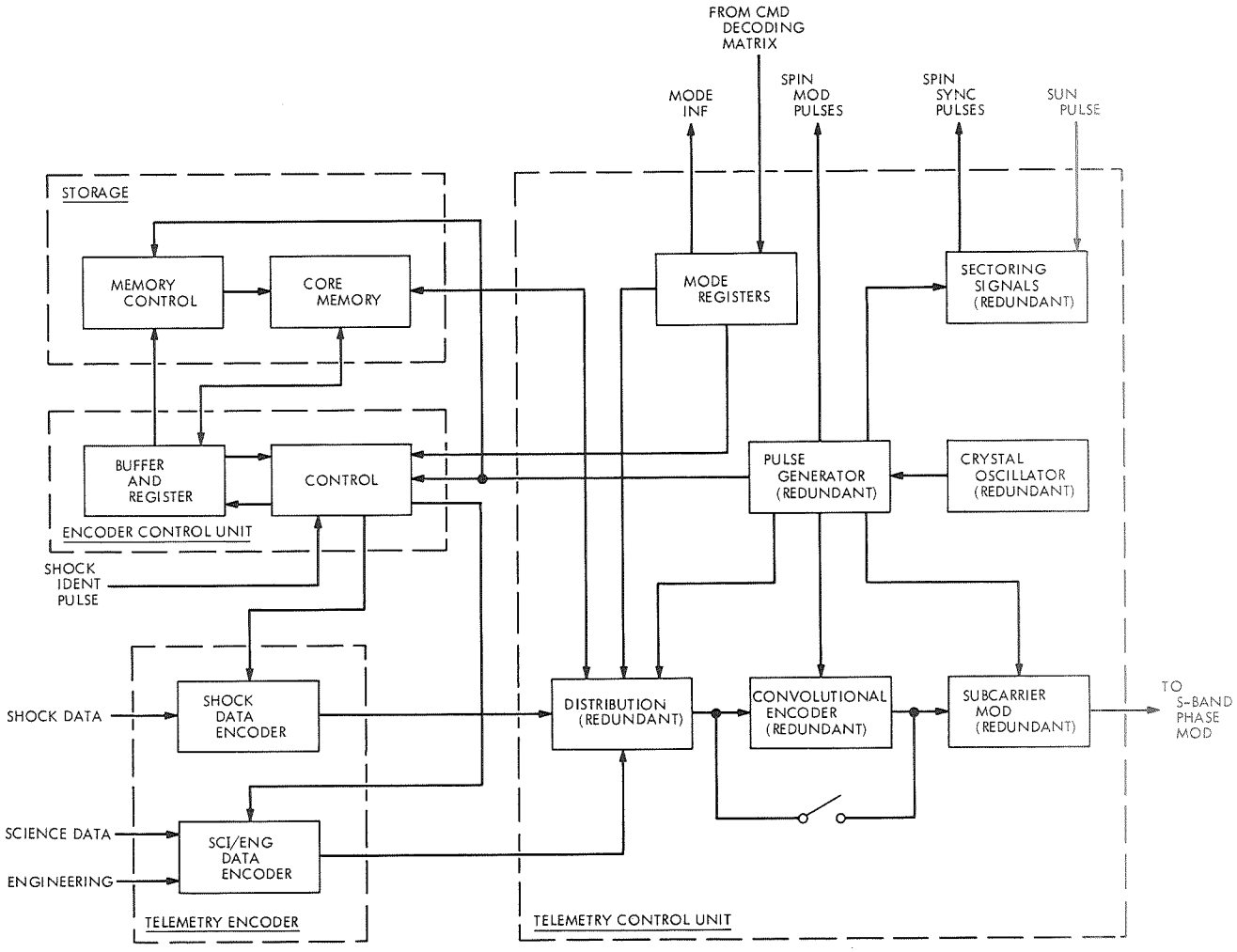

Fig. 4. Functional block diagram of *Helios* spacecraft telemetry subsystem

Mariner Mars 1971 Mission Support

R. P. Laeser
Mission Support Office

All requirements for Deep Space Network (DSN) capabilities needed to support Mariner Mars 1971 Mars orbital operations have been compiled and reiterated with the implementing organizations. Trade-offs between schedule and capability have been made in some instances. This article describes the resulting planned configuration, by network system.

In Technical Report 32-1526, Vol. III, the DSN configuration for support of the *Mariner* Mars 1971 launch and cruise was described. That configuration was significantly different from the one originally planned because of the realities of implementation scheduling. Similar problems have forced a decrease in available DSN capabilities for support of *Mariner* Mars 1971 Mars orbit operations. The resulting configurations, by network systems, are described in the following tables and figures. The method of presentation is the same as in the previous article. Table 1 and Figs. 1 and 2 apply to the telemetry system; Table 2 and Fig. 3 apply to the command system; Table 3 and Figs. 4 and 5 apply to the tracking system; Table 4 and Fig. 6 apply to the monitor system; Table 5 and Fig. 7 to the operations control system; Table 6 and Fig. 8 to the simulation system; and Table 7 to intersystem capabilities. The simulation system will be used to support training for the orbital period.

For each capability listed in a table, a figure reference is given to the corresponding element in the cross-referenced figure; in some cases the block on a figure is numbered and figure reference 2-(1) is interpreted as Fig. 2, Block (1).

The major change that was made between the original plan and the plan described here is that all high-rate telemetry processing and all master data record (MDR) and experiment data record (EDR) processing was eliminated from the 360/75. A plan to interface the Project-supplied mission and test computer(s) (MTC) to the GCF high-speed data lines will be implemented to accomplish these functions.

Table 1. Telemetry system

Planned orbital operations capabilities	Reference
A. DSIF	
1. Hardware ability to demodulate, synchronize and decode all MM'71 data	1-DSIF
2. TCP telemetry software	
a. Acquire synchronized 50 bps through 16.2-kbps telemetry for SSA/BDA	1-TCP
b. Format 50 bps through 2 kbps data and output over HSDL	1-TCP
c. Format selected 50 bps science and output via TTY	1-TCP
d. At DSS 14, format 1-16 kbps data and output over WBDL	1-TCP
e. Record all received data on a digital ODR	1-ODR
3. ODR validation program to operate on TCP	1-TCP
4. Playback specified portions of ODR at HSDL rate	1-TCP
5. Analog record receiver and SDA outputs	1-DSIF
6. Playback analog SDA recording with ground received time	1-DSIF
7. Hardware/software must simultaneously provide:	
a. Command, engineering telemetry (8⅓ or 33⅓, and science telemetry (50 bps, 1 kbps, or 2 kbps) using one 920 computer	1-DSIF
b. 1, 2, 4, 8, or 16 kbps telemetry using second 920 computer (DSS 14 only)	1-DSIF
B. GCF	
1. 50-kbps WBDL from DSS 14 to SFOF	1-WBDL
C. SFOF	
1. 360/75 Telemetry software for engineering (8⅓ or 33⅓) data	
a. Automatic stream selection	2-(2)
b. Place real-time data on SDR	2-(6)
c. Place ODR replay data on SDR (at HSDL rate)	1-360
d. SDR/MDR summary display	2-(6)
e. Fix discrepancies	
(1) Display formats	2-(5)
(2) Special processing—derived channels	2-(4)
2. 360/75 Telemetry software for 50 bps science data	
a. Automatic stream selection	2-(2)
b. Place real-time data on SDR	2-(6)
c. Place ODR replay data on SDR (at HSDL rate)	1-360
d. SDR/MDR summary display	2-(6)
e. Decommutate	2-(3)
f. Display TTY character printer formats	2-(5)
g. Display 1443 formats	2-(5)
h. Display DTV formats	2-(5)
3. 360/75 Telemetry software for all low rate telemetry	
a. SDR recovery after failure	1-360
b. SDR write to tape	1-360
c. Summary processor (statistical)	1-360
d. Recall from SDR for display	2-(6)
e. TAG formats for 1443 (2)	2-(5)
f. TAG DTV formats (2)	2-(5)
g. TAG formats for character printers (2)	2-(5)
h. DSN monitor data in telemetry displays	1-360
i. Telemetry-monitor interface	1-360
j. Continue ground channel processing in absence of telemetry data	1-360

Table 2. Command system

Planned orbital operations capabilities	Reference
A. DSIF	
1. Fix TCP software discrepancies known at launch, including alarms, stack recall	3-TCP
2. Playback to SFOF selected portions of ODR from TCP	3-TCP
B. GCF	
C. SFOF	
1. 360/75 command software	
a. Display alarms consistent with A.1	3-360
b. Generate and validate command SDR	3-360
c. Place ODR replay data on SDR	3-360
d. Generate command MDR providing merge of playback, card, or tape data	3-360
e. Recovery of SDR and other key command information after failure	3-360
f. Command/monitor interface	3-360
g. Modify DTV stack recall display	3-360
h. Block DTV format of commands entered and for each: transmit time, verify status, enable status, confirm/abort results	3-360 3-DTV
i. Display of "spacecraft event time" and "earth received time" in confirm/abort display	3-360

Table 3. Tracking system

Planned orbital operations capabilities	Reference
A. DSIF	
1. Range data and 10 sample/sec doppler (DTS) to SFOF via HSDL from DSS 14	A-DTS
2. 20 μsec inter-station time synchronization	—
3. Acquire open loop receiver data (Occultation Experiment Support) at DSS 14, 41, and 62 and analog record	—
4. Digitize open loop data in real time at DSS 14	—
5. Digitize, at CTA 21, analog recordings of open loop data mailed from DSS 41 and 62	—
B. GCF	
C. SFOF	
1. Hardware	
a. 360/75-1108 electrical interface	4-ELEC
2. 360/75 software	
a. Transfer SDR to 1108 via electrical interface	5-(1)
b. Recovery of SDR after failure	5-(1)
c. MDR (archive) generation and validation	5-(1)
d. Project tape (or equivalent disk) certification	5-(1)
e. Accept spacecraft ephemeris from 1108 via electrical interface	5-(3)
f. 1108 spacecraft ephemeris tape conversions on operational 360/75	5-(3)
g. Add antenna limits to predicts	5-(3)
h. View periods without full predicts run	5-(3)
i. Reduce predict wall clock run time	
(1) Loaded system, 3 DSS, 24 h, Mars orbit—30 min.	5-(3)
(2) Same conditions—15 min.	5-(3)
j. Occultation predicts	5-(3)
k. Pseudo-residual alarms and tolerance setting	5-(2)
l. Pseudo-residual ϕ factor selection	5-(2)
m. Real-time accountability and outage alarms	4-360
n. Tracking Alarms Processor (TAP) DTV display	4-360
o. Generate SDR file of tracking data charged particle and troposphere calibration factors (MEDIA)	4-360
p. Fix discrepancies	
(1) Comm Processor/360 tracking software "channel" data transfer problem	4-360
(2) Predict track syn. freq. logic, including display	5-(3)
(3) Add "Sign" to printout of TRAG records and DRVID	4-360
(4) Add spacecraft frequencies to ϕ factor check tape	5-(3)
q. Process high speed metric data from DTS	
(1) Basic I/O logic	4-360
(2) Display of data and alarm blocks	4-360
(3) All other processing same as TTY data	4-360
r. Compute timing polynomials in background mode (PLATO)	4-360
s. Tracking data selection for transmission to Project	4-360
t. Light-time interface to other systems/programs	4-360
u. Add pseudo-residual quality index to SDR	4-360
v. Locked file in predicts to allow controlled changes of constants	5-(3)

Table 4. Monitor system

Planned orbital operations capabilities	Reference
A. DSIF	
B. GCF	
C. SFOF	
1. 360/75 SFOF monitor software	
a. Acquire and display status/configuration of 360/75 computer, input/output devices, and interfaces with 1108 and communications processor	6-360
b. Accept status data from SFOF telemetry and command software	6-360
2. 360/75 DSN monitor software	
a. Accept and display data from SFOF monitor software	6-360
b. Assemble monitor criteria data and use to generate alarms (including new requirements)	6-360
c. Display alarms on digital TV and character printer	6-360

Table 5. Operations control system

Planned orbital operations capabilities	Reference
A. DSIF	
1. Display telemetry/RF predicts on line printer as received via high speed from SFOF	7-DIS
2. Generate antenna pointing system drive tape from tracking predicts via high speed or TTY	7-APS
B. GCF	
C. SFOF	
1. 360/75 Operations control software	
a. Sequence of Events Generation (SEG) program, real time, meeting negotiated requirements of SRD DSW-2-3040	7-360
b. 1443 page print of output routed traffic	7-360
c. Repair output router floating point	7-360
d. TTY multiple routing indicator	7-360

Table 6. Simulation system

Planned orbital operations capabilities	Reference
A. DSIF	
1. All capabilities available for launch also available at DSS 14 and 62	8-SCA
2. Accept high rate data via WBDL and generate fixed high rate pattern at DSS 14 and CTA 21	8-SCA
3. Perform automatic signal attenuation on carrier	8-ATT
B. GCF	
1. High speed data between Simulation Center and DSS 12, 14, 41, 51, 62, and SFOF	8-HSD
2. Wideband data between Simulation Center and DSS 14, CTA 21 and SFOF	8-WBDL
C. Simulation center (SIMCEN)	
1. 6050 software	
a. Generate maneuver responsive TTY tracking data for up to three DSS	8-6050
b. Accept high rate science data from digital recording	8-6050
c. Format and distribute b. to DSS 14 and CTA 21 via wideband, simultaneous with HSDL telemetry activity	8-6050
d. Format and distribute b. to SFOF via wideband, simultaneous with HSDL telemetry, command, tracking, and monitor activity	8-6050
e. Simulate DTS tracking data interaction with SFOF via HSDL, simultaneous with c. and/or d.	8-6050
f. Format and distribute engineering and 50 bps science via HSDL	8-6050
D. SFOF	
1. Generate on 360/75 time-ordered ϕ factor tapes for tracking simulation input	8-360

Table 7. Intersystem

Planned orbital operations capabilities	Reference
A. DSIF	
1. One 920 computer must perform the following processing simultaneously:	1-TCP 3-TCP
a. Telemetry: one 2.025 kbps plus one 33⅓ (including TTY engineering) or one 50 bps plus one 33⅓ (including TTY engineering and science)	
b. Command: maximum activity for one spacecraft	
c. Other: DIS interface, AGC and SNR conversions, lock status handling	
B. GCF	
1. One 4.8 kbps HSDL must carry a maximum load consisting of:	1-HSD 3-HSD 6-HSD$_1$
a. Telemetry: one 2.025 kbps plus 33⅓ bps engineering	
b. Command: traffic representative of two command transmissions per minute	
c. Monitor: 14 blocks per minute	
C. SFOF	
1. Perform the following processing simultaneously (refer to each system for details):	1-360 3-360
a. Telemetry: real-time processing of any legal combination of MM '71 data (one live and one simulated spacecraft)	4-360 6-360 7-360
b. Command: real-time processing (one spacecraft)	
c. Tracking: real-time processing, including pseudo-residuals, plus predicts (one live and one simulated spacecraft). Includes high speed tracking data from DTS	
d. Monitor: all real-time processing	
e. Operations Control: output routing of predicts, sequence or schedule	
f. Other large (analysis) programs, including: MDR/EDR, COMGEN, SEG, SPOP, SCISIM, AMPS, LIBSET, OCCULTATION, SCILIB, UVS DISPLAY, IRR DISPLAY	

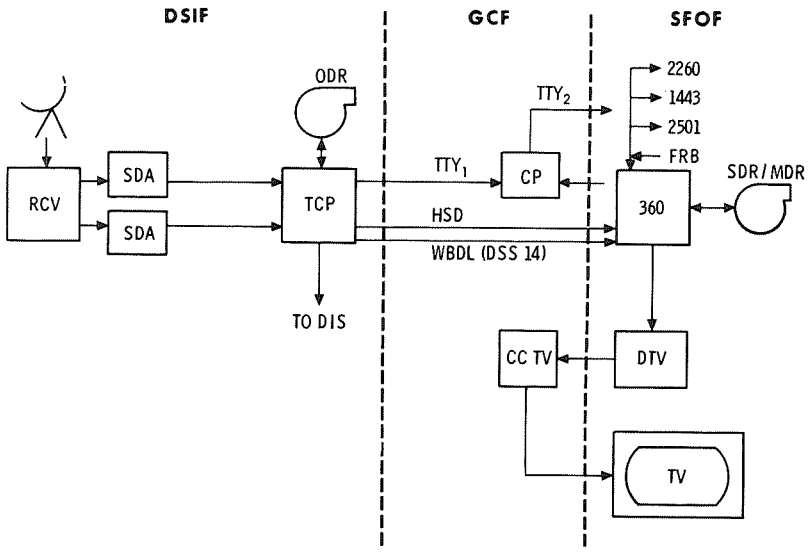

Fig. 1. Telemetry system

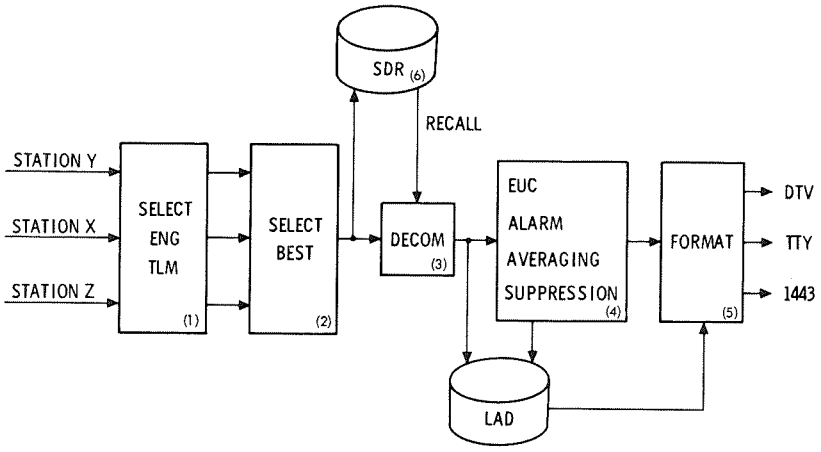

Fig. 2. Telemetry inside the 360 computer

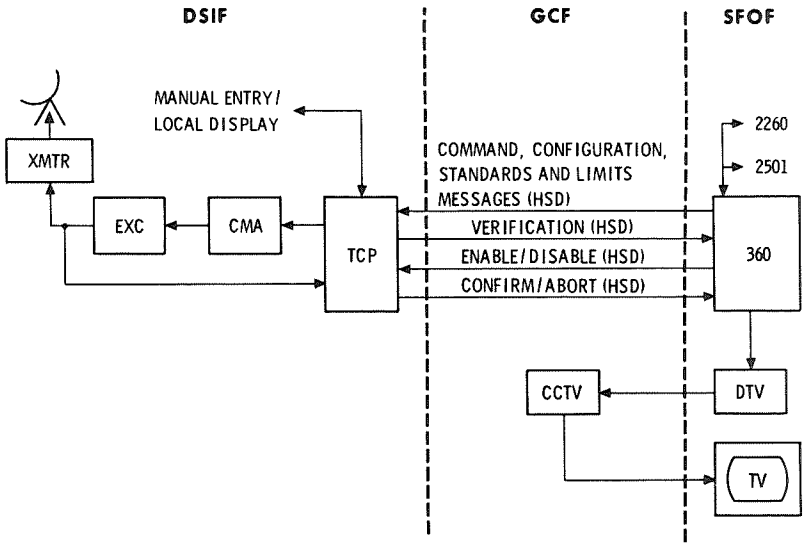

Fig. 3. Command system

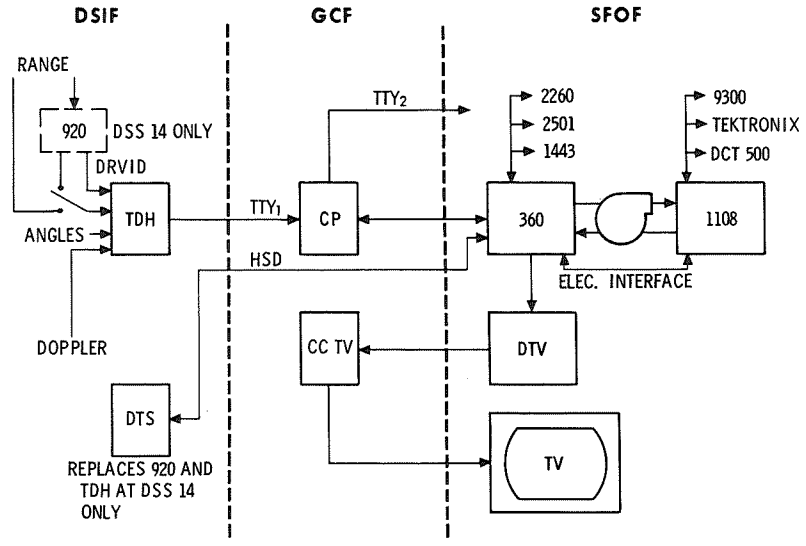

Fig. 4. Tracking system

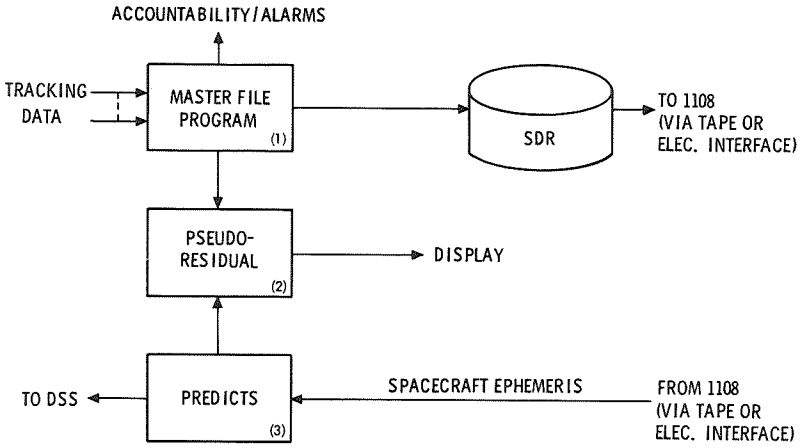

Fig. 5. Tracking inside the 360 computer

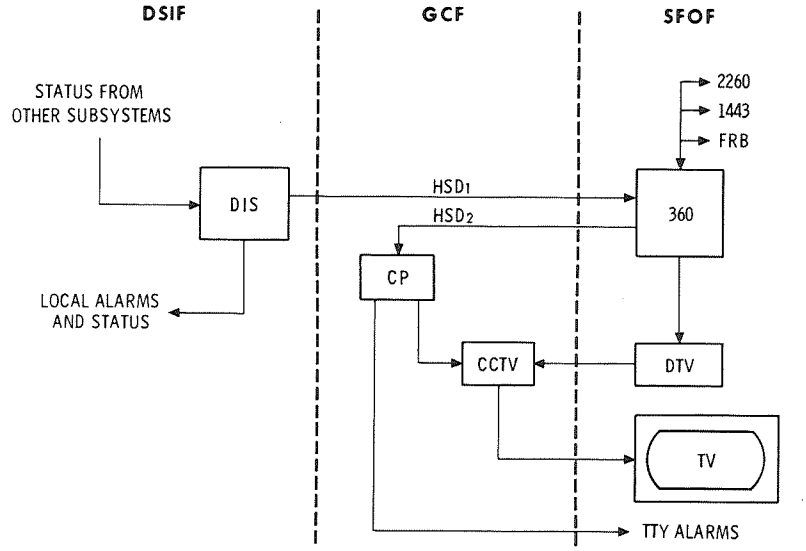

Fig. 6. Monitor system

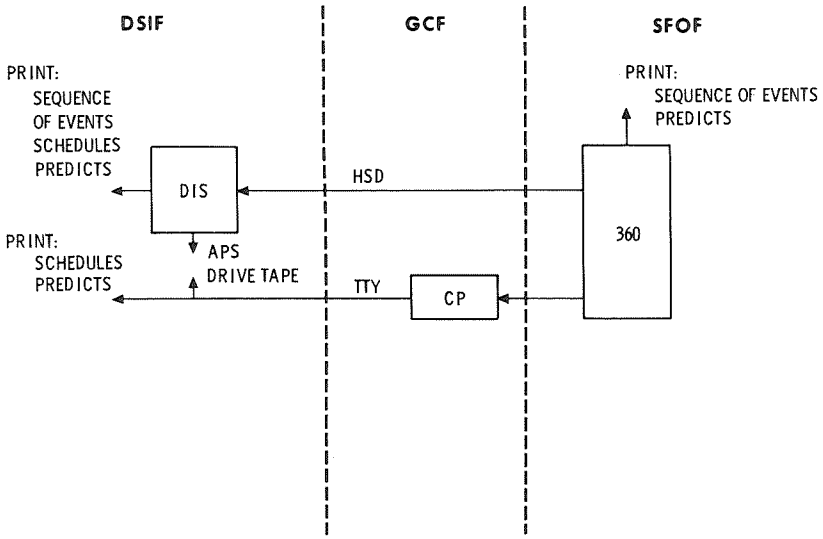

Fig. 7. Operations control system

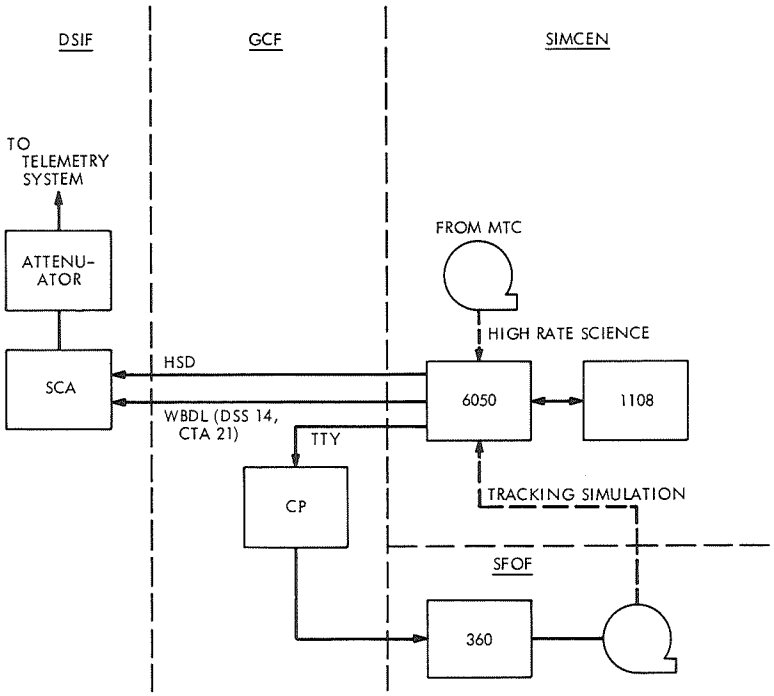

Fig. 8. Simulation system

Viking Mission Support

D. J. Mudgway
Mission Support Office

Previous issues of the Deep Space Network (DSN) Space Programs Summary and the DSN Progress Report devoted attention to management and organization, Deep Space Network configurations for telemetry, command, and tracking, and, more recently, to the influence of the DSN in the design of the Viking mission orbiters and landers. Beginning with this issue of the DSN Progress Report, attention will be focused on reporting Viking-related activity in certain specific areas, as the DSN interface organization progresses from the planning through operational phases of the Viking missions. This article takes up the question of DSN support for Viking navigation and traces progress since the latter part of 1970 through the present time.

I. Introduction

In Refs. 1, 2, and 3, Tracking and Data System (TDS) plans for support of *Viking* were described with particular reference to management and organization, technical documentation, and DSN configurations for telemetry, command, and tracking. Following the redirection of the Project from the 1973 to the 1975 opportunity, attention was devoted to achieving a better understanding of the influence of DSN capabilities and constraints on the design of the *Viking* 1975 Mission.

In Refs. 4, 5, and 6, these questions were addressed in the areas of *Viking* trajectories, *Viking* Orbiters and Landers, and telecommunications including telemetry, command, and tracking. This and subsequent articles will describe significant *Viking*-related activity as the DSN interface organization progresses through the planning, implementation, testing, and operational stages of the mission.

II. Background

Since the decision was made by the Project to use the Type II trajectory described in Ref. 4, a great deal of attention has been given by the Project and the DSN to properly identifying requirements and capabilities respectively for radio metric data needed to accomplish the *Viking* navigation function.

The basic radio metric data provided by the DSN to the *Viking* Project consist of the following items:

(1) Doppler.

(2) Range.

(3) Timing.

These basic data are supplemented with additional information which permits the prime data to be evaluated

prior to their use in the Flight Project's orbit determination and navigation processes. The supplementary data include the following items:

(1) Specifications on station parameters, such as accuracy and stability of frequency, timing, phase delay, group delay, etc.

(2) Deep Space Station (DSS) status.

(3) Calibration data for interplanetary medium effects.

(4) Identification of data type, by station and spacecraft.

Because the quality of the radio metric data provided by the DSN directly influences the realization of the navigation goals, the *Viking* Project places great emphasis on the identification of all uncertainties in the data and the reduction of all error sources to the absolute minimum.

While the DSN supports a continuing program aimed at achieving objectives such as these for all flight projects, the exact details of the navigation support provided by the DSN for any particular project depends on its specific requirements.

III. Navigation Requirements

The *Viking* requirements for navigation-related data were first presented to the DSN in Ref. 7, following an extensive review with the *Viking* Project Office in January 1971 at the Langley Research Center.

Table 1 compares the mission requirements on system design (MRSD) as given in Ref. 7 with the DSN capability as presented at that time. The DSN capabilities given in the table are based on the material appearing in Ref. 8 and are consistent with DSN planning for the *Viking* era as reflected in Ref. 9.

Several of the parameters are of special significance to the navigation function and are discussed below.

A. Doppler

Noise in the doppler data arises from two principal sources within the DSSs:

(1) High-frequency noise in the Receiver, Exciter, Transmitter Subsystems. Over a 60-second averaging period, this amounts to 0.00007 meters/second (rms).

(2) Oscillator frequency instability in the Frequency and Timing Subsystem (FTS), which contributes 0.00075 meters/second (rms) over a 60-second period. This assumes a stability of 5 parts in 10^{12} in the FTS oscillators.

When added RSS-wise and converted to a 3-sigma value, the value of 2.1 mm/s given in Table 1 is obtained.

The doppler phase stability is also a function of two DSS parameters:

(1) Variation in electrical path length through the RF system, having a value of 0.5 meters over 12 hours.

(2) Stability of the DSS transmitter frequency (5×10^{-12}) over one round-trip light time (RTLT). For RTLT of 2400 seconds, this is equivalent to 1.8 meters.

The RSS addition of these two contributions gives the 3-sigma value of 5.5 meters/12 hours given in Table 1.

The two remaining doppler quantities of interest, i.e., offset and rate, arise from estimates of the worst possible case *Viking* trajectories where the earth/spacecraft radial velocity might reach ± 17 km/s with accelerations as high as 2.7 m/s^2. Given adequate signal margins in the receiver RF tracking loops, this presents no problem to the Deep Space Instrumentation Facility (DSIF), except that the doppler offset could cross into an adjoining channel as explained in Ref. 5.

B. Ranging

In considering planetary ranging at all 64-meter stations for support of *Viking*, the following error characteristics must be taken into account:

(1) High-frequency noise, which arises in the ranging receiver, depends on both the ratio of ranging power to noise power and on the time between independent samples. Both of these parameters are under the control of the flight project. A typical value for $P_r/N_0 = +4$ dB with a sample time of 250 seconds gives an uncertainty in each independent range sample of 3 meters (rms). A set of curves relating these variables has been developed and is included in Ref. 10.

(2) Further errors in the range measurement result from the accumulated effect of several other factors:

(a) Instability of the ranging modulation group delay in passing through the RF system contributes about 2 meters uncertainty over a 12-hour period.

(b) Absolute frequency error of 1×10^{-11} over 1000 seconds is equivalent to an error of 1.5 meters.

(c) A timing measurement error of 30 microseconds causes a further error of 1 meter for an earth/spacecraft radial velocity of 30 km/s.

(d) The zero-delay device used to calibrate the station ranging system contains an uncertainty of 2.5 meters.

The 3-sigma value of the RSS total of these uncertainties produced the 12-meter value for range delay given in Table 1.

The overall uncertainty of the ranging system measurements is obtained by including the noise contribution with the delay uncertainties and taking the RSS total. This approach gives a value of approximately 7 meters (rms) which has been adopted as the current DSN standard for ranging uncertainty.

The remaining ranging-related items are concerned with the acquisition time of the standard operational DSN planetary ranging system (Tau) relative to that of the developmental ranging system (Mu).

The figures given in the table reflect the Project's earlier interest in the Mu system where the acquisition time was given by

$$T_{acq}\,(\mathrm{Mu}) = 74\frac{N_0}{P_r} \approx 240 \text{ seconds}$$

where

N_0 = noise power in the ranging receiver

P_r = ranging power in the ranging receiver

By comparison, the standard DSN operational planetary ranging system (Tau) under the same conditions had an acquisition time given by

$$T_{acq}\,(\mathrm{Tau}) = 4550\frac{N_0}{P_r} \approx 14800 \text{ seconds}$$

All other parameters in both systems remain the same.

More recent developments in this area are discussed in *Section IV*.

C. Differenced Ranging Versus Integrated Doppler

The difference between S-band doppler phase delay and S-band ranging group delay is of prime importance in calibrating out the effect of charged particles in the ionosphere and interplanetary medium on the doppler data. This technique takes advantage of the fact that charged particles affect range increments obtained from the accumulated doppler count and those obtained from differencing range measurements by nearly equal but opposite amounts. The doppler phase velocity is advanced while the ranging group velocity is retarded. The Differenced Ranging Versus Integrated Doppler (DRVID) technique is described in Ref. 11.

It is obvious that the stability of the difference between the phase and group delays has a direct influence on the quality of the calibration data obtained from DRVID.

The DSN value for this parameter expressed in terms of the uncorrelated drift over a 12-hour period is estimated to be 10 nanoseconds or 1.5 meters.

In the operational planetary ranging system planned for *Viking*, the DRVID data will be available as soon as the clock or highest frequency component of the range code has been acquired by the ground receivers. This will take 1 to 10% of the time required for the full code acquisition, which in turn depends on signal-to-noise considerations as described above. The minimum acquisition time of about 80 seconds applies in both cases. The ranging acquisition sequence for the Tau system is shown in Fig. 1. It would appear, therefore, that there should be no difficulty in satisfying the Project's requirements for DRVID data within 15 minutes of receipt of two-way doppler under reasonable signal-to-noise conditions.

D. Timing

In the *Viking* time period, the DSN expects to have the lunar time sync system in operational use throughout the 64-meter network. This will provide 20-microsecond (one sigma) timing synchronization between 64-meter stations and between National Bureau of Standards (NBS) and the Goldstone master clock. The *Viking* timing

requirements given in Table 1 can easily be met by this capability.

E. Equivalent Station Locations

The Project requires a tracking system model for which the equivalent station location errors will not exceed the following values:

Equivalent station radius error r_s = 4.5 meters

Equivalent station longitude error r_λ = 9.0 meters

Since these equivalent station location errors are the result of combining many parameters into a specific model of the Project's choosing, the DSN is responsible only for providing the parameters listed in Table 1, either by means of a specification or a magnetic tape containing the desired calibration data. The DSN will, however, assist the Project in developing an error model suitable to its needs.

IV. Recent Progress

Since the original discussions on the navigation requirements, a considerable refinement in both the Project's statement of requirements and the DSN statement of capabilities has taken place. The progress in this area is reflected mainly in the sections of the SIRD (Ref. 8) dealing with radio metric requirements.

Requirements for S- and X-band performance data have been added as an adjunct to the radio science experiments as well as to provide an alternative to the DRVID technique for charged-particle calibration.

The need for rapid ranging acquisition on the Lander, discussed in Ref. 6, has been restated in terms of a single uplink rather than dual simultaneous uplinks. This allows the use of a single high-power (100 kW or greater) uplink which provides sufficient ranging power at the Lander or Orbiter to achieve the acquisition time desired with the standard DSN operational planetary ranging system (Tau). In constraining *Viking* flight operations to a single uplink during ranging periods when rapid acquisition is required, this solution is not entirely satisfactory, but it is acceptable for short periods when the single uplink constraint can be tolerated.

V. Conclusion

With the publication of the SIRD, the statement of Project navigation requirements is virtually complete. However, much remains to be done to fully understand, identify, and separate the TDS and Orbiter or Lander contributions to total system errors. This work is necessary in order to allow the DSN response to the SIRD, that is, the NASA Support Plan, to be prepared by the end of this year in accordance with the *Viking*/TDS schedule.

It is quite likely that the continuing DSN process of refining its navigation-related capabilities could result in the availability of radio metric data of significantly improved quality by the time of the *Viking* Mission. Care is being taken to ensure that the mission design is such that advantage can be taken of these improvements, should they eventuate, to enhance the mission navigation process.

References

1. Mudgway, D. J., "*Viking* Mission Support," in *The Deep Space Network*, Space Programs Summary 37-61, Vol. II, pp. 26–28. Jet Propulsion Laboratory, Pasadena, Calif., Jan. 31, 1970.
2. Mudgway, D. J., "*Viking* Mission Support," in *The Deep Space Network*, Space Programs Summary 37-62, Vol. II, pp. 12–22. Jet Propulsion Laboratory, Pasadena, Calif., Mar. 31, 1970.

References (contd)

3. Mudgway, D. J., "DSN Support for *Viking*," in *The Deep Space Network*, Space Programs Summary 37-63, Vol. II, p. 14. Jet Propulsion Laboratory, Pasadena, Calif., May 31, 1970.

4. Mudgway, D. J., "*Viking* Mission Support," in *The Deep Space Network Progress Report*, Technical Report 32-1526, Vol. I, pp. 7–10. Jet Propulsion Laboratory, Pasadena, Calif., Feb. 15, 1971.

5. Mudgway, D. J., "*Viking* Mission Support," in *The Deep Space Network Progress Report*, Technical Report 32-1526, Vol. II, pp. 28–32. Jet Propulsion Laboratory, Pasadena, Calif., Apr. 15, 1971.

6. Mudgway, D. J., "*Viking* Mission Support," in *The Deep Space Network Progress Report*, Technical Report 32-1526, Vol. III, pp. 38–45. Jet Propulsion Laboratory, Pasadena, Calif., Jun. 15, 1971.

7. Viking 75 Project Mission Requirements on System Design, RS-3703001, Appendix A, Langley Research Center, Hampton, Va., Mar. 26, 1971.

8. Viking 75 Support Instrumentation Requirements Document, RD-3713008 (Review Copy), Langley Research Center, Hampton, Va., Jun. 1, 1971.

9. Deep Space Network System Requirements 820-9, Rev. A, DSN Tracking System, 1972-1975, Jun. 15, 1971 (JPL internal document).

10. DSN Standard Practice 810-5, Rev. A, Change 2, May 15, 1971, DSN/Flight Project Interface Design Handbook, Oct. 1, 1970 (JPL internal document).

11. MacDoran, P. F., and Wimberly, R. N., "Charged-Particle Calibrations From Differenced Range Versus Integrated Doppler—Preliminary Results From *Mariner* Mars 1969," in *The Deep Space Network*, Space Programs Summary 37-58, Vol. II, pp. 73–77. Jet Propulsion Laboratory, Pasadena, Calif., Jul. 31, 1969.

Table 1. *Viking* metric data quality[a]

Parameter	MRSD requirements	DSN capabilities
Angle error (peak value)	0.06 deg	0.06 deg
Angle resolution	0.002 deg	0.002 deg
Doppler noise	2.1 mm/s	2.1 mm/s
Doppler phase delay stability	6 m/12 h	5.5 m/12 h
Doppler offset	±262 kHz	±207 kHz
Doppler rate	41 Hz/s	>50 Hz/s
Ranging group delay	15 m	12 m
Ranging high-frequency noise	15 m	3 m (rms)
Ranging acquisition time	30 min	<4 min
Ranging ambiguity	>3000 km	150,000 km
DRVID		
Phase/group delay	4.5 m/12 h	4.5 m/12 h
Acquisition time	15 min	15 min
Timing		
Master clock to NBS	1 ms	60 μs
Interstation time sync	150 μs	60 μs
Equivalent station locations (σ_{R_S}, σ_λ)	4.5 m, 9.0 m	—
DSS locations (σ_{R_S}, σ_λ)	—	0.5 m, 1.0 m
Polar motion (σ_X, σ_Y)	—	0.7 m, 0.7 m
Predicted earth rotation (UTI)	—	4.0 ms
Charged particles (DRVID)	—	1.0 m/12 h
Tropospheric refraction	—	0.5 m/12 h
Electrical path length	—	0.5 m/12 h
Frequency instability	—	5×10^{-12}

[a]3-sigma values unless stated otherwise.

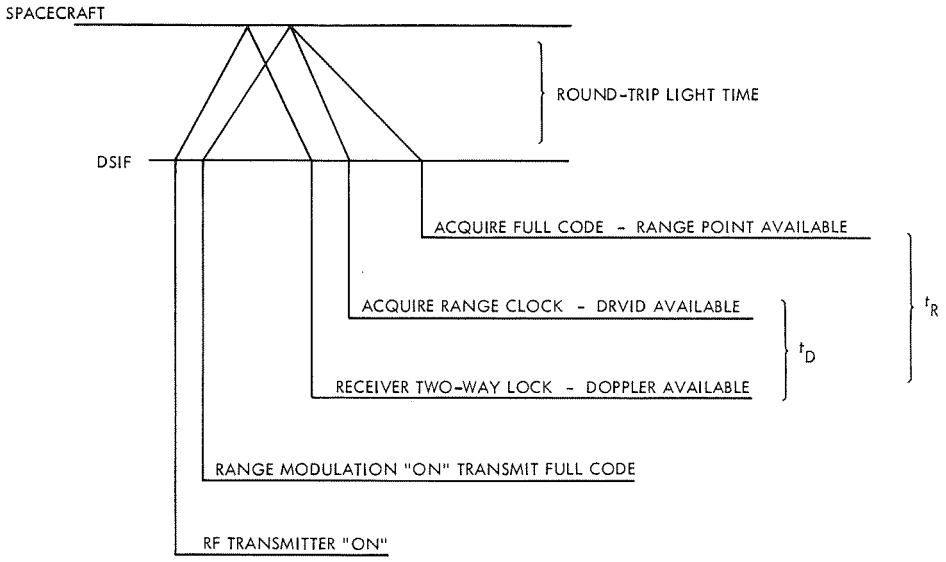

Fig. 1. Operational planetary ranging acquisition sequence

Radio Science Support

K. W. Linnes
Mission Support Office

Since 1967, radio scientists have used the Deep Space Network (DSN) 26- and 64-meter antenna stations to investigate pulsars, to study the effects of solar corona on radio signals, and to observe radio emissions of X-ray sources. Very long baseline interferometry (VLBI) techniques have also been used for high-resolution studies of quasars. Several VLBI observations that were accomplished during the reporting period are summarized.

I. Introduction

The 26- and 64-meter antenna stations of the DSN have been used for several years to support radio science experiments. NASA, JPL, and university scientists have used key DSN facilities whose particular and unique capabilities were required for the performance of the experiments. In order to formalize the method of selecting experiments and experimenters, a Radio Astronomy Experiment Selection (RAES) Panel was formed in 1969. Notice of availability of these facilities was placed in professional journals to inform the scientific community that they were available for limited use by qualified radio scientists (Ref. 1). No charge is made for use of the standard DSN facilities and equipment; special equipment, however, must be provided by the experimenters. A summary of all experiments conducted through April 1971 was reported in Ref. 2.

II. Radio Science Operations

A very long baseline interferometry (VLBI) experiment indicated in the previous report (Ref. 2, page 51) was recently approved, and performed on May 30 and June 25, 1971. The experiment was for the purpose of high-resolution studies of extra-galactic sources at 3 cm and involved simultaneous observations using the 22-meter antenna at the Crimean Astrophysical Observatory (CAO), the 43-meter antenna at the National Radio Astronomy Observatory (NRAO) in Greenbank, West Virginia, and the DSN 64-meter antenna station at Goldstone, California. The USSR experimenters were from CAO and also the Institute for Cosmic Research; the U.S. experimenters are from NRAO, Cornell University, and Caltech. The observations were conducted satisfactorily and the magnetic tapes from the various observatories were taken to NRAO for processing. At Goldstone, experimental equipment in the 8-GHz range was used with a system temperature of about 30 K. At all stations, wideband recording terminals, designated Mark II, were supplied by the NRAO. Timing synchronization between stations was achieved by NRAO personnel flying a rubidium frequency standard from the U.S. station to the CAO via Copenhagen and Leningrad.

Results of the X-band VLBI (8 GHz) measurements made in February 1971 by M. Cohen of Caltech, K. Kellermann and B. Clark of NRAO, and D. Jauncey of Cornell University were submitted for publication in June (Ref. 3). These measurements confirm the millisecond-of-arc structure of 3C279 reported by Shapiro from his measurements in connection with his general relativity experiment (Ref. 4).

In June, Shapiro repeated his measurements using the Goldstone 64-meter station and the MIT Haystack antenna used earlier. The data have been returned to MIT for processing. Further measurements will have to be deferred until the fall of 1971 because the X-band feed cone is being removed from the 64-meter antenna for several months as part of some upgrading and reconfiguration activities.

An observation at S-band at medium bandwidth between the 64-meter antenna at Goldstone and the 26-meter antenna at Woomera, Australia, was made in a continuing series of observations by Australian and Caltech experimenters (Ref. 2).

III. RAES Panel Activities

The RAES Panel approved the repetition of the Goldstone–Haystack observations at X-band. No other new proposals were received during this reporting period.

References

1. *Bulletin of the American Astronomical Society,* Vol. 2, No. 1, p. 177, 1970.
2. Linnes, K. W., Sato, T., and Spitzmesser, D., "Radio Science Support," in *The Deep Space Network Progress Report,* Technical Report 32-1526, Vol. III, pp. 46–51. Jet Propulsion Laboratory, Pasadena, Calif., Jun. 15, 1971.
3. Cohen, M., et al., "The Small Scale Structure of Radio Galaxies and Quasars at 3.8 cm," *Astrophys. J.* (in press).
4. Shapiro, I., et al., "Quasars: Mc/Arc Structure Revealed by Very Long Baseline Interferometry," *Science,* Vol. 172, p. 52, Apr. 2, 1971.

Application of Differenced Tracking Data Types to the Zero Declination and Process Noise Problems

K. H. Rourke and V. J. Ondrasik
Tracking and Orbit Determination Section

A preliminary analysis of the information content inherent in differenced doppler and differenced range data [Quasi-VLBI (very long baseline interferometry)] is made to illustrate why these data types may be superior to conventional data types, when the spacecraft is at a low declination or is subject to unmodelable accelerations. This simple analysis, based upon a 3 parameter model of the range and range-rate observables, shows that in certain circumstances the differenced data types can be expected to improve the accuracy of the orbit determination solution. Some hardware and calibration requirements which will insure that the data will be of sufficient quality are briefly discussed.

I. Introduction

This article considers the use of differenced simultaneous or near simultaneous tracking data from two widely separated tracking stations as a countermeasure for two particularly troublesome problems that occur in determining the orbit of an interplanetary spacecraft, namely, the zero declination and process noise problems. The process noise problem refers to the difficulties encountered in determining the orbit of a spacecraft that is subject to random non-gravitational acceleration uncertainties. The acceleration uncertainties, although often negligible in their direct effect on the physical orbit of a spacecraft, can severely limit the capability of actually solving for the orbit on the basis of conventional tracking data types. The zero declination problem is a more familiar difficulty, i.e., obtaining accurate short arc solutions with zero declination, declination insensitive doppler data. The problem is particularly acute when the spacecraft random accelerations degrade longer arc solutions. The following presentation indicates that the differenced data techniques promise significant improvements in orbit determination performance, particularly in cases for which the zero declination or process noise problems are a limiting factor. The degree of improvement is, however, contingent on projected, although not overly optimistic, tracking instrumentation and system calibration capabilities.

Presently only two-way doppler and three-way doppler are simultaneously available at separate tracking stations. This discussion broadens the selection in considering simultaneous two-way and three-way range and nearly simultaneous two-way range measurements, one before and one after an interstation handover. Three-way range has never been used as an explicit data type, yet it is equivalent to station-to-station timing techniques that have been used for lunar spacecraft tracking. There should be no difficulty in implementing the three-way ranging with the planetary instrumentation (see Ref. 1). This pre-

liminary analysis treats the simultaneous data in differenced form, i.e., two-way minus three-way doppler, two-way minus three-way range, and two-way range minus near simultaneous two-way range. This approach need only be an artifice for revealing the advantages of the simultaneous tracking data in circumventing the process noise and zero declination problems. Although explicit differencing may prove to be a satisfactory mode of incorporating the simultaneous data, a more efficient "optimal" use of the data entails a direct combination of both data types with a suitably designed orbit determination filter.

The differenced data types, two-way minus three-way doppler and two-way minus three-way range are analogous to the VLBI (very long baseline interferometery) data types, fringe rate, and time delay, respectively, and hence are sometimes referred to as quasi-VLBI data. (Two-way minus two-way range contains the same information as time delay VLBI, yet has different error characteristics as explained later.) Williams in Ref. 2 discusses the characteristics of VLBI tracking, primarily with regard to geophysical parameter determinations and he points out that in spite of the remarkable precision available to VLBI techniques their direct application to spacecraft orbit determination is limited by the same tracking platform and propagation media uncertainties affecting the conventional tracking data. The direct use of actual VLBI measurements for spacecraft navigation is in addition hindered by the rather special data processing requirements associated with interferometery. The conventional tracking data VLBI analogs, however, provide the special VLBI characteristics discussed in this article with the conventional tracking data acquisition ease and adequate measurement precision (with respect to expected navigation requirements and calibration accuracies). These comments are not intended to minimize the promise of VLBI in aiding Earth-based interplanetary navigation since, although VLBI may be inconvenient for direct spacecraft tracking, it is expected to be valuable in tracking platform calibration.

The discussion of differenced tracking data proceeds in the following with an analysis of two-way minus three-way doppler as a means for circumventing the process noise problem. The treatment serves principally as a motivation for the use of the simultaneous two-way and three-way data and as an identification of associated major error sources. The next segment of the discussion considers differenced range data types for use in alleviating the zero declination problem, and delineates the major expected error sources.

II. Differenced Doppler

Differenced simultaneous doppler (two-way doppler minus three-way doppler) promises to be less sensitive to short-term spacecraft random accelerations than conventional two-way doppler. This effect is easily motivated with the familiar Hamilton/Melbourne range rate representation of doppler residuals (see Ref. 3):

$$\Delta\dot{\rho} = a + b\sin\omega t + c\cos\omega t + n(t)$$

with

$$a = \Delta\dot{r}(t)$$
$$b = -r_s\omega\sin\delta\Delta\delta(t)$$
$$c = -r_s\omega\cos\delta\Delta\alpha(t)$$

where $\Delta\dot{r}$, $\Delta\delta$, and $\Delta\alpha$ are instantaneous corrections to the distant spacecraft's geocentric range rate, declination, and right ascension over the duration of the pass. Parameters r_s, ω, and δ are station radius from the spin axis, Earth rotation rate, and spacecraft nominal declination, respectively. The time $t = 0$ corresponds to nominal meridian crossing to allow simpler expressions for b and c. The function $n(t)$ represents a data noise process. This representation implies that the information available from a single pass of doppler data can be expressed in terms of estimates of the spacecraft's geocentric range rate, declination, and right ascension. The difficulties arising from random spacecraft acceleration can be visualized as follows: accelerations affect the data most strongly through the a-term, short-term acceleration variations will introduce short-term velocity variation, and these components then introduce errors into the b and c determinations, thereby corrupting the right ascension and declination solutions.

Consider for example a moderate spacecraft random acceleration of 5×10^{-11} km/s^2. (Acceleration uncertainties can be expected to range from the 10^{-12} km/s^2 affecting ballistic spacecraft to the 10^{-9} km/s^2 affecting a thrusting solar electric spacecraft.) The worst possible 1-day degradation in b and c is produced by a radial acceleration of the form

$$a_r \sim (5 \times 10^{-11})\cos(\omega t + \phi)$$

inducing an effective station location error of magnitude

$$\frac{5 \times 10^{-11}}{\omega^2} \sim 10 \text{ meters}$$

Thus, relatively small acceleration uncertainties can conceivably cause significant spacecraft position measurements.

Consider now topocentric range rate observed from two separated tracking stations

$$\Delta\dot{\rho}_1(t) = \Delta\dot{r}(t) + b_1 \sin \omega t + c_1 \cos \omega t + n_1$$
$$\Delta\dot{\rho}_2(t) = \Delta\dot{r}(t) + b_2 \sin \omega t + c_2 \cos \omega t + n_2$$

The parameters b_1, b_2, c_1, c_2 are linear expressions in the $\Delta\alpha$ and $\Delta\delta$ corrections, their explicit form depending on the particular time reference used in the above representations. Two-way doppler residuals obtained at station 1 can be expressed as $2\,\Delta\dot{\rho}_1$. Three-way doppler residuals available at station 3 are of the form $\Delta\dot{\rho}_1 + \Delta\dot{\rho}_2 - C\Delta f/f$ where the $C\Delta f/f$ term arises from the frequency standard discrepancy, Δf between stations 1 and 2. The difference of two-way doppler from station 1 and 3-way doppler from station 2 is represented as

$$\Delta\dot{\rho}_1 - \Delta\dot{\rho}_2 + C\Delta f/f = C\Delta f/f + (b_1 - b_2) \sin \omega t + (c_1 - c_2) \cos \omega t \quad (1)$$

over the overlap $\psi_1 \leq \omega t \leq \psi_2$. The geocentric range rate terms subtract out and are replaced by a "velocity bias" $C\Delta f/f$ arising from the relative station to station frequency standard bias $\Delta f/f$ (C = speed of light). Herein lies the motivation for differenced doppler data: in the presence of large unmodelable random acceleration, the differenced doppler allows separation of $\Delta\delta$ and $\Delta\alpha$ determination, through $b_1 - b_2$ and $c_1 - c_2$, from a corrupted $\Delta\dot{r}$ determination. The technique is hindered, however, by the introduction of a velocity bias uncertainty in the place of the geocentric range rate uncertainty. Clearly, the differenced doppler data can be effective in circumventing process noise effects only as long as the uncertainties arising from frequency standard instability are significantly less than the process noise uncertainties expected in the conventional doppler data.

The differenced doppler data is formally identical to VLBI fringe rate data (with respect to the above representation), hence the term quasi-VLBI. This correspondence includes the velocity bias term that arises from the tracking station frequency standard biases. The only essential difference between the differenced doppler and fringe rate VLBI (in the case of spacecraft tracking) lies in the different data resolution capabilities inherent to the two techniques. The geometric relationships characteristic of either fringe rate VLBI or differenced doppler can be visualized as shown in Fig. 1, where $\bar{r}_{s_1}$ and $\bar{r}_{s_2}$ are equatorial projections of the two tracking station radius vectors. Associated with those data types is the projected "base line" $\bar{r}_{s_1} - \bar{r}_{s_2}$. The differenced data can be viewed as conventional doppler (minus the geocentric effects) observed from a "pseudo-station" located at $\frac{1}{2}(\bar{r}_{s_1} - \bar{r}_{s_2})$ during the overlap of stations 1 and 2.

The short overlap durations and the offset tracking configurations associated with the geometries of widely separated tracking stations can diminish the precision of the $\Delta\delta$ and $\Delta\alpha$ determinations. In contrast to the usual Hamilton/Melbourne analysis, determinations of the parameters $b = b_1 - b_2$ and $c = c_1 - c_2$ as well as $\Delta\delta$ and $\Delta\alpha$ cannot generally be considered as independent, complicating a detailed error analysis such as provided by Ref. 3. In any case

$$\sigma_b^2 + \sigma_c^2 = \omega^2 r_B^2 (\sin^2 \delta\, \sigma_a^2 + \cos^2 \delta\, \sigma_\delta^2)$$

depends only on the pass width and the data noise where σ_a^2, σ_b^2, σ_a^2, σ_δ^2 are the variances of the a, b, $\Delta\alpha$, and $\Delta\delta$ determinations based on the data in Eq. (1) (assuming a particular data noise variance σ_n^2). r_B is the baseline projection length $|\bar{r}_{s_1} - \bar{r}_{s_2}|$. Estimates that are sufficient for the purposes of this discussion can then be obtained from

$$\sin^2 \delta\, \sigma_\delta^2 \leq (\sigma_b^2 + \sigma_c^2)/r_B^2\omega^2$$
$$\cos^2 \delta\, \sigma_a^2 \leq (\sigma_b^2 + \sigma_c^2)/r_B^2\omega^2$$

The α and δ variances, therefore, have bounds that depend on the overlap width $\psi_2 - \psi_1$ and the projected baseline length r_B. These quantities vary considerably with the particular tracking station pair. Table 1 presents the baseline and projected baseline (obtained from Ref. 2) length and overlap variations for a selection of DSN tracking station pairs. The overlap varies approximately linearly with spacecraft nominal declination for pairs in the same northern or southern hemisphere. The strength of a given station pair increases with the available overlap width, yet large overlap widths go with short baseline projections, e.g., station pair 51–61, which tend to diminish the strength of the station pair. The α and δ variances also depend on the spacecraft nominal declination, with declination solutions becoming degenerate near $\delta = 0$ in analogy to conventional doppler.

Figure 2 presents curves of $(\sigma_b^2 + \sigma_c^2)^{1/2}/\omega$ (scaled as effective station location errors) as functions of overlap half-width and *a priori* velocity bias uncertainty. The values are based on 1 mm/s data taken at 1-minute intervals. The *a priori* velocity bias uncertainty as well as the

overlap width are seen to strongly affect the precision of the a and b, and accordingly the $\Delta\alpha$ and $\Delta\delta$ determinations. The effect of good *a priori* velocity bias information is particularly dramatic for the short overlap widths that are available from typical station pairs. For instance, an *a priori* velocity bias certainty of 0.1 mm/s ($\Delta f/f < 3 \times 10^{-13}$) allows 3-meter effective station location error determinations of $\Delta\alpha$ and $\Delta\delta$ for a nominal 30-deg half pass width. This dependence on velocity bias *a priori* implies that long-term frequency standard stability is a critical factor affecting the capability of the differenced data in determining the spacecraft's right ascension and declination.

Short-term frequency instabilities, particularly diurnal variations, produce $\Delta\delta$ and $\Delta\alpha$ errors in the same way short-term acceleration variations affect two-way doppler. Figure 3 shows the relation between short-term frequency stability and rss b and c accuracy (assuming otherwise perfect b and c determinations). The domains of two available frequency standards (hydrogen and Rubidium) are also indicated (see Ref. 4). Rubidium associated accuracies are on the order of 30 meters in effective station location whereas the hydrogen accuracies are bounded by 3 meters. (Hydrogen maser stability of 5×10^{-13} is conservative.) Three-meter accuracies are compatible with the performance requirements of modern interplanetary navigation while 30-meter accuracies are not. This and the above comments regarding long-term stabilities imply that the useful application of two-way/three-way doppler tracking requires hydrogen frequency standards at each tracking station.

The preceding analysis is not intended to imply that the sole use of two-way minus three-way doppler or, equivalently, fringe rate VLBI is an efficient use of the data received at both stations from the spacecraft. The differenced data is effective in allowing separation of topocentric and geocentric tracking information—even in the case of a spacecraft experiencing large random accelerations. Ultimately, maximum information is extracted if concurrent two-way and three-way data are processed together with a suitably designed orbit determination filter that takes advantage of the known random acceleration characteristics. The differenced data provides, nevertheless, an adequate conceptualization for preliminary analysis as well as a straightforward first approximation to an "optimal" treatment of concurrent two-way and three-way doppler data.

The scope of this article's treatment of differenced doppler data is the influence of process noise on the information available from only a single tracking pass, i.e., the data available over periods of less than one day. Orbit determination solutions require data over several days and, although short-term accuracies do determine ultimate orbit determination performance, the correspondence between short-term and longer-term accuracy is by no means a simple one. This is particularly true in the case of acceleration uncertainties since they directly affect the spacecraft's position and velocity. The topic of longer arc orbit determination is presented in the next article[1] of this volume.

III. Differenced Range

The two-way minus three-way doppler is analogous to fringe rate or narrow band VLBI. A time delay or wide-band VLBI analogue can be implemented by differencing range measurements taken at separate tracking stations.

As mentioned previously, two modes are considered for differenced range time delay measurement, namely, two-way range minus simultaneous three-way range and two-way minus near simultaneous two-way range. The two-way minus two-way technique is motivated by the difficulties encountered in obtaining sufficiently precise tracking station clock synchronization for acceptable three-way range accuracies. Three-way synchronization errors are directly involved in the signal arrival measurement so that a timing error Δt produces a range difference error of $C\Delta t$, i.e., at a rate of 300 meters/microsecond. Two-way minus two-way station synchronization, however, introduces an error into the measurement epoch specification producing range difference errors $\dot{\rho}\Delta t$, where $\dot{\rho}$ is the spacecraft's range rate, thus resulting in only $\sim$10-mm errors per microsecond timing error. Since best synchronization accuracies to date (see Ref. 1) are in the 5-microsecond range, the use of the simultaneous differenced range requires advanced methods (e.g., stellar source VLBI or extraction from the tracking data). The timing bias can be expected to drift at 13 meters/day for oscillator stabilities at 5×10^{-13}, implying that the timing bias calibrations or solutions will require frequent updating. It is unclear if two-way minus three-way range is superior to differenced doppler in the case that timing bias is extracted from the spacecraft tracking data.

The measurement geometry associated with either the pseudo or "real" wide-band VLBI is illustrated in Fig. 4.

---

[1]Ondrasik, V. J., and Rourke, K. H., "An Analytical Study of the Advantages Which Differenced Tracking Data May Offer for Ameliorating the Effects of Unknown Spacecraft Accelerations" (this volume).

The signal time delay, baseline length and signal source direction are seen to be related as follows:

$$\tau = \frac{D}{C} \cos \phi$$

The time delay expression can be related in equatorial coordinates as

$$\tau = \frac{1}{C} [z_B \sin \delta + r_B \cos \delta \cos (\alpha - \alpha_B)]$$

where z_B, r_B, and α_B are baseline z height, equatorial projection length, and right ascension at the time of the delay measurement. Since the delay measurement allows short arc solutions of equatorial angles, differenced range data exhibits the same advantages of insensitivity to process noise as does differenced doppler. In contrast to differenced doppler, however, the time delay permits zero declination, declination solutions, since near zero declination

$$C\Delta\tau \sim z_B \cos \delta \, \Delta\delta$$

so that general time delay errors, $C\Delta\tau$, produce declination errors

$$\Delta\delta \sim \frac{1}{\cos \delta} \frac{C\Delta\tau}{z_B}$$

Short arc determinations on the basis of doppler data (conventional or differenced) are on the other hand degraded by errors of the form

$$\Delta\delta \sim \frac{1}{\tan \delta} \frac{\Delta r_s}{r_s}$$

where Δr_s and Δr_B, in the case of the differenced data, are assumed to be the limiting error sources (see Ref. 3). Figure 5 displays these relationships in terms of position errors at 10^8 km for varying nominal declinations and $C\Delta\tau$ error levels. Typical values are assigned to z_B, r_s, and Δr_s: 7000 km (Goldstone, Canberra), 5000 km, and 1.5 meters, respectively. The figure makes clear the potential of differenced range measurements for alleviating the zero declination problem—assuming that $C\Delta\tau$ errors can be restricted to the sub-10-meter domain. Such an assumption, however, cannot be taken lightly. The conventional application of range measurements regards 10-meter accuracy as entirely adequate (provided that stabilities permit DRVID calibrations, see Ref. 5). Differenced range quasi-VLBI finds 10-meter range measurement marginal with 1-meter measurement system accuracies an attractive goal.

Differenced range measurement errors can be placed in the following general categories:

(1) General baseline errors, including geocentric station location errors, polar motion, and UT1 errors.

(2) Transmission media errors, including ionosphere and space plasma charged-particle effects and tropospheric refraction errors.

(3) General instrumentation errors, including those of signal arrival time measurement, local clock synchronization and rate stability, spacecraft transponder delay, and ground delay.

The influence of baseline errors on the differenced range time delay measurement can be presented in terms of the following differential expression of differenced range:

$$\begin{aligned}\Delta\rho_1 - \Delta\rho_2 = C\Delta\tau \\ &= z_B \cos \delta - r_B \sin \delta \cos (\alpha - \alpha_B) \, \Delta\delta \\ &\quad - r_B \cos \delta \sin (\alpha - \alpha_B) (\Delta\alpha - \Delta\alpha_B) + \sin \delta \Delta z_B \\ &\quad + \cos \delta \cos (\alpha - \alpha_B) \, \Delta r_B\end{aligned}$$

where Δz_B, Δr_B, and $\Delta\alpha_B$ are corrections to the baseline parameters z_B, r_B and $\Delta\alpha_B$. The baseline errors Δr_B and $r_B \Delta\alpha_B$ are less than 3 meters on the basis of station r_s and λ accuracies of 1.5 and 3 meters, respectively (see Ref. 5). The sin $\delta\Delta z_B$ error is a maximum of 8.5 meters at $\delta = 23.5°$ assuming individual station z height accuracies of 15 meters. The z_B errors can be improved on the basis of preliminary differenced range determinations. Note that declination determinations at zero declination are insensitive to z_B errors.

The influence of baseline errors on differenced range orbit determination accuracy is in any case essentially equivalent to the influence of station location errors on conventional tracking data orbit determination accuracy (except that the differenced data exhibits no singularity at zero declination). The crucial accuracies affecting the feasibility of effective differenced range measurements lie in the media and instrumentation error categories. Adequate estimates of these accuracies are difficult to obtain at this time, since, as mentioned previously, meter-level ranging accuracies have heretofore been considered unnecessary. Thus, current specifications are expected to be overly pessimistic with regard to differenced range applications. Table 2 presents media calibration and instrumentation accuracies for both simultaneous and near simultaneous techniques. In light of the uncertainty regarding the actual possible accuracies, several values are quoted for each error source, including expected present capability and upper and lower values for projected

future capability. The future quotations include earliest availability dates. The projected accuracies are illustrated in Fig. 6. Specific references are cited where possible. (The future accuracy capabilities are drawn from Ref. 9 that addresses several specific quasi-VLBI configurations.) These values indicate that meaningful demonstrations of differenced range techniques can be conducted at present and that the future goal of 1-meter level differenced range measurements is indeed a plausible one. The promise of differenced range techniques will become more clear with more detailed analysis and experimental verification of range instrument capabilities in the 3-meter domain, and sub-meter charged particle and troposphere calibration capability.

IV. Concluding Remarks

This article presents reasons why data taken simultaneously or nearly simultaneously from widely separated stations is a partial solution to the zero declination and process noise problems. This analysis should not, however, be conceived of as proving the value of the differenced data. To be able to state with assurance that the differenced data will substantially improve spacecraft navigation, it will be necessary to undertake a thorough accuracy study using analysis tools which are a direct analogue of operational software. Such a study is currently underway and will be reported on in the future. The faith which one may put in the results of this study will be highly dependent on the quality of the information which describes the performance of the frequency standards, ranging machines, and calibration procedures. Ultimately, credible information regarding measurement system performance can only be obtained by an analysis of actual radio tracking measurements taken from an interplanetary spacecraft. Presently plans are underway for acquiring this data during the *Mariner IX* mission.

Acknowledgment

The material presented in this article cannot be credited to the authors alone. The authors wish to acknowledge the valuable contributions of insight and encouragement from D. W. Curkendall, T. W. Hamilton, D. W. Trask, J. G. Williams, and O. H. von Roos.

References

1. Martin, W., Borncamp, F., and Brummer, E., "A Method for Precision Measurement of Synchronization Errors in Tracking Station Clocks," AGARD Conference Proceedings Number Twenty-Eight, Technivision Series, Slough, England, Jan. 1970.

2. Williams, J. G., "Very Long Baseline Interferometry and Its Sensitivity to Geophysical and Astronomical Effects," in *The Deep Space Network*, Space Programs Summary 37-62, Vol. II, pp. 49–55. Jet Propulsion Laboratory, Pasadena, Calif., Mar. 31, 1970.

3. Hamilton, T. W., and Melbourne, W. G., "Information Content of a Single Pass of Doppler Data from a Distant Spacecraft," in *The Deep Space Network*, Space Programs Summary 37-39, Vol. III, pp. 18–23. Jet Propulsion Laboratory, Pasadena, Calif., May 31, 1966.

4. Levine, M. W., and Vessof, R. F., "Hydrogen-Maser Time and Frequency Standard at Agassiz Observatory," *Radio Science*, Vol. 5, No. 10, pp. 1287–1292, Oct. 1970.

5. Mulhall, B. D., et al., *Tracking System Analytic Calibration Activities for the Mariner Mars 1969 Mission*, Technical Report 32-1499. Jet Propulsion Laboratory, Pasadena, Calif., Nov. 15, 1970.

6. Ondrasik, V. J., Mulhall, B. D., and Mottinger, N. A., "A Cursory Examination of the Effect of Space Plasma on *Mariner V* and *Pioneer IX* Navigation With Implications for *Mariner* Mars 1971 TSAC," in *The Deep Space Network*, Space Programs Summary 37-60, Vol. II, pp. 89–94. Jet Propulsion Laboratory, Pasadena, Calif., Nov. 30, 1969.

7. Ondrasik, V. J., and Thuleen, K. L., "Variations in the Zenith Tropospheric Range Effect Computed From Radiosonde Balloon Data," in *The Deep Space Network*, Space Programs Summary 37-65, Vol. II, pp. 25–35. Jet Propulsion Laboratory, Pasadena, Calif., Sept. 30, 1970.

8. Miller, L. F., Ondrasik, V. J., and Chao, C. C., "A Cursory Examination of the Sensitivity of the Tropospheric Range and Doppler Effects to the Shape of the Refractivity Profile," in *The Deep Space Network Progress Report*, Technical Report 32-1526, Vol. I, pp. 22–30. Jet Propulsion Laboratory, Pasadena, Calif., Feb. 15, 1971.

9. Hamilton, T. W., *Error Sources for VLBI-Like Spacecraft Measurements*, IOM 71-37 (JPL internal document).

Table 1. Differenced tracking data parameters for principal DSN station pairs

Station pair	Baseline length D, km	Baseline z height z_B, km	Equatorial projection length r_B, km	Overlap, deg	
				$\delta = 23.5°$	$\delta = -23.5°$
DSSs 14–42 (Goldstone–Canberra)	10590	7350	7630	85.9	85.9
DSSs 14–61 (Goldstone–Madrid)	8390	441	8380	106.8	27.9
DSSs 14–51 (Goldstone–Johannesburg)	12260	6440	10430	35.4	35.4
DSSs 42–51 (Canberra–Johannesburg)	9589	906	9546	28.7	88.7
DSSs 42–61 (Canberra–Madrid)	12515	7790	9795	26.8	26.8
DSSs 51–61 (Johannesburg–Madrid)	7524	6884	3038	148.1	148.1

Table 2. Differenced range measurement errors

Error source	Present capability, m		Present configuration	Projected capability, m				Projected configuration
				Upper value		Lower value		
	Simultaneous	Near simultaneous		Simultaneous	Near simultaneous	Simultaneous	Near simultaneous	
Charged particles	1[a,b]	1	Faraday rotation	0.1	0.5			S-X down link, 1976
Troposphere	1[a,c,d]	1	Constant model	0.5	0.5			Historical data improved mapping, 1973
Signal arrival time/ground delay	10[e]	10[e]	*Mariner* Mars 1971 planetary systems	10	10	1	1	
Clock sync	1000[e]	1	3 μs	1	1			Star source VLBI, 1976
Clock rate at 1 AU	3[f]	3	Rb standard $\sim 10^{-11}$	0.3	0.3			H standard, 1973
Transponder delay instability	0.1	1	*Mariner* Mars 1971	0.1	1			

[a]Reference 5.
[b]Reference 6.
[c]Reference 7.
[d]Reference 8.
[e]Reference 9.
[f]Reference 4.

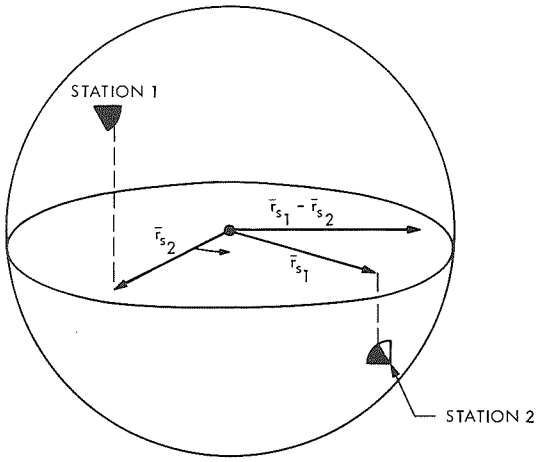

Fig. 1. Differenced data geometry

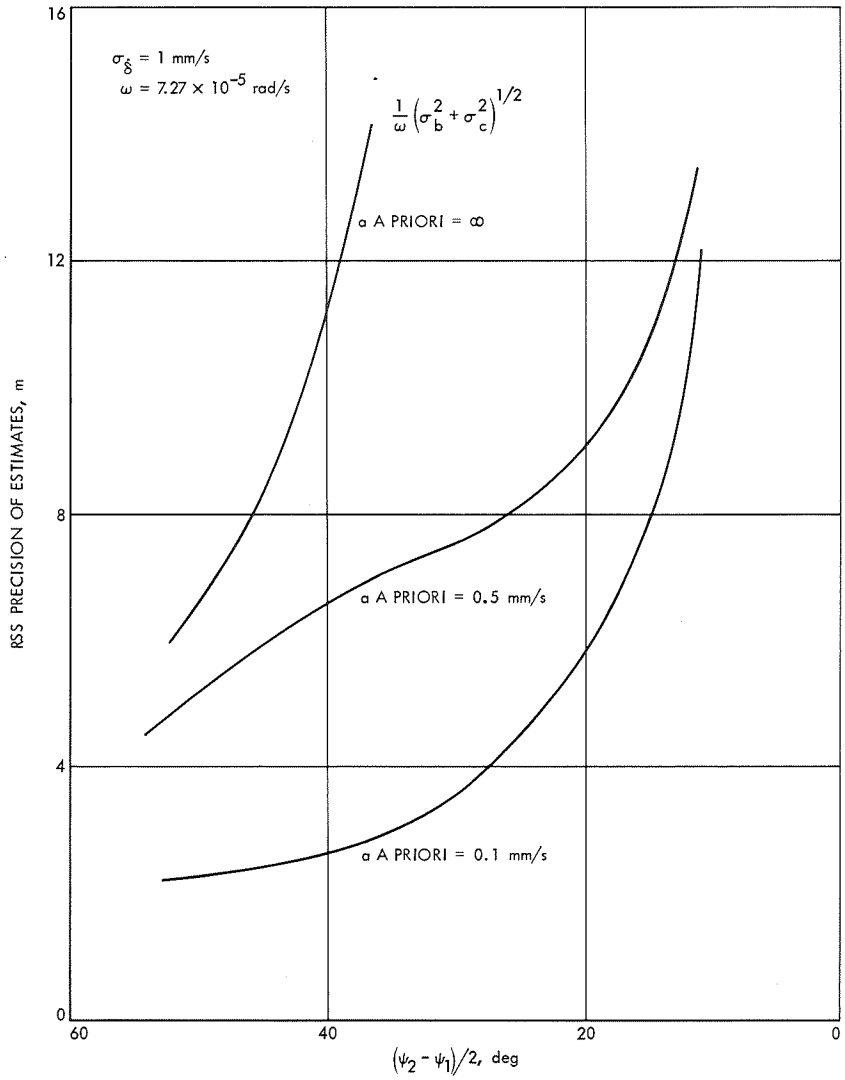

Fig. 2. Precision of *b* and *c* parameters as a function of overlap halfwidth and *a a priori*

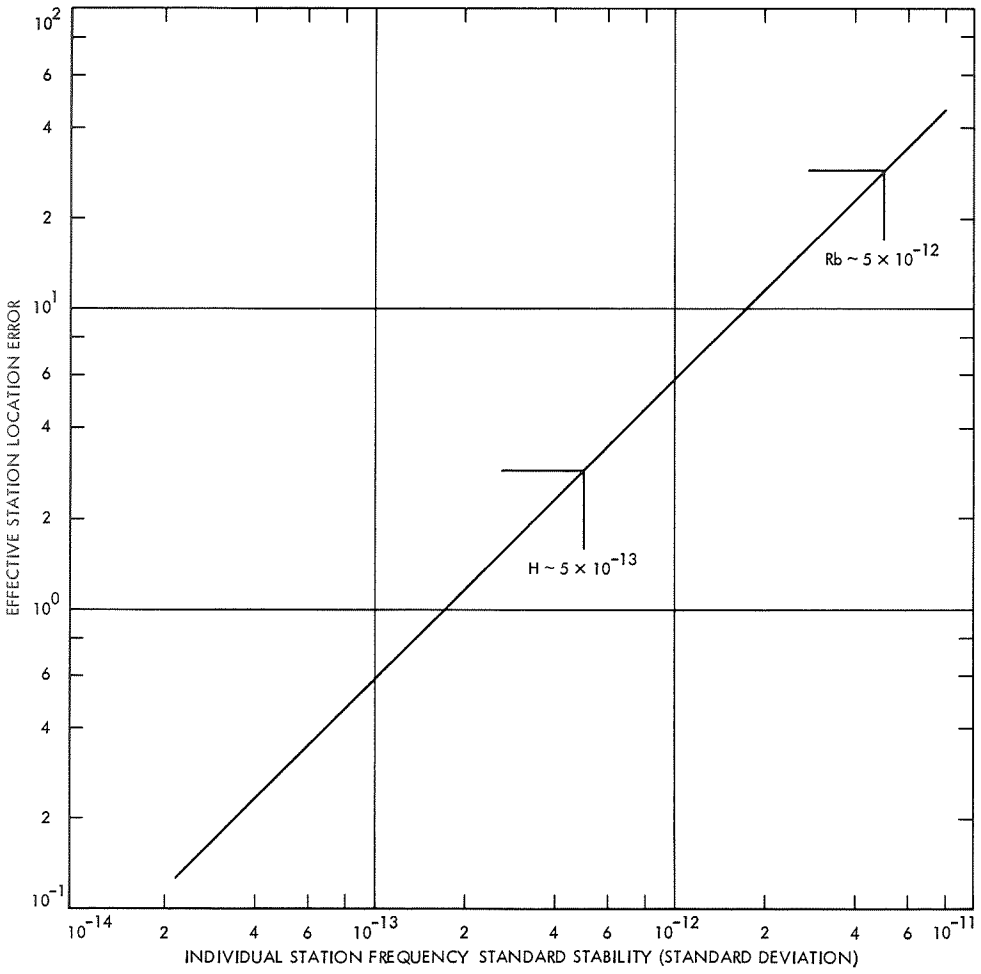

Fig. 3. Effective station location error due to worst case frequency standard drift

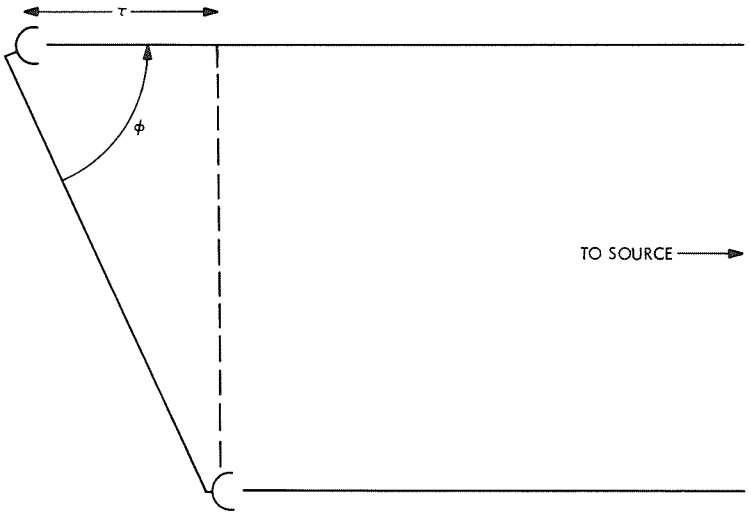

Fig. 4. Signal time delay

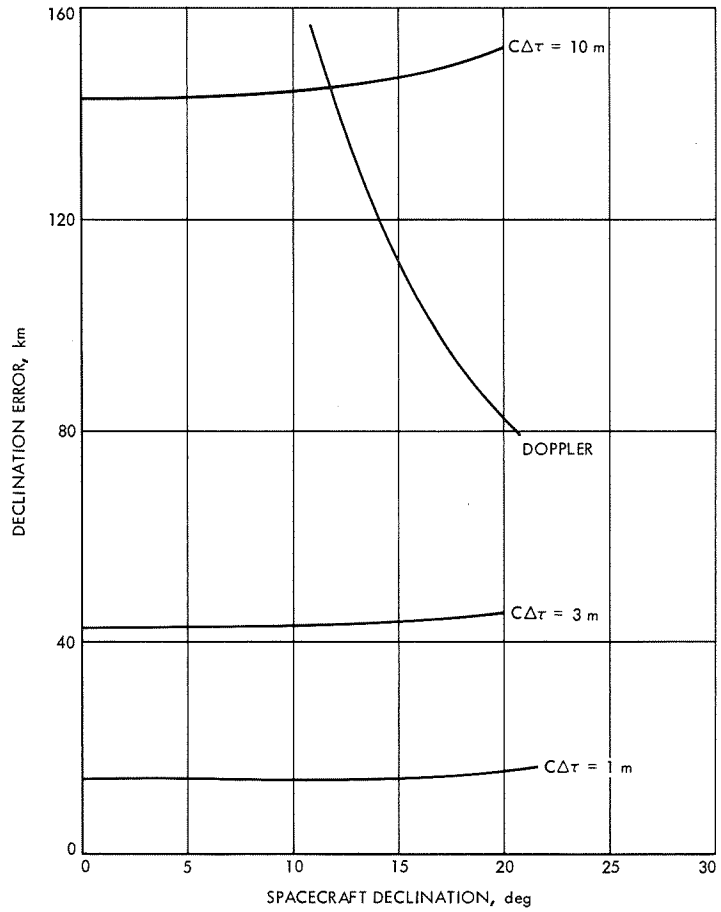

Fig. 5. Doppler and differenced range declination determination error

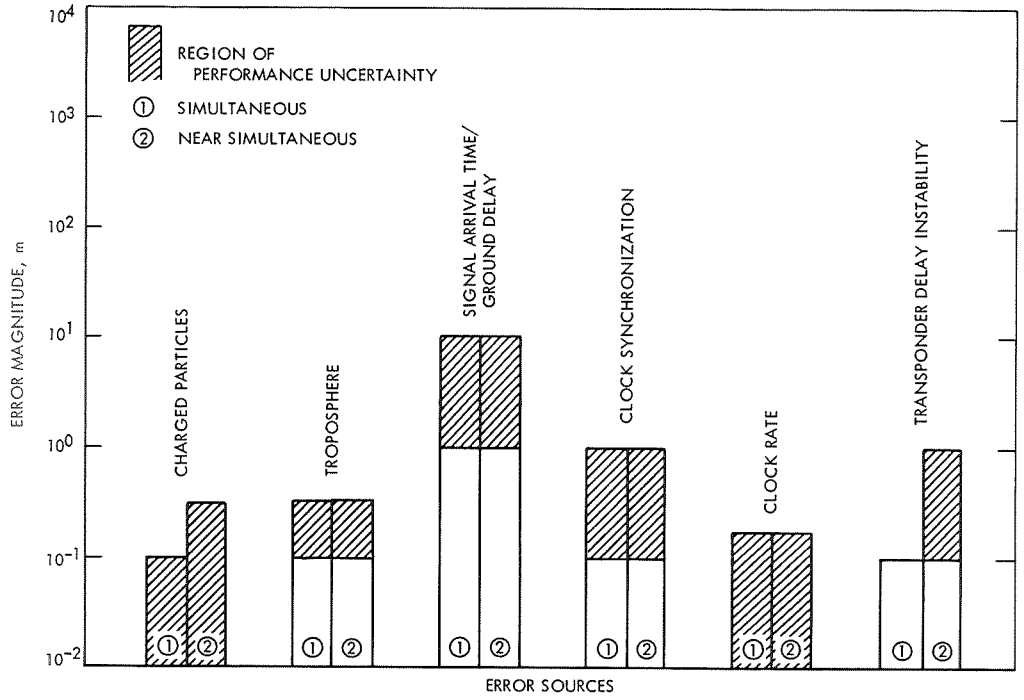

Fig. 6. Future configuration differenced range error sources

An Analytical Study of the Advantages Which Differenced Tracking Data May Offer for Ameliorating the Effects of Unknown Spacecraft Accelerations

V. J. Ondrasik and K. H. Rourke
Tracking and Orbit Determination Section

Using the six parameter representation of the range-rate observable, arguments are presented to show why differenced data may more effectively diminish the effects of unmodelable spacecraft accelerations than the conventional tracking data. For a Viking spacecraft experiencing unknown constant accelerations, the orbit determination solution using differenced data may be two orders of magnitude better than the solution obtained from conventional tracking data.

I. Introduction

In the previous article,[1] some preliminary analysis was performed to examine the advantages of using data taken simultaneously, or nearly simultaneously, from two widely separated tracking stations. In particular, it was shown that the deleterious effect of unmodeled accelerations on the estimate of the spacecraft state may be substantially reduced by differencing the data obtained in this manner. To further illustrate the reasons why differenced data may be superior to conventional data, and, in addition, to obtain some idea of the degree of this superiority, conventional and differenced data were separately used to compute estimates of the position and velocity of a *Viking* spacecraft subject to unmodeled constant accelerations. Since the primary purpose of undertaking this investigation is to gain an increased understanding of the orbit determination process, the range rate observable will be represented by an analytical model involving six parameters.

II. The Six Parameter Model

As explained in Ref. 1, this six parameter model is developed by first expanding the range-rate observable, in terms of the ratio between the geocentric distances of the observing station and spacecraft, to obtain the following equation:

$$\dot{\rho} = \dot{r} - z_s \dot{\delta} \cos\delta + r_s (\dot{\phi} - \dot{\alpha}) \cos\delta (\phi - \alpha) + r_s \dot{\delta} \sin\delta \cos(\phi - \alpha) \quad (1)$$

where

r = spacecraft geocentric range

δ = spacecraft declination

[1]Rourke, K. H., and Ondrasik, V. J., "Application of Differenced Tracking Data Types to the Zero Declination and Process Noise Problem" (this volume).

α = spacecraft right ascension

r_s = station's distance off the Earth's spin axis

z_s = station's distance above the Earth's equator

ϕ = station's right ascension

$\dot{a} = \dfrac{da}{dt}$

The six parameter model results from assuming that the time-varying quantities involved in Eq. (1) may be represented by the following first-order expansions in time:

$$\begin{aligned}
\dot{r} &= \dot{r}_0 + \ddot{r}_0 t \\
\delta &= \delta_0 + \dot{\delta}_0 t \\
\alpha &= \alpha_0 + \dot{\alpha}_0 t \\
\dot{\delta} &= \dot{\delta}_0 + \ddot{\delta}_0 t \\
\dot{\alpha} &= \dot{\alpha}_0 + \ddot{\alpha}_0 t \\
\phi &= \phi_0 + \dot{\theta} t
\end{aligned} \tag{2}$$

where a_0 denotes that the quantity a is evaluated at $t = 0$. Substituting Eq. (2) into Eq. (1) yields

$$\begin{aligned}
\dot{\rho}(t) = {} & a + b \sin(\phi_0 - \alpha_0 + \dot{\theta} t) + c \cos(\phi_0 - \alpha_0 + \dot{\theta} t) \\
& + dt + et \sin(\phi_0 - \alpha_0 + \dot{\theta} t) \\
& + ft \cos(\phi_0 - \alpha_0 + \dot{\theta} t)
\end{aligned} \tag{3}$$

where

$$\begin{aligned}
a &= \dot{r}_0 - z_s \dot{\delta}_0 \cos\delta_0 \\
b &= r_s (\dot{\theta} - \dot{\alpha}_0) \cos\delta_0 \\
c &= r_s \dot{\delta}_0 \sin\delta_0 \\
d &= \ddot{r}_0 + z_s (\dot{\delta}_0^2 \sin\delta_0 - \ddot{\delta}_0 \cos\delta_0) \\
e &= r_s [-(\dot{\theta} - 2\dot{\alpha}_0) \dot{\delta}_0 \sin\delta_0 - \ddot{\alpha}_0 \sin\delta] \\
f &= r_s [-(\dot{\theta} - \dot{\alpha}_0) \dot{\alpha}_0 \cos\delta_0 + \dot{\delta}_0^2 \cos\delta_0 + \ddot{\delta}_0 \sin\delta_0] \\
\dot{\theta} &= 0.729 \times 10^{-4} \text{ rad/s}
\end{aligned} \tag{4}$$

Since $\ddot{r}_0$, $\ddot{\delta}_0$, and $\ddot{\alpha}_0$ are not independent of r_0, δ_0, α_0, $\dot{r}_0$, $\dot{\delta}_0$, and $\dot{\alpha}_0$, the expressions in Eq. (4) for the coefficients *a–f* are not suitable for analysis. However, as shown in Ref. 1, the relationships between these quantities may be found, and result in the following equations:

$$\begin{aligned}
a &= \dot{r}_0 - z_s (\dot{\delta}_0 \cos\delta_0) \\
b &= r_s (\dot{\theta}_0 - \dot{\alpha}_0) \cos\delta_0 \\
c &= r_s \dot{\delta}_0 \sin\delta_0 \\
d &= \ddot{r}_{g0} + r_0 (\dot{\delta}_0^2 + \dot{\alpha}_0^2 \cos^2\delta_0) \\
&\quad + z_s \left(\dot{\delta}_0^2 \sin\delta_0 + \dot{\alpha}_0^2 \cos^2\delta_0 \sin\delta_0 \right. \\
&\quad \left. + 2 \frac{\dot{r}_0}{r_0} \cos\delta_0 - \ddot{\delta}_{g0} \cos\delta_0 \right) \\
e &= r_s \left(- \dot{\theta}_0 \dot{\delta}_0 \sin\delta_0 + 2 \frac{\dot{r}_0}{r_0} \dot{\alpha}_0 \cos\delta_0 - \ddot{\alpha}_{g0} \right) \\
f &= r_s \left(- \dot{\theta}_0 \dot{\alpha}_0 \cos\delta_0 + \dot{\alpha}_0^2 \cos^3\delta_0 + \dot{\delta}_0^2 \cos\delta_0 \right. \\
&\quad \left. - 2 \frac{\dot{r}_0}{r_0} \dot{\delta}_0 \sin\delta_0 + \ddot{\delta}_{g0} \sin\delta_0 \right) \\
\ddot{r}_g &= - \mu \left[\frac{r}{r_p^3} - r_e \left(\frac{1}{r_p^3} - \frac{1}{r_e^3} \right) \right. \\
&\quad \left. \times < \cos\delta \cos\delta_s \cos(\alpha - \alpha_s) + \sin\delta \sin\delta_s > \right] \\
\ddot{\delta}_g &= - \mu \frac{r_e}{r} \left(\frac{1}{r_p^3} - \frac{1}{r_e^3} \right) \\
&\quad \times < \sin\delta \cos\delta_s \cos(\alpha - \alpha_s) - \cos\delta \sin\delta_s > \\
\ddot{\alpha}_g &= - \mu \frac{r_e}{r} \left(\frac{1}{r_p^3} - \frac{1}{r_e^3} \right) \cos\delta \sin(\alpha - \alpha_s) \\
r_p &= \{ r^2 + r_e^2 - 2 r r_e [\cos\delta \cos\delta_s \cos(\alpha - \alpha_s) \\
&\quad + \sin\delta \sin\delta_s] \}^{1/2} \\
r_e &= \text{distance from Earth to Sun} \\
\delta_s &= \text{declination of the Sun} \\
\alpha_s &= \text{right ascension of the Sun} \\
\mu &= \text{gravitational constant of the Sun}
\end{aligned} \tag{5}$$

Any error analysis based upon this model proceeds by treating the coefficients *a–f* as data points which describe the range-rate observable. However, these "data" points are not independent, and in fact may be highly correlated. The correlations and appropriate weights associated with these coefficients may be expressed by the following information matrix:

$$J_a = \frac{N}{\sigma_{\dot\rho}^2}\frac{1}{\int_\rho d\psi}\begin{bmatrix} \int_\rho d\psi & \int_\rho \sin\psi\, d\psi & \int_\rho \cos\psi\, d\psi & \int_\rho \psi\, d\psi & \int_\rho \psi \sin\psi\, d\psi & \int_\rho \psi\cos\psi\, d\psi \\ & \int_\rho \sin^2\psi\, d\psi & \int_\rho \sin\psi\cos\psi\, d\psi & \int_\rho \psi\sin\psi\, d\psi & \int_\rho \psi\sin^2\psi\, d\psi & \int_\rho \psi\sin\psi\cos\psi\, d\psi \\ & & \int_\rho \cos^2\psi\, d\psi & \int_\rho \psi\cos\psi\, d\psi & \int_\rho \psi\sin\psi\cos\psi\, d\psi & \int_\rho \psi\cos^2\psi\, d\psi \\ & & & \int_\rho \psi^2\, d\psi & \int_\rho \psi^2\sin\psi\, d\psi & \int_\rho \psi^2\cos\psi\, d\psi \\ & & & & \int_\rho \psi^2\sin^{-2}\psi\, d\psi & \int_\rho \psi^2\sin\psi\cos\psi\, d\psi \\ & & & & & \int_\rho \psi^2\cos^2\psi\, d\psi \end{bmatrix} \tag{6}$$

where

$\psi = \dot\theta t$

$\sigma_{\dot\rho}^2$ = variance of the white noise associated with the range-rate measurements

N = number of range-rate data points

$\int_\rho$ indicates that the integral extends over the full tracking interval, but has a non-zero contribution only when data is being taken

In using the six coefficients *a–f* as data points, the estimation filter accepts residuals in *a–f*, which have been generated in some manner, and modifies the six elements of the spacecraft state such that the residuals in $\dot\rho(t)$ are minimized. If the residuals in *a–f* are generated by an error source (e.g., unmodeled non-gravitational accelerations), there will be a resulting error in the spacecraft state. Using the classical least-squares technique, this solution procedure may be written as

$$\Delta\mathbf{x}_{\dot\rho}^{\bullet} = \Lambda_{\dot\rho}^{\bullet} A^T J_a \Delta\mathbf{a} \tag{7}$$

where

$\Delta\mathbf{x}_{\dot\rho}^{\bullet}$ = solution vector for the spacecraft state resulting from the use of range-rate data only

$\Delta\mathbf{a}$ = a vector representing changes in the coefficients *a–f* which have been generated in some manner

$\Lambda_{\dot\rho}^{\bullet} = (A^T J_a A)^{-1}$ = state covariance resulting from the use of range-rate data only

$$A = \frac{\partial(a,b,c,d,e,f)}{\partial(r_0, \delta_0, \alpha_0, \dot r_0, \dot\delta_0, \dot\alpha_0)} \tag{8}$$

The effect of including range data in the solution may be represented by supplying *a priori* information to the information matrix as shown below:

$$\Delta\mathbf{x}_r = \Lambda_r A^T J_a \Delta\mathbf{a} \tag{9}$$

where

$\Delta\mathbf{x}_r$ = solution vector for the spacecraft state resulting from the use of range rate and range data

$$\Lambda_r = [A^T J_a A + J_r(\text{ap})]^{-1}$$

$$J_r(\text{ap}) = \begin{bmatrix} \sigma_r^2(\text{ap}) & 0 \\ 0 & 0 \end{bmatrix}$$

$\sigma_r(\text{ap})$ = *a priori* standard deviation of the geocentric range

(10)

III. Specification of Tracking Patterns and Trajectory Information

The possible advantages inherent in the differenced range-rate data will be illustrated by comparing (1) the covariances, and (2) the solution error produced by constant unknown accelerations, when these quantities are computed separately, using the differenced data and the conventional range-rate data. The particular example that will be chosen involves the *Viking* trajectory described in Table 1 and the use of tracking patterns shown in Fig. 1. These tracking passes are essentially horizon to horizon and since the epoch has been chosen to occur at the meridian crossing of DSS 14, only the DSS 14 tracking pattern will be symmetric.

The standard deviation of the coefficients *a–f*, for data arcs containing pass 1, passes 1–3, passes 1–5, and passes 1–7 of Fig. 1 are easily calculated from Eq. (7) and are shown in Fig. 2. In this figure the standard deviations resulting from the symmetric passes of DSS 14 are labeled with (SYM) and those resulting from the non-symmetric passes which will be used for the differenced data are labeled by (NON-SYM). It should be noted that when more than one pass of data is used the standard deviations resulting from the symmetric passes (which will be used with the conventional data) are approximately an order of magnitude lower than those resulting from the use of non-symmetric passes (which will be used with the differenced data).

IV. Spacecraft State Standard Deviations and Errors Resulting From the Use of Conventional Data

If the components of the unknown, constant, non-gravitational acceleration are expressed in the r_0, δ_0, α_0 coordinate system, it is easily seen from Eq. (4) that these accelerations produce errors in the coefficients describing the conventional range rate of an amount given below:

$$\Delta a = 0$$

$$\Delta b = 0$$

$$\Delta c = 0$$

$$\Delta d = \Delta\ddot{k}_r - \frac{\tilde{z}_s}{r}\cos\delta_0\,\Delta\ddot{k}_\delta$$

$$\Delta e = -\frac{r_s}{r}\cos\delta_0\,\Delta\ddot{k}_\alpha$$

$$\Delta f = \frac{r_s}{r}\sin\delta_0\,\Delta\ddot{k}_\delta \qquad (11)$$

where

$\Delta\ddot{k}_{r,\,\delta,\,\alpha}$ = components of the unknown, constant, non-gravitational accelerations

The errors in the coefficients, *a–f*, produced by a constant non-gravitational acceleration of amount 10^{-12} km/s^2 in all three components are shown in Table 2.

The errors in the estimate of the spacecraft state and the associated computed standard deviations may now be obtained by using Eqs. (7) and (8) for conventional range-rate data only and by using Eqs. (9) and (10) for the conventional range-rate data supplemented by a range point. The results are shown in Figs. 3 and 4, where the quantities resulting from the use of conventional range-rate data only and conventional range-rate data plus a range point are labeled by $(\dot{\rho})$ and $(\dot{\rho}, r_0)$, respectively. To avoid numerical difficulties the solutions involving range data were performed by starting with the *a priori* information listed in Table 3.

One of the most notable features of Fig. 3 is that the errors generated by the range-rate data only solutions are constant, while the errors generated by the range-rate data supplemented by a range point depend upon the data arc. The doppler only solutions are constant because the six data points and six solve-for parameters are related in such a manner that allows the residuals to be reduced to zero. However, when the range is deleted from the solution, there are only five solve-for parameters and the residuals cannot be set to zero, only minimized. This minimization is dependent upon the correlations, which are a function of time, and hence the solution will be a function of time. A further examination of Fig. 3 shows that an unknown acceleration will produce errors primarily in the range estimate, if range-rate data only is used and in the estimates of the declination and right ascension rates if a range measurement is also used. These results may be easily explained. From Eq. (10) it is apparent that unknown accelerations in the radial direction are about four orders of magnitude more important than accelerations perpendicular to the radial direction. The solution filter will account for this spurious radial acceleration by adjusting the gravitational, and centrifugal accelerations. Since the range enters most strongly into the range-rate observable through the gravitational acceleration, if it is available for estimation, almost all of the error will emerge in this quantity. A very good approximation to a range error produced by a constant acceleration may often be obtained by using the following equation:

$$\Delta r = \frac{\Delta\ddot{k}}{\partial\dot{d}/\partial r} \qquad (12)$$

where

$\Delta\ddot{k}$ = constant acceleration error

$\partial\dot{d}/\partial r \approx m/r_p^3(2 - 3\sin^2\psi) + (\dot{\alpha}^2\cos^2\delta + \dot{\delta}^2)$ (Ref. 1)

ψ = Earth–spacecraft–Sun angle

For the example under consideration, Eq. (12) gives an approximation to the range error of 50.8 km, which is very close to the result shown in Fig. 3. If the range has been essentially deleted from the solution by the *a priori* information, the radial acceleration will be absorbed in the

centrifugal acceleration term, because any change in the gravitational acceleration would now require changes in δ and α which are well determined by the b and c coefficients. An error in the centrifugal accelerations will manifest itself as errors in $\dot{\alpha}$ and $\dot{\delta}$. Simple equations for $\Delta\dot{\alpha}$ and $\Delta\dot{\delta}$ comparable to the Δr equation above cannot be written down because $\dot{\delta}$ and $\dot{\alpha}$ are also strongly involved in the e and f coefficients. Although the errors in the δ and α directions are less than a kilometer, they are included because the results scale directly with the magnitude of the accelerations and for those typical of solar electric spacecraft the errors could be three orders of magnitude larger than those shown in Fig. 3.

V. The Six Parameter Model for Differenced Data

The six parameter model representing the differenced range-rate data may be obtained by first using Eq. (3) to express separately the topocentric range rate from two stations as shown below:

$$\dot{\rho}_1(t) = a_1 + b_1 \sin(\dot{\theta}t) + c_1 \cos(\dot{\theta}t) + d_1 t + e_1 t \sin(\dot{\theta}t) + f_1 t \cos(\dot{\theta}t)$$

$$\dot{\rho}_2(t) = a_2 + b_2 \sin(\lambda_{21} + \dot{\theta}t) + c_2 \cos(\lambda_{21} + \dot{\theta}t) + d_2 t + e_2 t \sin(\lambda_2 + \dot{\theta}t) + f_2 t \cos(\lambda_{21} + \dot{\theta}t)$$

where

$$\lambda_{21} = \lambda_2 - \lambda_1$$

$t = 0$ occurs at meridian crossing of station 1

Clearly the differenced range rate, $\nabla\dot{\rho}$, may be represented by the difference between these two equations as shown below:

$$\nabla\dot{\rho} = a_d + b_d \sin(\dot{\theta}t) + c_d \cos(\dot{\theta}t) + d_d t + e_d t \sin(\dot{\theta}t) + f_d t \cos(\dot{\theta}t) \quad (13)$$

where

$$a_d = -(z_{s_1} - z_{s_2})\,\dot{\delta}\cos\delta$$

$$b_d = b_1 - (b_2 \cos\lambda_{21} - c_2 \sin\lambda_{21})$$

$$c_d = c_1 - (c_2 \cos\lambda_{21} + b_2 \sin\lambda_{21})$$

$$d_d = (z_s - z_{sz})(\dot{\delta}_0^2 \sin\delta_0 - \ddot{\delta}_0 \cos\delta_0)$$

$$= (z_s - z_{sz})\left(\dot{\delta}_0^2 \sin\delta_0 + \dot{\alpha}_0^2 \cos\delta_0 \sin\delta_0 + 2\frac{\dot{r}_0}{r_0}\dot{\delta}_0 \cos\delta_0 - \ddot{\delta}_{g0} \cos\delta_0\right)$$

$$e_d = e_1 - (e_2 \cos\lambda_{21} - f_2 \sin\lambda_{21})$$

$$f_d = f_1 - (f_2 \cos\lambda_{21} + e_2 \sin\lambda_{21}) \quad (14)$$

The a_d and d_d terms have been written explicitly to show that the geocentric range rate and accelerations have cancelled out and no longer appear in the coefficients. The covariance and solutions using differenced range-rate data only and differenced range-rate data supplemented by a range point may be obtained by using Eqs. (7)–(10) with the a–f coefficients replaced by the a_d–f_d coefficients of Eq. (14). As was pointed out in the previous article (Footnote 1), the differencing procedure introduces problems associated with the frequency standard. However, for the sake of clarity, these oscillator-induced problems will be ignored.

VI. Spacecraft State Variances and Errors Resulting From the Use of Differenced Data

The unknown constant non-gravitational accelerations of 10^{-12} km/s^2 considered previously will produce errors in the a_d–f_d coefficients of the amount shown in Table 2. It is readily apparent from this table that the error in d_d is now of the same size as the errors in the e_d and f_d coefficients.

The formal covariance, and errors in spacecraft state due to unknown constant accelerations, may now be computed for the data arcs shown in Fig. 1, and are illustrated in Figs. 3 and 4. In these figures, the quantities which result from the use of differenced range-rate data only are labeled by (DIFF $\dot{\rho}$) and those which result from the use of differenced range-rate supplemented by a range point are labeled by (DIFF $\dot{\rho}$, r_0). An examination of Fig. 3 shows that, as was the case for conventional data, the acceleration errors are absorbed by either the range or $\dot{\delta}$ and $\dot{\alpha}$.

VII. Comparison Between the Conventional and Differenced Data Results

To obtain a clear comparison between the spacecraft states standard deviations and errors generated by the two data types under consideration, each quantity in Fig. 3 or 4 computed from differenced data was divided by the same quantity computed from conventional data. The results of following this procedure for the standard deviations and errors computed from five passes are shown in Table 4.

Bearing in mind the assumptions upon which this analysis has been based, an examination of Table 4 and

Figs. 3 and 4 leads to the following tentative conclusions regarding the use of conventional and differenced range-rate data to obtain a spacecraft state solution in the presence of unknown constant accelerations:

(1) The differenced data cannot determine the range or range rate.

(2) The formal standard deviations for δ, α, $\dot{\delta}$, and $\dot{\alpha}$ are generally slightly better using the conventional data if more than one pass of data is used.

(3) For solutions involving range-rate data only, unknown constant accelerations produce errors in the spacecraft state which are generally about the same size, irrespective of whether conventional or differenced data is used.

(4) If a range point is included in the data set, errors in δ, α, $\dot{\delta}$, and $\dot{\alpha}$ produced by unknown constant accelerations of equal magnitude in three orthogonal directions, are at least 100 times smaller if differenced range-rate data is used rather than the conventional range-rate data.

The fact that the differenced data cannot estimate the geocentric range or range rate is not surprising because the portions of the range-rate observable which is most effective in determining these quantities have been intentionally eliminated in the differencing process. This is not a serious matter because the range and range rate can be determined from the conventional data.

The main advantage of differenced range-rate data over conventional range-rate data is that state estimates obtained from the differenced data are not degraded nearly as much by unmodeled radial accelerations as estimates obtained from conventional range-rate data as was mentioned above. It is this feature that raises the promise that using differenced doppler data may be at least a partial solution to the process noise problem.

Before leaving this section it should be mentioned once more that the analysis performed here is representative of a real physical situation only to the degree that the six parameter model is representative of the range-rate observable and that the unknown accelerations are constant.

VIII. Summary and Discussion

The purpose of the analysis carried out in the previous sections was motivated by the desire to increase our understanding of how the differencing techniques ameliorates the effect of unmodelable accelerations, and also to obtain some idea of how effective these techniques may be. By making use of the six parameter representation of the range-rate observable, it was shown, once again, that the unmodeled accelerations which severely degrade the solution are those occurring in the radial direction. It appears that the effect of these accelerations can be substantially reduced by differencing the data taken simultaneously from two tracking stations. For the *Viking* trajectory, which was used as an example, the unmodeled constant accelerations degraded the conventional data solution two orders of magnitude more than the differenced data solution.

Although the analysis presented in this article indicates that differenced data may be very useful in diminishing the effects of unmodelable accelerations, before any real confidence may be acquired in this technique it will be necessary to perform an uncompromised accuracy analysis study. Such a study is currently underway and will be reported on in the near future.

Reference

1. Ondrasik, V. J., and Curkendall, D. W., "A First-Order Theory for Use in Investigating the Information Content Contained in a Few Days of Radio Tracking Data," in *The Deep Space Network Progress Report*, Technical Report 32-1526, Vol. III, pp. 77–93. Jet Propulsion Laboratory, Pasadena, Calif., June 15, 1971.

Table 1. *Viking* trajectory information

Quantity	Value
r_0	0.8854×10^8 km
δ_0	20.31 deg
α_0	57.76 deg
$\dot{r}_0$	15.32 km/s
$\dot{\delta}_0$	0.2278×10^{-7} rad/s
$\dot{\alpha}_0$	0.8896×10^{-7} rad/s
t_0	1976 Jan 22 3^h 33^m meridian crossing at DSS 14

Table 2. Errors in *a–f* produced by a constant acceleration

Conventional coefficients	Error[a]	Differenced coefficients	Error[a]
a	0	a_d	0
b	0	b_d	0
c	0	c_d	0
d	9.9996×10^{-13}	d_d	-7.7869×10^{-17}
e	-5.5120×10^{-17}	e_d	-3.8737×10^{-17}
f	2.0400×10^{-17}	f_d	-3.3122×10^{-17}

[a]Produced by $\Delta\ddot{k}_{r,\delta,\alpha} = 10^{-12}$ km/s^2

Table 3. *A priori* information for the spacecraft state

Spacecraft coordinate	*A priori* value
r	10^{-3} km
δ	10^{-8} rad
α	10^{-8} rad
$\dot{r}$	10^{-2} km/s
$\dot{\delta}$	10^{-10} rad/s
$\dot{\alpha}$	10^{-10} rad/s

Table 4. Comparisons of standard deviations and errors obtained by using conventional and differenced range-rate data

Coordinate	σ (diff)/σ (conv)		Δ (diff)/Δ (conv)[a]	
	Range rate only	Range rate + range	Range rate only	Range rate + range
r	2.34×10^3	1	−0.942	—
δ	4.08	1.65	−3.79	0.0109
α	2.62	0.516	0.00196	0.00244
$\dot{r}$	2.12×10^7	6.07×10^5	4.76×10^6	9.23×10
$\dot{\delta}$	2.78×10	0.0713	0.0000345	0.00626
$\dot{\alpha}$	2.35	1.29	3.76	0.00400

[a]For unmodeled constant acceleration of 10^{-12} km/s^2.

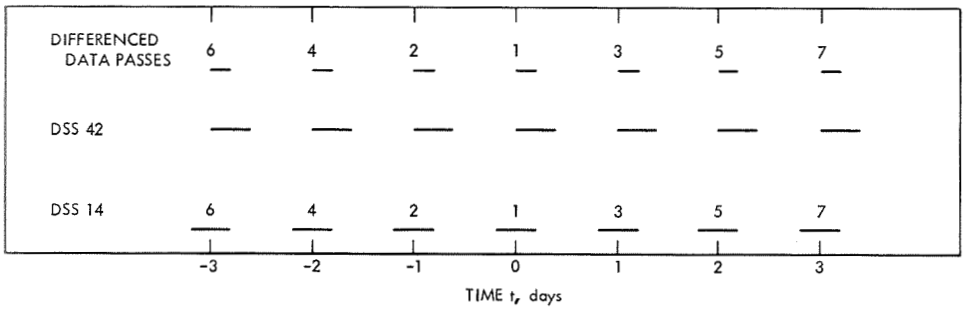

Fig. 1. Tracking patterns and pass numbers

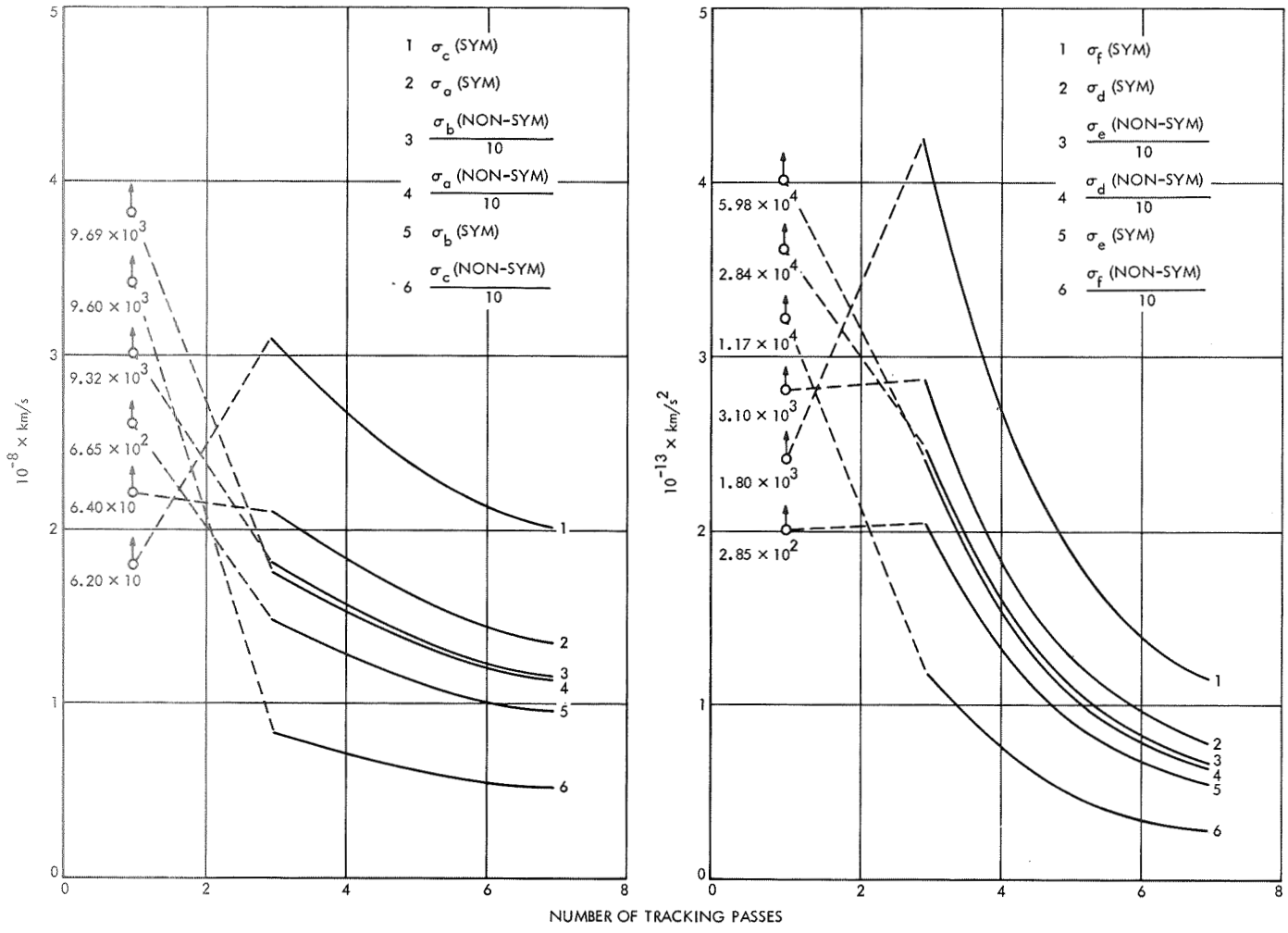

Fig. 2. Standard deviations of $a \rightarrow f$

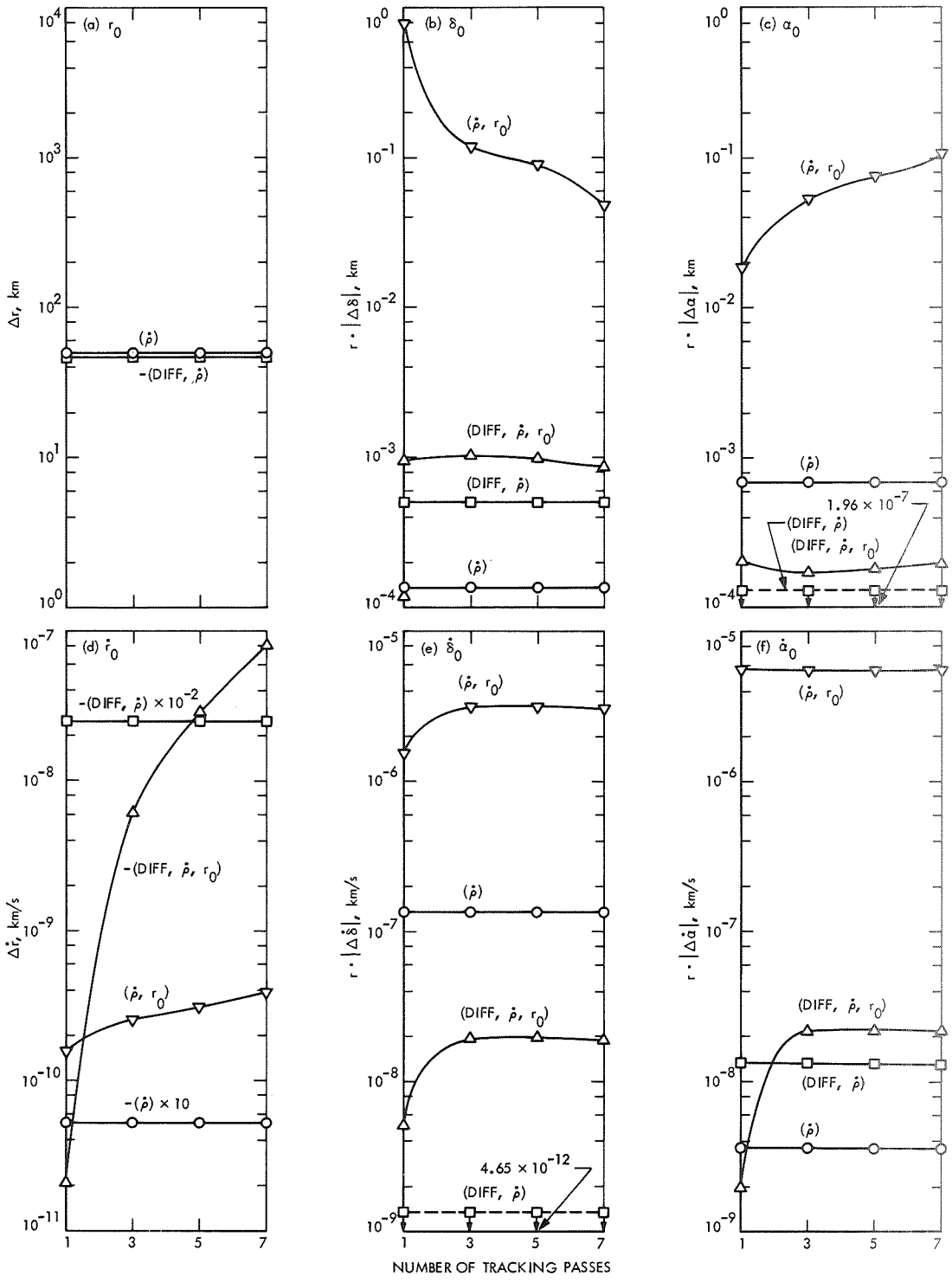

Fig. 3. Spacecraft state errors produced by unmodeled constant accelerations of 10^{-12} km/s^2 when conventional and differenced data are used

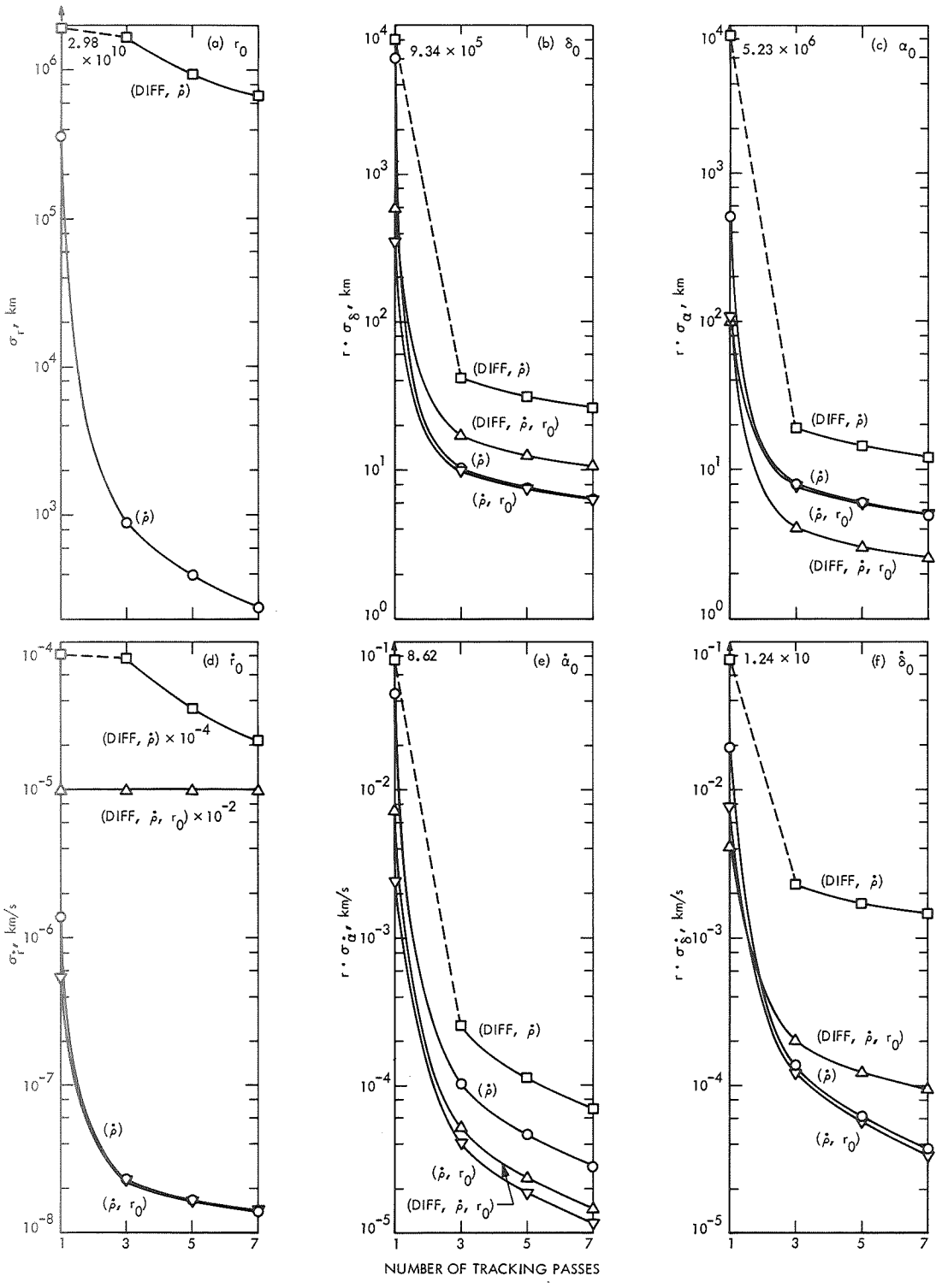

Fig. 4. Spacecraft state standard deviations and errors resulting from the use of conventional and differenced data

An Examination of the Effects of Station Longitude Errors on Doppler Plus Range and Doppler Only Orbit Determination Solutions With an Emphasis on a *Viking* Mission Trajectory

V. J. Ondrasik and N. A. Mottinger
Tracking and Orbit Determination Section

During the early Viking Mission accuracy analysis studies, it was discovered that station location errors may degrade the navigation more for doppler plus range solutions than for doppler only solutions. An explanation of this seemingly curious occurrence is given.

I. Introduction

Early in the *Viking* Mission accuracy analysis studies, a set of statistics describing the effect of station location errors on navigational accuracies were obtained which at first glance were hard to believe. These statistics, which were generated by a weighted least-squares batch solution filter operating on data supplied by the *Viking* trajectory and tracking station described in Table 1, are shown in Fig. 1 and involve the behavior of the semimajor axis (SMAA) of the error ellipse in the B-plane (described in Fig. 2) when various amounts of data were included in the solution. The standard deviation of SMAA given in Fig. 1 were computed by the Double Precision Orbit Determination Program (DPODP, Mod 5.2) consider option (Ref. 1). These consider standard deviations reflect the influence that both data noise and constant errors in particular parameters may have on the orbit determination solution.

The interesting feature of Fig. 1 is that, although initially the doppler plus range solution is superior to the doppler only solution, as more data is included the situation is reversed. This degradation of the solution by the addition of more information was very curious and required more of an explanation than just stating that it is a manifestation of an improperly modeled filter.

II. Verification of the DPODP Consider Option

When the results given in Fig. 1 were first acquired, one possible explanation was that the DPODP consider option was not working properly. A verification of the consider option for one parameter, p, may be obtained by first using the procedure outlined in Table 2 to determine the effect that a constant error in p may have on the solution.

Figure 3 contains errors in $\mathbf{B} \cdot \mathbf{R}$ obtained by following the above procedure for a station longitude error. The

longitude error was chosen for investigation because it is primarily responsible for the results shown in Fig. 1.

Also included in Fig. 3 are the computed standard deviations in $\mathbb{B} \cdot \mathbb{R}$ resulting from data noise alone, σ_d, and the consider standard deviation, σ_c, describing a station longitude error of 3 meters. If the consider option is working properly, the following equation will be satisfied:

$$\sigma_c^2 = \sigma_d^2 + [\Delta (\mathbf{B} \cdot \mathbf{R})]^2 \tag{1}$$

Substitution of the numbers contained in Fig. 3 into this equation did maintain the equality and it was therefore concluded that the consider option was working properly.

III. Spherical Spacecraft State Errors at Epoch

In order to explain the behavior of the standard deviation of the SMAA shown in Fig. 1, it is necessary to remove the effects of mapping nearly six months to encounter and examine the spacecraft state errors at epoch. Figure 4 contains the errors in the spacecraft state at epoch, in spherical coordinates, produced by a longitude error of 3 meters, when doppler only and doppler plus range data are included in the solution. It should be noted that the doppler only solutions may require a few days of data before stabilizing.

Starting with the results in Figs. 3 and 4, one may construct the following explanation of the results shown in Fig. 1:

(1) Initially the data noise is the dominant error source and the addition of range data reduces the effect of the data noise to such an extent that the doppler plus range solution is superior to the doppler only solution.

(2) As more data is included in the solution the effect of data noise is reduced and the station longitude error becomes the dominant error source.

(3) The station longitude error translates primarily into right ascension and range errors for doppler only solutions or right ascension, declination rate and right ascension rate errors for doppler plus range solutions.

(4) After a six-month mapping the velocity errors are magnified to such an extent that the doppler only solution will be superior to the doppler plus range solution.

IV. Analytical Explanation of Spacecraft Errors Produced by a Station Longitude Error

The problem has now been reduced from explaining the effects of station location errors at encounter to explaining these effects at epoch. To obtain such an explanation, it is convenient to use an analytic model of the observable.

For data arcs of a few days the spacecraft state errors produced by a station longitude error can be grossly predicted by the 6 parameter model. This model is described in Ref. 2 and uses the following equation to represent the range-rate or doppler observables:

$$\dot{\rho} = a + b \sin \omega t + c \cos \omega t + dt + e\omega t \sin \omega t + f\omega t \cos \omega t \tag{2}$$

where

$a = \dot{r}_0$

$b = r_s \omega \cos \delta_0$

$c = b\epsilon$

$d = \ddot{r}_{g0} + r_0 (\dot{\delta}_0^2 + \dot{\alpha}_0^2 \cos^2 \delta_0)$

$e = -r_s (\dot{\delta}_0 \sin \delta_0 - \epsilon \dot{\alpha}_0 \cos \delta_0)$

$f = -r_s (\dot{\alpha}_0 \cos \delta_0 + \epsilon \dot{\delta}_0 \sin \delta_0)$

$\dot{\rho}$ = topocentric range rate

$$\ddot{r}_{g0} = -\mu \left\{ \frac{r_0}{r_{p0}^3} - r_e \left(\frac{1}{r_{p0}^3} - \frac{1}{r_{p0}^3} \right) \times [\cos \delta_0 \cos \delta_{s0} \cos (\alpha_0 - \alpha_{s0}) + \sin \delta_0 \sin \delta_{s0}] \right\}$$

= geocentric acceleration

$\epsilon = (\lambda - \lambda^*) - (\alpha - \alpha^*)$

μ = solar gravitational constant

r_e = Sun–Earth distance

$$r_p = \{r^2 + r_c^2 - 2r\, r_e [\cos \delta \cos \delta_s \times \cos (\alpha - \alpha_s) + \sin \delta \sin \delta_s]\}^{1/2}$$

= Sun spacecraft distance

δ_s = declination of the Sun

α_s = right ascension of the Sun

x^* = *a priori* value of x

$\dot{x} = \dfrac{dx}{dt}$

$x_0 = x(t = 0)$

t = time past meridian crossing

For the *Viking* trajectory of Table 2, this representation retains its usefulness for data arcs of a few days in length.

As briefly described in the previous article[1] and more fully in Ref. 2, an error analysis using Eq. (2) proceeds by using the 6 coefficients $a \rightarrow f$ as correlated data points which described the information contained in the range-rate observable. These data points may then be used to obtain solutions and the associated covariances. In particular, an error in the station longitude will produce errors in the c, e, and f coefficients, which will be treated as "before-the-fit" residuals. The solution filter will then generate compensating errors in the spacecraft state to minimize the "after-the-fit" residuals in a least-squares sense. The results of following this procedure are also included in Fig. 4 for data arcs of two and four days and are in fairly good agreement with the DPODP values.

The physical process behind the results illustrated in Fig. 4 may be understood by examining Eq. (2). As mentioned previously, a longitude error will produce errors in the c, e, and f coefficients. Since the longitude and right ascension enter into these coefficients in the same way, the solution filter will want to make a compensating error in the right ascension. However, this change in the right ascension will produce a change in the d, or acceleration coefficient of Eq. (2), since the gravitation acceleration is a function of the spacecraft right ascension. This change in d must be accounted for by errors in the remaining components of the spacecraft state. For a doppler only solution, the error will appear in the range because the range occurs only in the d coefficient and therefore a change in the range affects this coefficient only. The range error, which will compensate for the change in d produced by the right ascension error, is given by the following equation:

$$\Delta r = \frac{\partial d/\partial \alpha}{\partial d/\partial r}\,\Delta\lambda$$

$$= \frac{0.489 \times 10^{-5}}{0.204 \times 10^{-13}} \times 0.524 \times 10^{-6} = 126 \text{ km} \qquad (3)$$

Using the numerical values associated with the *Viking* trajectory of Table 1 yields the result shown in Eq. (3). This value is almost identical to the range error found by extrapolating the stable DPODP solutions of Fig. 4.

When the doppler data is supplemented by a range point, the range is essentially deleted from the solution and cannot be used to cancel the error in the acceleration coefficient produced by the right ascension error. Since the declination is strongly determined by the b coefficient, the acceleration coefficient error will be compensated for by errors in $\dot{\delta}$ and $\dot{\alpha}$. It is not possible to obtain a simple equation analogous to Eq. (3) to express these velocity errors because $\dot{\delta}$ and $\dot{\alpha}$ are also contained in the e and f coefficients.

V. Summary

The preceding section has shown that for fairly short data arcs a station longitude error will produce an error in the spacecraft's right ascension. This right ascension error will in turn generate an error in the spacecraft's geocentric acceleration. To minimize the effects of this acceleration error, compensating errors will be made in the range for doppler only solutions, and in $\dot{\delta}$ and $\dot{\alpha}$ for doppler plus range solutions. If these errors are mapped over a sufficiently long period of time, the velocity errors of the doppler plus range solution may assume a greater importance than the position errors of the doppler only solution. It is for this reason that station location errors may degrade doppler and range solutions more than doppler only solutions when an improperly modeled solution filter is used. This is the set of circumstances which lead to the seemingly strange *Viking* accuracy analysis results illustrated in Fig. 1.

[1]Ondrasik, V. J., and Rourke, K. H., "An Analytical Study of the Advantages Which Differenced Tracking Data May Offer for Ameliorating the Effects of Unknown Spacecraft Accelerations" (this volume).

References

1. Moyer, T. D., *Mathematical Formulation of the Double-Precision Orbit Determination Program (DPODP),* Technical Report 32-1527, pp. 109–117. Jet Propulsion Laboratory, Pasadena, Calif., May 15, 1971.

2. Ondrasik, V. J., and Curkendall, D. W., "A First-Order Theory for Use in Investigating the Information Content Contained in a Few Days of Radio Tracking Data," in *The Deep Space Network Progress Report,* Technical Report 32-1526, Vol. III, pp. 77–93. Jet Propulsion Laboratory, Pasadena, Calif., June 15, 1971.

Table 1. Description of the *Viking* trajectory

Geocentric coordinate[a]	Value
r = range	0.885×10^8 km
δ = declination	20.3 deg
α = right ascension	58.1 deg
$\dot{r}$ = range rate	15.3 km/s
$\dot{\delta}$ = declination rate	0.245×10^{-7} rad/s
$\dot{\alpha}$ = right ascension rate	0.890×10^{-7} rad/s
r_s = station distance off the spin axis	5.20×10^3 km
λ = station longitude	243 deg

[a]Epoch 1976 Jan 21.
Encounter 1976 July 14.

Table 2. Procedure for determining the errors in the solution produced by a constant error in a particular parameter

Step	Operation
1	Simulate the observed data using a particular value of the parameter, p_0.
2	Calculate the computed data using another value of the parameter, $p_c = p_0 + \Delta p$.
3	Form the (observed–computed) residuals.
4	Obtain the solution, with p not included in the solution set.

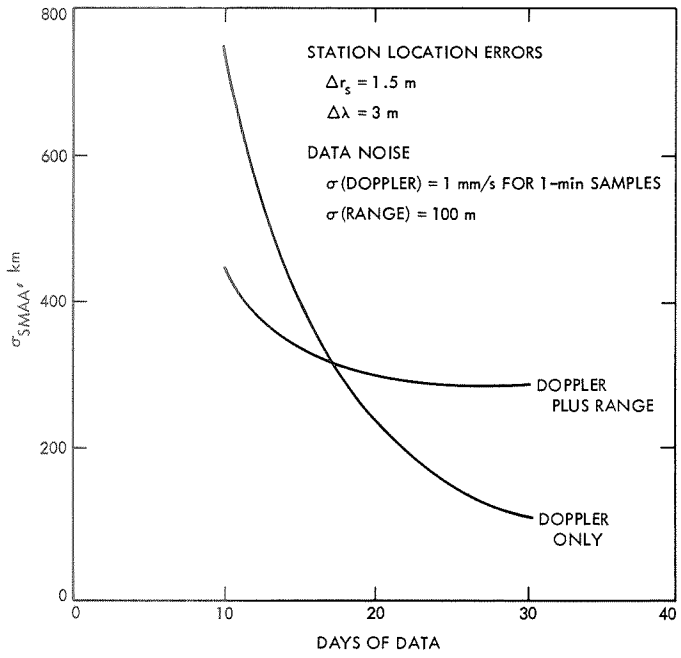

Fig. 1. Consider SMAA for doppler and doppler plus range solutions

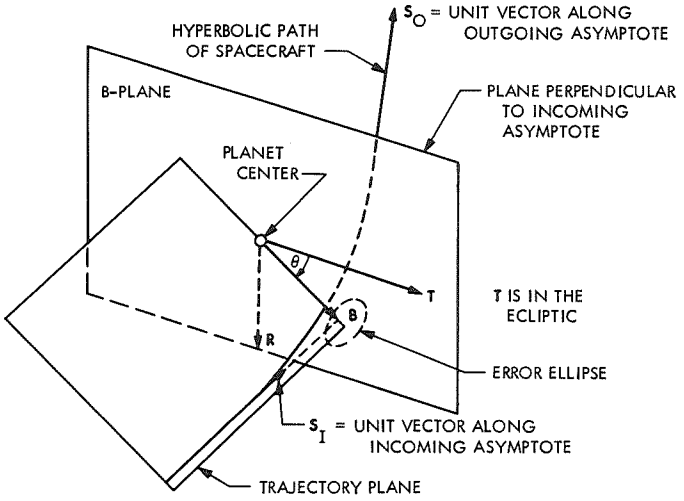

Fig. 2. B-plane and error ellipse

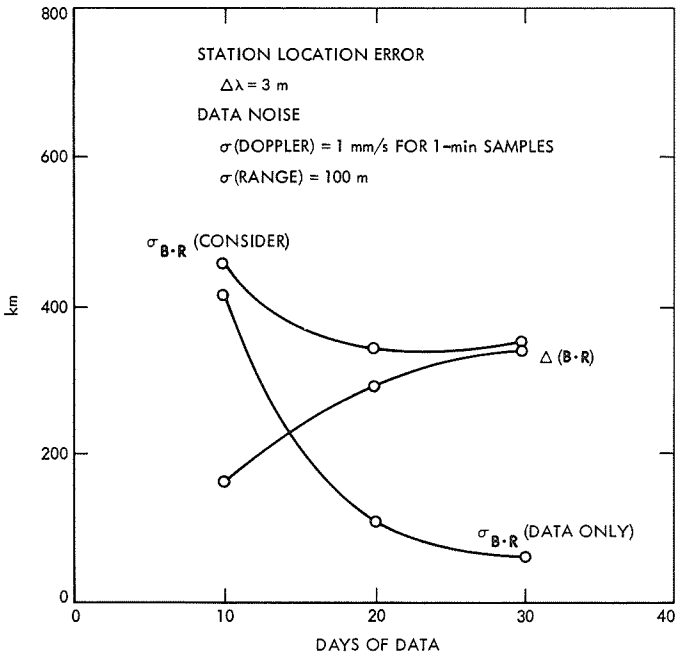

Fig. 3. Errors in B · R produced by a station longitude error of 3 meters

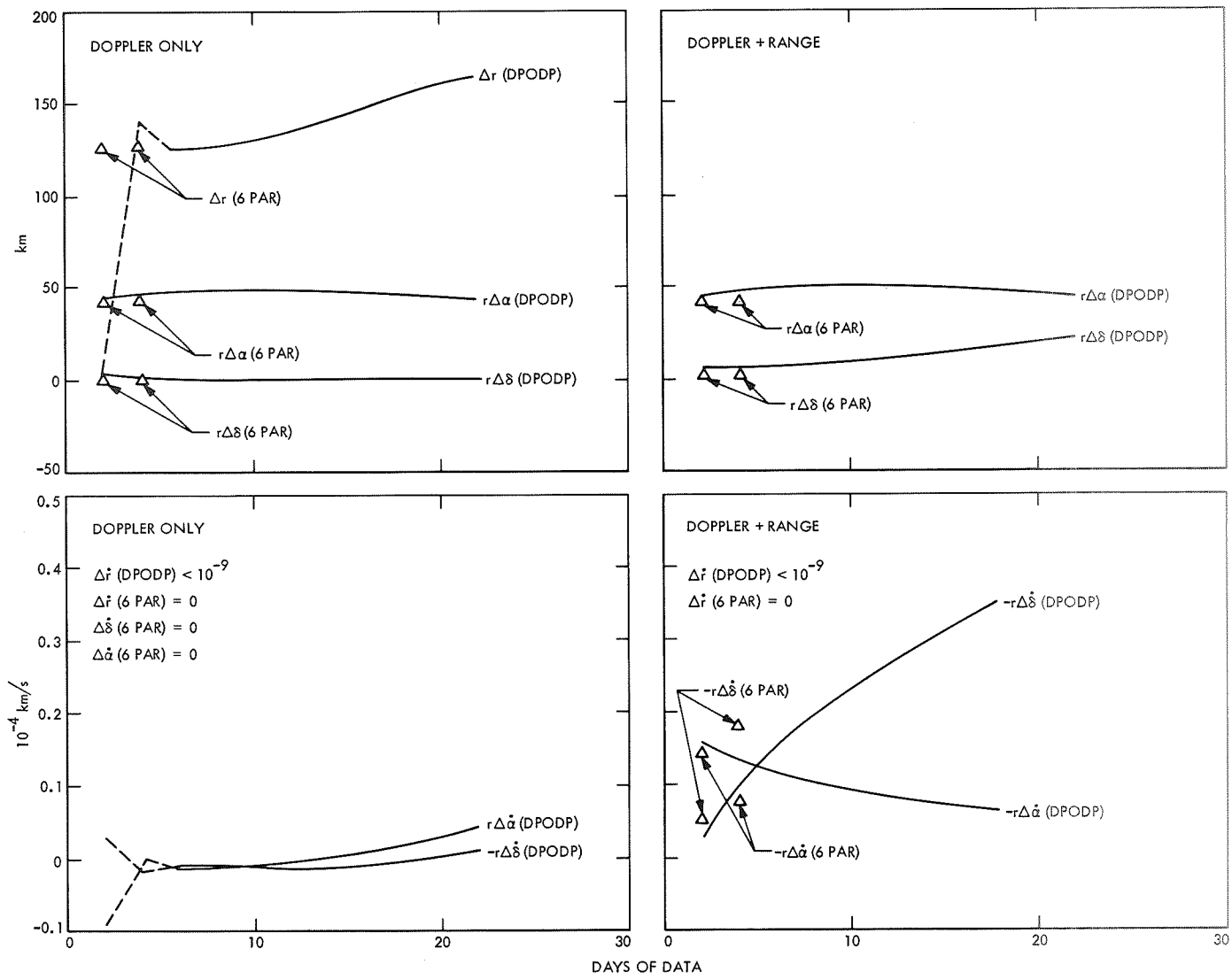

Fig. 4. Spherical spacecraft state errors produced by a station longitude error of 3 meters

Digital Period Detector Oscilloscope Trigger

W. A. Lushbaugh
Communications Systems Research Section

Due to the increased complexity of new digital equipment, there has arisen a need for more sophisticated test equipment. This article describes a piece of equipment for obtaining an optimum trigger for an oscilloscope. This equipment accepts a periodic digital sequence and its associated clock, and outputs a single pulse once per period. This output is intended to be used as the external trigger for an oscilloscope. A digital readout of the numerical value of the period is also provided to enable determination of the correct trigger to be used for a multitrace display.

I. Introduction

Due to the increased complexity of new digital equipment, there has arisen a need for more sophisticated test equipment. The digital period detector oscilloscope trigger (DIPDOT) is a piece of test equipment which accepts a periodic digital sequence and its associated clock, derives the period of this sequence, and outputs a single pulse once per period. A digital readout of the number of clock pulses in the period appears on the front panel. The output pulse is intended to be used as the external trigger input to an oscilloscope, thereby enabling the display of sequences for which no other sync is available and which will not self-trigger. The digital readout can be used to check that the external trigger being supplied to a multi-trace display has the correct period necessary to properly display all traces in their true phase relationship. Use of the DIPDOT to detect the period of the longest length sequence of a multi-trace display will also ensure the maximum brightness possible for such a display.

II. Design Aims

It was desired to have the DIPDOT use as little hardware as possible. Obviously an easy method of finding the period of a sequence is to store a number of bits of the sequence larger than the greatest expected period and do a simple correlation on these bits until the minimum period is found. However, since it was decided that the device would not be useful unless it could determine periods of at least several thousand bits, the mass memory approach was abandoned and a serial scheme adopted. The serial version uses a minimum of sequence memory (actually only one bit) but instead, observes the sequence over many of its periods to extract the necessary information.

III. The Algorithm

A sequence $f(n)$, $n = 1, 2, \cdots$, has period P if

$$f(n) = f(n + P)$$

for all n and P is the smallest such number for which this equation is satisfied. To ensure that the P found by the DIPDOT is indeed the smallest such value, the first hypothesis H is one, i.e., it is first assumed that all the

bits of the sequence are equal. This assumption is held and every bit of the sequence examined until a difference is observed. At this point the hypothesis is set to 2 and the sequence is searched for an adjacent 1–0 combination of bits.

After the 1–0 is found every (non-overlapping) pair of bits following is examined for agreement with 1–0. This mode of operation will continue until a disagreement is found, at which time H is set to 3, the device waits for an adjacent 1–0 and then checks every pair of bits spaced three units from the 1 for the 1–0 agreement. Iteration continues in this manner until an H is found such that a 1–0 combination is found M times spaced H apart, where M is the largest period expected. The search up to this point will be referred to as Mode I.

The 1–0 window was chosen because every sequence of period greater than 1 has such a combination and because many digital sequences encountered in practice have a low density of *ones* or *zeros* leading to a low number of transitions. Thus the DIPDOT locks onto a significant point in low density sequences (i.e., the probability of passing a large number of tests when H is not correct is low) while in more random sequences nothing is lost since all two-bit windows would have approximately the same density.

The job of finding the correct period is not completed when an M is found such that M consecutive tests show no errors. However it is certain that H and P, the actual period, have a common factor. Thus the H-2 bits between the 1–0 windows must be checked for agreement. This second part of the algorithm, which will be referred to as Mode II, uses a time-saving method developed by Dr. E. Rodemich and is described below:

IV. Rodemich Verification Method

THEOREM. *If a periodic sequence $f(n)$, $n = 1, 2, \cdots$, has period $P < M$ and it satisfies the following set of relations:*

$$f(kH + a_l) = f(a_l), \qquad 0 \leq k \leq \frac{M}{\ell} - 1$$
$$\ell = 1, 2, \cdots, H$$

with $a_1 = 0$ and

$$a_{l+1} = a_l + \left(\frac{M}{\ell} - 1\right) H + 1$$

then $P \mid H$.

Proof: If $P = ab$ and $H = ac$ with $(b, c) = 1$ notice that the relations

$$f(kH + a_l) = f(a_l), \qquad 0 \leq k \leq \frac{P}{a} - 1$$
$$1 \leq \ell \leq a$$

are included in the above.

Define $f_l(m) = f(am + a_l)$ and note that f_l has a period dividing b, i.e., $f_l(m + \lambda b) = f_l(m)$ now

$$f_l(kc) = f_l(0) \qquad 0 \leq k \leq \frac{P}{a} - 1 = b - 1$$

since

$$f_l(kc) = f(kca + a_l) = f(a_l) = f_l(0)$$

observe $\{kc\} \equiv \{0, 1, \cdots, b-1\} \mod b$ because if $k_1 \neq k_2$

$$k_1 c - k_2 c \neq \alpha b$$

because $(b, c) = 1$ and $|k_1 - k_2| < b$

$$\therefore f_l \text{ is constant for } 1 \leq \ell \leq a$$

By definition $a_l \equiv \ell - 1 \pmod{a}$ so that if $y \equiv z \pmod{a}$ any such y can be expressed as $y = y_1 a + a_l$ for some a_l and $z = z_1 a + a_l$

$$\therefore f(y) = f_l(y_1) = f_l(z_1) = f(z)$$

which means that the period of f divides a, i.e.,

$$P \mid A \Rightarrow b = 1 \Rightarrow P \mid H$$

V. Consequences of Theorem

The first set of tests for a given hypothesis H is given by

$$f(kH) = f(0) \qquad 0 \leq k \leq M - 1$$

which amounts to the Mode I algorithm described above. The Rodemich Theorem now says to move over 1 bit in the sequence, i.e., starting at $a_2 = (M-1)H + 1$ and verify that

$$f(kH + a_2) = f(a_2) \qquad 0 \leq k \leq \frac{M}{2} - 1$$

i.e., only do half as many tests as were done the first time. After this move over one bit and do $M/3$-1 tests,

then $M/4$-1 etc. Thus the total number of observed bits to verify that $P|H$ is

$$T = \sum_{\ell=1}^{H}\left(\frac{M-1}{\ell}\right)H + 1 \approx MH \ln H$$

But due to the way in which the hypotheses are formed, i.e., starting at $H = 1$ and incrementing by one each time any test fails, the first H found is actually P. Thus

$$T \approx MP \ln P$$

which is the lowest value found to date for this quantity.

VI. Calculation Time in Mode I

The calculation time for H to go from 1 to P in mode I can be significant. The time is not only a function of P but of the structure of the particular sequence. A lower bound for the length of time can be calculated for sequence with only one 1–0 transition. In this case all hypotheses except the correct one fail the first test in the series. Since the device then waits for the 1–0 transition (or P time units) to test the next hypothesis this minimum time is approximately $(P-1)^2$ units. Actually a pseudo-random sequence with a probability of 1/4 of finding a 1–0 window is slightly faster and has a Mode I computation time of approximately

$$T_{M_I}(Pn) \approx \sum_{n=1}^{P}\left[\left(\frac{4}{3}n + 4\right)\right]$$

$$= 4P + \frac{4}{3}\frac{P(P+1)}{2} = \frac{2P^2}{3} + 4\frac{2}{3}P$$

The worst-case sequence is not known, but the following example takes particularly long.

Consider the sequence

$$f(0) = f(2) = f(4) = \cdots = f(M-4) = 0$$
$$f(1) = f(3) = f(5) = \cdots = f(M-1) = 1$$

and $f(M-2) = 1$, i.e.,

n	0	1	2	3	4	5	$\cdots$	$(M-4)$	$(M-3)$	$(M-2)$	$(M-1)$
f_n	0	1	0	1	0	1	$\cdots$	0	1	1	1

Every even hypothesis for this sequence will look good and conceivably pass most of the series of tests. Thus the upper bound on the total acquisition time is given by

$$T_{MAX} \approx (M-1)\sum_{h=1}^{M/2}\sum_{\ell=1}^{h}\frac{2h}{\ell} \approx \frac{M^3}{4}\ln M$$

and for $M = 10^4$ as in the final design T_{MAX} could be on the order of 10^{12} clock periods of the sequence.

VII. Hardware

Figure 1 shows a block diagram of the DIPDOT. There is a hypothesis register and two countdown circuits which deliver pulses at a rate determined by the number held in the hypothesis register. Two countdown circuits were used so that one of them may be held fixed during Mode II to provide a useful sync to the scope earlier than if only one device were used. This second countdown circuit is not completely extraneous because it is the phase difference between its output and the output of the first countdown circuit that enables the $\div\ell$ feature of the Rodemich method. During Mode I, the two countdown networks are held in the same phase, and the $\div\ell$ flip-flop sets on CD1 = 1 and resets on CD2 = 0; i.e., one time unit later so that only one clock pulse gets to the M counter every H clock periods. In Mode II, which is entered when the M counter reaches full scale for the first time, one clock pulse is deleted from the CD1 circuit, and a new one-bit sample of the sequence is taken at this new phase. The $\div\ell$ flip-flop now is set for 2 clock pulses every H times, causing the M counter to count twice as fast as it did in Mode I. After $M/2$ observations have been made, the M counter reaches full-scale, causing CD1 to shift over another unit in the sequence, a new sample to be taken and the $\div\ell$ flip-flop to stay up three time periods every time CD2 reaches 1. In general then, M/ℓ samples are taken at the ℓth iteration, in accordance with the above theorem.

When the CD1 and CD2 outputs finally get back to their original phase, it means that all the prescribed tests are finished and that the hypothesis has been verified. The completion of this verification is communicated to the operator of the device by the shutting off of the decimal point in front of each digit of the digital readout.

A. Start Sequence

Since the DIPDOT never reduces the number in the hypothesis register, a start button is provided to restart the search. The start button produces the following sequence of events: all registers are reset to zero, then a single pulse is supplied to the hypothesis register to advance its count to 1, and sequence clock is supplied only to the M counter. The system then checks to see if

the sequence actually does have period 1, i.e., that all bits are equal. If two different bits are found (i.e., an adjacent 1–0 combination) the start sequence is over and operation, described in the foregoing as Mode I, starts. If the sequence does have all bits equal, this start mode will never be terminated, but after M consecutive equal bits have been observed, the decimal points on the display will go out, signifying that the period has been verified.

It should be noted at this point that the machine actually never stops checking the input sequence and that, if it has verified period 1 and at some later time the period changes, the device will automatically find the new period if it is less than M.

B. Return to Mode I

Actually many sequences can pass all the tests of Mode I with a wrong hypothesis. This results in the discovery of an error in Mode II which entails a slightly different sequence of events to occur than if this happened in Mode I. Actually it is very much like the start sequence in that all the registers except the hypothesis register have to be reset. This realigns the CD1 and CD2 circuits to their original phase and puts the system back into Mode I.

VIII. Improved Methods of Period Detection

It is obvious that the method used for period detection can be improved at the cost of system complexity. If each test, described above, tested N consecutive bits of the sequence, the search time in Mode I would obviously be less than at present (especially if the N-bits examined were constrained to have at least one 1–0 combination), and the time to verify (Mode II) the hypothesis would be divided by at least N. The major drawback to such a design is that all periods less than N would become special cases in the logic design of the device.

Other improvements can easily be thought of, e.g., checking the parity of the number of *ones* in the hypothesized period as well as looking at the bits every H time units. Every approach of this type examined to date seems only to enable some new sequence to be found that would cause the calculation time in Mode I to remain excessive.

IX. The Prime Method

A completely different approach to the problem would utilize a property of prime numbers. An easily proved theorem is the following:

THEOREM. *If M is a prime number $> P$ then the set*

$$\{kM\} \equiv \{0, 1, 2, \cdots, P-1\}$$

mod P, $k = 0, 1, 2, \cdots, P-1$.

Proof. Suppose $k_1 M \equiv k_2 M \bmod P$, i.e.,

$$k_1 M = \alpha_1 P + B_1$$
$$k_2 M = \alpha_2 P + B_1$$

then

$$P(\alpha_1 - \alpha_2) = M(k_1 - k_2)$$

and since $P \nmid M$ and $|k_1 - k_2| < P$, this implies

$$\alpha_1 = \alpha_2$$

This theorem implies that the set of equations

$$f(kM) = f(kM + H) \qquad k = 0, \cdots, M-1$$

reduce mod P for any $P < M$ to the set of relations

$$f(0) = f(H)$$
$$f(1) = f(H+1)$$
$$\vdots$$
$$f(H-1) = f(2H-1)$$

so that if H is the lowest number that satisfies this set of relations we have by definition $H = P$ for the sequence in question. This theorem implies that a period detector could be built that takes a new sample of an input sequence, e.g., every 10,007 (the smallest prime greater than 10^4) time units, verifies that $f(10{,}007 \cdot k) = f(10{,}0007 \cdot k + H)$ for $k = 1, 2, \cdots, 10{,}007$ and if all tests are satisfied, the period is verified. The time to verify a given hypothesis is seen to be approximately

$$T \cong M^2$$

which is independent of the period and a smaller time than the present design if $P > 1382$. For periods in the range of 10^4 the prime machine approaches 9.2 times (i.e., ln 10^4) the speed of the present design.

X. Conclusions

The DIPDOT was designed in support of the Viterbi Decoder project (Ref. 1) and was used extensively in the debugging stage of that project. Since the decoder uses 10-bit serial arithmetic, many small period data sequence inputs would lead to arithmetic register periods of 1024 nodes (10240 bits) or some multiple thereof. By looking at the sign bit of these circulating numbers (using a word marker as clock) the DIPDOT was able to obtain sync to display extremely long bit streams. At one point in the debugging, it appeared that the decoder had a hardware malfunction, but by obtaining the proper sync on a bit stream, it was found that an oversight in the design had permitted the machine, when first turned on, to enter and hang up in an undesired, incorrect mode of operation.

In summary, when a digital machine is misperforming, some part or parts of it are not operating with their designed periods, and a device such as the DIPDOT is essential in order to give a proper oscilloscope display of what is happening. Figures 2 and 3 are photographs of the DIPDOT assembly. Figure 2 is the original prototype which was later modified for box mounting with integral power supply.

Reference

1. Lushbaugh, W. A., "Information Systems: Hardware Version of an Optimal Convolutional Decoder," in *The Deep Space Network Progress Report*, Technical Report 32-1526, Vol. II, pp. 49–55. Jet Propulsion Laboratory, Pasadena, Calif., April 15, 1971.

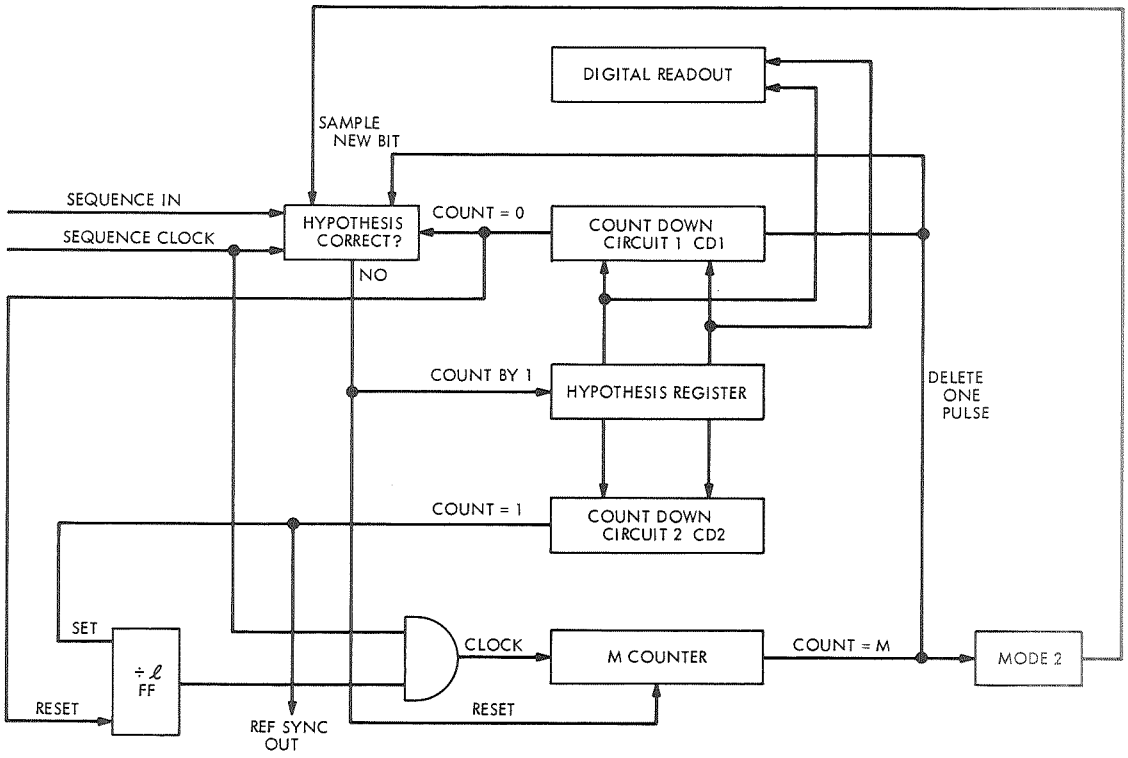

Fig. 1. DIPDOT block diagram

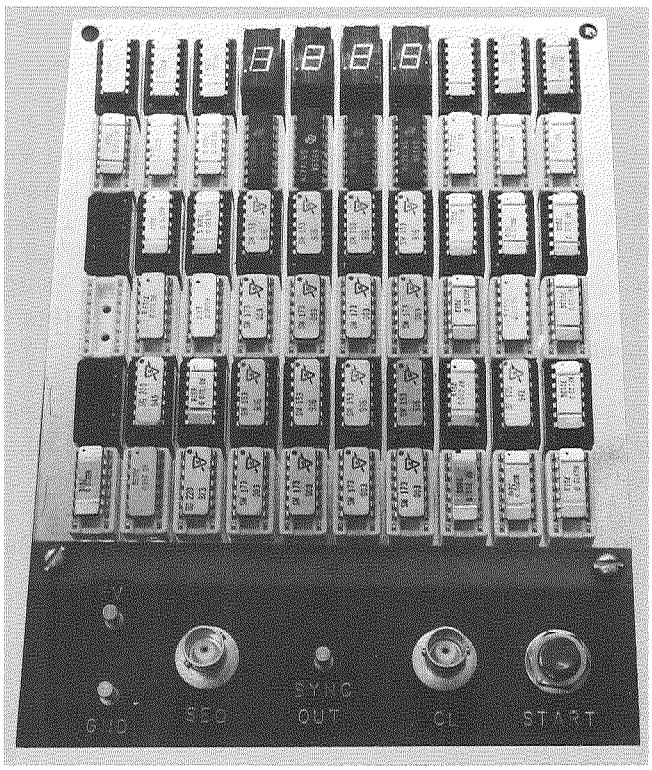

Fig. 2. DIPDOT prototype assembly

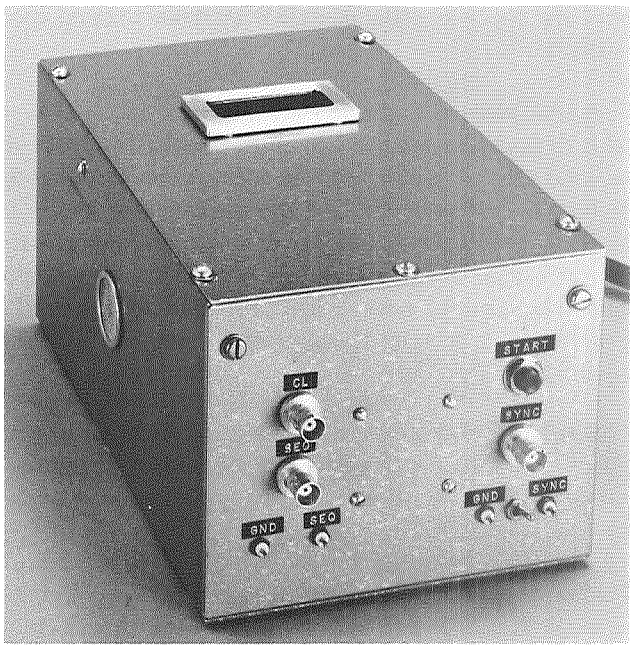

Fig. 3. DIPDOT assembly with box mounting and integral power supply

Generation of the Ford Sequence of Length 2^n, n Large

H. Fredricksen
Communications Systems Research Section

This article presents three algorithms for forming the Ford sequence of length 2^n and compares the storage requirements for each of the three. These sequences are used in checkout of digital communications equipment.

I. Introduction

Shift register sequences have had application in code generation, prescribed period sequence generation for countdown circuits, and PN shift register sequences have been used for recovering signals from noise in deep space transmissions.

A special sequence period for a shift register of n stages is the deBruijn sequence of length 2^n. In the deBruijn sequence all 2^n possible n-tuples occur once as n successive bits of the cyclic shift of the sequence of length 2^n. These sequences have been used in forming comma-free codes of higher index, as random bit generators when all 2^n possible subsequences of length n are required, and as a test sequence to map through all 2^n states of a Viterbi convolutional decoder.

The method most often used to find a deBruijn sequence of length 2^n is to find a primitive polynomial of degree n over GF[2]. When the primitive polynomial is wired into a shift register, a sequence of length $2^n - 1$ is formed, if care is taken to avoid the all-zero cycle of length 1. An extra logical expression is then required to "add" the zero sequence into the PN sequence to form the deBruijn sequence of length 2^n.

There are $\phi(2^n - 1)/n$ primitive polynomials of degree n. But since there are $2^{2^{n-1}-n}$ deBruijn sequences of length 2^n, we see the "linear" deBruijn sequences form a vanishingly small fraction of all deBruijn sequences. Also to find a primitive polynomial of high degree is not necessarily an easy task.

Unfortunately, to generate a nonlinear deBruijn sequence is not generally easy either. There is an algorithm, which we attribute to Ford (Ref. 1) which yields a nonlinear deBruijn sequence. In Ref. 2 the Ford algorithm is investigated and the positions of the truth table for its generation are determined. The algorithms for the Ford sequence generation are given below.

However, to form the Ford sequence using Ford's original algorithm or the algorithm for the truth table requires 2^n bits of storage in the first case, or $(n-1) \times (Z(n)-1)$ bits of storage in the second, where $Z(n)-1$ is the number of positions which are equal to 1 in the truth table generation and $Z(n)$ is given by

$$Z(n) = \frac{1}{n} \sum_{d/n} \phi(d)\, 2^{n/d}$$

We give a new algorithm below which yields the Ford sequence and requires no storage beyond two holding registers of length n bits. The algorithm is valid even for very large n.

II. Algorithms for Generation of Ford Sequence

Ford's Algorithm. Let $x_0 = x_1 = \cdots = x_{n-1} = 0$. The x_{n+k}th bit is a 1 if the n-tuple $x_{k+1}x_{k+2} \cdots x_{k+n-1}$ 1 has not occurred previously in the sequence, otherwise it is a 0.

Proof of Ford's Algorithm. The process must terminate at $1000 \cdots 0$ for if it terminates at $y_0, y_1, \cdots, y_{n-1} \neq 10 \cdots 0$, then $y_0 \cdots y_{n-1}$ must have occurred at least twice in the sequence, which is not permitted. Also every n-tuple must be on the sequence for if $z_0 \cdots z_{n-1}$ is not on the sequence then neither is one of its possible successors, in particular $z_1 \cdots z_{n-1}$ 0. Continuing we see $z_2 \cdots z_{n-1}$ 0 0 is not on the sequence, and finally we find that $100 \cdots 0$ is not on the sequence.

We now present the algorithm which determines the truth table for the Ford sequence.

Algorithm 1

(1) Form the pure cycle decomposition of the deBruijn graph, i.e., choose all cycles of length ℓ, $\ell \mid n$.

(2) For each cycle (excepting (0)), find the maximum element, $m_i = 2^{r_i}k_i$, k_i odd, $r_i \geq 0$.

(3) $\alpha_i = (k_i - 1)/2$.

Algorithm 1 yields $Z(n) - 1$ positions α_i which are the positions which are 1 in the truth table, where $Z(n)$ is the number of cycles of length ℓ, $\ell \mid n$.

Verification of Algorithm 1 is given in Ref. 2. Ford's algorithm requires the whole sequence be saved for the generation and Algorithm 1 requires the saving of the positions $0, y_1, \cdots, y_{n-1}$ which will take the 1 successor $y_1, \cdots, y_{n-1}, 1$.

We now give an algorithm to produce the Ford sequence for large n. The algorithm is similar to Algorithm 1. Algorithm 2 will produce the next n-tuple of the Ford sequence from the current n-tuple.

Algorithm 2

(1) $\beta_0 = (0, 0, 0, \cdots, 0)$, the starting n-tuple of all zeros. (From $\beta_i = (b_1, b_2, \cdots, b_n)$, we produce $\beta_{i+1} = (b_2, b_3, \cdots, b_{n+1})$).

(2) Form $\beta_i^* = (b_2, b_3, \cdots, b_n, 1)$.

(3) Consider all cyclic shifts of β_i^* to find the maximum element M_i on the cycle

$$\beta_i^*, M_i = (b_i \cdots b_n, 1; b_2 \cdots b_{i-1})$$

(4) If $b_2 = b_3 = \cdots = b_{i-1} = 0$, then

$$\beta_{i+1} = (b_2, b_3, \cdots, b_n, \overline{b}_1)$$

otherwise $\beta_{i+1} = (b_2, \cdots, b_n, b_1)$.

Proof

Algorithm 2 follows easily from Algorithm 1. If

$$b_2 = b_3 = \cdots = b_{i-1} = 0$$

then the maximum element on one of the pure cycles in Algorithm 1 is

$$m_i = 2^{i-2}\left[1 + \sum_{j=1}^{n-i+1} b_{n-j+1}\,2^j\right]$$

and

$$1 + \sum_{j=1}^{n-i+1} b_{n-j+1}\,2^j = k_i \text{ of Algorithm 1}$$

$$\sum_{j=0}^{n-i} b_{n-j+1}\,2^j = \alpha_i \text{ of Algorithm 1}$$

Algorithm 2 requires saving only the present state β_i and the current largest value of the shift of the vector β_i^*.

References

1. Ford, L. R., Jr., *A Cyclic Arrangement of M-tuples*, Report No. P-1071. Rand Corp., Santa Monica, Calif., Apr. 23, 1957.

2. Fredricksen, H., "The Lexicographically Least deBruijn Cycle," *Journal of Combinatorial Theory*, Vol. 9, No. 1, pp. 1–5, July 1970.

Weights in the Third-Order Reed-Muller Codes

H. van Tilborg
Communications Systems Research Section

In order to obtain performance superior to that of the (32,6) first-order Reed-Muller Code used on Mariner Mars 1969 and 1971 spacecraft, bandwidth limitations make it necessary to consider Reed-Muller codes of higher orders. In this paper, we investigate the weights which can actually occur in the third-order Reed-Muller codes of lengths 256 and 512. For length 256, we succeed in finding the exact set of integers which occur as weights. For length 512, we do the same, except that we cannot decide whether 140 and 372 occur as weights or not. We show, however, that there are no words of weight 132 or 380, a result which adumbrates an important new theorem on Reed-Muller codes.

I. Introduction

Reed-Muller (RM) codes are among the most useful binary block codes. For instance, the first-order RM code of length 32 is the celebrated (32,6) biorthogonal code which was used on *Mariners* Mars '69 and '71. In order to obtain performance superior to that of the (32,6) code, one would like to use a longer RM code. Unfortunately, the bandwidth requirements of longer *first*-order RM codes are such as to render them useless for NASA missions. However, higher order RM codes require less bandwidth at a fixed length than the first order codes, and so it becomes important to investigate the feasibility of implementing these codes.

As a first step in this direction, researchers have begun to investigate the weight spectrum of these codes. The weight spectrum of the first-order RM code is trivial: except for the all-zero word and the all-one word, all words have weight half the block length. Recently, through the work of Kasami, Berlekamp, and Sloane, the complete weight enumerator for the second-order RM codes has been obtained.

The weight enumerator for the third-order RM codes, however, remains unknown, although for lengths 128 or less it can be obtained by various *ad hoc* techniques. In this paper we investigate the weight enumerator for the third-order RM code of lengths 256 and 512, with the preliminary goal being to identify those weights which actually occur in these codes. For length 256, our result is that all weights which are not eliminated by known theorems can actually occur. For 512, however, we discover that, although no previous theorem suggests it, no words of weights 132 or 380 occur; this adumbrates an important new theorem on RM codes. Finally, weights 140 and 372 remain undecided; i.e., we can neither show that they do not occur nor exhibit words of that weight.[1]

II. Summary of Known Results

RM(r;2^m) denotes the rth order RM code of length 2^m. The following theorems are known:

THEOREM 1 (Ref. 1). *The minimum distance d in RM (r;2^m) is 2^{m-r}.*

THEOREM 2 (Ref. 2). *If*

$$\sum_{i=0}^{2^m} A_i z_i$$

is the weight enumerator of RM $(r;2^m)$ then

$$A_i = A_{2^m - i}$$

THEOREM 3 (McEliece, from Ref. 1). *For the same weight enumerator,*

$$i \not\equiv 0 \pmod{2^{\lceil \frac{m}{r} \rceil - 1}} \text{ implies } A_i = 0$$

By the definition of RM $(r;2^m)$ (Ref. 1) each code vector corresponds with an rth degree polynomial in m variables over GF (2), and the weight of this vector is the number of times that this polynomial has value 1.

So instead of studying the vectors we can study the polynomials. In this paper we need both points of view. We denote by $|f|_m$ the number of times that f, as a function of m variables, is 1.

Example. Let f be an rth degree polynomial in m variables (over GF (2)); then Theorem 1 says

$$|f|_m = 0 \text{ or } |f|_m \geq 2^{m-r}$$

and Theorem 3 says $|f|_m$ is divisible by $2^{\lceil \frac{m}{r} \rceil - 1}$

THEOREM 4 (T. Kasami and N. Tokura from Ref. 3). *If f is an rth degree polynomial of m variables, $r \leq 2$ and $0 < |f|_m < 2^{m-r+1}$ $(0 < |f|_m < 2d)$, then f is transformable by any appropriate affine transformation of the variables into one of the following forms:*

(4a) $x_1 x_2 \cdots x_{r-\mu}(x_{r-\mu+1} \cdots x_\mu + x_{\mu+1} \cdots x_{\mu+r})$
where $m \geq r + \mu \quad r \geq \mu \geq 3$, or

(4b) $x_1 \cdots x_{r-2}(x_{r-1}x_r + x_{r+1}x_{r+2} + \cdots + x_{r+2\mu-3}x_{r+2\mu-2})$
where $m - r + 2 \geq 2\mu \geq 2$

and in both cases

(4c) $|f|_m = 2^{m-r+1} - 2^{m-r+1-\mu}$
$= 2d - 2d \cdot 2^{-\mu}$

Remark. $|f|_m$ is invariant under affine transformation so that this theorem characterizes the codewords with weight $< 2d$.

[1]Since this paper was written it has been possible to show that no words of weight 140 or 372 occur, either. In addition, the weight enumerator for the third-order code of length 256 has been found.

THEOREM 5 (McEliece, Ref. 1).

$$|f|_m = \sum_{\substack{g \subset f \\ g \neq 0}} (-1)^{|g|} 2^{|g| + \nu(g) - 1}$$

where

$|g|$ = *the number of terms in the polynomial* g

$\nu(g)$ = *the number of variables not involved in* g

$g \subset f$ *means all terms of* g *are terms of* f

As an immediate consequence of Theorem 5 we find

$$|f(x_1, \cdots, x_{m-2}) + x_{m-1}x_m|_m = 2^{m-2} + 2 \cdot |f(x_1, \cdots, x_{m-2})|_{m-2} \quad (1)$$

$$|f(x_1, \cdots, x_{m-3}) + x_{m-2}x_{m-1}x_m|_m = 2^{m-3} + 6 \cdot |f(x_1, \cdots, x_{m-3})|_{m-3} \quad (2)$$

$$|f(x_1, \cdots, x_{m-3}) + x_{m-2}x_{m-1}x_m + x_m|_m = 3 \cdot 2^{m-3} + 2 \cdot |f(x_1, \cdots, x_{m-3})|_{m-3} \quad (3)$$

These relations will be useful in the next paragraph.

III. Tables

We start our work with some tables. We wish to know whether there are more gaps in the weight enumerator than those given by Theorems 1 through 4. We have formulated Tables 1 and 2 for RM $(3;2^8)$ and RM $(3;2^9)$. By Theorem 2 we are only interested in weights up to 2^{m-1}, and because we are looking for gaps, we only need to find code words of a certain weight to see that there is no gap.

We did not succeed in finding a codeword of weight 132 or 140. We are therefore left with only the possible gaps $A_{132} = 0$ or $A_{140} = 0$. In the next section we will show that $A_{132} = 0$.

For a while we believed that if one adds to a codeword $c \in$ RM $(3;2^m)$ an appropriate codeword $d \in$ RM $(2;2^m)$, the weight of $c + d$ would be less than twice the minimum distance in RM $(3;2^m)$ so that Theorem 4 would be applicable. However, by counting the number of codewords in the second- and third-order RM codes and the number of equivalence classes of the codewords of weights less than $2d$, it can be shown that this cannot be true for $m = 9$.

IV. $A_{132}=0$ in RM(3;2^9)

Let $f(x_1, \cdots, x_9) = p(x_1, \cdots, x_8) + x_9\, q(x_1, \cdots, x_8)$; then $|f|_9 = |p|_8 + |p+q|_8$.

LEMMA 1. *If* $f(x_1, \cdots, x_9) = p(x_1, \cdots, x_8) + x_9\, q(x_1, \cdots, x_8)$ *and* $|p|_8 > |p+q|_8$ *then there is* $f'(x_1, \cdots, x_9) = p'(x_1, \cdots, x_8) + x_9\, q'(x_1, \cdots, x_8)$ *with* $|p'|_8 < |p'+q'|_8$, $|p'|_8 = |p+q|_8$, $|p'+q'|_8 = |p|_8$ *and therefore* $|f|_9 = |f'|_9$.

Proof. Take $p'(x_1, \cdots, x_8) = p(x_1, \cdots, x_8) + q(x_1, \cdots, x_8)$ and $q'(x_1, \cdots, x_8) = q(x_1, \cdots, x_8)$. Q.E.D.

If $f(x_1, \cdots, x_9) = p(x, \cdots, x_8) + x_9\, q(x_1, \cdots, x_8)$ is a third-degree polynomial then $p(x_1 \cdots, x_8)$ is of third degree and $q(x_1, \cdots, x_8)$ of second degree. By Lemma 1 we need only look for a polynomial $p(x_1, \cdots, x_8)$ of third degree and a polynomial $q(x_1, \cdots, x_8)$ of second degree with the property $|p|_8 + |p+q|_8 = 132$ and $|p|_8 \leqq |p+q|_8$. The occurring weights in the third order RM code of length 2^8 are 0,32,48,56,64,68,72, $\cdots$, so by Lemma 1 we only have to consider $|p|_8 = 0,32,48,56,64$. This proves Lemma 2.

LEMMA 2. *If* $f(x_1, \cdots, x_9) = p(x_1, \cdots, x_8) + x_9\, q(x_1, \cdots, x_8)$ *has weight 132, then we may assume*

$$(|p|_8, |p+q|_8) = \text{a) } (0,132) \text{ or}$$
$$\text{b) } (32,100) \text{ or}$$
$$\text{c) } (48,84) \text{ or}$$
$$\text{d) } (56,76) \text{ or}$$
$$\text{e) } (64,68)$$

We now consider these possibilities separately.

(a) $(|p|_8, |p+q|_8) = (0,132)$

$|p|_8 = 0$ implies $p \equiv 0$, so we want $|q|_8 = 132$ but q is second degree, and 132 does not occur in RM(2;2^8). (See Theorem 3.) So (a) is impossible.

(b) $(|p|_8, |p+q|_8) = (32,100)$

By Theorem 4 is p transformable to $x_1x_2x_3$. So the question is, is there a second polynomial $q(x_1, \cdots, x_8)$ with

$$|x_1x_2x_3 + q(x_1, \cdots, x_8)|_8 = 100?$$
$$|x_1x_2x_3 + q(x_1, x_2, \cdots, x_8)|_8 = |q(0, x_2, \cdots, x_8)|_7 + |x_2x_3 + q(1, x_2, \cdots, x_8)|_7$$

Both terms are weights in RM(2;2^7) and by Theorem 3 divisible by 8; but 100 is not divisible by 8.

Conclusion. (b) is impossible.

(c) $(|p|_8, |p+q|_8) = (48,84)$

Theorem 4 shows that p is equivalent to $x_1(x_2x_3 + x_4x_5)$. By the same reasoning as in (b),

$$|x_1(x_2x_3 + x_4x_5) + q(x_1, \cdots, x_8)|_8 = |q(0, x_2, \cdots, x_8)|_7 + |x_2x_3 + x_4x_5 + q(1, x_2, \cdots, x_8)|_7$$

and is therefore divisible by 8, but 84 is not divisible by 8. Thus (c) is impossible.

(d) $(|p|_8, |p+q|_8) = (56,76)$

Theorem 4 gives that p is equivalent to $x_1(x_2x_3 + x_4x_5 + x_6x_7)$ or to $x_1x_2x_3 + x_4x_5x_6$. $x_1(x_2x_3 + x_4x_5 + x_6x_7)$ can be excluded in the same way as (c) because 76 is not divisible by 8. So we want to find a second degree polynomial $q(x_1, \cdots, x_8)$ with $|x_1x_2x_3 + x_4x_5x_6 + q(x_1, \cdots, x_8)|_8 = 76$. This turns out to be impossible.

(d1) Suppose x_7x_8 is a term in $q(x_1, \cdots, x_8)$, so

$$q(x_1, \cdots, x_8) = p(x_1, \cdots, x_6) + x_7 a(x_1, \cdots, x_6) + x_8 b(x_1, \cdots, x_6) + x_7x_8$$

p is second degree, a and b first degree. Consider the affine transformation $x_7' = x_7 + b(x_1, \cdots, x_6)$ $x_8' = x_8 + a(x_1, \cdots, x_6)$ $x_i' = x_i$, $i = 1, \cdots, 6$ which does not affect $x_1x_2x_3 + x_4x_5x_6$. This transformation reduces our problem to: can $|x_1x_2x_3 + x_4x_5x_6 + p'(x_1, \cdots, x_6) + x_7x_8|_8$ be 76? Equation (1) gives us that this form is $64 + |x_1x_2x_3 + x_4x_5x_6 + p'(x_1, \cdots, x_6)|_6$ and Theorem 1 gives that this last part is 0 or $\geqq 16$; so it is never 76.

(d2) Suppose now that x_7x_8 is not a term in $q(x_1, \cdots, x_8)$, so $q(x_1, \cdots, x_8) = p(x_1, \cdots, x_6) + x_7 a(x_1, \cdots, x_6) + x_8 b(x_1, \cdots, x_6)$. p is second degree; a and b first degree. If $a = 0$ then $|x_1x_2x_3 + x_4x_5x_6 + p(x_1, \cdots, x_6) + x_8 b(x_1, \cdots, x_6)|_8 = 2|x_1x_2x_3 + x_4x_5x_6 + p(x_1, \cdots, x_6) + x_8 b(x_1, \cdots, x_6)|_7$ and so by Theorem 3 is divisible by 8; but 76 is not divisible by 8.

So $a \not\equiv 0$ and also $b \not\equiv 0$. If $a \equiv 1$ then $|x_1x_2x_3 + x_4x_5x_6 + p(x_1, \cdots, x_6) + x_7 + x_8 b(x_1, \cdots, x_6)|_8 = 2^7$ and not 76. So $a \not\equiv 1$, and also $b \not\equiv 1$. So both a and b are affinely equivalent to x_1, not necessarily simultaneously.

Therefore, $x_1x_2x_3 + x_4x_5x_6 + q(x_1, \cdots, x_8)$ has to be equivalent to either: (1) $k(x_1, \cdots, x_6) + x_1x_7 + x_1x_8$ if $a = b$, or (2) $k(x_1, \cdots, x_6) + x_1x_7 + x_2x_8$ if $a \neq b$, where $k(x_1, \cdots, x_6)$ is of third degree. In (1) apply $x_8' = x_8 + x_7$,

$x_i' = x_i$, $i \neq 8$ and then we are in a previous case. In (2) $|k(x_1, \cdots, x_6) + x_1x_7 + x_2x_8|_8 = |k(0, x_2, \cdots, x_6) + x_2x_8|_7$ $+ |k(1, x_2, \cdots, x_6) + x_7 + x_2x_8|_7 = |k(0, x_2, \cdots, x_6)$ $+ x_2x_8|_7 + 64$ and is therefore by Theorem 1 $\geqq 16 + 64 =$ 80. Conclusion: (d) is also impossible.

LEMMA 3. *If* $|f(x_1, \cdots, x_9)|_9 = 132$ *for* $f \in RM(3;2^9)$, *then for any* i, $(|f(x_i = 0)|_8, |f(x_i = 1)|_8) = (64,68)$ *or* $(68,64)$.

LEMMA 4. *If* $f(x_1, \cdots, x_9) \in RM(3;2^9)$ *and* $|f|_9 = 132$, *then* $(|f(0, 0, x_3, \cdots, x_9)|_7, |f(0, 1, x_3, \cdots, x_9)|_7,$ $|f(1, 0, x_3, \cdots, x_9)|_7, |f(1, 1, x_3, \cdots, x_9)|_7) = (32,32,32,36)$ *or* $32,32,36,32)$ *or* $(32,36,32,32)$ *or* $(36,32,32,32)$.

Proof. Divide the word into the four parts corresponding to $(x_1, x_2) = (0,0)(0,1)(1,0)(1,1)$:

x_1:	0	0	1	1
x_2:	0	1	0	1
	a	b	c	d

and let a, b, c, and d be the weights of these parts. Then from Lemma 3

$$\begin{aligned} a + b = 64, \quad & c + d = 68 && A_1 \\ \text{or } a + b = 68, \quad & c + d = 64 && A_2 \\ \text{and } a + c = 64, \quad & b + d = 68 && B_1 \\ \text{or } a + c = 68, \quad & b + d = 64 && B_2 \end{aligned}$$

This gives four possible weight structures:

(1) A_1B_1	$64 - b$	b	b	$68 - b$
(2) A_1B_2	$64 - b$	b	$b + 4$	$64 - b$
(3) A_2B_1	$68 - b$	b	$b - 4$	$68 - b$
(4) A_2B_2	$68 - b$	b	b	$64 - b$

By $x_2' = x_2 + 1$, (2) is equivalent to (1); by $x_1' = x_1 + 1$, (3) is equivalent to (1); by $x_1' = x_1 + 1$, $x_2' = x_2 + 1$, (4) is equivalent to (1). So every codeword of weight 132 is in one of the forms (1) (2) (3) or (4) and is transformable into form (1). Under the transformation $x_1' = x_1 + x_2$, $x_2' = x_2$, (1) goes into the form

$$(64 - b, \quad 68 - b, \quad b, \quad b)$$

and this form has to be equivalent with (1) (2) (3) or (4). This is only possible if $b = 32$ or $b = 34$, but $b = 34$ is excluded by Theorem 3. (Each part $\in$ RM $(3;2^7)$) for $b = 32$, (1) is (32,32,32,36), (2) is (32,32,36,32), (3) is (32,36,35,32), (4) is (36,32,32,32). Q.E.D.

LEMMA 5. *Let* $f(x_1, \cdots, x_m)$ *be a third degree polynomial which is not a second degree polynomial of* m *variables. Then* f *can be transformed by an appropriate affine transformation into* $x_1x_2x_3 + x_1 p(x_4, \cdots, x_m)$ $+ x_2 q(x_4, \cdots, x_m) + x_3 r(x_4, \cdots, x_m) + k(x_4, \cdots, x_m)$ *where* p, q *and* r *are polynomials of degree 2 and* k *of degree 3.*

Proof. w.l.o.g. $f(x_1, \cdots, x_m) = x_1x_2x_3 + x_1x_2a(x_4, \cdots, x_m)$ $+ x_1x_3b(x_4, \cdots, x_m) + x_2x_3c(x_4, \cdots, x_m) + x_1p(x_4, \cdots, x_m)$ $+ x_2q(x_4, \cdots, x_m) + x_3r(x_4, \cdots, x_m) + k(x_4, \cdots, x_m)$ where a, b and c have degree 1, p, q, and r have degree 2 and k has degree 3. The substitution of

$$x_3' = x_3 + a(x_4, \cdots, x_m)\, x_i' = x_i, i \neq 3$$

cancels $x_1x_2a(x_8, \cdots, x_m)$, affects only p, q, and k, which remain of 2nd, 2nd, and 3rd degree. Now the substitution $x_2' = x_2 + b(x_8, \cdots, x_m)\, x_1' = x_1 + c(x_8, \cdots, x_m)$ proves the theorem.

If $f(x_1, \cdots, x_9)$ is a third degree polynomial, we can divide it in the 8 parts where $(x_1, x_2, x_3) = (0,0,0) \cdots (1,1,1)$ and each part corresponds with a code word in RM $(3;2^6)$. We use the symbols p, q, r and k for the polynomial and the corresponding codeword.

Form 1. $x_1x_2x_3 + x_1p(x_4, \cdots, x_9) + x_2q(x_4, \cdots, x_9)$ $+ x_3r(x_4, \cdots, x_9) + k(x_4, \cdots, x_9)$ is of the form

Position	0	1	2	3	4	5	6	7
x_1	0	0	0	0	1	1	1	1
x_2	0	0	1	1	0	0	1	1
x_3	0	1	0	1	0	1	0	1
								1
					p	p	p	p
			q	q			q	q
		r		r		r		r
	k	k	k	k	k	k	k	k

We will need this form constantly in the rest of this proof.

LEMMA 6. *If there is a codeword of weight 132 in* RM $(3;2^9)$ *then when it is transformed into Form 1, the weight of the position 6 and 7 has to be 36. Therefore (by Lemma 4) the positions 0 and 1, 2 and 3, 4 and 5 all have weight 32.*

Proof. Lemma 4 gives that 6, 7 has weight 32 or 36, so assume 6, 7 has weight 32, and that 2, 3 has weight 32. 2, 3 is an element in RM $(3;2^7)$ like 0, 1 and 4, 5 and 6, 7. 2, 3 is $k(x_4, \cdots, x_9) + q(x_4, \cdots, x_9) + x_3 r(x_4, \cdots, x_9)$ and has weight 32. 6, 7 is $k(x_4, \cdots, x_9) + q(x_4, \cdots, x_9) + p(x_4, \cdots, x_9) + x_3 r(x_4, \cdots, x_9) + x_3$ and has weight 32 (by assumption). So we see that $6, 7 = 2, 3 + p(x_4, \cdots, x_9) + x_3$. Now $|p(x_4, \cdots, x_9) + x_3|_7 = 2^6 = 64$, so we have added to 2, 3 (weight 32) a word of weight 64 ($p(x_4, \cdots, x_9) + x_3$) and we get 6, 7, which also has weight 32. This is only possible if the positions of the *ones* of 2, 3 are a subset of the positions of the ones of $p(x_4, \cdots, x_9) + x_3$. This is equivalent to $p(x_8, \cdots, x_9) + x_3 = 0$ implies $k(x_4, \cdots, x_9) + q(x_4, \cdots, x_9) + x_3 r(x_4, \cdots, x_9) = 0$. In general, if a and b are polynomials over GF (2) and $a = 0$ implies $b = 0$, $b = b\,a$. So $k + q + x_3 r = (k + q + x_3 r)(p + x_3)$. Comparing the coefficients of x_3 gives

LEMMA 7. $k = pr + q$.

This implies that the positions 2, 3 (of Lemma 5) have the form

2	3
pr	$(p + 1)\,r$

if $r = 0$, pr and $(p + 1)\,r$ are both zero. If $r = 1$ then pr and $(p + 1)\,r$ are complementary. So 2, 3 has weight equal to the weight of r. But 2, 3 has weight 32, so $|r|_6 = 32$.

Supposition 1. 0, 1 has weight 36, so that 4, 5 has weight 32 (like 2, 3). If we now compare 4, 5 with 6, 7 (as we did above with 2, 3 and 6, 7), we find $k = qr + p$. Together with Lemma 7 this gives $r(p + q) = p + q$ or

LEMMA 8. *$r = 0$ implies $p + q = 0$.*

Now we divide positions 0 and 1 into the parts, where $r = 0$ and $r = 1$ (remember that $|r|_6 = 32$); then 0, 1 looks like

x_3	0	0	1	1
r	0	1	0	1
	$k(r = 0)$	$k(r = 1)$	$k(r = 0)$	$k(r = 1) + 1$
	u	v	w	x

v and x are complementary and so together have weight 32. The total weight is 36 (by assumption), so

LEMMA 9. *k has weight 2 on the positions where $r = 0$.*

Now we divide positions 6 and 7 into the parts where $r = 0$ and $r = 1$. Then 6, 7 looks like (by Lemma 8)

x_3	0	0	1	1
r	0	1	0	1
	$k(r = 0)$	$k(r = 1) + p(r = 1) + q(r = 1)$	$k(r = 0) + 1$	$k(r = 1) + p(r = 1) + q(r = 1)$
	a	b	c	d

$b = d$ and a and c are complementary, and so together have weight 32. The total weight is 32, so $b = d = 0$. So position $6 = (a, b) = (a, 0)$ and has weight 2 by Lemma 9. But position 6 is a codeword in RM $(3;2^6)$ and by Theorem 1 weight 2 is impossible. Hence, 0, 1 must have weight 32.

Supposition 2. 4, 5 has weight 36 and hence 0, 1 has weight 32. If we now compare 0, 1 with 6, 7 (the same way as done above with 4, 5 and 6, 7 and also with 2, 3 and 6, 7), we find $k = (p + q)\,r$ so $r = 0$ implies $k = 0$ and because $k = pr + q$ (Lemma 7), $r = 0$ implies $q = 0$. If we now compare 4, 5 with 6, 7 the same way as at the end of A), we get the same contradiction. The only assumption made is that 6, 7 has weight 32. The conclusion is that its weight is not 32 and by Lemma 3 its weight is 36. Q.E.D.

LEMMA 10. *If $x_1x_2x_3 + x_1 p(x_4, \cdots, x_9) + x_2 q(x_4, \cdots, x_9) + x_3 r(x_4, \cdots, x_9) + k(x_4, \cdots, x_9)$ has weight 132, where p, q and r are of degree 2 and k of degree 3, then $|p|_6 = |q|_6 = |r|_6 = 28$.*

Proof. We have seen that 0, 1 in Form 1 has weight 32, so $|r + k|_6 + |k|_6 = 32$ and $|r|_6 - |k|_6 \leqq |r + k|_6 = 32 - |k|_6$ so $|r|_6 = 32$. 6, 7 in Form 1 has weight 36, so $|r + 1|_6 - |p + q + k|_6 \leqq |r + p + q + k + 1|_6 = 36 - |p + q + k|$ or $|r + 1|_6 \leqq 36$, so $|r|_6 \geqq 28$. So $28 \leqq |r|_6 \leqq 32$. But $r \in$ RM $(2;2^6)$, so Form 1 gives that $|r|_6$ is 28 or 32.

Suppose $|r|_6 = 32$. If we look at positions 0 and 1, then we see that 0 and 1 are complementary on the positions where $r = 1$, so have weight 32 on these positions (32 positions). Because the total weight is 32 (Lemma 6), we see that $r = 0$ implies $k = 0$.

By the same reasoning on 2, 3, $r = 0$ implies $k + q = 0$, and on 4, 5 $r = 0$ implies $k + p = 0$. So we have $r = 0$ implies $(k = 0)$ and $(p = 0)$ and $(q = 0)$. This gives for positions 6, 7:

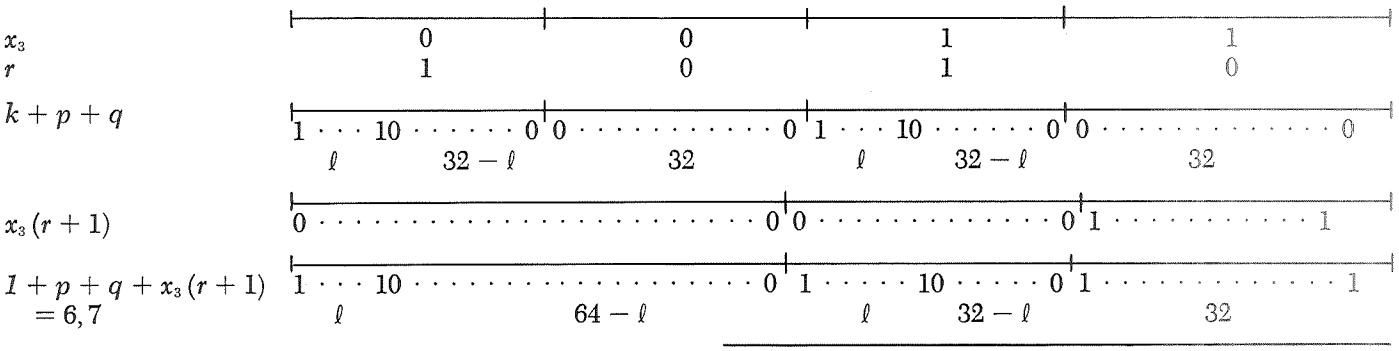

So $2\ell + 32 = 36$ or $\ell = 2$ but $|k+p+q|_6 = \ell$ ($k+p+q$ is position 6) so $\ell = 0$ or $\ell \geqq 8$ by Theorem 1. This is a contradiction, hence $|r| = 28$. By interchanging x_1 and x_3 or x_2 and x_3 we also get $|p| = |q| = 28$. Q.E.D.

Theorem 5. *In RM (3;2⁹), $A_{132} = 0$.*

Proof. $|f|_9 = 132$. Then by Lemma 4 f can be written in the form Lemma 5, and by Lemma 10 $|p| = |q| = |r| = 28$. Positions 0, 1 have weight 32, so $|k + x_3 r|_7 = 32$.

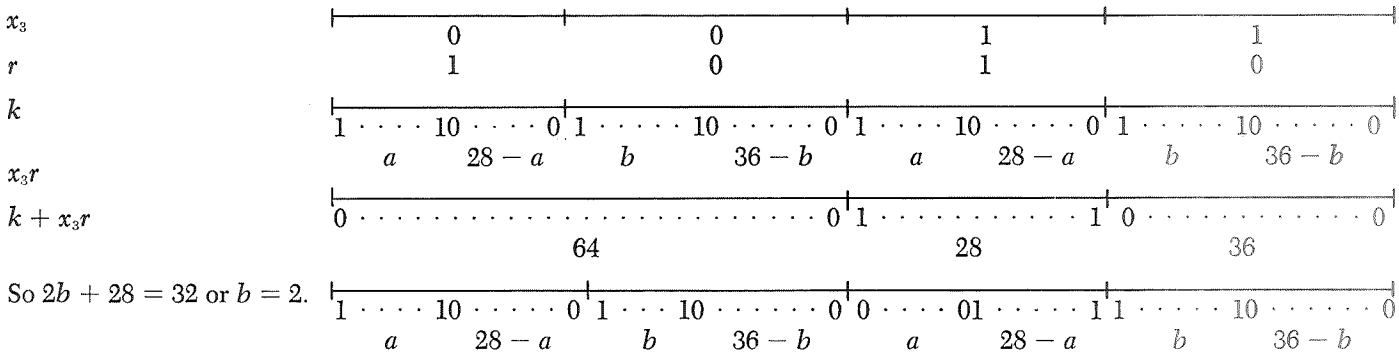

Hence the work k has two ones on the positions where $r = 0$. By a similar argument on 2, 3 and 4, 3 we see that the same holds for $k + p$ and $k + q$. Because $k + p + q = k + (k + p) + (k + q)$, we know that

Lemma 11. *$k + p + q$ has $\leqq 6$ ones on the positions where $r = 0$.*

Now we look again at 6, 7: $|k + p + q + x_3(r + 1)|_6 = 36$.

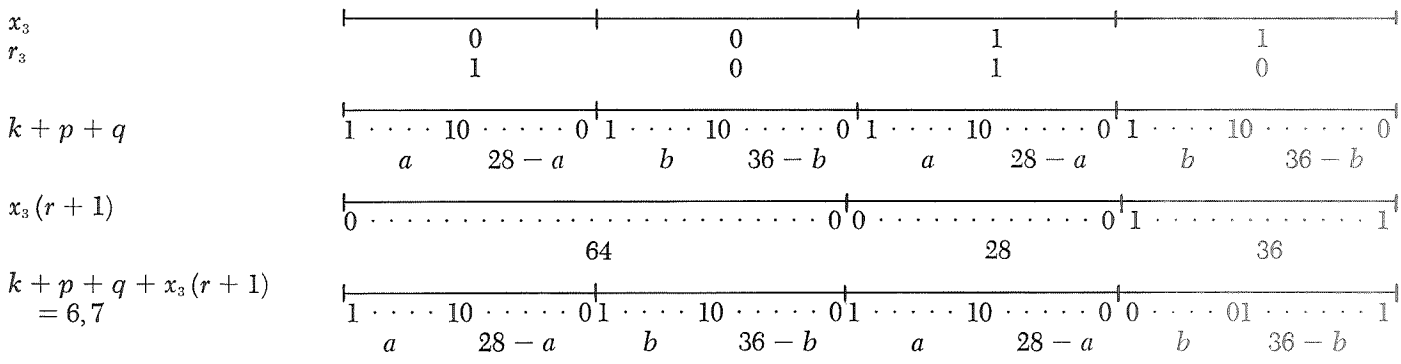

So $2a + 36 = 36$, or $a = 0$. That means that all the ones of $k + p + q$ are on the positions where $r = 0$. But by Lemma 11 this is a contradiction with Theorem 1 ($k + p + q \in$ RM (3;2⁶)) unless $k + p + q = 0$.

So the only possibility for a codeword of weight 132 is $k = p + q$, but then $k = p + q$ and $k = q + r$ and hence $p = q = r$, and that means $k = p + q = 0$ and that is impossible because then $32 = |k + x_3 r|_7 = |x_3 r|_7 = |r|_6 = 28$. Q.E.D.

References

1. van Lint, J. H., "Coding Theory," *Springer Lecture Notes in Mathematics No. 201*, Springer-Verlag, Berlin, 1971.

2. Berlekamp, E. R., *Algebraic Coding Theory*, pp. 361–367. McGraw Hill Book Co., Inc., New York, 1968.

3. Kasami, T., and Tokura, N., "On the Weight Structure of Reed-Muller Codes," *IEEE Trans. Inf. Theory*, Vol. IT-16, No. 6, pp. 752–758, Nov. 1970.

Table 1. RM $(3;2^s)$

Weight w	Words of this weight	Comment
0	0	
32	$x_1x_2x_3$	by (4b); ϵ RM $(3;2^3)$
48	$x_1(x_2x_3 + x_4x_5)$	by (4b); ϵ RM $(3;2^5)$
56	$x_1(x_2x_3 + x_4x_5x_6x_7)$ $x_1x_2x_3 + x_4x_5x_6$	by (4b); ϵ RM $(3;2^7)$ by (4a); ϵ RM $(3;2^6)$
64	x_1x_2	$w = 2d$; ϵ RM $(2;2^5)$
68	$x_1(x_2x_3 + x_4x_5) + x_6x_7x_8$	Compare with $w = 48$ and apply Eq. (2)
72	$x_1x_2x_3 + x_4x_5x_6 + x_1x_4$	ϵ RM $(3;2^6)$
76	$x_1(x_2x_3 + x_4x_5) +$ $x_6x_7x_8 + x_1x_6$	
80	$x_1x_2x_3 + x_4x_5$	ϵ RM $(3;2^5)$
84	$x_1(x_2x_3 + x_4x_5) +$ $x_6x_7x_8 + x_2x_6$	
88	$x_1(x_2x_3 + x_4x_5) + x_6x_7$	ϵ RM $(3;2^7)$; compare with $w = 48$ and apply Eq. (1)
92	$x_1x_2x_3 + x_4x_5x_6 + x_7x_8$	compare with $w = 56$ and apply Eq. (1)
96	$x_1x_2 + x_3x_4$	ϵ RM $(2;2^4)$
100	$x_1x_2x_3 + x_4x_5x_6 +$ $x_1x_4 + x_7x_8$	compare with $w = 72$ and apply Eq. (1)
104	$x_1x_2x_3 + x_4x_5 + x_6x_7$	compare with $w = 80$ and apply Eq. (1); ϵ RM $(3;27)$
108	$x_1(x_2x_3 + x_4x_5) +$ $x_6x_7x_8 + x_6$	compare with $w = 48$ and apply Eq. (3)
112	$x_1x_2 + x_3x_4 + x_5x_6$	ϵ RM $(2;2^6)$
116	$x_1x_2x_3 + x_4x_5 +$ $x_6x_7x_8 + x_6$	compare with $w = 80$ and apply Eq. (3)
120	$x_1x_2 + x_3x_4 + x_5x_6 + x_7x_8$	ϵ RM $(2;2^8)$
124	$x_1x_2x_3 + x_4x_5x_6 +$ $x_7x_8 + x_1x_4$	
128	x_1	ϵ RM $(1;2^1)$; $128 = 2^{m-1}$
$d = 2^{s-3} = 32$, $2^{\left\lceil \frac{s}{3} \right\rceil - 1} = 4$, so the weights are divisible by 4		

This table shows that there are no gaps in RM $(3;2^s)$ other than the ones already known.

Table 2. RM $(3;2^9)$

Weight w	Words of this weight	Comment
0	0	
64	$x_1x_2x_3$	by (4b); see $w = 32$ in RM $(3;2^8)$
96	$x_1(x_2x_3 + x_4x_5)$	by (4b); see $w = 48$ in RM $(3;2^8)$
112	$x_1(x_2x_3 + x_4x_5 + x_6x_7)$ $x_1x_2x_3 + x_4x_5x_6$	by (4b); see $w = 56$ in RM $(3;2^8)$ by (4a); see $w = 56$ in RM $(3;2^8)$
120	$x_1(x_2x_3 + x_4x_5 + x_6x_7 + x_8x_9)$	by (4b)
128	x_1x_2	$128 = 2d$; ϵ RM $(2;2^2)$
132	?	
136	$x_1(x_2x_3 + x_4x_5) + x_6x_7x_8$	ϵ RM $(3;2^8)$; see $w = 68$ in Table 1
140	?	
144	$x_1(x_2x_3 + x_4x_5 + x_6x_7) + x_1$	ϵ RM $(3;2^7)$
148	$x_1x_2x_3 + x_4x_5x_6 + x_7x_8x_9$	compare with $s = 112$ in this table and apply Eq. (2)
152	$x_1(x_2x_3 + x_4x_5) + x_6x_7x_8 + x_1x_6$	ϵ RM $(3;2^8)$; see $w = 76$ in Table 1
156	$x_1x_2x_3 + x_4x_5x_6 + x_7x_8x_9 + x_1x_4x_7$	
160	$x_1x_2x_3 + x_4x_5$	ϵ RM $(3;2^5)$
164	$x_1(x_2x_3 + x_4x_5 + x_6x_7) + x_2x_4x_8 + x_3x_5x_9$	
168	$x_1(x_2x_3 + x_4x_5) + x_6x_7x_8 + x_2x_6$	ϵ RM $(3;2^8)$; see $n = 84$ in Table 1
172	$x_1x_2x_3 + x_4x_5x_6 + x_1x_4 + x_7x_8x_9$	compare with $w = 72$ in Table 1 and apply Eq. (2)
176	$x_1(x_2x_3 + x_4x_5) + x_6x_7$	ϵ RM $(3;2^7)$
180	$x_1(x_2x_3 + x_4x_5 + x_6x_7 + x_8x_9) + x_2x_3x_4 + x_5x_6x_7$	
184	$x_1x_2x_3 + x_4x_5x_6 + x_9x_8$	ϵ RM $(3;2^8)$; see $n = 92$ in Table 1
188	$x_1(x_2x_3 + x_4x_5 + x_6x_7 + x_8x_9)$ $x_1 + x_2x_3x_4 + x_5x_6x_7$	

Weight w	Words of this weight	Comment
192	$x_1x_2 + x_3x_4$	ϵ RM $(2;2^4)$
196	$x_1x_2x_3 + x_4x_5x_6 + x_1 + x_1x_4 + x_7x_8x_9$	Apply Eq. (2) on first four terms
200	$x_1x_2x_3 + x_4x_5x_6 + x_1x_4 + x_7x_8$	ϵ RM $(3;2^8)$; see $w = 100$ in Table 1
204	$x_1(x_2x_3 + x_4x_5 + x_6x_7) + x_2x_4x_8 + x_3x_5x_9 + x_1$	Compare with $w = 64$
208	$x_1x_2x_3 + x_4x_5x_6 + x_1$	ϵ RM $(3;2^6)$
212	$x_1x_2x_3 + x_4x_5x_6 + x_7x_8x_9 + x_1x_4x_7 + x_1$	
216	$x_1(x_2x_3 + x_4x_5) + x_6x_7x_8 + x_6$	ϵ RM $(3;2^8)$; see $w = 108$ in Table 1
220	$x_1x_2x_3 + x_4x_5x_6 + x_7x_8x_9 + x_1$	Apply Eq. (2) or (3)
224	$x_1x_2 + x_3x_4 + x_5x_6$	ϵ RM $(2;2^6)$
	$x_1x_2 + x_3x_4x_5 + x_3$	ϵ RM $(3;2^5)$
228	$x_1x_2x_3 + x_4x_5x_6 + x_1x_4 + x_7x_8x_9 + x_7$	Compare with $w = 72$ in Table 1 and apply Eq. (3)
232	$x_1x_2x_3 + x_4x_5 + x_6x_7x_8 + x_6$	Compare with $w = 80$ in Table 1 and apply Eq. (3)
236	$x_1(x_2x_3 + x_4x_5 + x_6x_7) + x_2x_4x_8 + x_3x_5x_9 + x_8$	
240	$x_1x_2 + x_3x_4 + x_5x_6 + x_7x_8$ $x_1x_2 + x_3x_4 + x_5x_6x_7 + x_5$	ϵ RM $(2;2^8)$; see $w = 110$ in Table 1 ϵ RM $(3;2^7)$; apply Eq. (3)
244	$x_1x_2x_3 + x_4x_5x_6 + x_1 + x_4 + x_7x_8x_9$	
248	$x_1x_2x_3 + x_4x_5x_6 + x_1 + x_4 + x_7x_8$	ϵ RM $(2;2^8)$; see $w = 124$ in Table 1
252	$x_1x_2x_3 + x_4x_5x_6 + x_7x_8x_9 + x_1 + x_4 + x_7$	Apply Eq. (3)
256	x_1	$w = 2^{m-1}$

$d = 2^{9-3} = 64$, $2\left[\frac{9}{3}\right]^{-1} = 4$

If $|f(x_1, \cdots, x_8)|_8 = k$, then $|f(x_1, \cdots, x_8)|_9 = 2k$, so half of the words in this table are elements of RM $(3;2^8)$

Detection of Failure Rate Increases

G. Lorden
California Institute of Technology

I. Eisenberger
Communications Systems Research Section

The problem of devising systematic policies for replacement of equipment subject to wear-out involves the detection of increases in failure rates. Detection procedures are defined as stopping times N with respect to the observed sequence of random failures. The concepts of "quickness of detection" and "frequency of false reactions" are made precise and a class of procedures is studied which optimizes the former asymptotically as the latter is reduced to zero. Results of Monte Carlo experiments are given which show that efficient quickness of detection is attainable simultaneously for various levels of increase in failure rates.

I. Introduction

The present formulation of the problem of detecting failure rate increases arose in the study of replacement policies for equipment which may possibly be subject to wear-out, under the assumption that little is known *a priori* about when the onset of wear-out is likely to occur, or even whether it will occur. The desired type of policy is a rule utilizing failure data themselves to determine that the failure rate has increased. When such determination has occurred, some previously specified action is taken, e.g., investigation of causes or ordering of replacements. It is desired that this action be taken as soon as possible after a specified level of increase in the failure rate has occurred, and it is by no means necessary to estimate when that increase began. Thus, in mathematical terms, the kind of statistical procedure sought is a stopping time N for an observed sequence of random variables $X_1, X_2, X_3, \cdots$. That is, N is a random variable with possible values 1, 2, $\cdots$, and ∞ (i.e., never stops), such that for every $n = 1, 2, \cdots$, the event $\{N = n\}$ depends on $X_1, \cdots, X_n$ only. The X_i's are times between successive failures, and are assumed to be independent, with exponential densities

$$f_{\lambda_i}(x) = \begin{cases} \lambda_i e^{-\lambda_i x}, & x \geqq 0 \\ 0, & x < 0 \end{cases} \qquad \lambda_i > 0, i = i, 2, \cdots \tag{1}$$

In order to define a simple criterion for quickness of reaction to increases in the failure rate, it is convenient to consider the following situation: For some $m = 1, 2, \cdots$,

$$\lambda_1 = \lambda_2 = \cdots = \lambda_{m-1} = \lambda \text{ (known)}$$

and

$$\lambda_m = \lambda_{m+1} = \cdots = (1+\theta)\lambda, \theta > 0 \tag{2}$$

Note that Eq. (2) specifies that the increase in failure rate from λ to $(1+\theta)\lambda$ occurs instantaneously after X_{m-1} is observed. Denote by P_m and E_m probabilities and expectations for $m = 1, 2, \cdots$, and denote the same by P_0 and E_0 when $\lambda = \lambda_1 = \lambda_2 = \cdots$. A reasonable measure of quickness of detection of increases occurring at time m is the smallest number C_m such that

$$E_m[N - (m-1) | X_1 = x_1, \cdots, X_{m-1} = x_{m-1}] \leqq C_m$$

for all $x_1, \cdots, x_{m-1}$ such that $N \geqq m$. As a kind of "worst case" criterion, define $\overline{E}_\theta N$ as the largest of the C_m's, i.e.,

$$\overline{E}_\theta N = \sup_{m \geqq 1} C_m \tag{3}$$

The desire to have small $\overline{E}_\theta N$ for $\theta > 0$ must, of course, be balanced against the need to have a controlled frequency of "false reactions." In other words, when there is no increase in failure rate, then N should be large, hopefully infinite. It is shown in Ref. 1, however, that in order to have $\overline{E}_0 N$ finite for some $\theta > 0$ it is necessary that N have finite expectation even under P_0. An appropriate type of restriction on false reactions, therefore, is

$$E_0 N \geqq \gamma > 1 \tag{4}$$

where γ is to be prescribed.

The problem under investigation can now be formulated more precisely. Among all stopping times N satisfying Eq. (4) for prescribed γ, determine one which minimizes (or nearly minimizes) $\overline{E}_\theta N$ over a specified range, $\theta_1 \leqq \theta \leqq \theta_2$. In Ref. 1, it is shown that as $\gamma \to \infty$ the minimum possible $\overline{E}_\theta N$ ($\theta > 0$ fixed) is asymptotic to

$$\frac{\log \gamma}{\log(1+\theta) - \dfrac{\theta}{1+\theta}} \tag{5}$$

where the denominator is the Kullback–Leibler information number when $(1+\theta)\lambda$ is true and the alternative is λ. In that paper, it is also demonstrated that a "maximum likelihood" procedure, $\hat{N}$, achieves the asymptotic minimum simultaneously for all $\theta > 0$. (The rate of approach to the asymptotic minimum depends on θ, however.) These procedures are defined for the present case of exponential distributions in *Section III* and computationally simpler modifications are introduced, along with Monte Carlo results. It is helpful to take up first the case of a single alternative $\theta > 0$, which will be done in *Section II*. *Section IV* treats the case where λ is unknown.

II. Simple Alternative

Motivated by the problem of control charts in quality control, E. S. Page (Ref. 2) proposed a general procedure for detecting a change from one density to another at an unknown location in a sequence of random variables. His procedure consists of repeated applications of a sequential probability ratio test (SPRT) which in the present context is definable by the inequalities (for fixed $\theta > 0$)

$$0 < n \log(1+\theta) - \theta S_n < \log \gamma \tag{6}$$

where $S_n = X_1 + \cdots + X_n$, γ is chosen > 1, and it is assumed from this point on that $\lambda = 1$ (which can always be achieved by scaling the X's). The procedure is to stop as soon as the right-hand inequality is violated, with the proviso that if the left-hand inequality is violated first all observations up to that point will be discarded and the procedure "recycled," with $S_1, S_2, \cdots$, denoting cumulative sums of the new observations.

The following equivalent formulation is convenient to apply: stop the first time that

$$T_n \geqq \log \gamma \tag{7}$$

where $T_0 = 0$ and for $n = 1, 2, \cdots$,

$$T_n = \max(0, T_{n-1} + \log(1+\theta) - \theta X_n) \tag{8}$$

It is illuminating also to view Page's procedure in another way. Stopping occurs when *for some* $k \geqq 1$ the last k observations, $X_{n-k+1}, \cdots, X_n$, are "significant" in the sense of a one-sided SPRT, i.e.,

$$k \log(1+\theta) - \theta(X_{n-k+1} + \cdots + X_n) \geqq \log \gamma$$

Let α, $1-\beta$, respectively, denote the probabilities under P_0, P_1 that the procedure stops before recycling. Then the expected number of cycles is evidently α^{-1}, $(1-\beta)^{-1}$, respectively. If N_1 denotes the number of observations required to violate either inequality, then by Wald's equation (Ref. 3) for the expected value of the sum of a random number of independent and identically distributed variables, the number N of observations taken by Page's procedure satisfies

$$E_0 N = \alpha^{-1} E_0 N_1 \tag{9}$$

and

$$E_\theta N = (1-\beta)^{-1} E_\theta N_1 \tag{10}$$

Furthermore,

$$\overline{E}_\theta N = (1-\beta)^{-1} E_\theta N_1 \tag{11}$$

since obviously $\overline{E}_\theta N \geqq E_\theta N$. And $\overline{E}_\theta N \leqq E_\theta N$ by the following argument. Observing $X_1 = x_1, \cdots, X_{m-1} = x_{m-1}$ determines that $T_{m-1} = t \geqq 0$ (depending on $x_1, \cdots, x_{m-1}$). Since $X_m, X_{m+1}, \cdots$, are independent of past X's, the sequence $T_m, T_{m+1}, \cdots$, behaves just as $T_1, T_2, \cdots$, would if one started with $T_0 = t \geqq 0$. Since this last obviously would not make any succeeding T's smaller, it would not increase the time required to reach $\log \gamma$. This proves Eq. (11).

Since $\alpha \leqq \gamma^{-1}$ by the usual estimates of SPRT error probabilities (Ref. 4), evidently

$$E_0 N \geqq \gamma \, E_0 N_1 \geqq \gamma$$

Furthermore $(1-\beta)^{-1} E_\theta N_1$ is asymptotic to $\log \gamma$ divided by the information number, by virtue of the usual Wald formulas for expected sample sizes. Thus Page's procedure does approach asymptotically the minimum $\overline{E}_\theta N$ (Expression 5).

Using Eqs. (9) and (11) one can obtain good approximations to $\overline{E}_0 N$ and $E_\theta N$ in terms of γ from the approximations of SPRT error probabilities and expected sample sizes for exponential densities given in Ref. 3. For the boundaries 0 and $\log \gamma$ in Expression (6), these approximations are as follows:

$$1-\beta = \alpha\gamma G(\theta) = \frac{\theta \gamma G(\theta)}{\gamma G(\theta)(1+\theta) - 1} \tag{12}$$

where

$$G(\theta) = \frac{(1+\theta)\log(1+\theta) - \theta}{\theta - \log(1+\theta)}$$

$$(\log(1+\theta) - \theta) E_0 N_1 = \alpha \log(\gamma(1+\theta)) - (1-\alpha)\theta \tag{13}$$

$$\left(\log(1+\theta) - \frac{\theta}{1+\theta}\right) E_\theta N_1 = (1-\beta) \times \left(\log\gamma + \frac{\frac{1}{2}(1+\theta)(\log(1+\theta))^2}{(1+\theta)\log(1+\theta) - \theta}\right) - \frac{\beta\theta}{1+\theta} \tag{14}$$

The approximations (12)–(14) give approximations to $\overline{E}_0 N$ and $E_\theta N$ by Eqs. (9) and (11). The accuracy of these approximations is indicated by the following comparison (Table 1) with the values based on the exact formulas in Ref. 5 (which entail considerably more calculation).

III. Composite Alternative

For the problem of minimizing $\overline{E}_\theta N$ over a range $\theta_1 \leqq \theta \leqq \theta_2$ subject to $E_0 N \geqq \gamma$, it is natural to consider simultaneous Page procedures. Performing Page's procedures simultaneously for all alternatives $\theta \in [\theta_1, \theta_2]$ results in stopping when for some $k \geqq 1$ the last k observations satisfy

$$\max_{\theta_1 \leqq \theta \leqq \theta_2} [k \log(1+\theta) - \theta (X_{n-k+1} + \cdots + X_n)] \geqq \log \gamma$$

This rule is computable since the indicated maximum is attained either at θ_1, or θ_2, or at the maximum likelihood estimate, given by $\hat{\theta} = (X_{n-k+1} + \cdots + X_n) k^{-1} - 1$. This is the procedure, $\hat{N}$, which achieves the asymptotic minimum (Expression 5) for every $\theta \in (\theta_1, \theta_2)$, as shown in Ref. 1. In that paper the computation of this type of procedure is discussed.

The results of preliminary Monte Carlo experiments indicated that in the "small sample case," i.e., $E_0 N \leqq 2000$, when θ_2/θ_1 is not very large, the improvement of $\overline{E}_\theta N$ for $\theta \in [\theta_1, \theta_2]$ achieved by $\hat{N}$ in comparison to Page's procedure is already achieved to a large extent by the simpler rule which uses two simultaneous Page procedures, one for each of the alternatives θ_1, θ_2. Accordingly, the following results are limited to this dual-Page procedure, $\tilde{N}$. Extensive Monte Carlo sampling was carried out with $\theta_1 = 0.5$ and $\theta_2 = 0.8$. Thus, the range of alternatives where efficient performance was most emphasized represented 50% to 80% increases in failure rate. The values $\gamma = 60$ and $\gamma = 100$ were chosen, resulting in estimates of $E_0 \tilde{N}$ equal to 508 and 936, respectively. The results are summarized in Table 2. (The tolerances given are sample variances.) Just as for a single Page procedure, $\overline{E}_\theta \tilde{N} = E_\theta \tilde{N}$ for $\theta > 0$.

The value $\theta = -0.1$ is included in Table 2 to indicate how $\tilde{N}$ performs if the true failure rate remains 10% less than the nominal value. In both cases $\gamma = 60, 100$, the frequency of false reactions is about one-third as large as when the failure rate equals the nominal value.

Note that the efficiency of $\tilde{N}$ is about 96% and 98%, respectively, for $\gamma = 60$, 100, and θ between 0.5 and 0.8 (the efficiency estimate of 100.1% resulting from sampling error). For θ outside the chosen interval [0.5, 0.8], the efficiency falls off gradually but is still quite high between 0.4 and 1.0, particularly for the smaller γ.

Comparison of the results for $\gamma = 60$ and 100 indicates that a much larger $E_0\tilde{N}$ is obtainable for a relatively small increase in $\overline{E}_\theta\tilde{N}$'s. An increase of about 15% in $E_\theta\tilde{N}$'s between the two cases yields nearly a doubling of $E_0\tilde{N}$.

For fixed γ, there is a convenient rule of thumb that fairly well approximates $E_\theta\tilde{N}$ over the indicated range; namely, $E_\theta\tilde{N}$ is inversely proportional to θ (or, equivalently, the percent increase in the failure rate). Table 3 indicates the accuracy of the approximation $\theta E_\theta\tilde{N} =$ constant in the case of the Monte Carlo results of Table 2. The rule of thumb exhibits a similar degree of accuracy in approximating the $E_\theta N$ (from Eqs. 10 and 14) of a Page procedure for θ with γ chosen (depending on θ) to achieve a prescribed E_0N (from Eqs. 9 and 13).

Having chosen θ_1, θ_2 for a dual-Page procedure, the problem naturally arises of how to select γ to achieve a prescribed E_0N. (The corresponding problem for a single-Page procedure is solvable by successive approximations using Eqs. 9 and 13.) Unfortunately, it seems to be very difficult to derive approximations for $E_0\tilde{N}$ in terms of γ. Bounds are obtainable, however, from the following simple considerations. In the case $\gamma = 60$, for example, the Page procedures for $\theta_1 = 0.5$ and $\theta_2 = 0.8$ have frequencies of false reaction, $1/E_0N$, equal to 1/588 and 1/1026, respectively, according to Eqs. (9) and (13). Evidently, the dual procedure $\tilde{N}$ has frequency of false reaction at least 1/588 and at most 1/1026 + 1/588 = 1/374. Thus, $374 < E_0\tilde{N} < 588$. Note that the Monte Carlo result of 508 is in fact closer to the upper bound, which is also true in the case $\gamma = 100$.

It is not very difficult to estimate $E_0\tilde{N}$ by Monte Carlo methods accurately enough to choose γ, once the range has been narrowed by using the bounds just described. Since the values of $\overline{E}_\theta\tilde{N}$ increase rather slowly compared to $E_0\tilde{N}$ as γ is made larger, there is little harm in choosing γ conservatively.

The single- and dual-Page procedures, N and $\tilde{N}$, and the maximum likelihood procedure $\hat{N}$ all have a pleasant property: when $\theta = 0$, the time to stop is approximately exponentially distributed. To see this for N, note that the cycles defined by Expression (6) are a sequence of Bernoulli trials, and stopping occurs upon the first failure to recycle (i.e., violation of the right-hand inequality). Thus, the number of cycles is geometrically distributed, and when γ (and hence the number of cycles) is large, the number of observations also is nearly geometrical (approximately exponential) in distribution. The same holds true for $\tilde{N}$ and $\hat{N}$, since recycling of the Page procedure for θ_1 entails (Ref. 1) recycling of the Page procedures for all $\theta > \theta_1$, i.e., the initial conditions are duplicated. The approximate exponential distribution gives a reasonable indication of the probabilities of "unlucky" early false reactions.

IV. The Case of Unknown λ

By dealing with the sequence of ratios S_2/S_1, S_3/S_2, $\cdots$, one can obviously develop procedures whose performance does not depend on the scale factor, λ. The sequence $\{S_n\}$ is a Poisson process (so long as the failure rate remains constant) and it is well known (Ref. 6) that the conditional distribution of S_n given $S_{n+1} = t$ is the same as the distribution of the largest of n independent variables uniformly distributed on $[0, t]$. Thus,

$$P(S_n \leqq x \mid S_{n+1} = t) = \begin{cases} \left(\frac{x}{t}\right)^n, & 0 \leqq x < t \\ 1, & x \geqq t \end{cases}$$

and hence

$$P\left(\left(\frac{S_n}{S_{n+1}}\right)^n \leqq u \mid S_{n+1} = t\right) = P\left(S_n \leqq u^{\frac{1}{n}} t \mid S_{n+1} = t\right) = \begin{cases} u, & 0 \leqq u \leqq 1 \\ 1, & u \geqq 1 \end{cases} \tag{15}$$

Since this last expression doesn't depend on t, evidently $(S_n/S_{n+1})^n$ is uniformly distributed on $(0, 1)$ and independent of S_{n+1}. In fact, $(S_n/S_{n+1})^n$ is independent of $S_{n+1}, \cdots, S_m$ (jointly) for any $m > n + 1$, since the conditional distributions above are unchanged if the condition $S_{n+1} = t$ is augmented by specifying $S_{n+2} = t_{n+2}, \cdots, S_m = t_m$. Therefore, $(S_n/S_{n+1})^n$ is evidently independent of $(S_{n+1}/S_{n+2})^{n+1}, \cdots, (S_{m-1}/S_m)^{m-1}$ jointly. For fixed m, the last statement is true for all $n < m - 1$, and hence

$$S_1/S_2, (S_2/S_3)^2, \cdots, (S_{m-1}/S_m)^{m-1}$$

are mutually independent (for every $m \geqq 3$). Thus, the random variables in the infinite sequence

$$S_1/S_2, (S_2/S_3)^2, (S_3/S_4)^3, \cdots$$

are independent and (by the remark following Eq. 15) each is uniformly distributed on (0, 1). It is easy to verify that if U is uniformly distributed on (0, 1), then $\log U^{-1}$ is exponentially distributed with mean 1. Thus,

$$\log \frac{S_2}{S_1}, 2 \log \frac{S_3}{S_2}, 3 \log \frac{S_4}{S_3}, \cdots \tag{16}$$

are independent and exponentially distributed with mean one, *regardless of the true value of* λ. The (single or dual) Page procedures of the preceding sections, when applied to the sequence (16), will therefore yield the same E_0N as before.

Under what circumstances will the sequence (16) be independent and exponentially distributed with mean $1/(1 + \theta)$? Obviously, it suffices that $S_1, S_2, \cdots$ have the same distribution as $W_1^{1/1+\theta}, W_2^{1/1+\theta}, \cdots$, where $\{W_n\}$ is a Poisson process. This is the case if, for example, the S_n's are the times of successive failures occurring in a family of repairable parts under the following assumptions. Their failure rate functions depend only on age (the effects of previous failures disappearing upon repair) and are Weibull with shape parameter $\alpha = 1/(1 + \theta)$ and arbitrary scale parameters (not necessarily the same for all parts).

The behavior of sequence (16) when the failure rate changes abruptly at time m can be described approximately by noting that

$$n \log \frac{S_{n+1}}{S_n} = \log \left(1 + \frac{X_{n+1}}{nX_n}\right)^n \approx \frac{X_{n+1}}{\overline{X}_n} \text{ for large } n \tag{17}$$

where $\overline{X}_n = S_n/n$. If the failure rate is λ for $X_1, \cdots, X_m$, then changing it to $(1 + \theta)\lambda$ thereafter multiplies $X_{m+1}, X_{m+2}, \cdots$ by $1/(1 + \theta)$, while $\overline{X}_n$ is largely unaffected so long as $n - m << m$. For $n >> m$, however, the contribution of $X_1, \cdots, X_m$ to $\overline{X}_n$ becomes small and $n \log (S_{n+1}/S_n)$ begins to approach an exponential distribution with mean one again. If the failure rate changes after X_m from a constant to a Weibull failure rate function with $\alpha = 1/(1 + \theta)$ (keeping the same scale parameter), then it is easy to see that for $n >> m$ the variables $n \log (S_{n+1}/S_n)$ will be approximately independent exponential with mean $1/(1 + \theta)$.

In summary, then, the application of the procedures studied in the preceding sections to the sequence (16) leaves E_0N unchanged and should result in efficient detection whenever the failure rate increases sharply and continues to increase in the form of a Weibull failure rate function.

References

1. Lorden, G., "Procedures for Reacting to a Change in Distribution" (submitted to *Ann. Math. Statist.*).
2. Page, E. S., "Continuous Inspection Schemes," *Biometrika*, Vol. 41, pp. 100–115, 1954.
3. Lorden, G., "Sequential Tests for Exponential Distributions" (submitted to *Ann. Math. Statist.*).
4. Wald, A., *Sequential Analysis*. John Wiley & Sons, Inc., New York, 1947.
5. Dvoretzky, A., Kiefer, J., and Wolfowitz, J., "Sequential Decision Problems for Processes with Continuous Time Parameter: Testing Hypotheses," *Ann. Math. Statist.*, Vol. 24, pp. 254–264, 1950.
6. Doob, J. L., *Stochastic Processes*. John Wiley & Sons, Inc., New York, 1953.

Table 1. Comparison of actual and approximate expected stopping times

θ	γ	$E_\theta N$		$E_\theta N$	
		Actual	Approximate	Actual	Approximate
0.4	20	422.1	418.5	47.9	47.8
0.6	50	676.0	673.6	36.4	36.4
0.9	40	342.0	340.3	20.2	20.2

Table 2. Number of observations before detection (Monte Carlo sampling)

	Value of θ								
	−0.1	0	0.25	0.4	0.5	0.6	0.8	1.0	1.5
$E_\theta\widetilde{N}$ (60)	1701	508	96.3	53.9	42.2	35.0	26.2	21.3	15.8
	±181	±21	±2.5	±1.2	±1.0	±0.7	±0.4	±0.3	±0.2
% Efficiency[a]			85.5	94.7	96.1	96.2	96.3	95.6	89.1
$E_\theta\widetilde{N}$ (100)	2756	936	128.0	69.0	48.3	40.5	30.2	24.5	17.6
	±236	±48	±3.5	±1.6	±1.0	±0.7	±0.5	±0.3	±0.2
% Efficiency[a]			81.5	89.8	100.1	98.1	97.2	95.6	91.1

[a]The efficiency was estimated using the ratio of (sampled) $E_\theta\widetilde{N}$ to the $E_\theta N$ of a Page procedure for θ having the same $E_\theta N$ as $E_\theta\widetilde{N}$ (sampled).

Table 3. Values of $\theta E_\theta\widetilde{N}$ (sampled)

γ	Value of θ						
	0.25	0.4	0.5	0.6	0.8	1.0	1.5
60	24.1	21.6	21.1	21.0	21.0	21.3	23.7
100	32.0	27.6	24.2	24.3	24.2	24.5	26.4

On the Blizard Decoding Algorithm

L. R. Welch
University of Southern California

This article presents an analysis and modification of the new Blizard decoding algorithm, which promises to give performance superior to any known practical decoding algorithm on the deep space channel.

I. Introduction

In Ref. 1, R. B. Blizard describes a new method for decoding binary linear error correcting codes. The algorithm was presented ad hoc and the description was sketchy. In an attempt to understand his process, I have developed a modification which has a partly logical, partly heuristic derivation as an approximation to the maximum likelihood estimator. The computational complexity of these algorithms is within the range of practicability, while for most codes it is impractical to implement the maximum likelihood estimate.

The mathematical foundation, given here, reveals the assumptions needed to derive the algorithms. It is, however, necessary that an investigation be carried out to determine the suitability of these algorithms for specific codes and channels.

II. Preliminaries

Let $m_1, \cdots, m_k$ be random variables which take on the values 0 and 1. Let G be a k by n matrix of 0's and 1's and define

$$T_j = \sum_{i=1}^{k} m_i G_{ij} \bmod 2, \qquad j = 1, 2, \cdots, n$$

The m_i's are message bits, the T_j's are transmitted bits, and G is the generating matrix of the code. Finally, let $p(Z|0)$ and $p(Z|1)$ be two probability densities and $Z_1, \cdots, Z_n$ be random variables whose joint density, given $m_1, \cdots, m_k$, is

$$P(Z_1, \cdots, Z_n | m_1, \cdots, m_k) = \prod_{j=1}^{n} p(Z_j | T_j) \qquad (1)$$

The Z_i's are the received symbols of a memoryless channel.

The decoding problem is to determine functions $\hat{m}_i(Z_1, \cdots, Z_n)$ which satisfy some performance criterion. If all messages are equally likely and minimum probability of word error is desired, then the estimator is the maximum likelihood estimator, $(m_1^*, \cdots, m_k^*)$ which satisfies

$$P(Z_1, \cdots, Z_n | m_1^*, \cdots, m_k^*) = \max_{m_1, \cdots, m_k} P(Z_1, \cdots, Z_n | m_1, \cdots, m_k) \qquad (2)$$

In practice this estimator is not easily computed (with the exception of Viterbi's dynamic programming algorithm for convolutional codes with small memory) so that approximations are required to minimize equipment.

III. Derivation of the Algorithm

The algorithm begins with tentative probabilities assigned to the m_i's and attempts to repetitively improve these estimates by using the estimates as *a priori* probabilities and replacing them by *a posteriori* probabilities using the Z_j's. The goal is to achieve the maximum likelihood estimator.

Let $\{P_\theta : \theta = (\theta_1, \cdots, \theta_k), |\theta_i| \leqq 1\}$ be a parametric family of probability functions defined as follows:

$$P_\theta(Z_1, \cdots, Z_n, m_1, \cdots, m_k) = \prod_{j=1}^{n} P(Z_j | T_j) \prod_{i=1}^{k} \left(\frac{1 + (-1)^{m_i} \theta_i}{2} \right) \tag{3}$$

where T_j is defined as before. There are other methods for parameterizing this family but the θ's are convenient since $E_\theta[(-1)^{m_i}] = \theta_i$.

Observe that

$$\begin{aligned} P_\theta(Z_1, \cdots, Z_n) &= \sum_{m_1, \cdots, m_k} P(Z_1, \cdots, Z_n | m_1, \cdots, m_k) P_\theta(m_1, \cdots, m_k) \\ &\leqq \sum_{m_1, \cdots, m_k} P(Z_1, \cdots, Z_n | m^*, \cdots, m_k^*) P_\theta(m_1, \cdots, m_k) \\ &= P(Z_1, \cdots, Z_n | m_1^*, \cdots, m_k^*) \\ &= P_{\theta^*}(Z_1, \cdots, Z_n) \end{aligned} \tag{4}$$

where $(m_1^*, \cdots, m_k^*)$ is defined by Eq. (2) and $\theta_j^* = (-1)^{m_j^*}$. Therefore, θ^* is a solution to the problem of finding that θ which maximizes $P_\theta(Z_1, \cdots, Z_n)$. Conversely, if the maximum likelihood estimate is unique, the solution to the parametric maximization problem is unique and is at $\theta_j^* = (-1)^{m_j^*}$.

From the probability model defined by θ, the *a posteriori* probabilities $P_\theta(m_i | Z_1, \cdots, Z_n)$ and the *a posteriori* expectations

$$\theta_i'(\theta, Z_1, \cdots, Z_n) = E_\theta[(-1)^{m_i} | Z_1, \cdots, Z_n] \tag{5}$$

can be computed. The substitution of θ' for θ induces a transformation, $\sigma(\theta)$ defined by Eq. (5) on the parameter space. This transformation has been studied (Refs. 2 and 3) and is known that

$$P_{\sigma(\theta)}(Z_1, \cdots, Z_n) \geqq P_\theta(Z_1, \cdots, Z_n)$$

with equality only if $\theta = \sigma(\theta)$. Further, $\theta = \sigma(\theta)$ only at stationary points of $P_\theta(Z_1, \cdots, Z_n)$ (regarded as a function of only θ). This fact suggests the following procedure: select some θ^0 and define recursively $\theta^t = \sigma(\theta^{t-1})$ for $t = 1, 2, \cdots$. The function values $P_{\theta^t}(Z_1, \cdots, Z_n)$ increase and for almost all choices of θ^0 (i.e., except for a set of Lebesque measure 0), the sequence will converge to a local maximum (Ref. 3). Hopefully, if θ^0 is in a neutral position, the maximum point will have enough influence on the trajectory to be the point of convergence.

Next, consider the formula for $\sigma(\theta)$. Algebraic manipulation of Eqs. (3) and (5) results in the equation

$$\frac{1 + \theta_i'}{1 - \theta_i'} = \frac{P_\theta(Z_1, \cdots, Z_n | m_i = 0)}{P_\theta(Z_1, \cdots, Z_n | m_i = 1)} \frac{1 + \theta_i}{1 - \theta_i} \tag{6}$$

where

$$P_\theta(Z_1, \cdots, Z_n | m_i = a) = \sum_{\substack{m_1, \cdots, m_k = 0, 1 \\ m_i = a}} \prod_{j=1}^{n} P(Z_j | m_1, \cdots, m_k) \prod_{l \neq i} \left(\frac{1 + (-1)^{m_l} \theta_l}{2} \right) \tag{7}$$

This formula is of little practical value since the work required to evaluate it grows exponentially with k. However, if we assume that $P_\theta(Z_1, \cdots, Z_n | m_i = a)$ is well approximated by

$$\prod_{j=1}^{n} P_\theta(Z_j | m_i = a)$$

(that is, the Z's are conditionally independent given m_i), then the work is significantly reduced and Eq. (6) becomes

$$\frac{1+\theta_i'}{1-\theta_i'} = \frac{1+\theta_i}{1-\theta_i} \prod_{j=1}^{n} \frac{P_\theta(Z_j | m_i = 0)}{P_\theta(Z_j | m_i = 1)} \tag{8}$$

The jth factor can be written in terms of channel probabilities as

$$\frac{P_\theta(Z_j | m_i = 0)}{P_\theta(Z_j | m_i = 1)} = \frac{p(Z_j|0) P_\theta(T_j = 0 | m_i = 0) + p(Z_j|1) P_\theta(T_j = 1 | m_i = 0)}{p(Z_j|0) P_\theta(T_j = 0 | m_i = 1) + p(Z_j|1) P_\theta(T_j = 1 | m_i = 1)} \tag{9}$$

Now

$$T_j = \prod_{l=1}^{k} g_{lj} m_l$$

so that

$$E_\theta[(-1)^{T_j} | m_i = 0] = E_\theta\left[\prod_l (-1)^{m_l} \,\middle|\, m_i = 0\right] = \prod_{l \neq i} \theta_l \tag{10}$$

where the products are over all l for which $g_{lj} = 1$. Labelling the last product in Eq. (10), β_{ij}, reduces Eq. (9) to

$$\frac{P_\theta(Z_j | m_i = 0)}{P_\theta(Z_j | m_i = 1)} = \frac{p(Z_j|0)(1+\beta_{ij}) + p(Z_j|1)(1-\beta_{ij})}{p(Z_j|0)(1-\beta_{ij}) + p(Z_j|1)(1+\beta_{ij})} \tag{11}$$

provided $g_{ij} = 1$. If $g_{ij} = 0$, the ratio is 1. Equation (8) can now be written

$$\frac{1+\theta_i'}{1-\theta_i'} = \frac{1+\theta_i}{1-\theta_i} \prod_j \frac{p(Z_j|0)(1+\beta_{ij}) + p(Z_j|1)(1-\beta_{ij})}{p(Z_j|0)(1-\beta_{ij}) + p(Z_j|1)(1+\beta_{ij})} \tag{12}$$

where the product is over all j with $g_{ij} = 1$.

With the exception of the factor $(1+\theta_i)/(1-\theta_i)$, Eq. (12) is equivalent to Blizard's transformation. This additional factor has a conservative effect. If the probability of $m_i = 0$ is close to one and the product in Eq. (12) is less than one, then the transformation with the $(1+\theta_i)/(1-\theta_i)$ factor lessens the probability a small amount. While the transformation without the factor switches the probability to less than one-half.

Blizard's initial probabilities can be obtained in a natural manner from Eq. (12) as follows. If all messages are assumed equally probable, the initial parameter $\theta^0 = (0, \cdots, 0)$. In this case $\beta_{ij} = 0$ unless the product defining β_{ij} is empty, in which case $\beta_{ij} = 1$. This corresponds to $Tj = m_i$. If there is only one value of j for which this is true, Eq. (12) reduces to

$$\frac{1+\theta_i'}{1-\theta_i'} = \frac{p(Z_j|0)}{p(Z_j|1)} \tag{13}$$

which corresponds to Blizard's initial probabilities.

The suitability of these algorithms depends upon two things. First, the assumption

$$P_\theta(Z_1, \cdots, Z_n | m_i = a) = \prod_j P_\theta(Z_j | m_i = a)$$

should not do too much violence to the probability model. And secondly, the product factor in Eq. (12) should have a distribution which is not clustered too near 1.

References

1. Blizard, R. B., *Study of Applications of Digital Techniques to Apollo S-Band Communications, Phase 2, Final Report*, NASA-MCR 70-419. Martin Marietta Corp., Nov. 1970.

2. Baum, L. E., and Eagon, J. A., "An Inequality with Applications to Statistical Prediction for Functions of Markov Processes," *Bull. Am. Math. Soc.*, Vol. 73, pp. 360–363, 1967.

3. Baum, L. E., and Sell, G. R., "Growth Transformations for Functions on Manifolds," *Pacific J. Math.*, Vol. 27, pp. 211–222, 1968.

Improved RF Calibration Techniques: System Operating Noise Temperature Calibrations

M. S. Reid
Communications Elements Research Section

The system operating noise temperatures of the S-band research operational cone at DSS 13 (Venus Deep Space Station) and the polarization diversity S-band cone at DSS 14 (Mars DSS) are reported for the period February 1 through May 31, 1971.

The system operating noise temperature performance of the low noise research cones at the Goldstone Deep Space Communications Complex (GDSCC) is reported for the period February 1 through May 31, 1971. The operating noise temperature calibrations were performed with the ambient termination technique (Ref. 1). The cones on which this technique[1] was used during this reporting period are:

(1) S-band research operational (SRO) cone at DSS 13.

(2) Polarization diversity S-band (PDS) cone at DSS 14.

The averaged operating noise temperature calibrations for the various cones, and other calibration data, are presented in Table 1. The calibration data were reduced with JPL computer program number 5841000, CTS20B.

[1]Most of the measurements were taken by JPL DSS 13 (Venus) and DSS 14 (Mars) personnel.

Measurement errors of each data point average are recorded under the appropriate number in Table 1. The indicated errors are the standard deviation of the individual measurements and of the means, respectively. They do not include instrumentation systematic errors. The averages were computed using only data with:

(1) Antenna at zenith.

(2) Clear weather.

(3) No RF spur in the passband.

(4) Probable error of computed operating noise temperature due to measurement dispersion less than 0.1 K.

Table 1 shows that the SRO cone was operated on the ground at zenith. Eleven measurement sets were taken within 24 hours (May 18 and 19, 1971). The average system operating noise temperature was 13.9 K, whereas

the average for the reporting period with the cone on the antenna at zenith, at the same frequency, was 17.0 K. Eight measurement sets were made at the ALSEP frequency (2278.5 MHz); the average system operating noise temperature at this frequency was 18.8 K. Furthermore, one data set was made at the ALSEP frequency with the maser connected to a standard-gain horn looking through a section of the antenna surface opened for this purpose. The antenna was at zenith and the system operating noise temperature in this configuration was 25.9 K.

Figures 1, 2, and 3 are plots of the system operating noise temperatures of the SRO cone as a function of time in day numbers, at 2388, 2295, and 2278.5 MHz, respectively. Figure 4 is a plot of the system operating noise temperature of the SRO cone on the ground at 2388 MHz. Similarly, Fig. 5 shows the data for the PDS cone at 2298 MHz, low noise path.

In all the figures, data that satisfy the four conditions stated above are plotted as asterisks, while data that fail one or more conditions are plotted as circles.

Reference

1. Stelzried, C. T., "Operating Noise-Temperature Calibrations of Low-Noise Receiving Systems," *Microwave J.*, Vol. 14, No. 6, pp. 41–48, June 1971.

Table 1. Averaged operating noise temperature calibrations for the low noise research cones at GDSCC

Station	DSS 13					DSS 14	
Cone	SRO					PDS	
Configuration	Cone on ground	Cone on antenna	Cone on antenna	Cone on antenna	Standard gain horn	Low noise path	Diplexed
Frequency, MHz	2388	2388	2295	2278.5	2278.5	2298	2292
Maser serial number	96S2	96S2	96S2	96S2	96S2	96S3	96S3
Maser temperature, K	5.2	5.2	5.2	5.2	5.2	4	4
Maser gain, dB	38.0 ±0.16/0.05 11 measurements	37.3 ±0.21/0.03 48 measurements	50.1 ±0.46/0.12 15 measurements	44.0 ±0.82/0.29 8 measurements	45.4 1 measurement	53.9 ±0.37/0.11 7 measurements	53.6 ±0.56/0.32 3 measurements
Follow-up noise temperature contribution, K	0.43 ±0.12/0.006 11 measurements	0.50 ±0.02/0.003 35 measurements	0.15 ±0.07/0.02 11 measurements	0.53 ±0.42/0.15 8 measurements	0.28 1 measurement	0.02 ±0.004/0.001 8 measurements	0.02 ±0.004/0.002 3 measurements
System operating noise temperature, K	13.9 ±0.39/0.11 11 measurements	17.0 ±0.27/0.05 35 measurements	16.0 ±0.50/0.14 11 measurements	18.8 ±0.31/0.15 8 measurements	25.9 ±0.27 1 measurement	19.6 ±0.67/0.24 8 measurements	23.8 ±0.40/0.22 3 measurements

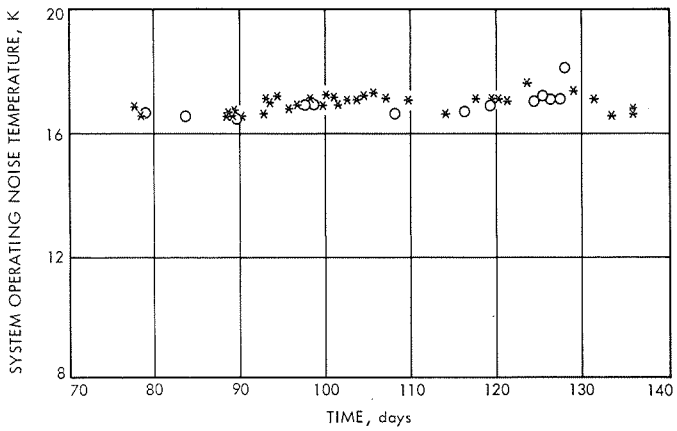

Fig. 1. System operating noise temperature of SRO cone at 2388 MHz at DSS 13

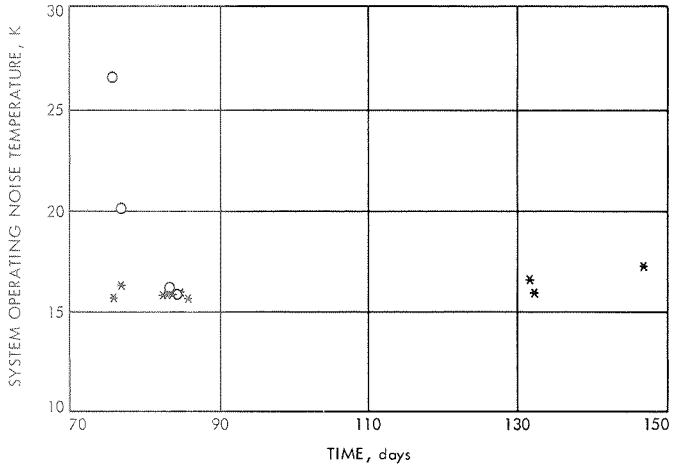

Fig. 2. System operating noise temperature of SRO cone at 2295 MHz at DSS 13

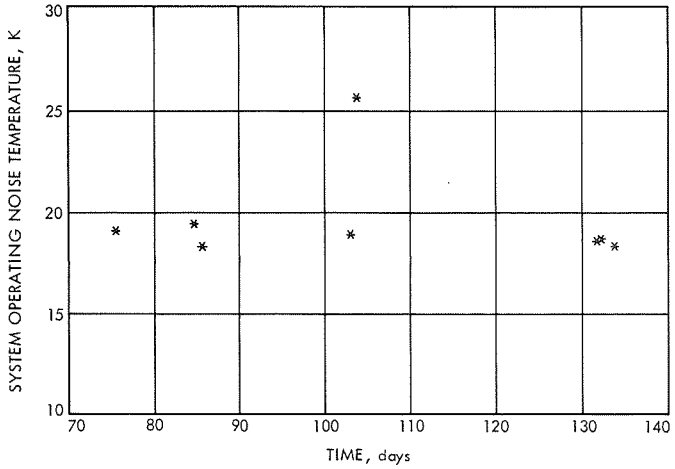

Fig. 3. System operating noise temperature of SRO cone at 2278.5 MHz at DSS 13

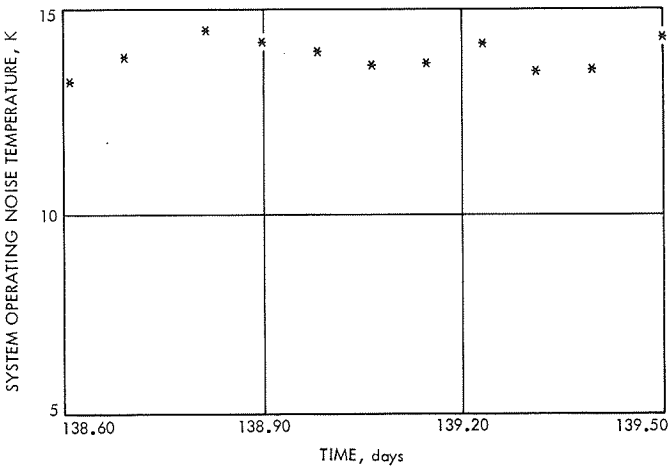

Fig. 4. System operating noise temperature of SRO cone at 2388 MHz on the ground at DSS 13

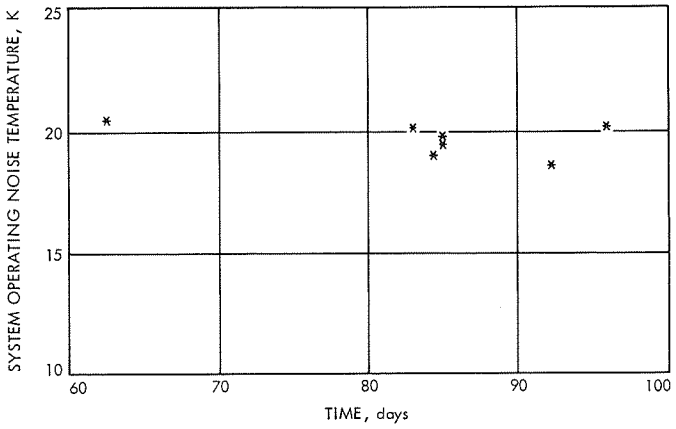

Fig. 5. System operating noise temperature of PDS cone at 2298 MHz at DSS 14

DSN Research and Technology Support

E. B. Jackson
R. F. Systems Development Section

Major activities of the Development Support Group at both DSS 13 (Venus Deep Space Station) and the Microwave Test Facility are presented, and accomplishments and progress for each are described. Activities include radio metric observations (20–25 GHz), pulsar observations and planetary radar, precision antenna gain measurement (RASCAL), weak source observations, 100-kW operational clock synchronization transmitter implementation, clock synchronization transmissions, and DSIF klystron testing.

The Development Support Group, Section 335, is currently engaged in the following activities at DSS 13 (Venus Deep Space Station) and the Microwave Test Facility (MTF) at GDSCC.

I. DSS 13 Activities

A. In Support of Section 325

Section 325 personnel continue to make extensive use of the 9-meter antenna using their 20–25 GHz radiometer. However, their observations are being concentrated on the planet Mars as it comes toward closest approach.

B. In Support of Section 331

1. Pulsars. The 20 pulsars tabulated in Ref. 1, page 158, continue to be regularly observed and data on pulse-to-pulse spacing, power density spectra, and pulse arrival time continue to be collected.

2. Planetary radar. The program continues with the emphasis having switched to the planet Mars, with precision ranging (to a resolution of better than 1500 meters) being accomplished thrice weekly in support of the *Viking* Project. Weekly ranging of the planet Venus to the same resolution also continues. The 2388-MHz 400-kW transmitter at DSS 14 has been reinstalled and ranging is now being done utilizing the DSS 14 64-meter antenna for both transmitting and receiving as well as continuing the bistatic ranging which utilizes the DSS 13 26-meter antenna for transmitting and the DSS 14 64-meter antenna for receiving.

C. In Support of Section 333

1. Precision antenna gain measurement. This effort has been named RAdio Source CALibration (RASCAL) and data are being taken utilizing the computer program described in Ref. 1, page 155, which has been titled SAmple and aVerAGE (SAVAGE).

2. Weak source observation. Data are being collected utilizing the Noise Adding Radiometer (NAR) technique. Radio sources regularly observed (weekly) include 3C218, 3C348, 3C353, 3C461, the planet Jupiter, and the Sun.

D. In Support of Section 335

The major support to this section is implementation of the 100-kW Operational Clock Synchronization Master

Transmitting Station. The high-voltage power supply, associated water and oil circulation systems, and the 450-kW heat exchanger have all been tested with four- and eight-hour heat runs at dc power levels up to 490 kW.

The power amplifier klystron has been received and installation of the amplifier, exciter, feed system, and waveguide will commence on July 1, 1971.

E. In Support of Section 337

Clock synchronization transmissions will continue to be made until July 1, 1971. At that time the system will be shut down to convert to the 100-kW configuration at the operational frequency of 7149.9 MHz. Stations to which transmissions are routinely being made include DSSs 14, 41, 42, 51, 62, and a station located at JPL in Pasadena.

II. Microwave Test Facility

A. In Support of Section 335

Utilizing the protoype construction capabilities of the facility, the driver amplifier for the 100-kW X-band clock synchronization amplifier klystron is being constructed and tested. Additionally, other support (machining, wiring, etc.) is being given to the project as needed.

B. In Support of Section 337

Testing of DSIF amplifier (10 and 20 kW) klystrons continues on an as-needed basis.

Reference

1. Jackson, E. B., "DSN Research and Technology Support," in *The Deep Space Network Progress Report*, Technical Report 32-1526, Vol. III, pp. 154–158. Jet Propulsion Laboratory, Pasadena, Calif., June 15, 1971.

S-Band Planetary Radar Receiver Development

C. F. Foster
R. F. Systems Development Section

This article describes the design modification of the DSS 14 bistatic radar receiver. This receiver is basically an open-loop superheterodyne receiver used for development of communication techniques. The modifications include wider bandwidths to support high-speed, high-resolution planetary mapping, and the redistribution of system gain to prevent noise saturation. The redesigned bistatic radar receiver has been installed at DSS 14 and is now being used in the Venus radar mapping experiment.

I. Introduction

The bistatic radar receiver (Ref. 1) has undergone extensive design changes because of improvements in several subsystems at DSS 14 [e.g., high-performance maser (Ref. 2) and hydrogen maser reference generator (Ref. 3)] and the need to support wide-bandwidth high-resolution radar mapping experiments. The IF frequency was changed from 455 kHz to 2.5 MHz with a bandwidth increase from 400 kHz to 2 MHz at the −3-dB points. The gain of the receiver was redistributed to prevent overloading on noise. The cabling, switching, and the frequency distribution system were simplified to provide more reliable operation.

II. Implementation

The recent installation of a high-performance maser and a microwave signal distribution system added 15 dB of S-band gain. This gain increase caused the S-band converter (Fig. 1) to overload on noise when looking at the ambient load, making it impossible to measure system noise temperature. The problem has been solved by redesigning the pre-amplifier and reducing its gain by 15 dB. The gain compression curves of the mixer preamplifier are shown in Fig. 2.

The redesigned 30- to 2.5-MHz converter (Fig. 1) consists of a 30-MHz power divider, tubular bandpass filter with a 3-dB bandwidth of 2 MHz, a switchable crystal filter module with either 3 MHz or 400 kHz, 3-dB bandwidths, wide-band double-balanced mixer, low-pass filter to remove the second local oscillator interference, and a video amplifier. The output of this converter is sent via the inter-site microwave link to DSS 13 for detection and data processing. (A plot of the two system bandwidths is shown in Figs. 3 and 4.)

A 30- to 50-MHz converter with a 10-MHz bandwidth was designed and installed in order to interface the bistatic radar receiver with the standard DSIF maser instrumentation eliminating the requirement for additional maser instrumentation to service the R&D receiver.

III. Conclusion

The bistatic radar receiver has been successfully modified and installed at DSS 14 and is being used to support the Venus radar mapping experiment.

References

1. Foster, C. F., "S-Band Planetary Radar Receiver Development," in *The Deep Space Network*, Space Programs Summary 37-41, Vol. III, pp. 107–110. Jet Propulsion Laboratory, Pasadena, Calif., Sept. 30, 1966.
2. Clauss, R., and Quinn, R., "Low-Noise Receivers: Microwave Maser Development," in *The Deep Space Network*, Space Programs Summary 37-58, Vol. II, pp. 50–52. Jet Propulsion Laboratory, Pasadena, Calif., July 31, 1969.
3. Sward, A., "Frequency Generation and Control: The Hydrogen Maser Frequency Standard," in *The Deep Space Network*, Space Programs Summary 37-59, Vol. II, pp. 40–43. Jet Propulsion Laboratory, Pasadena, Calif., Sept. 30, 1969.

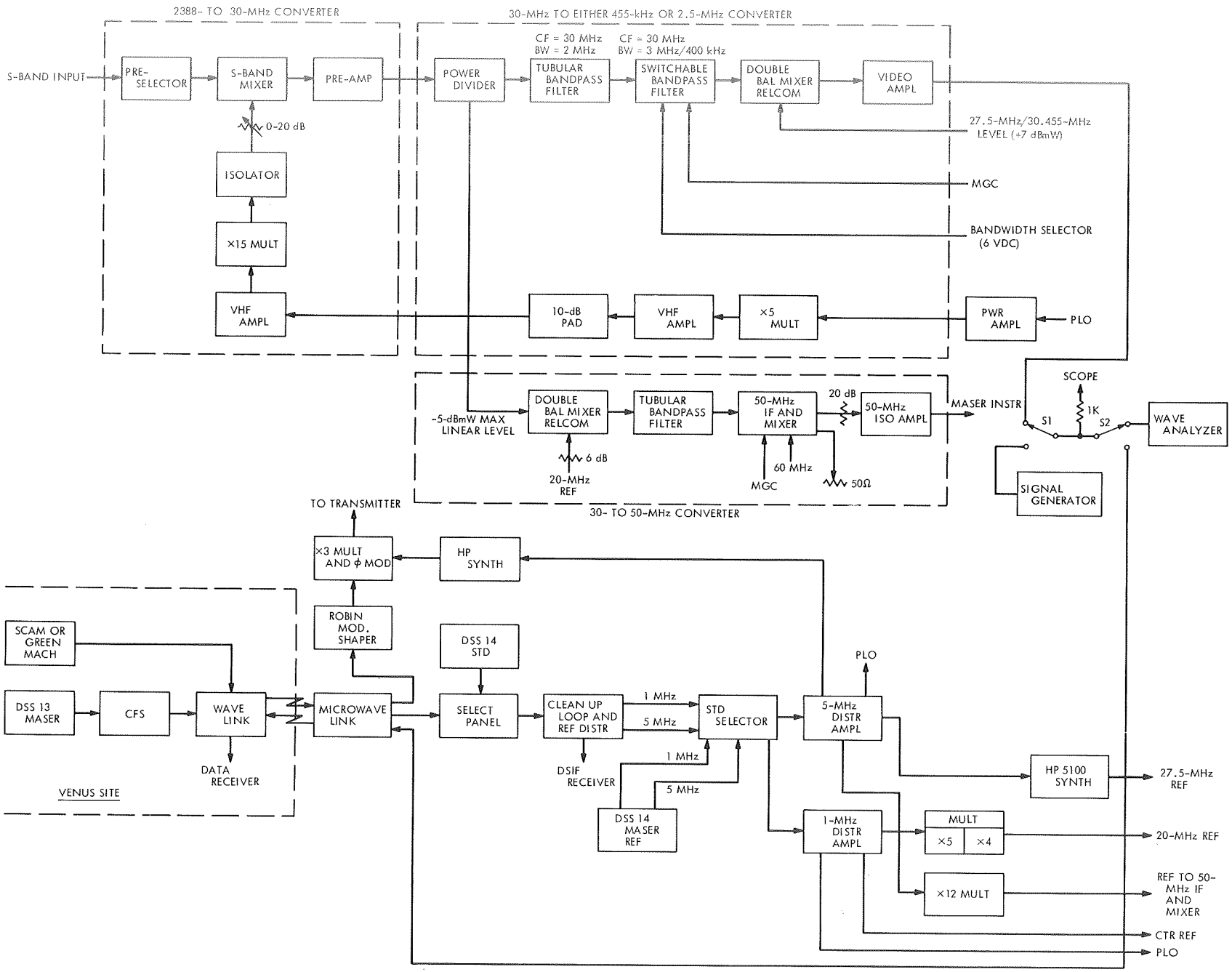

Fig. 1. Bistatic radar receiver block diagram

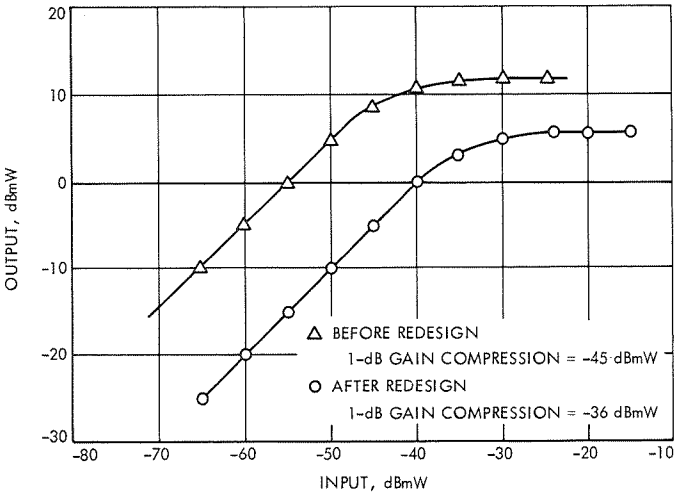

Fig. 2. Mixer/pre-amplifier gain curve

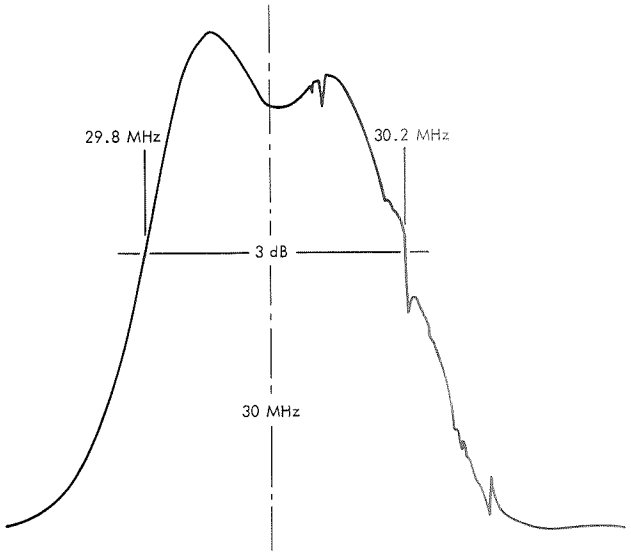

Fig. 3. Bistatic radar receiver: overall bandpass narrow filter

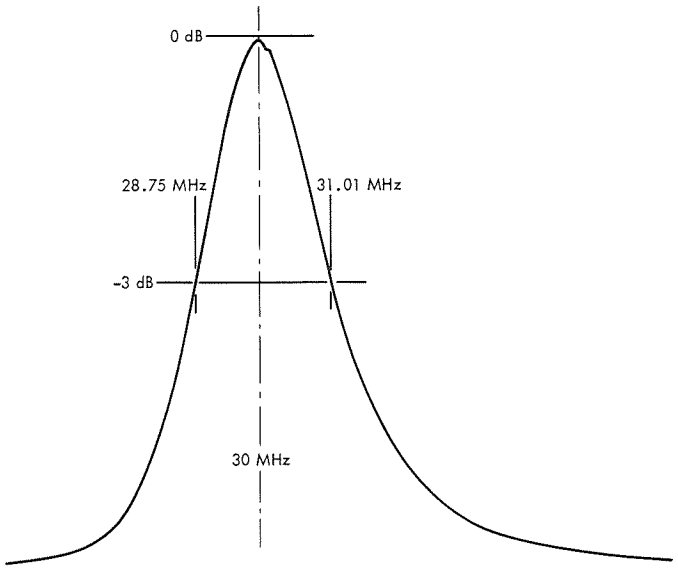

Fig. 4. Bistatic radar receiver: overall bandpass wide-band filter

SFOF Digital Television Display Subassembly

F. L. Singleton
SFOF/GCF Development Section

This article describes the Space Flight Operations Facility (SFOF) digital television display subassembly, which is a part of the digital television assembly. It accepts input digital data from the computer subassembly, converts it to video data, stores it and provides a continuous television-compatible video output which is distributed throughout the SFOF. The display subassembly consists of a system control unit, four display generator units and various hardcopy generation equipment.

I. Introduction

The digital television display subassembly is a part of the digital television assembly (DTV) of the user terminal and display subsystem in the SFOF. The purpose of the DTV is to provide flight projects and DSN users with volatile real-time displays of spacecraft data and DSN equipment status. As a part of the DTV, the display subassembly provides a digital-to-video conversion capability with storage and refresh capability for multiple channels of alphanumeric and graphic information display. This subassembly is shown in Fig. 1. The display subassembly and the computer subassembly make up the DTV. This article supplements two previous ones on the DTV (Ref. 1) and the computer subassembly (Ref. 2).

The display subassembly includes interfacing equipment, display generation equipment and hardcopy equipment. This article provides details on the display subassembly design approach, interface characteristics, and display generation capability. "SFOF Digital Television Hardcopy Equipment," by K. Kawano and F. L. Singleton in this issue, discusses the hardcopy generation capability.

II. Display Subassembly Requirements

Within the DTV, the display subassembly's primary purpose is the conversion of digital information into a video format and outputting this video data. To achieve this purpose, the display subassembly must be able to accept formatted digital data, convert this data into a video signal containing alphanumeric and graphic data suitable for TV display, provide multichannel storage of the video signals, and constantly refresh the video signal outputs to the TV displays.

Because the display subassembly outputs are distributed to standard TV monitors, these video outputs must meet standard TV format requirements. This format is as follows: A standard TV frame consists of a horizontal raster of 480 visible scan lines. Each frame consists of two fields A and B with 240 visible scan lines each. The two fields are scanned on the television screen alternately so that the 240 scan lines in one field physically interlace with those of the other field. The rate at which the fields are scanned is 60 per second, a rate which is sufficiently fast to appear to the human eye as a single visible display. In order to update data on the screen, the display subassembly must be able to address specific locations on the screen in either field.

III. Design Approach

The input to the display subassembly is digital data from the computer subassembly. The system control unit (SCU) serves as the interface between the computer subassembly and the display subassembly. Digital data is accepted by the SCU and passed on to the display generators or the hardcopy equipment.

The conversion of digital data into TV-compatible video data required digital data buffering, logic for channel selection, alphanumeric character generation, graphic data generation, address location, and timing synchronization. These functions were combined into a display generator unit for each 20 DTV channels.

In order to provide multichannel storage for video data, a mass storage device was required. To be TV-compatible required constant refreshing of display outputs in synchronism with the existing TV distribution equipment. The design approach which satisfied both mass storage and constant refreshing was a rotating mass memory device. A disk memory was selected for this design because it was a rotating mass memory device that could be synchronized to the TV distribution equipment. Storage for 20 DTV channels was provided on each of four disk memory units.

Input and output interfaces to the disk memory and amplifiers for video output were included in the display generator logic, providing common logic for 20 DTV channels in each of four display generators.

Because the data conversion and storage capability was provided in 20 channel increments, future expansion capability was made by allowing interfaces for up to six display generators on the SCU. This provision permits expansion to 120 channels.

IV. Functional Description of the DTV Display Subassembly

This subassembly consists of the following units: one system control unit, four display generators, one display image buffer, twelve copy request units and twelve hardcopy printers (Fig. 2).

The display image buffer, copy request units, and hardcopy printers are all part of the hardcopy equipment.

Each of these units has been provided to meet the requirements for the display subassembly. In the following discussion, the functional aspects of the display subassembly are described in an attempt to provide a better understanding of how the design approach has been implemented.

V. Digital Input Interface

The display subassembly under the control of the computer subassembly generates video displays and hardcopy outputs. The SCU interfaces with the computer subassembly and provides overall integration of the display subassembly. Although the SCU receives two input sources from the computer subassembly, only one input at a time can have control of the SCU and therefore of the display subassembly. SCU circuitry locks out the second input when the first is connected until a complete message is transferred.

The SCU, acting much like a peripheral controller to the computer subassembly, routes the data and instructions to the computer-specified unit in the display subassembly. The SCU, as commanded by the computer subassembly, connects to a specific device (such as a display generator) and transfers the incoming digital data to that device on a demand-response basis.

In addition to data routing, the SCU also provides a data translation function by packing two 12-bit bytes input from the computer subassembly into one 16-bit word for output to the display generators. Unused portions of each 12-bit byte are discarded.

VI. Display Generation

Four display generators are attached to the SCU by a common data bus. Only one display generator at a time is selected for data transfer. Each of these units is identical to the other and contains the necessary logic for data conversion and output to the TV monitors. A block diagram of the display generator is shown in Fig. 3. The various logic blocks shown in that figure are used in the discussion to follow.

The data to be displayed on the DTV channels may be alphanumeric or graphic. Each display generator has both alphanumeric and graphic data generation capability. The alphanumeric characters consist of 96 characters selectable by standard 7-bit American Standard Code for Information Interchange (ASCII) codes. The

graphic data can be displayed in several modes as selected by instructions in the digital buffer memory; either as specific 8-bit patterns contained in the data, as 8-bit by 12-line matrix of data bits contained in the data, or as horizontal and vertical line segments with specified start and end points. The graphics capability discussed is the inherent hardware capability within the display subassembly.

Within the connected display generator, all instructions and data are first transferred into a digital buffer memory. The digital buffer can store up to 256 16-bit words, either instructions or data. It also holds these instructions and data so that they can be output repeatedly, when required in generating characters or other display data on more than one line or field of the screen.

To generate video displays, the display generation logic reads out data in sequence from the digital buffer memory. The general sequence of data read out from the digital buffer is as follows: (1) an instruction selecting the mode of operation (e.g., alphanumeric or graphic) is output to the control logic; (2) an instruction selecting the DTV channel and the corresponding disk memory channel is output to the channel select logic; (3) instructions selecting the starting X and Y addresses are loaded into the element and line address registers; and (4) these instructions are followed by alphanumeric or graphic data.

The channel select logic enables the correct gating in the write electronics so that data can be written on the selected channel. The element and line address registers store the addresses for selecting the appropriate location on the disk memory.

In order to convert alphanumeric data into a video display output, the data is transferred from the digital buffer to the character data generation logic. There the ASCII code selects the corresponding matrix from the alphanumeric read-only-memory. Then, sequential readout of the correct bit pattern from the read-only-memory occurs when the disk memory reaches the desired X and Y locations. With graphic data, the digital data is transferred through the graphic data generation logic.

The data selection and control logic selects either alphanumeric inputs from the alphanumeric read-only-memory or direct graphic data inputs from the graphic data generation logic and presents them to the input of the write electronics.

When the element and line address stored in the X and Y registers agree with the actual disk position as read out by the element and line counters, the comparison logic causes the write enable logic to command the write electronics to write data on the disk memory channel selected. Data written on a disk memory channel is automatically output as video data which is then displayed on the TV screens throughout the SFOF.

The display information may consist of up to 3200 alphanumeric characters in the 96-character ASCII set, any of various graphic modes, and may be positioned anywhere on a television screen. Alphanumeric or graphic data can be individually added or deleted without disturbing an existing display. The display generation logic can generate dark images on a light background or light images on a dark background, as well as generate four selectable character sizes.

VII. Timing Considerations

In all modes of operation, it is important to write the video bit patterns on exact locations of the disk which correspond to the desired television screen location. To accomplish this correspondence, a prerecorded clock signal from the disk memory is output to the element (X) and line (Y) counters of the display generator. The element and line counters count the stored clock signal and issue a binary code that designates the exact position of the rotating disk. The position of the disk is compared with the desired starting position for writing the next byte of information. A write-enable signal is generated at coincidence of these positions and remains enabled until the control logic determines the end of the operation in progress.

VIII. Disk Memory Data Storage

The video bit pattern generated by the display generator is stored on 80 tracks of a disk memory and then used to generate or refresh a video display on 20 video channel outputs. The data bits are written on the disk on four parallel tracks per DTV channel simultaneously at a nominal 3 MHz rate. The write data bits are stored 4-bits in parallel on the disk, but when read from the disk, are shifted from a parallel to a serial 12-MHz bit stream. Each stored data bit corresponds to an element address on the television monitor screen.

Data bits are written as either a logic 1 or logic 0 signal by the write electronics. The data bit written as

a logic 1 is caused by a flux transition in one direction and a data bit written as a logic 0 is caused by a flux transition in the opposite direction on the surface of the disk.

The manner in which the element and line counters count allows data to be recorded on the disk memory in a format identical to the horizontal scan television raster. It is recorded basically in the same time sequence as it is displayed on the TV screen. However, since physical location on the disk surface corresponds to a physical location on the screen, the individual elements of each line plus retrace and blanking times must be allowed for in disk recording. Also, since most data is recorded on both fields of the display, the data must be recorded on the disk on the first recorded field and on the second recorded field, half a revolution away on the disk.

This means that nearly all digital input data must be held over for processing on both fields of the disk memory (and display). The digital buffer memory is utilized to accomplish this. Data can be read from the digital buffer once for processing in field A and then read out again, 1/60th of a second later, for processing in field B. Data is held in the digital buffer until it is no longer required for display generation.

IX. Video Output Distribution

Each of the four display generators provides conditioning of the twenty disk memory channel outputs to provide a continuous noncomposite video signal output through video amplifiers to the television distribution equipment for 80 DTV channels. This equipment distributes these 80 channels to TV monitors throughout the SFOF.

This conditioning provides the correct signal levels and impedances but the manner in which the video data is recorded on the disk memory provides the proper TV-compatible signal content.

The video output frequency and frame synchronism are directly related to the disk memory rotation. Correct video output transmission has been accomplished by synchronizing the speed of rotation of the disk memory in each display generator to the SFOF-supplied TV sync. A servo control unit is associated with each disk memory which derives its output from the TV synchronizing signals. This output provides speed control signals to the disk memory motor and matches its speed to the TV sync rate.

Each rotation of the disk memory will cause one complete TV frame to be output per DTV channel. When this disk is synced to the TV sync source, it will rotate at 30 rev/s, producing a 30-frame/s or 60-field/s output rate.

X. Hardcopy Interface

Each display generator supplies a one channel video bit pattern output for use in hardcopy generation. Under control of the display image buffer (DIB), the DIB monitor channel in each display generator can be switched to output any one of the twenty DTV channels in that display generator. This data is presented to the DIB for use in recording and printing a hardcopy of any DTV channel.

XI. Conclusion

The DTV display subassembly was designed to meet the requirements for digital-to-video conversion, storage, and refresh of 80 video output channels. This design utilizes disk memories for video storage and refresh, and provides input digital buffering to allow optimum use of the disk memories. The resultant video data is ready for output to the existing television monitors used throughout the SFOF. This display has been operating in support of the current DSN commitments to *Mariner* '71 since January, 1971. The expanded 80-channel capability and hardcopy expansion were installed in March, 1971, in preparation for expanded DSN support for the *Pioneer F* mission.

References

1. Singleton, F. L., "SFOF Digital Television Assembly," in *The Deep Space Network*, Space Programs Summary 37-65, Vol. II, pp. 86–91. Jet Propulsion Laboratory, Pasadena, Calif., Sept. 30, 1970.

2. Leach, G. E., "SFOF Digital Television Computer Subassembly," in *The Deep Space Network Progress Report*, Technical Report 32-1526, Vol. III, pp. 175–178. Jet Propulsion Laboratory, Pasadena, Calif., June 15, 1971.

Fig. 1. DTV display subassembly

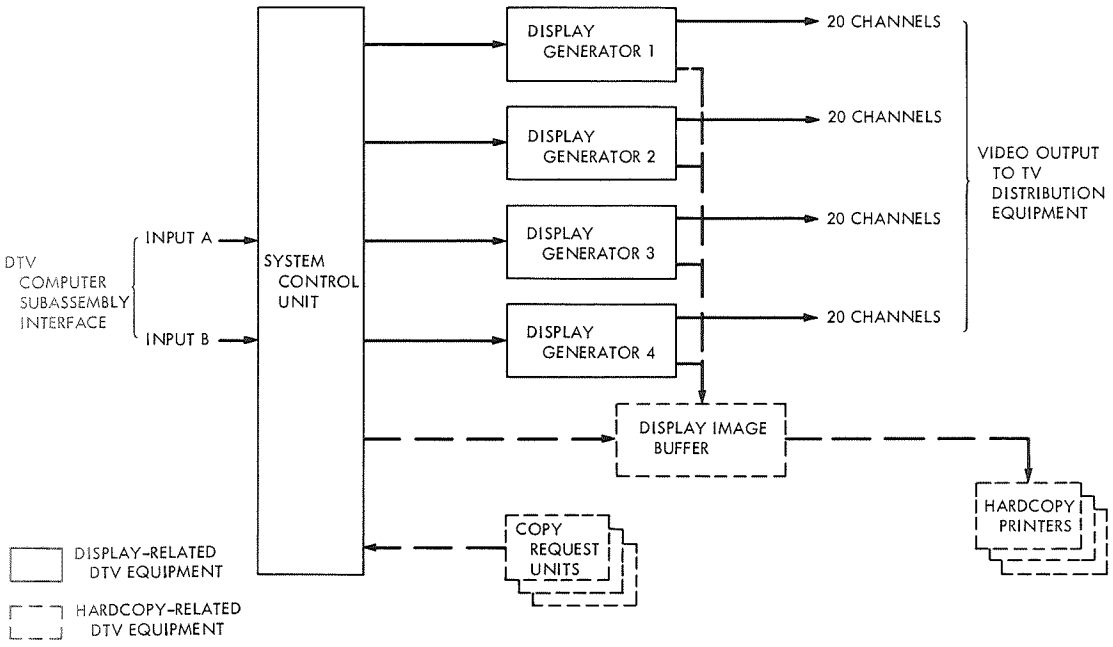

Fig. 2. DTV display subassembly block diagram

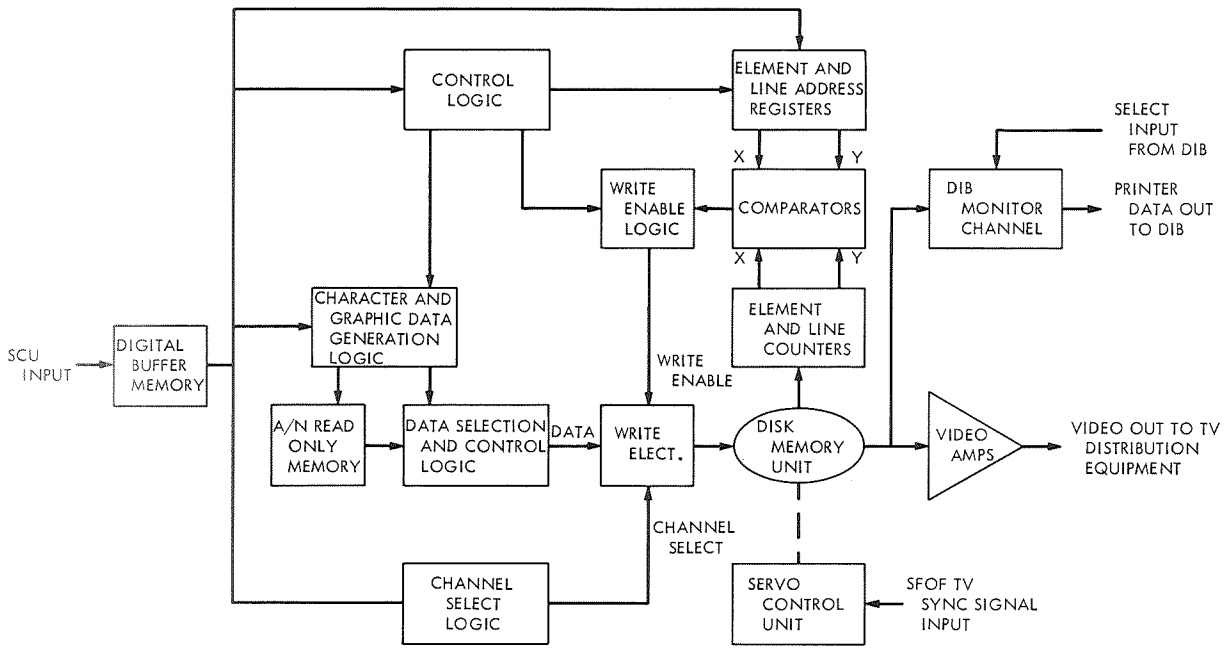

Fig. 3. Display generator block diagram

SFOF Digital Television Hardcopy Equipment

F. L. Singleton and K. Kawano
SFOF/GCF Development Section

The Space Flight Operations Facility (SFOF) digital television display subassembly has a hardcopy generation capability in addition to its display generation capability. The hardcopy capability is discussed in this article.

The display subassembly hardcopy equipment consists of a system control unit, twelve copy request units, a display image buffer and twelve hardcopy printers. The hardcopy equipment can make a print of any digital television display channel upon request.

I. Introduction

The SFOF Digital Television Assembly (DTV) has the capability to provide a hardcopy print of any DTV display channel when requested. This capability is provided within the display subassembly of the DTV. The DTV was previously discussed in Ref. 1. The display generation capability of the display subassembly is discussed in "SFOF Digital Television Display Subassembly," by F. L. Singleton in this issue. This article discusses the hardcopy capability of the display subassembly.

II. Requirements

The DTV is used in the SFOF for display of data for real-time usage. Each user has displayed data unique to his usage. In the course of operations, there will be displayed data that the user will need for a period longer than the normal update of his DTV display. This display may be needed to compare a parameter with subsequent displays or the display may need to be used in an area removed from the DTV display. Recall of stored data to a line printer for this purpose would not be practical. A conveniently located hardcopy system that allows printout of selected DTV images is required.

III. Design Approach

In order to meet the requirements for hardcopy output, the following decisions were made:

a. There will be several hardcopy devices distributed in the various user areas for user convenience.

b. An exact image of the DTV display will be printed for output accuracy.

c. High-speed printing is not required because of the low frequency of usage.

d. Any interference with display updates to produce a hardcopy will be minimized to maintain maximum throughput of DTV data.

Both the copy request units and hardcopy printers will be located in the various user areas of the SFOF.

Hardcopy requests will be initiated by the user at his copy request unit and the requested display will be printed by the printer associated with that copy request unit.

Copy requests will be input to the DTV computer subassembly and it will issue output instructions causing a print to be made. This will allow the computer subassembly to inhibit data output to a DTV display channel while its data is being recorded for printer output. However, it is desirable to reduce the amount of time data output is inhibited to a display generator of the display subassembly. Thus, an intermediate hardcopy controller will store the display data and output it to the hardcopy printer in the format and at the rate required by that printer. This controller is called the display image buffer (DIB) and it performs the various data transfer functions required to make a print of a display on a given DTV channel.

IV. Description of the DTV Hardcopy Equipment

The hardcopy equipment consists of twelve copy request units (CRU), the display image buffer (DIB), twelve hardcopy printers, and portions of the system control unit (SCU). A block diagram of the DTV display subassembly is shown in Fig. 1 with the hardcopy equipment identified in solid lines. A functional description of this equipment follows.

V. Copy Request Unit

The CRU is used to request printouts from a hardcopy printer. This unit is shown in Fig. 2. Each CRU consists of two thumbwheel digiswitches for DTV channel selection and an ENTER button for requesting hardcopy prints. The unit is interfaced to the computer subassembly through the SCU.

When a copy request button is pushed, an interrupt signal is routed to the computer subassembly by the SCU. The interrupt activates a hardcopy request sequence. The computer subassembly causes the SCU to output to it the digiswitch settings of all CRUs. Each CRU is associated with a specific printer and a request from that unit will cause a print to be outputted by its associated printer.

The computer subassembly will then connect to the DIB through the SCU and issue a record and print instruction. This instruction tells the DIB to record the selected DTV channel on the print channel associated with the requesting CRU and output that data by the printer.

The *enter* button light on the CRU is normally lit to indicate that it is ready to accept requests. When the button is pressed, the light will go out until the computer has taken the request. Any subsequent request will not be honored until the light turns back on. Once a request has been honored, another request can be made; however, before this second request can be acted upon, the print cycle for the first request must be completed. Therefore the light will remain out for the second request until the first print cycle is completed. At that point another request will be honored and will be acted upon when the second print cycle is completed.

There is a CRU associated with the maintenance monitor TV in the display subassembly. It is named the display request unit (DRU) and is located directly below the maintenance monitor. Its operation is exactly the same as that of a CRU except that the output is an immediate video display on the maintenance monitor. The image on the monitor is generated directly from the DIB disk memory. This monitor and DRU are used exclusively for DTV maintenance purposes.

VI. Display Image Buffer

The DIB acts as the hardcopy controller within the display subassembly. The DIB interfaces with the SCU, the display generators, and the hardcopy printers. The DIB contains the disk memory storage of hardcopy output data and the selection and interface logic to transfer any display generator DTV channel video signal into its disk memory storage and to convert this video data into printer-compatible data and output it to hardcopy printers.

The DIB is activated by a Record and Print instruction originating in the DTV computer subassembly as a result of a hardcopy request. Each instruction is transmitted to the DIB via the SCU. The instruction identifies the display generator, the display generator DTV channel, and the printer channel to be selected.

Each Record and Print instruction causes the following operations to occur: (1) The DIB outputs a select

signal to each display generator selecting the specified display generator channel; (2) The DIB selects the printer channel for recording on the disk memory, (3) The DIB enables the selected display generator input to the disk memory, and (4) The DIB records the video data from the display generator on the disk memory channel. (5) The DIB also issues a printer start signal, and after the printer is up to speed, (6) it outputs digital data at printer rates to the hardcopy printer. After the end of data transmission the DIB then (7) outputs a paper advance signal until the correct paper width for a 21.6 × 27.9 cm (8.5 × 11 in.) sheet of paper has been output.

Upon issuance of a Record and Print instruction, output of video display data to the affected display generator will be inhibited until the data is transferred from the display generator to the DIB disk memory storage. This data is transferred at a 3-MHz rate. Upon completion of transfer, the display generator is released for updates. The transfer normally requires two disk revolutions (1/15 s). Never is this inhibit time greater than 1/10 s. The above sequence is the Record portion of the Record and Print operation.

The Print operation for each instruction includes the following: (1) The DIB issues a paper start signal to the selected printer which starts the paper while the printer motor comes up to speed. After 0.5 s of paper movement, the DIB (2) starts data readout from its storage. (3) Data which creates the first scan line of a video image is transferred to the print buffer at 63 kHz rate. (4) The data is then printed as a row of dots as it would appear on a TV screen. (5) At the next scan line time (1/60 s) the next line is printed. This process takes place until all 480 lines, which constitute the visible DTV image, are printed. This process requires 8 s. At the conclusion of this process, the print cycle is over. However, the paper movement continues for another 2.5 s to allow for the bottom margin of the print. Each print cycle is about 11 s. A new print cycle will not be initiated until this paper movement is completed.

During the operations described in the foregoing,several more instructions to record and print images from other display channels to other printers may occur. Each command will be honored in sequence by the transfer of the image from the display storage to its print storage. However, once a print cycle has started, all printers are synchronized with it and no new cycle can be initiated until its completion. Thus, all new print requests will wait in their storage until a new print cycle starts. A new cycle can be started immediately after the conclusion of its predecessor and no paper stoppages need to occur on a printer already in motion. All the waiting printers will now start in unison and proceed with the print process described above. The printer just concluding its prints has the margin paper advance time mentioned above to receive a new print image.

The DIB is presently configured for 12 printer outputs and one monitor output.

VII. Hardcopy Printer

The DTV hardcopy printer is a Gould, Model 4800, electrostatic printer. A photo of this printer is shown in Fig. 3. The printer prints on a 27.9 cm-(11-in.) wide roll of paper which is continuously advanced during the print cycle. The printing process occurs by passing the paper over a write head where the paper is charged with a print pattern. The paper is then passed over a liquid toner bath where it picks up charged particles to form dark images on the white paper. As the paper advances it dries so that the copy output is nearly dry as it comes out of the printer and is completely dry within seconds after it comes out of the printer.

The printer accepts a 63 kHz digital bit stream input and converts it into an exact image of the DTV display, 640 elements by 480 lines. The image occupies an area 15.2 × 20.3 cm (6 × 8 in.) within a page of 21.6 × 27.9 cm (8.5 × 11 in.). The printer paper advance and line printing are both controlled by signals from the DIB. A sample of the hardcopy print is shown in Fig. 4.

The hardcopy printer and the copy request units are designed so that they may be located up to 305 m (1000 ft) from the DTV.

VIII. Expansion Capability

The Display subassembly is designed to have expansion capability. The hardcopy unit, currently, has the capability to drive 12 printers and one TV monitor. The unit is capable of 19 printers and a monitor or 20 printers without a monitor.

Currently, there are 12 CRUs. The unit is capable of up to 32 CRUs including the DRU. The current DTV software does not use more than one CRU per printer. However, future software will allow more than one user the capability to get prints from one shared printer.

IX. Conclusion

The SFOF Digital Television Assembly is provided with a hardcopy capability to support operations and development. An exact replica of the real time-display may be printed for near-real-time usage.

The hardcopy capability can be expanded for future usage. Currently, the DSN system operations area, the *Mariner* Mars '71 mission support areas, and the development areas are being supported by DTV hardcopy capability. The *Pioneer F* mission support areas are being configured and will also be supported by DTV hardcopy capability.

Reference

1. Singleton, F. L., "SFOF Digital Television Assembly," in *The Deep Space Network,* Space Programs Summary 37-65, Vol. II, pp. 86–91. Jet Propulsion Laboratory, Pasadena, Calif., Sept. 30, 1970.

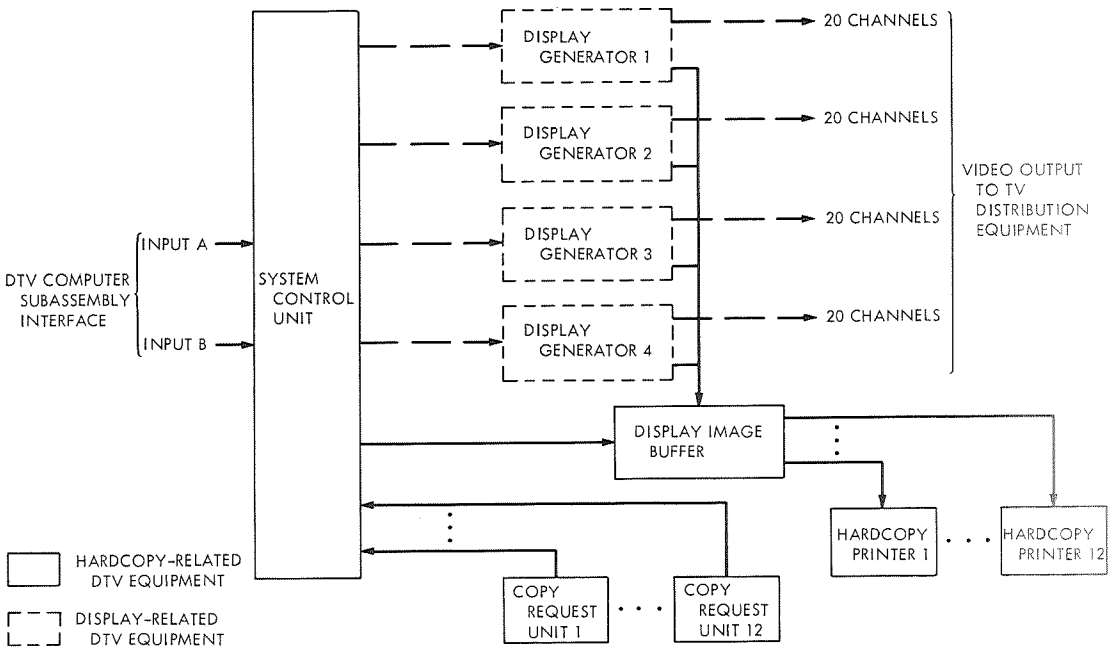

Fig. 1. DTV display subassembly block diagram

Fig. 2. DTV copy request unit

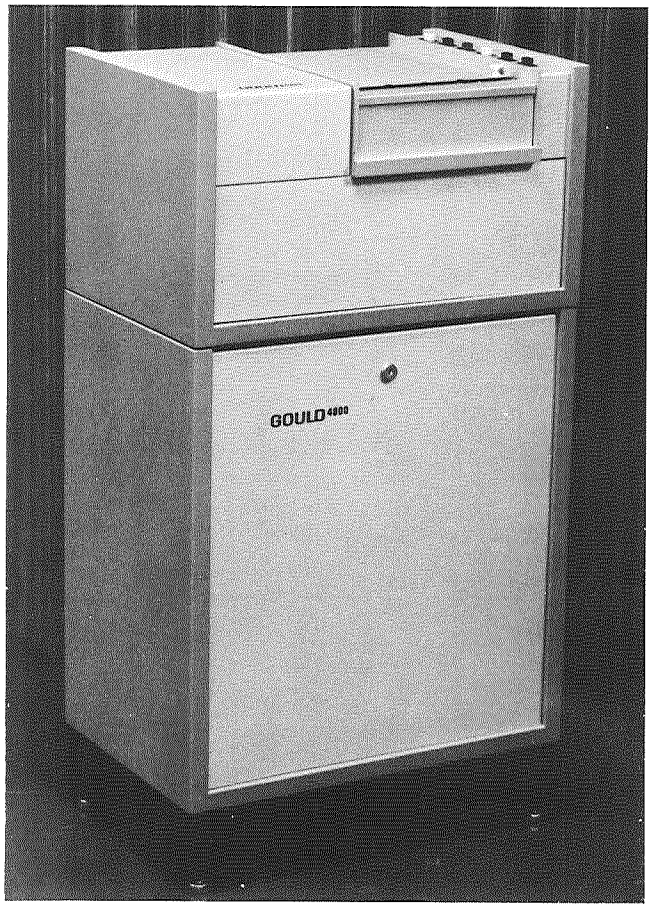

Fig. 3. DTV hardcopy printer

PRINT WIDTH 20 cm (8 in.)

PRINT HEIGHT 15 cm (6 in.)

```
SC-84 DSS-14   17:00:58 312-13   FORMAT646
DPQ=2
 S/C ID          STP NUMBR       G CONF E
  M71-1           0410.1        R1D2TACB
  15:32:11
 P GYRO/SS       Y GYRO/SS       R GYRO/FP
    51              79              66

 P POS/AGA       Y POS/BGA       R POS CRS
    59              69              64
                                  -.2039E-01
 CT INTENS       +X-Y N2 M       COUNTER 2
    68             .2699E+01          1
   .1250E+01
 ADAP GATE       -X+Y N2 M       COUNTER 3
     0             .2690E+01          2
   .0000E+00
 CT CONE         S/C POWER       30V REG P
     0             .2147E+03        .3491E+00
   .0000E+00
```

Fig. 4. Typical hardcopy print example

Mark IIIA Simulation Center Diagnostic Software

C. F. Leahey
SFOF/GCF Development Section

The expansion and reconfiguration of the Deep Space Network (DSN) simulation center to the Mark IIIA configuration necessitated the modification of existing diagnostic software and the development of new diagnostic and test programs. This article describes the characteristics of the diagnostics which were developed for the EMR 6050-Univac 1108 interface and the Interactive Alphanumeric Television Display System.

I. Introduction

The Mark IIIA Simulation Center is presently undergoing development activity in preparation for *Mariner* Mars '71 and *Pioneer F* support. This activity was described in Ref. 1.

The expansion and reconfiguration of the input/output necessitated the modification of existing diagnostic software and the development of new diagnostic and test programs for the SIMCEN. This article describes the characteristics of the diagnostics which were developed for the EMR 6050–Univac 1108 interface and the Interactive Alphanumeric Television System. The EMR 6050–Univac 1108 interface is described in Ref. 2 and the Interactive Alphanumeric Television System is described in Ref. 3.

Other changes were made to the SIMCEN diagnostic software to update the diagnostics to conform to the Mark IIIA configuration as described in Ref. 1.

II. Description

A. EMR 6050–Univac 1108 Interface Diagnostic Software

The EMR 6050–Univac 1108 interface diagnostic software tests the 50-kbits/s serial interface by sending selected patterns to the Univac 1108, receiving the same patterns back, and comparing the data received with the data sent. If the data does not compare, both the sent and received words are printed on the line printer. Additional error detection is provided by a priority interrupt.

There are five individual tests provided by this program. Each of these tests uses a different bit pattern. Any one or all of these tests may be run, depending on the option selected by the operator:

Test 1. Run all tests.

Test 2. Square wave pattern.

Test 3. All zeros pattern.

Test 4. Alternate bits pattern.

Test 5. Random pattern.

Test 6. Six-bit alphanumeric progression pattern.

A separate test (Test 99) has been added to notify the 1108 of the termination of testing. When Test 99 is selected, one block of data with a unique code in data word No. 1 is sent to the 1108. This tells the 1108 that testing is being terminated and it is no longer necessary for the user program that services the 6050 diagnostic to remain in core. The diagnostic does not wait for a reply but immediately terminates itself.

Data is always sent from the 6050 in 100-word blocks preceded by a sync word and followed by an end-of-text word (see Fig. 1 for format).

Data received has the control words stripped off by the hardware. Data may be received in either of two ways (modes) determined by the selected option. In the "single mode," one 100-word block is received for each 100-word block sent. The 100 words received are actually the first 100 words of a 250-word transmission from the 1108. The entire 250 words are received by the 6050 but only the first 100 are checked. In the "multiple mode," five 100-word blocks are received for each 100-word block sent. These five blocks are identical; however, they actually are sent from the 1108 and received by the 6050 as two 250-word blocks.

The data received is compared word-for-word with the data sent; and, if an error is detected, both words are printed in octal under the headings of "expected" and "received." Also included is the block number and the relative location of the word in the block (0–99). An alternative is available as an option. This alternative is to print all data received whether in error or not. This data is printed in the form of an octal dump one block at a time.

Added error detection consists of an interrupt which is activated by one of five error conditions detected and indicated by the interface assembly. The five error conditions are:

(1) *Collision* indicates an attempt to transmit data from the 1108 to the 6050 during the time that data is being transmitted to the 1108 from the 6050.

(2) *Parity* indicates incorrect parity exists in the data received from the 1108.

(3) *Data set* indicates a condition exists at the data set which will not allow successful transmission of data.

(4) *Underflow* indicates the number of words received is less than the number of words expected.

(5) *Overflow* indicates the number of words received is greater than the number of words expected.

There is no software method of indicating which of the five conditions caused the interrupt; however, indicators on the interface assembly panel are available for visual use.

The diagnostic will not transmit a second block of data to the 1108 until the first block has been received back from the 1108.

If the 1108 program is operating in the Real Time mode, an inquiry message or request-to-send block must be sent (see Fig. 2 for format) prior to sending a block of data; however, no response is required from the 1108, and the data block may be sent 10 ms after sending the inquiry message. If the 1108 program is operating in the Super Demand mode, the inquiry or request-to-send is not used. The data block is sent immediately.

B. Interactive Alphanumeric Television Display System Diagnostic Software

The Interactive Alphanumeric Television (IATV) Display System diagnostic software consists of seven tests and an executive routine. The executive routine and the tests are described in the following paragraphs:

Executive Routine. The executive routine operates a pre-test initialization sequence which determines which tests and equipment are required and whether or not the required units are ready. It then sequences the station and test operation.

Test One. This test mode operates all the tests described in the succeeding paragraphs.

Test Two—Basic Channel Functions. This test generates conditions and issues commands to test the channel adapter status word and the multiplexer status word. One of the two printers is used to generate interrupts. If a printer is not available, interrupt status bits in the channel adapter and the multiplexer will not be tested.

Test Three—Station Functions. The following station control functions are tested:

(1) Select alphanumeric mode

(2) Select graph mode

(3) Enable refresh

(4) Disable refresh

(5) Enable transmit

(6) Disable transmit

(7) Request status

Test Four—Cursor Addressing and Movement. Cursor address register functions are tested by loading and reading a complement pattern and by issuing all cursor control characters in displaying a visual pattern.

Test Five—Marching Alpha and Data Transfer. In this test, a marching alphanumeric pattern is written and read back to detect data transfer and interrupt sequence errors. An error summary is printed at the end of each pass, and (with the log option) data errors are logged in hexadecimal.

Test Six—Echo Test. The stations are polled for transmit ready or interrupt conditions. When one of these conditions exists, the line on which the cursor is located is read in and then written to the station 19 times to fill the screen.

Test Seven—Hardcopy Test. An 80-character, marching alpha pattern is cycled in six 12-line blocks so that each character is printed in every type position. End of print operation interrupts are monitored and errors are logged.

III. Summary

In this era of expanding technology, it is becoming commonplace to interface data processing devices such as the EMR 6050 and the Univac 1108 computers and to have alphanumeric CRT-keyboard display systems as computer input/output devices. Given these types of systems, it is important to design meaningful diagnostic and test programs to provide a high level of assurance that the devices are working properly, and if not, to provide some meaningful error indications so that the problem can be fixed in a short time.

These were the problems here. The diagnostic routines generated were conceptually relatively simple, but in their simplicity, they were able to accomplish the complex task of providing a high level of confidence that the computers were talking to each other in the same language and without errors and that the IATV system was working properly.

References

1. Polansky, R. G., "DSN Mark IIIA Simulation Center Development," in *The Deep Space Network*, Space Programs Summary 37-65, Vol. II, pp. 94–96. Jet Propulsion Laboratory, Pasadena, Calif., Sept. 30, 1970.
2. Leahey, C. F., "Mark IIIA Simulation Center EMR 6050–Univac 1108 Computer Interface," in *The Deep Space Network*, Technical Report 32-1526, Vol. I, pp. 88–92. Jet Propulsion Laboratory, Pasadena, Calif., Feb. 15, 1971.
3. Leahey, C. F., "Mark IIIA Simulation Center Interactive Alphanumeric Television System," in *The Deep Space Network*, Technical Report 32-1526, Vol. II, pp. 100–107. Jet Propulsion Laboratory, Pasadena, Calif., Apr. 15, 1971.

SYNC WORD	26_8	26_8	00	00
DATA WORD 1	XX	XX	XX	XX
DATA WORD 2	YY	YY	YY	YY
DATA WORD 100	ZZ	ZZ	ZZ	ZZ
END-OF-TEXT WORD	00	00	00	00

Fig. 1. Data block format

WORD 1	03_8	05_8	26_8	26_8
WORD 2	00	00	00	00

Fig. 2. Request-to-send block format

GCF High-Speed Data System Design and Implementation for 1971–1972

R. H. Evans
SFOF/GCF Development Section

The Deep Space Network (DSN) Ground Communications Facility (GCF) high-speed data system capabilities were significantly upgraded to meet the 1971–1972 era requirements. In general, those requirements doubled the data transmission rate to 4800 bps, added block demultiplexing at the remote stations, provided for block synchronous outbound transmission from the SFOF, and provided positive labeling of error-free blocks. This article discusses the major detail design problems encountered in implementing these requirements.

I. Introduction

This article discusses the hardware design and implementation problems in upgrading the Ground Communications Facility (GCF) High-Speed Data System (HSS) capabilities to meet the new functional design requirements set forth in Ref. 1 for the 1971–1972 era. Numerous design problems were encountered from the initial systems design conceptual stage to the detailed hardware and wiring implementation of the various assemblies. The problems concerning the general system design concepts are discussed in Ref. 2. The major detail design problems encountered with implementing the various new functions in the high-speed data assemblies (HSDAs) of the HSS are the subjects of this article.

The major tasks and new functional design requirements, to provide the DSN support required of the GCF HSS in the 1971–1972 era, are discussed in the sections that follow. Figure 1 depicts the GCF HSS and the new interface capabilities as discussed in this article.

II. Design and Implementation

A. Upgrading of the Data Transmission Rate From 2400 bps to 4800 bps

Throughout the DSN/GCF, the HSD circuit interface with the NASA Communications Network (NASCOM) is on the digital side of the data transmission equipment which NASCOM provides. In this case, NASCOM provided new Western Electric Co. (WECo) 203A Data Sets, which operate at the 4800-bps speed.

It was soon evident that the replacement of the 205B (2400 bps data set) with the new 203A would significantly impact the mechanical and electrical design of the HSDAs. Additionally, the operation of the HSS and

the data flow control aspect (affecting the data source/sink HSS users) would also be significantly affected.

The 203A Data Sets have a timed "training"[1] sequence feature to compensate for imperfect amplitude and envelope delay response of the line.

The timed training sequence, after its initiation by manual or automatic means, is controlled by the transmitter.

The Data Set Request to Send (RS) signal control lead is wired in the ON condition in all GCF HSD assemblies. Therefore, the initial training start time after circuit connection is controlled by the remote receiver. After the initial training, the receiver will signal for a "retrain"[2] automatically when it detects a loss of carrier which exceeds an allowable hold-over time, or when the signal quality falls below threshold. The receiver, after a preset time delay, will signal through the associated transmitter by phase shifting an auxiliary signal to the remote data set. The phase shift will immediately cause a momentary OFF interrupt of the remote transmitter RS signal and that transmitter will go through the timed training sequence; thereby the automatic retrain of the troubled side of the full duplex (FDX) circuit is completed. The other receiver would signal for and receive a retrain in the same manner over its own signaling and retrain loop.

The transmitter, whose RS signal lead has been momentarily turned OFF to initiate a training sequence, will turn OFF the Clear to Send (CS) signal to its associated data source which stops the flow of data from that source immediately and *without any warning*. At the conclusion of the training sequence (nominally 7.9 sec), the CS signal will be turned back ON. This clearly demonstrates that the 203A CS signal can be affected by the remote receiver—automatically—and without any warning. The GCF HSS, due to this new data set feature, then placed this additional design constraint on all HSS users. It was essential that all users reexamine their data flow control mechanisms and consider the probability of backlogging due to this added "system" control factor.

[1]Training: Five different time sequenced signal modes are automatically sent by the transmitter to permit the remote receivers' automatic equalization and timing synchronization features to fine adjust prior to transmission of data. The training period for the data sets used is a nominal 7.9 sec.

[2]Retrain: Same as training, but occurs after initial startup (training).

In order to provide the HSDA operator with the necessary indicators and controls to monitor the data set performance, and to manually initiate and observe the time-sequenced training events, a Data Set Control Panel was designed. This new Data Set Control Panel provides a momentary action indicator switch for interrupting the RS signal from normal ON to OFF. An ON/OFF indicator switch was included to inhibit the Automatic Retrain feature if desired, and ON/OFF indicators were provided for the CS, Data Set Ready (DSR), Carrier Off Delayed (COD), and Signal Quality (SQ) signals.

The last, but not least, design impact was the mechanical packaging problem of mounting the 203A Data Set in a DSS Comm Equipment Subsystem (DCES) HSDA. The DSIF standard rack design provides for 48-cm (19 in.) rack mounting space only; the 203A requires 58-cm (23-in.) mounting space. The 203A could not be operated in an "on-end" position. By special agreement with the DSIF, a deviation from the standard rack design was granted; and a new GCF-DCES rack was designed to accommodate two data sets in the bottom half. The top half was designed for standard 48-cm equipment mounting to accommodate the new BDXR equipment units.

B. Addition of BDXRs on Both the Prime and Backup Channels at CTA 21 and Each DSS Except DSS 13

(The GCF high-speed data block demultiplexer design and implementation is discussed in Ref. 3.)

The BDXR equipment is used in the DCES HSDAs located at CTA 21 and the DSSs. Previous to this upgrade to meet the 1971-1972 era requirements, the HSDA signal interface with the on-site computers (OSCs) for both the Transmit (TX) and Receive (RX) data functions was through the BMXRs.

Two BDXRs (one each for the prime and backup channels) along with their associated BDXR patch and test panel were mounted in the top half of the new rack as previously mentioned. The *receive* data and clock signal leads from the error detection decoders were rerouted to the BDXRs in the new rack.

The BDXRs, described in Ref. 3, operate in conjunction with the BDXR patch and test panel which is designed to provide ready access to all signal leads for monitoring, test, and substituting of through connections via patchcords. Only the prime channel BDXR

ports are cabled through from the BDXR patch and test panel for interface to the OSCs. The backup channel *receive* equipment can be substituted for the prime channel by application of patchcords. The patchcord method was a "value engineering" judgment so that the GCF mean time to restore requirement could be met in the simplest manner.

Value engineering considerations also reduced the functions that the BDXR was to perform. Since adequate HSDA self-test capability existed elsewhere, its need in the BDXR was not mandatory. However, it was required that the BDXR contain a simple test mode (front panel accessible) to check the programmed data block routing codes.

C. Provide for Block Synchronous Outbound HSD via BMXRs From the SFOF Comm Terminal Subsystem (SCTS) HSDA

The design of the BMXRs, although originally designed together with the BMXR switch and test panel (S&TP) for exclusive use in the DCES HSDA, was unchanged for its application in the SCTS HSDA. However, a new BMXR patch and test panel was designed to eliminate the BMXR "select" switch function of the S&TP but provide the required "test/operate" switch function. The new patch and test panel accommodates all four ports of three BMXRs providing test, monitor, and patch jacks; and the required "test/operate" switch and switch function for each port.

Past experience in interfacing with the SFOF had shown that various mission-dependent requirements occur from time to time to support Complementary Analysis Teams (CATs) with HS capability. Also, as the GCF and DSN monitoring systems become more sophisticated, the HSDA design must follow these changes.

The SCTS HSDA interfacing schemes are therefore designed to accommodate relatively large numbers of receive-data and monitor signal lead interfaces, along with the four transmit-data source interfaces provided through each BMXR.

A new high-speed data interface module (HIM) was designed. The HIM provides an isolated and controllable point of flexible interconnection between all HSDA signal leads and the data source/sinks. Inputs and outputs of the line driving and distribution amplifiers are also interconnected in the HIM.

It was necessary to insure that the electrical characteristics specified in EIA Standard RS 232-C were met at the points of interface. To assure RS 232-C requirements would be met, all interface cables used were designed and provided as part of the HSDA. All interfacing cables are therefore under centralized design control, and the HSDA wire line interface is remoted to the connector panel in the data source/sink users cabinet.

D. Provide Positive Labeling of Error-Free Blocks Received Throughout the GCF

The error detection decoders, as originally designed, labeled only those blocks that were received with errors detected while the decoder was in the lock mode (decoder "invalid"). The error status bits of error laden blocks received while in the non-lock "search" mode were unchanged and appeared to the data sink the same as error-free blocks.

The advent of the DSN multi-mission command system required positive error-free transmission of the command data from the SFOF to the DSSs through the GCF HSS. The decision was made that the decoder would be modified to label only those blocks received error-free. The DSIF computers, when operating under the DSN multi-mission command system mode, would be required to examine each block received for the positive error-free label. The DSIF computer would call for retransmissions of those blocks not containing the positive label until all command data blocks were received error-free.

Modification kits and instructions were sent to all field locations where the modification was accomplished by field personnel.

E. Provide Three Channels of HSD Equipment to the Simulation Center (SIMCEN), Each Capable of Independent Operation

The DCES HSDA that was installed in the SIMCEN was configured and wired the same as those provided at the DSSs, but was installed in standard SFOF-type cabinets. The DCES HSDA provided in these cabinets for use with the SIMCEN took on a unique appearance when rewired and reconfigured to provide simultaneous operation over three channels.

The same new BMXR patch and test panel previously described was used with the new three channel capabilities to provide three separate channel connections to the SIMCEN data source/sink interface. The cables

connecting the HSDA to the interface connector panel were provided as part of the HSDA and were of the special new design previously mentioned. Every effort was made to keep cabinet wiring changes to a minimum and all installation and modification effort was completed with the racks installed in their SIMCEN location.

The reconfiguration design and documentation effort was a sizeable task requiring new rack and wiring diagrams, a special cabling design package, and a new Operations and Maintenance Manual.

F. Provide a HSD Regeneration Assembly (HSRA) at the Area Comm Terminal (ACT) Located at the Goldstone Deep Space Communications Complex (DSCC)

The Area Comm Terminal Subsystem (ACTS) located at the Goldstone DSCC previously did not contain any HSD equipment. With respect to the HSS, the ACT was simply the point of interconnect where off-complex HSD circuits were interconnected to HSD circuits from DSSs 11, 12, and 14. To satisfy the flexible interconnect requirements normally attributed to such a trunking center, the transmission characteristics of each data circuit should, as a minimum, meet equivalent American Telephone and Telegraph Co. C-2 specifications. A specific long-term error rate can be expected when operating 203A data sets over a single C-2 grade circuit: if two C-2 grade circuits are interconnected with a 203A regenerator, the error rate can be expected to increase by a factor of two. Therefore, an ACTS HSRA was installed at the ACT. The HSRA is sized to regenerate, simultaneously, three full duplex HSD circuits. Additionally, landline (cable) HSD circuits interconnecting DSS 14 and DSS 11 to the ACT were equipped with custom-designed line equalization equipment to meet the C-2 specifications.

III. Summary

The effects of upgrading the GCF HSS to meet the requirements set forth for the 1971–1972 era are summarized as follows:

(1) The number of HSDAs was increased by one with the new installation of the HSRA at the Goldstone DSCC ACT.

(2) The DCES HSDAs equipped at CTA 21 and all DSSs except DSS 13 are fully and identically equipped with prime and backup channel equipment, including the new Block Demultiplexer equipment.

(3) The DCES HSDA equipped at the DSN SIMCEN is now a unique three-channel assembly. The three channels are configured for independent use through a new BMXR patch and test panel. This is the only DCES HSDA not equipped with the block demultiplexer capability.

(4) The SCTS HSDA has been changed significantly. Not only are the additional DSN-GCF interface requirements discussed herein accommodated, but the new NASCOM West Coast Switching Center requirements are also integrated.

(5) More details on the various types of HSDAs appear in succeeding articles.[3]

[3]For related articles covering more details on the HSDAs, see articles by Yinger, Brunder, and Rothrock in this issue.

References

1. McClure, J. P., "Ground Communications Facility Functional Design for 1971–1972," in *The Deep Space Network*, Space Programs Summary 37-66, Vol. II, pp. 99–102. Jet Propulsion Laboratory, Pasadena, California, November 30, 1970.

2. Nightingale, D., "High-Speed System Design Mark IIIA," in *The Deep Space Network*, Space Programs Summary 37-66, Vol. II, pp. 103–105. Jet Propulsion Laboratory, Pasadena, Calif., Nov. 30, 1970.

3. Evans, R. H., "High-Speed Data Block Demultiplexer," in *The Deep Space Network*, Space Programs Summary 37-66, Vol. II, pp. 105–106. Jet Propulsion Laboratory, Pasadena, Calif., Nov. 30, 1970.

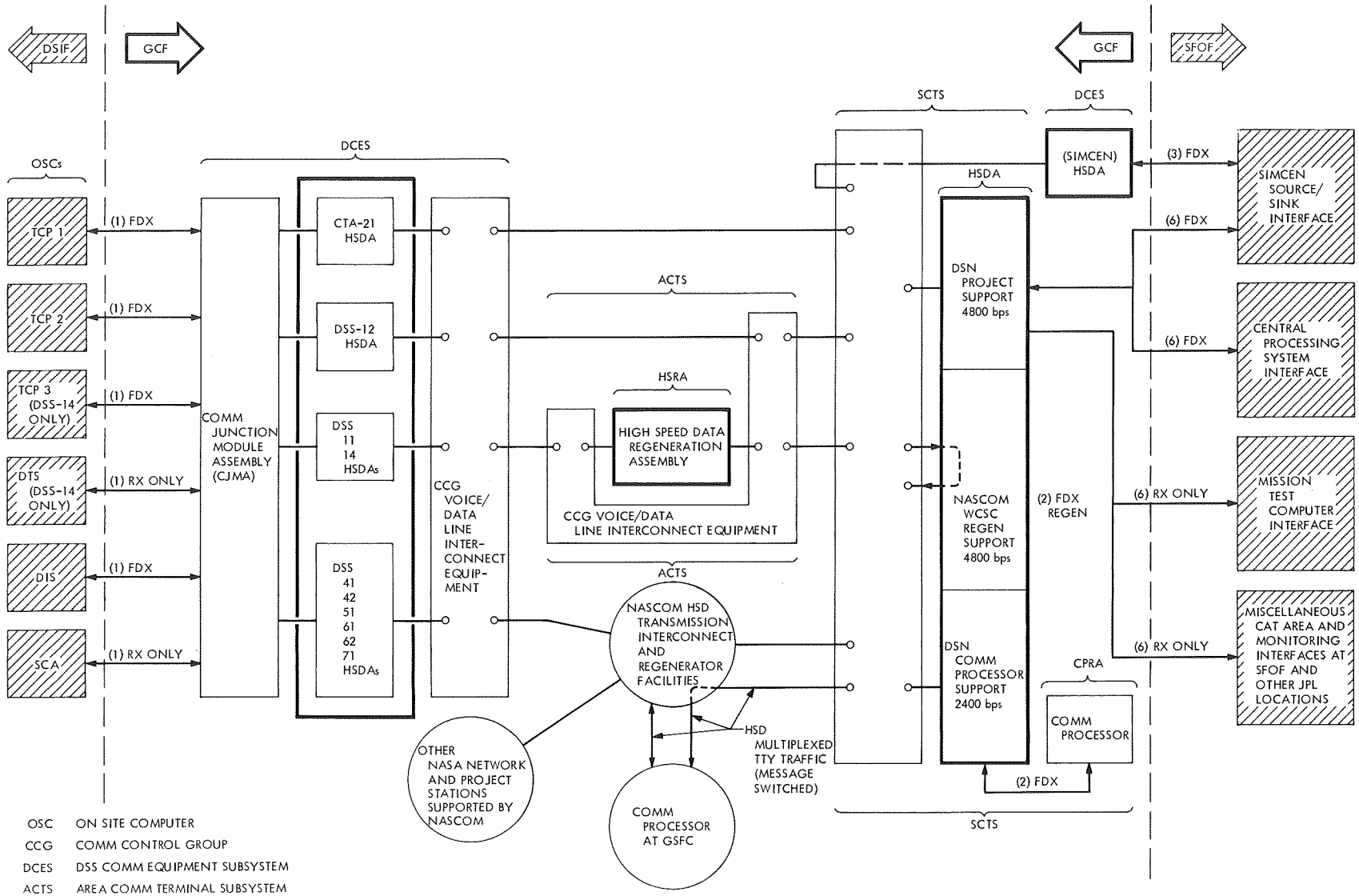

Fig. 1. DSN–GCF high-speed data system general interfaces 1971–1972 configuration

GCF DSS Communications Equipment Subsystem High-Speed Data Assembly

E. L. Yinger
SFOF/GCF Development Section

This article describes the functional operation of the Ground Communications Facility (GCF)-developed and supplied high-speed data assembly now in use at each Deep Space Station (DSS), except DSS 13 (Venus DSS), and CTA 21 (JPL Compatibility Test Area at Pasadena). The article discusses the subassemblies used, including those developed and incorporated during the latest reconfiguration, to fulfill the GCF High-Speed System requirements for the 1971–1972 period. The assembly is used to convert all high-speed data leaving the DSS to a form suitable for transmission to the Space Flight Operations Facility and converts all high-speed data entering the DSS to a form suitable for use by the on-station computers.

I. Introduction

This article discusses the functional operation of the major subassemblies (Fig. 1) making up the 1971–1972 configuration of the Ground Communications Facility (GCF)–DSS Communications Equipment Subsystem (DCES)–High-Speed Data Assembly (HSDA). This article will also briefly note the changes made to the pre-1971–1972 configuration of the DCES–HSDA described in Ref. 1 and implemented in accordance with System Design information contained in Refs. 2 and 3 and the Evans article[1] in this issue.

[1]Evans, R. H., "GCF High-Speed Data System Design and Implementation for 1971–1972" (this issue).

II. Purpose of DCES–HSDA

The DCES–HSDA selects data from the Deep Space Instrumentation Facility (DSIF) on-station computers (OSC) and converts them to a form suitable for transmission to the Space Flight Operations Facility (SFOF). It also converts the data transmitted from the SFOF to a form suitable for use by the OSCs and distributes the data to the appropriate OSCs.

The transmission portion of the DCES–HSDA provides automatic priority selection of transmission from a maximum of four OSCs, continuous data transmission by the automatic addition of filler data, block error

detection encoding, and the conversion of digital data blocks to a form suitable for transmission to the SFOF.

The receive portion of the DCES–HSDA provides the conversion of the voice band data from the SFOF to digital data, block error detection decoding, and the inspection of the User Dependent Type (UDT) code of the received data to determine the appropriate distribution of received data to any combination of up to six OSCs.

The information transmitted and received by the DCES–HSDA is organized in standard message segments of 1200-bit data blocks. Each data block consists of a header, data, and an ending (see Fig. 2).

(1) The header, provided by the data source, is 120 bits long and is represented by lines 1 through 5 of Fig. 2. The sync code is bits 1 through 24. The source code, bits 25 through 32, identifies the transmitting station. The destination code is bits 33 through 40. The block format code, bits 41 through 48, identifies block size and whether the block contains computer-generated data or block multiplexer (BMXR)-generated filler data. The UDT, bits 52 through 58, is inspected by the block demultiplexer (BDXR) to determine the distribution of received data to OSCs.

    The rest of the header, provided for data user only, is self explanatory except for the Multiple Mission Support Area (MMSA) code bits 97–98. The MMSA code is used to identify the tracking station in those instances where data blocks transmitted from any given tracking station contain data received from a spacecraft being tracked by another station.

(2) The data section contains 1044 bits. The data section may be computer-generated data or filler or test data from the BMXR.

(3) The ending is the last 36 bits, prepared and added by the encoder before transmission. The ending contains the 3-bit error status code and the 33-bit error control code. The decoder inspects each received data block and changes the three error status bits to ones if no error is detected.

For purposes of the ensuing discussion transmitted data (SD) will be followed from a DSIF OSC through the DCES–HSDA and received data (RD) through the DCES–HSDA into the DSIF OSCs. The DCES–HSDA now consists of three equipment racks, one of which was added in 1970 as described by Evans (Footnote 1).

III. Transmitted Data Flow Through the DCES–HSDA

A. Data Source

Up to four OSCs may initiate request-to-send (RS) control signals to the BMXR when they are ready to transmit data to the SFOF. When the BMXR is ready to pass data, it will initiate a clear-to-send signal to the highest priority OSC with its RS signal on. One bit time later that OSC must begin transfer of its 1164-bit data block. The transmitting OSC must turn off its RS immediately after bit time 1164 for at least one bit time.

B. Block Multiplexer Switch and Test Panel

Data from an OSC enters the BMXR switch and test panel (switch) where it is routed to one of two BMXRs. The BMXR switch provides for independent switching of data, control and timing signals between four OSCs and the two BMXRs. The switching is not operationally done on an individual basis however. Only one channel, prime or backup, may have access to the one HSD line to SFOF (Ref. 2) so all four OSCs are always switched to access the same BMXR via the BMXR switch.

In the pre-1971–1972 configuration of the DCES–HSDA, the BMXR switch and BMXRs also passed received data from SFOF to all four OSC inputs. That functional requirement is now obsoleted with the addition of the BDXRs as discussed in Ref. 4.

C. Block Multiplexer

The SD flow from the BMXR is continuous block formatted data selected on a priority basis from up to four OSCs or from the BMXR's internal preprogrammed filler block generator. The priority order of transmission from the OSCs through the BMXR is established by the setting of the priority switches on the BMXR.

At bit time zero the BMXR will begin transfer of a data block to the encoder. At the time the 1164th bit is received in the encoder, the encoder will turn off its clear-to-send (CS) signal to the BMXR. At the same time the transmitting source (OSC) must turn off its RS signal for at least one bit time and the BMXR begins its search for the source of the next data block. If the transmitting source of the last data block turns its RS

signal on before bit time 1198, the BMXR will consider its priority in the selection of a source for the next data block. At bit time 1198 the BMXR makes its selection. At bit time 1199 the encoder turns on the CS signal, and at bit time zero the selected source will begin sending its 1164-bit data block. If no OSC has its RS signal on at bit time 1198, when the BMXR is making the source selection, the BMXR will select its own filler block generator as a source of the next data block, thereby retaining continuous data transmission. The filler block generator is always the lowest priority selection of the BMXR.

D. Encoder

The encoder monitors and controls the flow of digital data from the OSCs going to the data set. Normal operation begins when the encoder receives an RS signal from the BMXR. The encoder then turns on and controls an RS signal to the data set. If the data set is ready, it will send a CS signal to the encoder. The encoder then completes the loop by turning on its CS signal to the BMXR. One bit time later the BMXR-selected data source will begin transfer of 1164 bits of data and the encoding process begins as described in Ref. 1. As the encoder receives the 1164th bit, it turns off the CS signal to the BMXR. As long as the DCES–HSDA is operating normally, the encoder will keep an RS signal to the data set turned on and the data set will keep its CS signal to the encoder turned on.

The encoder completes its processing of a data block by inserting three *zero* bits (the error status code) followed by the 33-bit error detection pattern as the data flows through the encoder from the BMXR to the data set. The encoder delays SD only one bit time in performing its encoding function.

E. Data Set Transmitter

The transmitter portion of the newly implemented Western Electric Co. 203A (4800 bps) full-duplex data set discussed by Evans (Footnote 1) is used primarily to convert encoded digital data input to an amplitude-modulated vestigial sideband voice frequency signal suitable for transmission to the SFOF via a standard voice frequency channel meeting American Telephone and Telegraph Co. specifications for a C2 grade transmission circuit. The data set also determines the bit rate and provides for synchronous transmission of data by providing the SD timing signal, Serial Clock Transmit (SCT), to the encoder, BMXR, and OSCs.

F. Data Set Control Panel

The new Data Set Control Panel (DSCP) discussed by Evans (Footnote 1) was designed and added to provide the operator with the required visual status indicators and a means to initiate a manual retrain of the associated 203A data sets.

G. Data Set Interface Module

The Data Set Interface Module (DSIM) was designed and added to provide a connector interface point between the prime and backup data sets and the audio frequency (AF) patch panel where the DCES–HSDA interfaces the one HSD line to the SFOF. The line input/output of the prime data set is normalled through the AF patch panel to the HSD line. If the operator wishes to place the backup data set on line, he must insert patchcords in the AF patch panel. The DSIM was equipped with attenuators to assure the proper signal levels at the DCES–HSDA interface with the transmission line to the SFOF.

IV. Received Data Flow Through the DCES–HSDA

A. Data Set Receiver

The receiver portion of the full-duplex data set discussed by Evans (Footnote 1) converts the amplitude modulated vestigial sideband voice frequency signal from the SFOF to serial digital data and routes it to the decoder. Under normal operating conditions a data block leaving the data set receiver will be exactly the same as it was as it left the encoder and entered the data set transmitter. The data set receiver also recovers an RD timing signal from the incoming data and routes it to the decoder, BDXR, and OSC as the Serial Clock Receive (SCR) signal.

B. Decoder

The decoder receives the incoming data blocks, via the interface buffers, and delays the data 1201 bits while it examines their validity as discussed in Ref. 1. The decoder then labels each error-free block by setting the three error status bits to 1's in accordance with Footnote 1 and forwards the data block to the BDXR.

C. BDXR and BDXR Patch and Test Panel

The BDXR and BDXR patch and test panel described in Ref. 3 were designed and added to direct each RD block only to the OSCs addressed in that data

block. The BDXR checks the UDT code information in bits 52 through 58 of each RD block and distributes the block accordingly.

The necessity for the addition of this demultiplexing capability was brought about by the increase in volume of received data and the change in data rate (from 2400 to 4800 bps) as explained in Ref. 4 and Footnote 1.

V. Data Flow Monitoring

Inputs and outputs of each subassembly are normalled through either the AF Patch and Test Jackfield, the DC Patch and Test Jackfield, the BMXR Switch and Test Jackpanel or the BDXR Patch and Test Panel. Signals passing between subassemblies may be monitored at one of the above-mentioned jackfields without interrupting data flow. When one of the visual status indicators on a subassembly signifies the presence of an abnormal condition, the operator may quickly isolate the anomaly and substitute, by using patchcords or switches, any or all backup subassemblies as required to restore normal operation. The DCES–HSDA also provides selected monitor signals for use in the monitor program. In general, the signals provide information on the configuration, mode of operation, and status of the subassemblies in use.

VI. Summary

The ten DCES–HSDAs located at CTA 21 and all DSSs (except DSS 13) have been upgraded as follows to meet the 1971–1972 HSS requirements:

(1) The Western Electric Co. (WECO) 205B (2400 bps) data sets were replaced with NASCOM-provided WECO 203A (4800 bps) data sets.

(2) Data Set Control Panels were designed and incorporated to provide the operator with a means of controlling the operation of the 203A data set and observing its status.

(3) Data Set Interface Modules were designed and incorporated to provide a connector interface for the 203A data sets and transmit/receive line level control.

(4) Block Demultiplexers (BDXR) were designed and incorporated to provide discriminate distribution of received data blocks to on-station computers (OSCs). The Block Demultiplexer Patch and test panels were designed to provide the necessary patch and test capability between the BDXR and OSCs.

(5) Two existing equipment racks were rewired and reconfigured, and one new rack was designed and added, to accommodate the new subassemblies added to the DCES–HSDA.

References

1. Nightingale, D., "High-Speed Data Communications for *Mariner* Mars 1969," in *The Deep Space Network*, Space Programs Summary 37-57, Vol. II, pp. 127–130. Jet Propulsion Laboratory, Pasadena, Calif., May 31, 1969.

2. McClure, J. P., "Ground Communications Facility Functional Design for 1971–1972," in *The Deep Space Network*, Space Programs Summary 37-66, Vol. II, pp. 99–102. Jet Propulsion Laboratory, Pasadena, Calif., Nov. 30, 1970.

3. Nightingale, D., "High-Speed System Design Mark IIIA," in *The Deep Space Network*, Space Programs Summary 37-66, Vol. II, pp. 103–105. Jet Propulsion Laboratory, Pasadena, Calif., Nov. 30, 1970.

4. Evans, R. H., "High-Speed Data Block Demultiplexer," in *The Deep Space Network*, Space Programs Summary 37-66, Vol. II, pp. 105–106. Jet Propulsion Laboratory, Pasadena, Calif., Nov. 30, 1970.

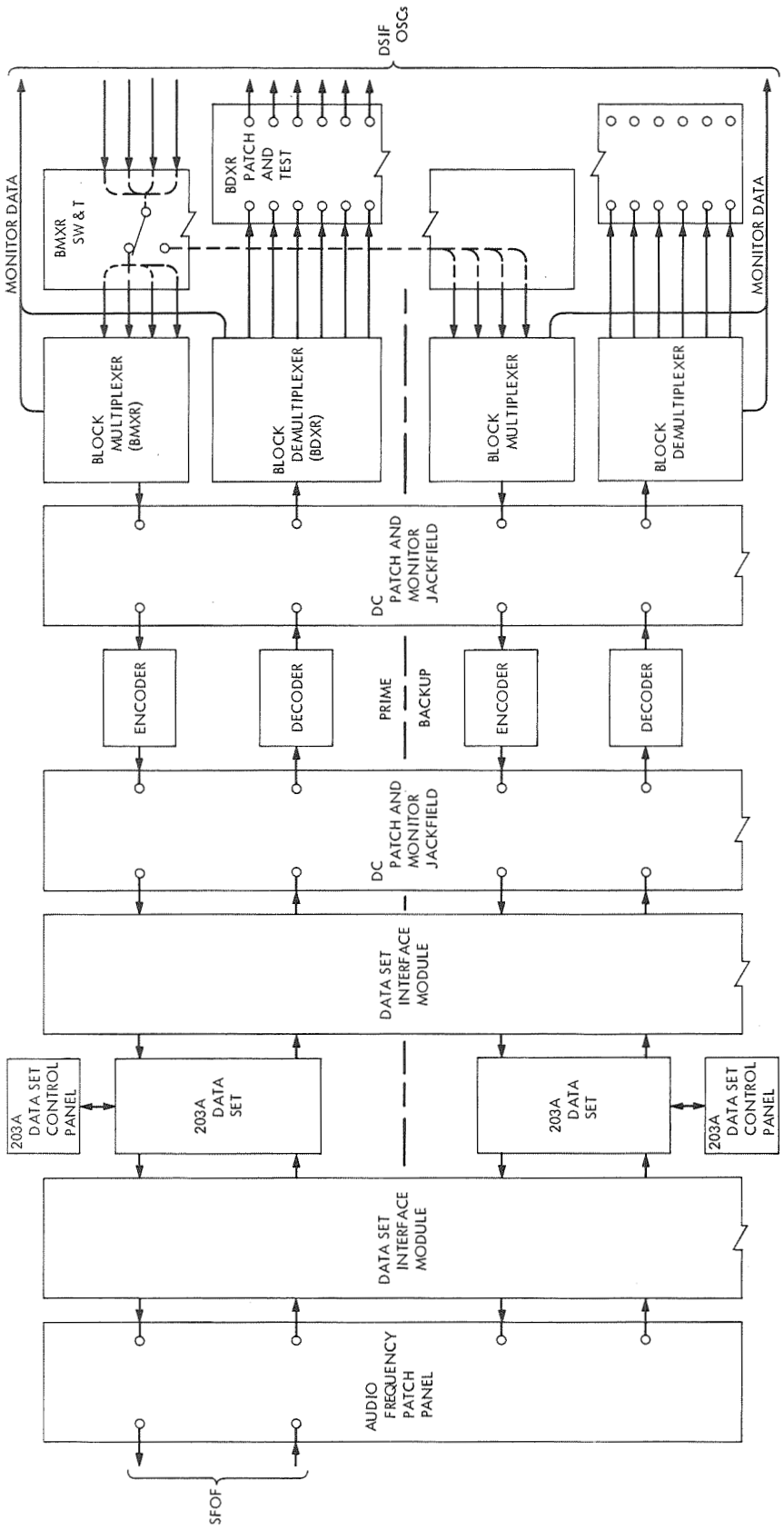

Fig. 1. DCES–HSDA functional block diagram 1971–1972 configuration

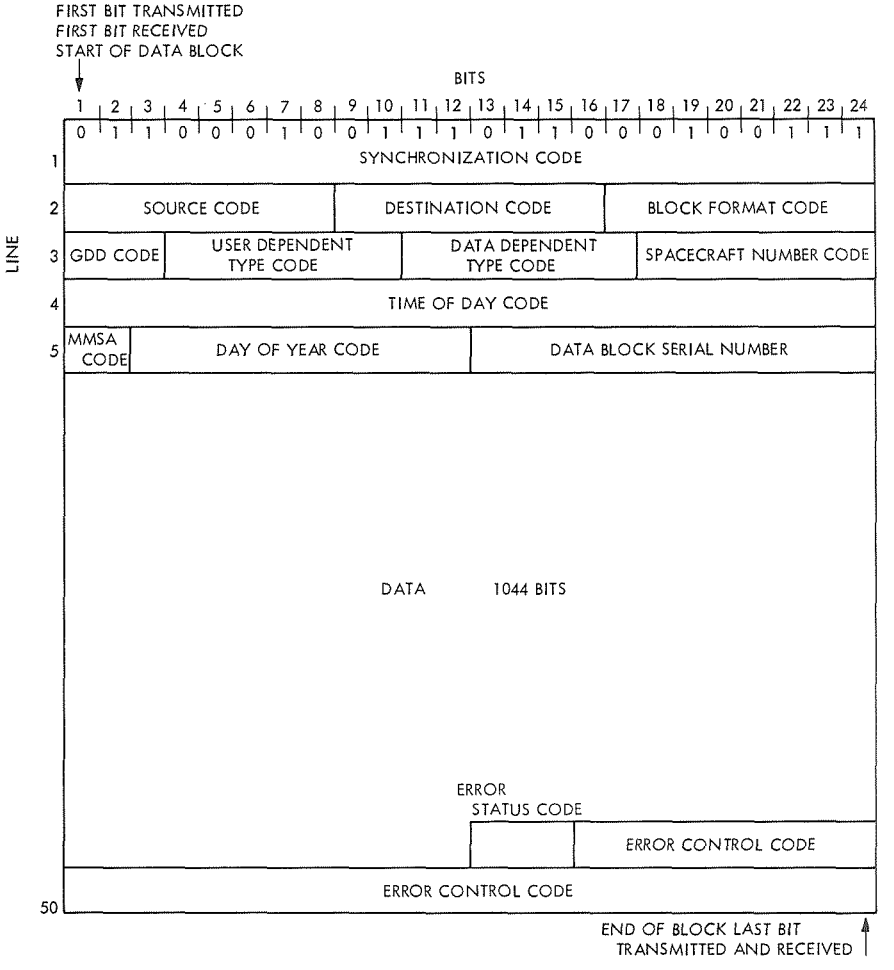

Fig. 2. Data block format

GCF SFOF Communications Terminal Subsystem High-Speed Data Assembly

G. J. Brunder
SFOF/GCF Development Section

New capabilities and equipment have been incorporated into the Space Flight Operations Facility Communications Terminal subsystem high-speed data assembly as a result of the 1970–1971 upgrade in support of the Deep Space Network. The distinct capabilities of the high-speed data assembly are discussed and the new 4800-bps high-speed data circuits and equipment are described on a functional level.

I. Introduction

The Space Flight Operations Facility Communications Terminal Subsystem (SCTS) high-speed data assembly (HSDA) is a full duplex data communication terminal that provides the necessary interface between the SFOF computers and the voice frequency data channels of the intersite transmission subsystem (ITS). Reference 1 provides information concerning the general configuration of the GCF 1971–1972 high-speed system. Reference 2 discusses equipment presently in operation in the SCTS high-speed data assembly.

The SCTS HSDA consists of 17 racks of equipment arranged to transmit, receive, process, test, monitor, switch, and distribute high-speed data.

The high-speed digital data is transmitted to and from three distinct entities, in audio form, over properly conditioned voice-grade circuits. The three external facilities connected to the SCTS high-speed data assembly are:

(1) The deep space station communications equipment subsystems (DCES). The transmission path utilized between the deep space stations and the SCTS high-speed data assembly is via the intersite transmission subsystem (ITS).

(2) Non-DSN project dependent locations. The transmission paths are GCF National Aeronautics and Space Administration Communications Network (NASCOM) circuits.

(3) Goddard Space Flight Center (GSFC) communications processor. NASCOM circuits and the SCTS high-speed data assembly interconnect the JPL and GSFC communications processors. Reference 3 discusses the functional capabilities of the JPL communications processor.

The intent of this article is to describe the general functional capabilities of the SCTS high-speed data assembly with particular emphasis on the new equipment and functional capabilities that have been incorporated into the assembly during the 1970–1971 upgrade.

II. SCTS High-Speed Data Assembly Configuration

A. 4800-bps High-Speed Data Circuits

Figure 1 depicts the general configuration and interface relationships of the 4800-bps HSD circuits used in support of the DSN. The upgrade of the data transmission rate from 2400 to 4800 bps is discussed in "GCF High-Speed Data System Design and Implementation," by R. H. Evans in this issue. The six full-duplex circuits provided by the HSD assembly are described below:

1. Transmit path. Each of the six transmit circuits can accept digital data from up to four different SFOF computers (data sources). All data sources are interfaced at the new HSD interface module (HIM).

a. HSD interface module. The HIM is JPL-designed equipment providing a highly flexible isolated distribution point for both HSD assembly data source and data sink signals. The HIM utilizes standardized connector panels, mounted in two racks, employing feed-through poke-home type Bendix connectors. The HIM is designed to accommodate many interface configurations due to the changing nature of the SCTS high-speed data assembly interface requirements.

b. Block multiplexer patch and test panel. From the HIM, the transmit signals are distributed to the new block multiplexer (BMXR) patch and test panel where connector ports can accommodate up to four data sources for each HSD circuit. Each panel provides for three HSD circuits. The panel also accesses the signals to patch, monitor and test jacks. A test/operate switch is provided to loop, in the "test" position, test signals through the BMXR patch and test panel and back to the BMXR, thus making the panel act as a data source for testing purposes. In the "operate" position the data source signals proceed to the BMXR input ports.

c. Block multiplexer. The BMXR permits up to four SFOF computers to time-share the transmit side of HSD line. This is accomplished on a priority basis, by multiplexing the block formatted data generated by the SFOF computers. When the SFOF computers are all idle the BMXR generates filler blocks to provide synchronous transmission on the HSD circuit.

The block formatted digital signals are transmitted to the encoder through a dc patch rack which provides signal access to patch, monitor and test jack facilities.

d. Encoder. The encoder performs the data block encoding for the error detection/encoding decoding (ED/ED) scheme. The ED/ED scheme provides for a positive method of monitoring the transmission of data between end terminals at the GCF.

The encoder affixes a 36-bit error detection pattern to the end of each data block before it is transmitted to the data set. The first 3 bits of the 36-bit pattern are an error status code and are always transmitted as binary zeros. The last 33 bits comprise a special coded polynomial derived from the encoding process.

e. Data set. The 203A data set is a Western Electric Co. full duplex unit. It converts the serial binary block-formatted data from the encoder into audio signals appropriate for the transmission circuit. Transmission is at a synchronous four-level amplitude modulated 4800-bps rate over four-wire C2-conditioned circuits. During the upgrade, 203A data sets replaced older 2400-bps 205B data sets in all six HSD channels.

f. Data set control panel. The JPL-designed data set control panel operates with the 203A data set. It provides visual monitoring of the operating status of the data set by displaying all the control signals at the data set digital interface. It also provides a switch to manually control the retrain initiation on the data circuit as described by Evans in this issue.

g. Attenuator panel. The audio signals are transmitted from the data set to a JPL-designed attenuator panel provided for use with both the transmit and receive sides of the data set audio circuit.

The attenuator panel contains pads that can accommodate plug-in resistors of variable values. Resistors thus can be selected to set the level of signal attenuation of the data set audio interface. The characteristics of the transmission path determine the signal levels to be selected.

The audio signals are then routed via audio patch, monitor and test jack facilities installed in a separate rack in the HSD assembly. Leaving the HSD assembly the signals are cabled to the audio switch assembly and are thence routed via the circuit distribution assembly (CDA) to the intersite transmission subsystem.

2. Receive path. The HSD audio signals received at the SFOF from an external location are routed to the audio switch assembly in the SFOF. The signals then enter the SCTS high-speed data assembly at the audio patch rack. Here the signals are accessible via patch, monitor and test jacks. The audio signals appear at the

203A data set after undergoing signal level adjustment in the attenuator panel discussed earlier in this article.

a. Data set. The 203A data set receiver demodulates, amplifies and automatically equalizes the incoming audio signal to compensate for the amplitude and delay distortions of the transmission facilities. The signal is then applied to an analog-to-digital converter, the output of which is transmitted to the decoder via dc patch, monitoring and test facilities in the dc patch rack.

b. Decoder. The decoder monitors the HSD received from the data set and performs a continuous decoding and error detection function within the error detection/encoding decoding scheme.

The decoder examines the complete data block, including the special 36-bit error detection pattern at the end of each block to determine whether or not the data block is error free. An error free block will pass the decoding process. This, together with sync pattern recognition, is used to validate the data block immediately prior to its output to the BMXR via dc jack access facilities.

If the decoder detects an invalid block (one containing errors), or cannot correctly identify the sync pattern, it performs a process obtaining a positive error status indication, discussed by Evans in this issue by changing the condition of the 3-bit error status code from binary "zeros" to binary "ones."

The decoder also informs the search alarm unit as to whether it recognizes a valid or invalid condition.

c. Search alarm unit. The search alarm unit was designed by JPL for use in the 1970–1971 upgrade to audibly and visually warn operations personnel of a loss of valid data or sync pattern recognition in the decoders. The loss must exceed a predetermined 5-sec time period while the decoder is in a "search" mode for an alarm condition to be initiated. The unit presently monitors all six SCTS HSDS high-speed data circuits simultaneously.

d. Block multiplexer. The BMXR receives the high-speed digital data from the decoder and drives four outputs, in parallel, through the BMXR patch and test panel jacks to the HSD interface module distribution interface.

e. HSD interface module. The HSD interface module distributes the received data, in parallel, to the central processing system, mission test computer, and the Simulation Center. A fourth parallel output is distributed to the line driver amplifier (LDA) rack.

f. Line driver amplifiers. The line driver amplifiers receive the digital input signals and drive three parallel output lines for each signal.

The LDA rack also has patch panels with patch, monitor and test jacks accessing each LDA input and output signal. The outputs are transmitted back to the HSD interface module where they are distributed to the GCF monitor areas, mission complimentary analysis team (CAT) areas, and to the teletype (TTY) character generators.

g. TTY character generator. The TTY character generator rack contains six on-line TTY character generators, one operational spare and related control panels, power supplies and test equipment.

Specific monitor signals are extended from the BMXR to the character generator. The character generator examines the status of the monitored signals for each data block and outputs one or two 8-level teletype characters to the communications processor. One 8-level character contains information indicating receipt of a valid data block, or detection of an invalid data block. Two 8-level characters, when sent, indicate degradation of the carrier and the loss of decoder block synchronization.

The JPL Communications Processor utilizes these data to drive a real-time display of high-speed data status. This display is provided on a digital TV format, via the SFOF internal communication subsystem (SICS), throughout the SFOF.

B. 4800-bps Full-Duplex Data Regeneration Circuits

Figure 2 represents the SCTS HSD assembly data terminal facilities provided for 4800-bps data regeneration of NASCOM data, in support of the West Coast Switching Center.

The facility consists of four Western Electric Co. 203A data sets arranged to provide two full-duplex (simultaneous two-way transmission of data) regeneration circuits. An additional 203A data set is provided as spare and may be substituted in place of a failed data set by the use of patchcords.

Data set control panels are also provided to display the operating status of each of the regeneration data sets and provide the means to select the receive timing signal from one data set to be used as the externally supplied transmit timing signal of the other data set.

The attenuator panel, previously discussed in this article, permits level adjustment of the audio transmit and receive signals at the data set audio (line) interface.

The dc and audio signals are also accessible at jack facilities to provide patch, monitor and test capability.

C. 2400-bps High-Speed Data Circuits

Three (including one spare) 2400-bps Western Electric Co. 205B data sets serve as data terminal facilities for high speed data circuits carrying multiplexed teletype data between the GSFC Communications Processor and the JPL Communications Processor.

At JPL, the digital data is transmitted through selected HSD line transfer relay paths to communication line terminals in the communications processor assembly. The relays are controlled by a transfer switch panel that can select either the on-line or off-line status of each HSD data circuit.

III. Summary

The 1970–1971 update of the SCTS high-speed data assembly provides an equipment configuration having the following capabilities:

(1) Six 4800-bps HSD circuits serving the DSN.

(2) Two 4800-bps full-duplex data regeneration circuits serving NASCOM West Coast Switching Center requirements.

(3) Three (including one spare) 2400-bps HSD circuits serving the JPL communications processor.

References

1. McClure, J. P., "Ground Communications Facility Functional Design for 1971–1972," in *The Deep Space Network,* Space Programs Summary 37-66, Vol. II, pp. 99–102. Jet Propulsion Laboratory, Pasadena, Calif., Nov. 30, 1970.
2. Nightingale, D., "High Speed Data Communications for *Mariner* Mars 1969," in *The Deep Space Network,* Space Programs Summary 37-57, Vol. II, pp. 127–129. Jet Propulsion Laboratory, Pasadena, Calif., May 31, 1969.
3. Turner, J. A., "JPL Communications Processor," in *The Deep Space Network,* Space Programs Summary 37-57, Vol. II, pp. 130–134. Jet Propulsion Laboratory, Pasadena, Calif., May 31, 1969.

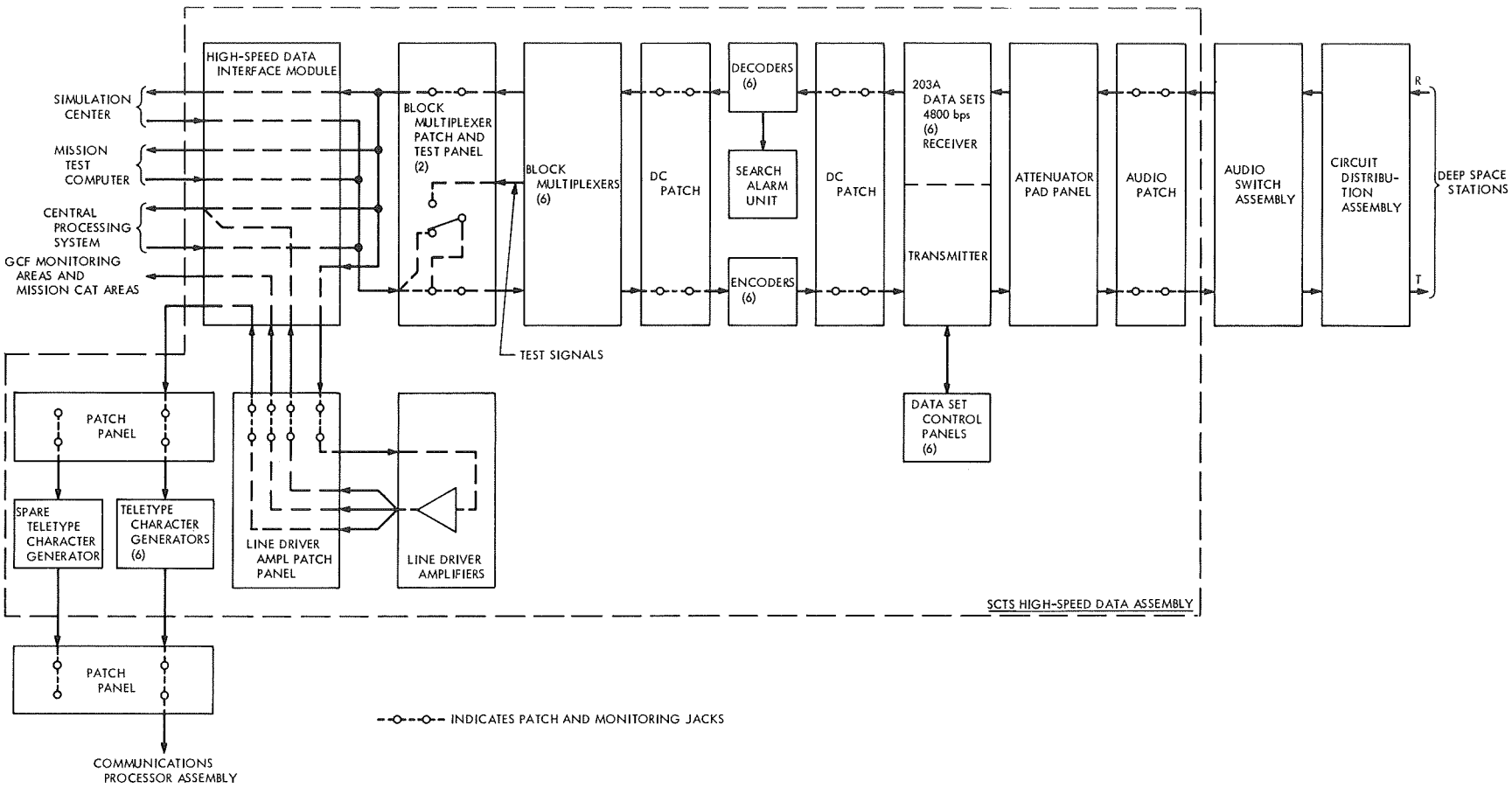

Fig. 1. SCTS HSDA 4800-bps high-speed data circuits functional block diagram

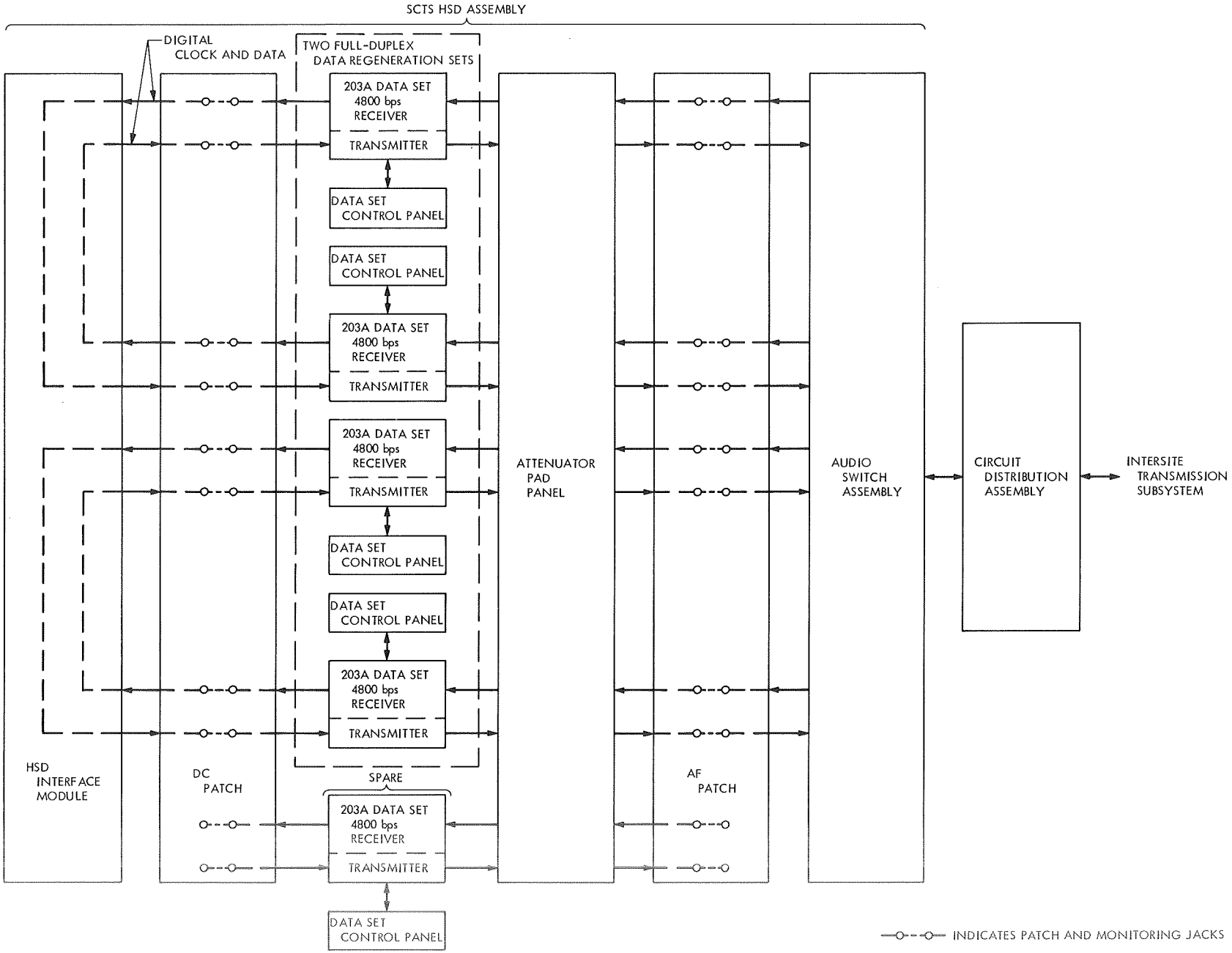

Fig. 2. SCTS HSDA 4800-bps data regeneration, functional block diagram

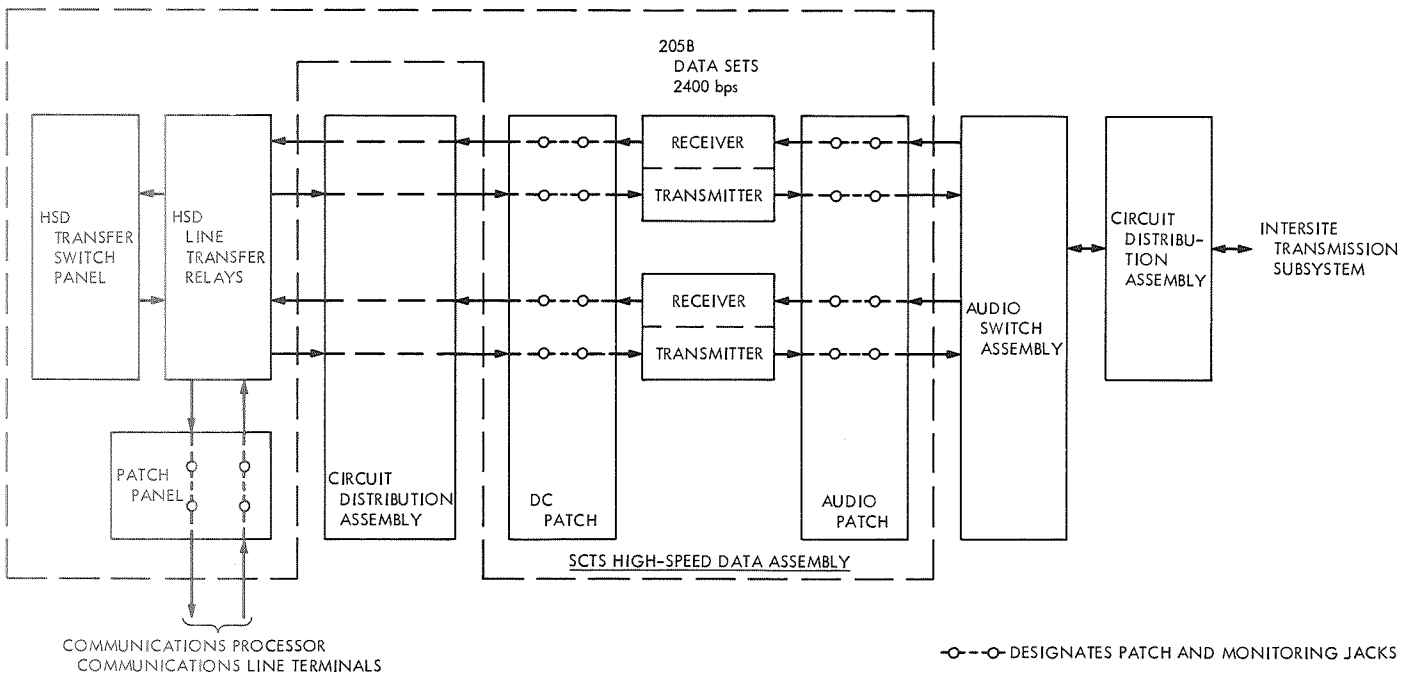

Fig. 3. SCTS HSDA 2400-bps HSD circuits functional block diagram

GCF Area Communications Terminal Subsystem High-Speed Data Regeneration Assembly

C. R. Rothrock
SFOF/GCF Development Section

The incorporation of a High-Speed Data Regeneration Assembly at the Area Communications Terminal located at the Goldstone Deep Space Communications Complex has provided the necessary interface for high-speed data entering or leaving the complex. The physical as well as electrical characteristics are described.

I. Introduction

This article describes the addition of a High-Speed Regeneration Assembly (HSRA) at the Area Communications Terminal (ACT) located at the Goldstone Deep Space Communication Center (DSC 10). DSC 10 is located within the Goldstone Deep Space Communications Complex (GDSCC). The Evans article[1] in this issue depicts the location functionally of the HSRA within the Ground Communications Facility (GCF).

The ACT is the trunking and interface center for all operational communications between the DSSs located at GDSCC and the outside world. The ACT provides the capability for routing and conditioning all communications entering or leaving the complex.

[1]Evans, R. H., "GCF High-Speed Data System Design and Implementation for 1971–1972" (this issue).

II. Physical Characteristics

In Fig. 1 the two bays on the right contain seven Western Electric 203A data sets. The two bays on the left contain the test equipment and patching jacks. The HSRA is self sustaining in that all the test equipment required to keep it in operation is an integral part of the assembly. *All test equipment* for this application is defined as test equipment required to maintain *on line* conditions.

The seven 203A data sets make up three full-duplex (FDX) circuits (transmission in both directions simultaneously). It takes a pair of data sets to make up one regeneration circuit. The seventh data set is used for a spare in the event of a failure.

The data set has two interfaces. One interface is on the digital side and the other interface is on the audio side. For regeneration application the digital sides of a pair of data sets are connected together. The audio sides of the data sets are connected to the transmission media.

III. Electrical Characteristics and Connections

The 203A data set converts digital information into audio information suitable for transmission over voice circuits in the 300- to 3000-Hz band. The transmission media must meet certain requirements to satisfy a specific long-term error rate as specified in Footnote 1.

These requirements are reiterated here for convenience. The transmission circuit of each data set (audio) should meet American Telephone and Telegraph C-2 specifications. A specific long-term error rate can be expected when operating the data set over a C-2 grade transmission circuit. If two C-2 grade circuits are operated in tandem, then the error rate can be expected to double.

Figure 2 depicts the main connection of a pair of data sets configured in a regeneration mode. These connections take place on the digital side. The Receive Data (RD) of one data set is connected to the Send Data (SD) of its conjugate. The Serial Clock Receiver (SCR) of the same data set is connected to the Serial Clock Transmitter External (SCTE) of its conjugate.

Audio information received by one data set is converted to digital information. The digital information is passed on to the second data set via the RD–SD connection. The second data set converts the digital information back into audio information to be retransmitted on to the transmission media. The SCTE–SCR connections guarantee that the transmitted information is in synchronization with the received information.

All digital and audio interface points are routed through patching jacks to facilitate testing and substitution of a failed data set. Test equipment is also terminated on jacks so that the *on-line condition* of the data sets can be monitored from the front of the bays.

In addition to the standard test equipment furnished, there is a Data Set Control Panel associated with each data set. The Data Set Control Panel provides for visual monitoring of critical digital and audio signal functions, and will indicate failure if one should arise. Those digital functions monitored are: Request to Send (RS), Clear to Send (CS), Data Set Ready (DSR), and Serial Clock Transmit External (SCTE). Audio signal functions monitored are: Carrier On (CO), Carrier On Delayed (COD), and Signal Quality (SQ).

IV. Summary

The HSRA installed at the ACT provides the capability of regenerating three high-speed full-duplex circuits with one data set used as a spare. In addition all test equipment (digital and audio) required to keep the HSRA *on line* is an integral part of the assembly. A Data Set Control Panel monitors visually critical digital and audio functions of the data sets. The HSRA provides the interface between off-complex high-speed data and all DSSs located at the Goldstone Deep Space Communications Complex.

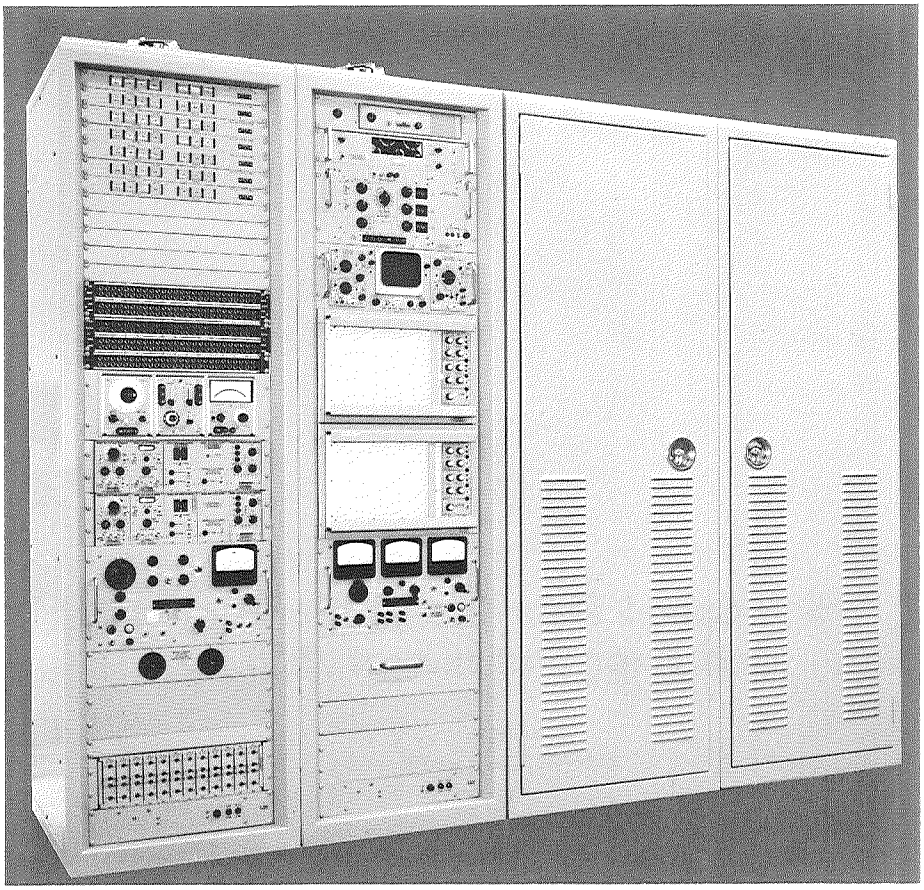

Fig. 1. High-Speed Regeneration Assembly

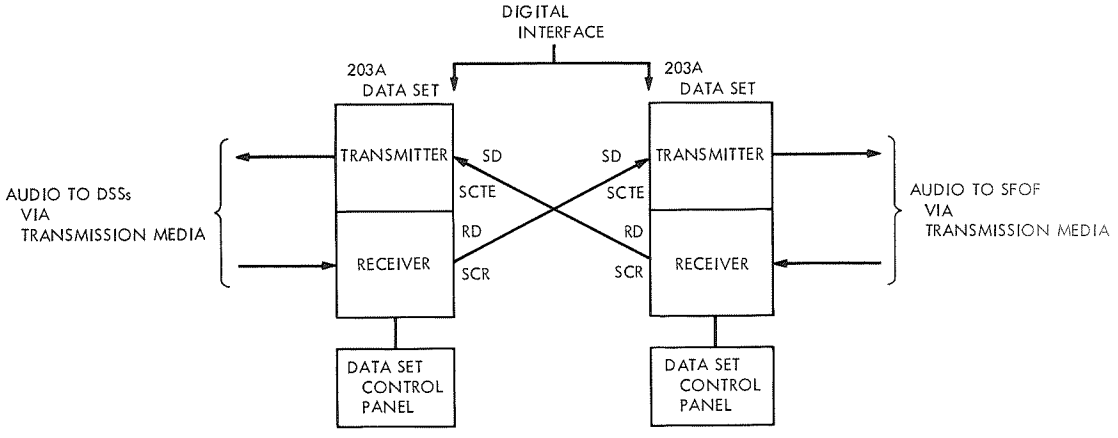

SD SEND DATA
RD RECEIVE DATA
SCR SERIAL CLOCK RECEIVER
SCTE SERIAL CLOCK TRANSMITTER EXTERNAL
→ DIRECTION OF SIGNAL FLOW

Fig. 2. Interconnect diagram

High-Speed Data System Performance and Error Statistics at 4800 bps

D. Nightingale
SFOF/GCF Development Section

A survey was conducted from March through June of 1971 to study the performance of the Ground Communications Facility upgraded High-Speed Data System. Operational and other user traffic was used as the basis for the tabulated results. This article describes the conditions under which the data were gathered and draws some conclusions based upon analysis of those data.

I. Introduction

The implementation of the upgraded High-Speed Data System (see Refs. 1 and 2), which introduced a number of new features into the transmission of data, also posed a number of questions. The questions involved the effect that user's operational data would have on total performance, on system reliability and on the occurrence of errors. This article attempts to develop some answers to these questions, using information gathered from real-time operational use of the system, as opposed to extracting measurement data from "controlled" tests. There are clearly a number of pitfalls in using a real-time approach as opposed to controlled tests; however, it is also evident that a more realistic set of conclusions can be drawn.

An explanation of the constraints, problems, and solutions and a tabulation of the actual statistics is developed in the following paragraphs. Wherever possible, any assumptions that were used will be indicated so that a progressive approach to the final results can be properly appreciated. This progressive technique was used for many reasons, among them being the time span involved (from early March 1971 to mid-June 1971), the varied types of activity during that time span, and the need to modify the meaning of observations resulting from the buildup in experience with the system.

The nature of the High-Speed Data System design, with its associated monitoring capability, led to the first limitation of this survey in which only traffic from the DSIF to the SFOF would be used for statistical analysis. The next bound was to use only DSSs 12, 14, 41, 51, 62, and 71 since these stations were engaged in the heaviest activity for both development and flight project support. Finally, all available data would be used to determine the performance of the system, permitting exclusions of data only where evidence could be found that the tabulated counts were erroneous.

II. Sources of Information, Method of Collection, and Analysis

The High-Speed Data System terminal equipment at JPL contains hardware items which provide the means to keep accurate records of the relevant monitored parameters. These data are fed to the GCF Communications Processor (CP) to drive a display for real-time technical control. Simultaneously, the CP maintains a log of this information and builds a summary for printout. Among the number counts contained in these summaries, four were selected as the prime source of statistical data:

(1) Count 1: Total number of data blocks received from a station during a scheduled operational activity.

(2) Count 2: Total number of data blocks received with transmission errors.

(3) Count 3: Total number of data blocks received in an out-of-sync condition.

(4) Count 4: Total time in seconds during which a loss of carrier signal was observed. Each second currently represents the loss of 4 data blocks.

The second source of information was the GCF Technical Controller's log and the Comm Chief's log. These were used to pinpoint anomalies that could adversely bias the summary counts mentioned above. Furthermore, these logs enabled the user of the system/station to be identified for further comparison and evaluation.

The printout of these summaries from the CP was provided on a weekly basis, each weekly report containing entries against each station on a per day basis. With these initial data, the logs were then scrutinized to uncover those periods which were clearly not of any value statistically, such as troubleshooting activities, procedural tests, associated difficulties, etc.

Lastly, there were periods during which the author made personal observations and notes of significant events to be used as a guide in establishing explanations for the later analyses.

These then were the major sources of data; others could be sought out and used on an "as-needed" basis.

The analysis itself was to take the form of an efficiency rating expressed in percent, and developed by summing together all data blocks either lost or received with errors as deficient blocks. Thus,

$$\text{Efficiency, \%} = \frac{\text{Count 1} - [\text{Count 2} + \text{Count 3} + 4\,(\text{Count 4})]}{\text{Count 1}} \times 100$$

It is therefore apparent that a figure of data block transfer efficiency will be the outcome. This method was used rather than a bit error rate since a data block received with errors contained an unknown number of bit errors, and it was virtually impossible to determine the number of bit errors in blocks received in an out-of-sync condition. It also should be evident that the efficiency rating thus established cannot be related to bit error rates without considerably more fine-grained statistical data.

III. Constraints, Problems, and Solutions

Certain constraints have already been indicated—namely that only data streams incoming to the SFOF were being monitored efficiently enough for adequate statistical data and that only specific stations would be used. Of further significant importance is the constraint of limited observational data, not only within the SFOF itself, but also at strategic points along each transmission path which, if available, might lead to the further deletion of erroneous number counts. Experience with this and other data transmission systems, however, leads to the conclusion that certain of these types of discrepancies tend to cancel one another out and can fairly safely be ignored.

The first problem to be faced was how to forecast or predict the results during the early stages of the survey and from them determine what additional information would need to be secured. The answer was readily available since, during the latter part of 1970 and into the first few weeks of 1971, acceptance tests (see Ref. 3) had been conducted in which similar statistics had been gathered. The unknown factor now being introduced was the addition of the user to the system. Such users would inevitably be involved in tests and development activities which of themselves would introduce degraded overall performance from a purely statistical point of view. Yet it could logically be expected that as more use

was made of the transmission capability, then a number of performance improvements should be apparent. For instance, procedures would be updated, software deficiencies would be exposed and rectified, hardware in the serial data streams would be modified as required to counter incompatibilities in overall network system designs, and interfaces between the various data sources and the processors in the SFOF would become "cleaner" and therefore more efficient as their weaknesses were found by the necessary tests.

As far as the purely communications portion of the end-to-end transmission of data was concerned, a great effort was made to provide the most efficient technical control and operational use procedures as possible. Extensive training and practice was given to all operators and careful coordination was established with the other agencies who would be involved in use of the high-speed capability.

This leads to the second problem. In using logs and other verbal reports, the reliability of the information contained therein, as it affected the results, was of concern. If taken at face value, then much valuable data could be erroneously deleted or, equally possibly, erroneous data could be inadvertently included. The solution became a matter of judgment and intuition, supported by questioning log entries whenever doubt existed. A substantial gain was made by this method since operations personnel subsequently improved the quality of such entries. To support this reporting activity, a secondary monitoring technique was introduced to deliver limited counts at a shorter sample rate than the daily printout available from the CP.

Yet another problem involved finding a method to feed back the early returns from the survey to the proper agencies, either users or communications operations, so that the indicated inefficiency could be corrected. It was found advantageous to make the user immediately aware, principally by verbal report, of suspected problems. It was also fairly straightforward to correct the activities of communications operations personnel when it was evident that errors either of judgement or of understanding were occurring and thereby causing a loss of efficiency.

Finally, there was the problem of the analysis itself and the results it would be expected to give. Of what value would this survey be, if the end result remained obscure and unintelligible? Thus, the efficiency equation expressed earlier was felt to represent in the simplest terms the sum total of all the data that were gathered.

IV. Tabulated Results and Observations

To make clear the magnitude of the data, some overall totals are given. During this survey, 20,807,024 data blocks were received at the SFOF. (Each data block contains 1200 bits.) This is equivalent to 60 days continuous operation at 4800 bps. A total of 230 separate station operational periods were scrutinized to provide additional background information and eliminate erroneous data.

Table 1 shows the tabulated results over the 13-week period of the survey. First, it is necessary to establish some reasonable standard against which the number counts and efficiency ratings can be judged. To do this we must make some assumptions: the first is that as time passes and experience is gained then human error is reduced to a negligible amount; the second is that software and hardware do not make random errors, therefore will either perform flawlessly or not at all. The next assumptions concern the transmission circuits alone, where it is expected that bit errors will occur in bursts at random, that each burst will create an average of 15 error bits and that such bursts will impact only 1 data block at a time.

Extensive tests on the circuits alone have produced evidence that the average long term bit error rate is 4 bit errors in every 10^5 bits transmitted. From the above assumptions it is clear that 15 bit errors require the transmission of $15/4 \times 10^5$ bits, which in turn equates to 312.5 data blocks of 1200 bits each. Thus, 1 data block will be "lost" in every 312.5 blocks transmitted, which gives an efficiency rating of 99.68% as the long term network average. This could also be viewed as the theoretical upper limit of network performance efficiency. The percentage figures in the right hand column of Table 1 should be compared with this limit.

It is now possible to make several interesting observations. First, it would be logical to expect a steady improvement in overall average efficiency for reasons which have already been given, and certainly the statistics bear this out. The reader is invited to extract the weekly figures for any particular station and observe the variations in performance that occurred. It is somewhat difficult to explain these variations in simple terms, since such a wide variety of activity was occurring. Among the more important events, it is significant to note that

during the weeks before the first *Mariner* Mars 1971 launch (May 8), the efficiency climbed to a peak. The inference is that tests and practice performed both by the DSN and the *Mariner* Mars Project with high-speed data had substantially improved the quantity of error-free and loss-free data arriving at the SFOF. The ensuing two- or three-week period reflects the return to test and development activity following the loss of the spacecraft. Again, as *Mariner IX* launch occurred (May 31), a noticeable upsurge was seen, to the extent that in the last week of recorded activity a figure of 99.46% was achieved. This is only slightly below the theoretical limit established earlier, and would indicate that the network as a whole is (or was) operating at just about peak efficiency.

There are clearly a mass of other trends and variations that can be developed and studied from the tabulated data. It is not the purpose of this article to try to consider all of them, since this would require an intimate knowledge of all activities at all locations at all times.

V. Conclusions

The first conclusion is that this survey can be considered an appetizer for what is yet to occur. Second, given good operating procedures, adequate training, and practice, operations personnel can provide the expected complement to a well-designed system. Third, all operations improve as important events approach and occur. Fourth, since the actual measured performance approached the theoretical limit, then the assumptions that were used to arrive at that limit are reasonably accurate.

References

1. McClure, J. P., "Ground Communications Facility Functional Design for 1971–1972," in *The Deep Space Network*, Space Programs Summary 37-66, Vol. II, pp. 99–102. Jet Propulsion Laboratory, Pasadena, Calif., Nov. 30, 1970.
2. Nightingale, D., "High-Speed System Design Mark IIIA," in *The Deep Space Network*, Space Programs Summary 37-66, Vol. II, pp. 103–105. Jet Propulsion Laboratory, Pasadena, Calif., Nov. 30, 1970.
3. Nightingale, D., and McClure, J. P., "Ground Communications Facility System Tests," in *The Deep Space Network Progress Report*, Technical Report 32-1526, Vol. III, pp. 190–192. Jet Propulsion Laboratory, Pasadena, Calif., June 15, 1971.

Table 1. Tabulated error statistics

Week ending	DSS	Data blocks received (Count 1)	Data block errors (Count 2)	Data blocks out of sync (Count 3)	Carrier off time (Count 4)	Efficiency, %	Overall average efficiency, %
Mar 13	12	229199	2923	801	1220	96.25	—
	14	38937	3	1	26	99.72	—
	41	168105	2846	1143	2	97.63	—
	51	225822	3076	739	611	97.23	—
	62	150658	279	634	1114	97.44	—
	71	273121	237	7630	1	97.12	—
	—	—	—	—	—	—	97.03
Mar 20	12	349945	4487	225	217	98.41	—
	14	179457	2276	1517	227	97.37	—
	41	596976	10552	8083	1332	95.99	—
	51	421239	3347	6162	913	96.88	—
	62	77897	780	1033	0	97.67	—
	71	x	x	x	x	x	—
	—	—	—	—	—	—	96.97
Mar 27	12	203530	1420	16466	559	90.11	—
	14	426558	3836	3278	899	97.49	—
	41	325740	1749	8307	35	96.87	—
	51	133716	258	2620	0	97.85	—
	62	327446	1551	3294	0	98.53	—
	71	x	x	x	x	x	—
	—	—	—	—	—	—	96.56
Apr 3	12	221110	1670	21	51	99.14	—
	14	296246	1487	10983	41	96.19	—
	41	257261	1433	3712	0	98.00	—
	51	430757	16429	1952	84	95.66	—
	62	258357	6373	311	498	96.64	—
	71	138882	139	3628	30	97.29	—
	—	—	—	—	—	—	96.81
Apr 10	12	487590	2553	26	303	99.23	—
	14	286038	2325	2446	1038	96.88	—
	41	319415	4796	584	158	98.27	—
	51	104505	439	5039	40	94.76	—
	62	103127	3264	6	0	96.83	—
	71	x	x	x	x	x	—
	—	—	—	—	—	—	98.04
Apr 17	12	594281	1526	438	588	99.57	—
	14	268374	776	3832	836	97.03	—
	41	851391	4463	5710	765	98.45	—
	51	607231	7751	11951	0	96.75	—
	62	402153	1029	10445	0	97.14	—
	71	143268	545	4020	0	96.82	—
	—	—	—	—	—	—	98.86
Apr 25	12	273866	1036	223	524	98.77	—
	14	246426	44	6	186	99.68	—
	41	103851	614	1495	12	97.92	—
	51	403043	3617	78	95	98.99	—
	62	215700	501	42	4	99.74	—
	71	140112	122	6	0	99.91	—
	—	—	—	—	—	—	99.17

Table 1 (contd)

Week ending	DSS	Data blocks received (Count 1)	Data block errors (Count 2)	Data blocks out of sync (Count 3)	Carrier off time (Count 4)	Efficiency, %	Overall average efficiency, %
May 2	12	207099	1158	68	741	97.98	—
	14	338607	162	442	116	99.68	—
	41	496186	2981	3598	507	98.26	—
	51	379374	1084	677	19	99.51	—
	62	195007	262	32	180	99.48	—
	71	107690	183	10	10	99.78	—
	—	—	—	—	—	—	99.02
May 8	12	101259	475	3	0	99.53	—
	14	x	x	x	x	x	—
	41	27780	94	3	0	99.65	—
	51	106946	297	639	0	99.12	—
	62	97181	1114	1187	15	97.57	—
	71	298579	934	41	0	99.68	—
	—	—	—	—	—	—	99.23
May 15	12	167127	186	462	140	99.28	—
	14	85311	91	2	25	99.77	—
	41	134103	493	2873	0	97.49	—
	51	204408	609	77	0	99.66	—
	62	94208	87	4	0	99.90	—
	71	79942	212	11	13	99.66	—
	—	—	—	—	—	—	99.24
May 21	12	x	x	x	x	x	—
	14	69426	92	1801	0	97.27	—
	41	112010	973	818	0	98.40	—
	51	106115	432	267	0	99.34	—
	62	85637	1284	1835	0	96.36	—
	71	117708	368	30	0	99.66	—
	—	—	—	—	—	—	98.39
May 30	12	25978	8	0	0	99.97	—
	14	82592	1827	2018	249	94.14	—
	41	13367	7	0	0	99.95	—
	51	195828	160	2415	1	98.68	—
	62	152594	242	18	29	99.75	—
	71	352146	570	3841	0	98.75	—
	—	—	—	—	—	—	98.51
Jun 6	12	1012827	127	7	65	99.96	—
	14	541496	2497	5	187	99.40	—
	41	1379902	3230	3736	142	99.45	—
	51	1353699	4762	8639	2	99.01	—
	62	123872	170	223	0	99.68	—
	71	214585	264	27	0	99.86	—
	—	—	—	—	—	—	99.46

Multiple-Mission Telemetry

W. Frey, R. Petrie, A. Lai, and R. Greenberg
DSIF Digital Systems Development Section

This article contains a status update of the Deep Space Instrumentation Facility (DSIF) Multiple-Mission Telemetry (MMT). Although the equipment covered in this report has been described in detail in earlier Deep Space Network (DSN) Space Programs Summary articles, it is now appropriate to provide information on the changes and new developments to the MMT system. Block diagrams depicting the various DSIF station MMT configurations and telemetry processing equipment added to support the Mariner Mars 1971 flight project are also included in this article.

I. Introduction

The Multiple-Mission Telemetry (MMT) *Mariner* Mars 1971 update has been successfully completed and the equipment is currently supporting the *Mariner* Mars 1971 flight project at the prime *Mariner* Mars 1971 DSIF stations. The MMT equipment added to the stations to support the mission is shown in Figs. 1 to 4. Four basic configurations have been implemented with the signal flow of each depicted in the figures. Detailed descriptions of the equipment involved were covered in Refs. 1 and 2. The purpose of this report is to provide an update on the status of the MMT *Mariner* Mars 1971 implementation.

The major elements of addition and change to the DSIF Multiple-Mission Telemetry System configuration for *Mariner* Mars 1971 were:

(1) Subcarrier Demodulator Assemblies (SDAs).

(2) Symbol Synchronizer Assemblies (SSAs).

(3) Block Decoder Assemblies (BDAs).

(4) Telemetry and Command Data Handling (TCD) modifications.

(5) MMT test software.

(6) High/low density digital tape recorders.

The current status of each of the above items is described below.

II. Subcarrier Demodulator Assemblies

Additional SDAs were procured to support the *Mariner* Mars 1971 mission requirements. Ten new units were obtained and implemented in the net. Deep Space Stations 12, 41, 62, 14, and CTA 21 received and installed two new SDAs.

In addition, all SDAs were implemented with new wide-band coherent amplitude detectors which provided better dc drift stability. The interface circuitry on all

SDAs was also modified to provide an additional output port of an unintegrated data stream to the Symbol Synchronizer Assembly.

III. Symbol Synchronizer Assemblies

The production model SSAs were fabricated and tested by Motorola, Inc., Government Electronics Division, Scottsdale, Arizona. A total of 19 SSA units and 9 sets of subassembly spares were procured by JPL under the Motorola contract.

All SSA units, subassembly spares and supporting documentation (e.g., O & M Manuals) have been supplied and installed in the DSN. The Deep Space Stations (DSSs) implemented with SSAs are: DSSs 12, 14, 41, 42, 51, 61, 62, 71, and CTA 21. Implementation was carried out jointly by Motorola, JPL, and station personnel. Training sessions at each DSS and at the GDSCC Training Center were held to familiarize site personnel with the theory and operation of the SSA.

The DSIF Maintenance Facility has been supplied with all the necessary test fixtures and test procedures with which to maintain all the SSAs in the DSIF.

Procurement action is presently underway to obtain two additional SSAs and one set of subassembly spares for MMT implementation at DSS 11.

IV. Block Decoder Assemblies

All BDAs were delivered on schedule and installed at DSSs 12, 41, 62, 14, 71, and CTA 21. There were no major problems at installation and system integration. The few failures were primarily due to circuit module component breakdown. Failures were disposed of by simple substitution. System checkout and evaluation indicated that the BDAs operated in accordance with specifications and operating curves. The operating BDAs have given no indication of any degradation from expected operating characteristics. All BDA spare assemblies, test fixtures, and documentation have been delivered to the network.

V. Telemetry and Command Data Handling Subsystem Modifications

The original article covering the modifications that were made to the TCD subsystem as a part of the MMT 1971 update was presented in Ref. 2. There are no functional changes to the TCD modification functional block diagram originally presented. However, certain engineering changes have been implemented to the TCP subassemblies to provide for better interface with the TCP computers:

(1) The TCP PIN/POT Interface Buffer Subassemblies have been modified with the addition of cable driver logic to provide for better buffered POT line signals to the HSD/WBD I/O Assemblies.

(2) The HSD/WBD I/O Assemblies have been modified with an automatic shut-down to eliminate a hang-up condition in the transmit mode as a result of either a computer halt or an operator-incurred halt. Modifications are also in progress in the HSD/WBD I/O Assemblies to eliminate susceptibility to noise.

(3) The TCP's Millisecond Clocks have been modified to operate with negative logic 1-pps and 1-kpps input signals from the Frequency Timing Subsystem (FTS).

The modifications as previously outlined in Ref. 2 have been implemented at all specified DSIF stations on schedule. The engineering changes listed above have been implemented and checked out at CTA 21. Subsequent implementation at all other DSIF Stations is presently being scheduled.

VI. MMT Test Software

As a part of the *Mariner* Mars 1971 MMT implementation, test software was developed to run in the TCP computers to verify proper operation of the new MMT assemblies added. This program exercises all equipment interfaces to the TCP computers and provides performance measurements to determine if the hardware is performing to specifications. The software assisted in the prototype development phase of the MMT equipment and was used to verify performance of the production model equipment when it was installed in the DSIF.

This test program has been identified as DOI-5087-TP by the DSIF program library. Program documentation was completed December 1, 1970 and transferred to the DSIF program library. The symbolic listing and magnetic tape containing complete source input accompanied the transmittal to the library.

The documentation covering the program capabilities, operation, and program listing was released by the DSIF program library in March 1971.

VII. High/Low Density Magnetic Tape Recorders

In order to provide the capability to create an ODR for telemetry data at the stations at the high data rates to be received at *Mariner* Mars 1971 encounter, new high-density tape recorders were procured. DSS 14 has been provided with two high-density recorder units to support the *Mariner* Mars 1971 mission. Each unit consists of dual tape recorders. The new recorders operate up to a recording density of 800 characters per inch versus 200 characters per inch on the old low-density recorders. This provides an advantage of being able to record a single reel of tape at the *Mariner* Mars 1971 high data rate for 85 minutes while the low-density unit would complete recording of a single reel in just 21 minutes. Thus, a great saving in tape usage is obtained. In addition, since each high-density unit has dual recorders, each TCP computer can switch over to the second recorder without any loss of data when a reel is full.

The dual high-density units were also installed on the TCP computers at CTA 21 and DSS 71 to assist in spacecraft compatibility testing and pre-launch checkout. At the stations where the high-density units were installed, the existing low-density units were replaced. The removed low-density units were then installed at the *Mariner* Mars 1971 prime 26-meter stations (DSSs 12, 41, and 62) to provide a dual low-density recording capability on each TCP computer for recording the lower data rates that occur at these stations.

References

1. Frey, W., Petrie, R., and Greenberg, R., "Multiple-Mission Telemetry System Project," in *The Deep Space Network*, Space Programs Summary 37-61, Vol. II, pp. 121–147. Jet Propulsion Laboratory, Pasadena, Calif., Jan. 31, 1970.
2. Frey, W., Petrie, R., Greenberg, R., McInnis, J., and Wengert, R., "Multiple Mission Telemetry 1971 Configuration," in *The Deep Space Network*, Space Programs Summary 37-63, Vol. II, pp. 63–77. Jet Propulsion Laboratory, Pasadena, Calif., May 31, 1970.

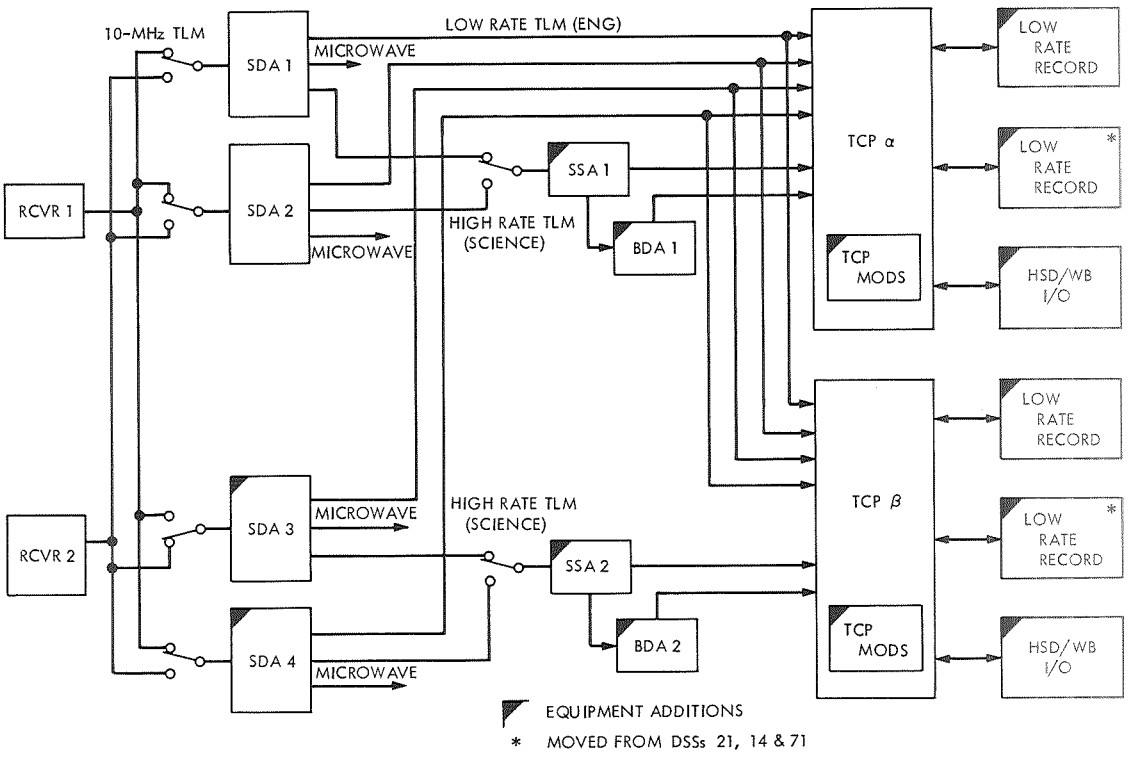

Fig. 1. MMT 1971 configuration signal flow diagram (DSSs 12, 41, and 62)

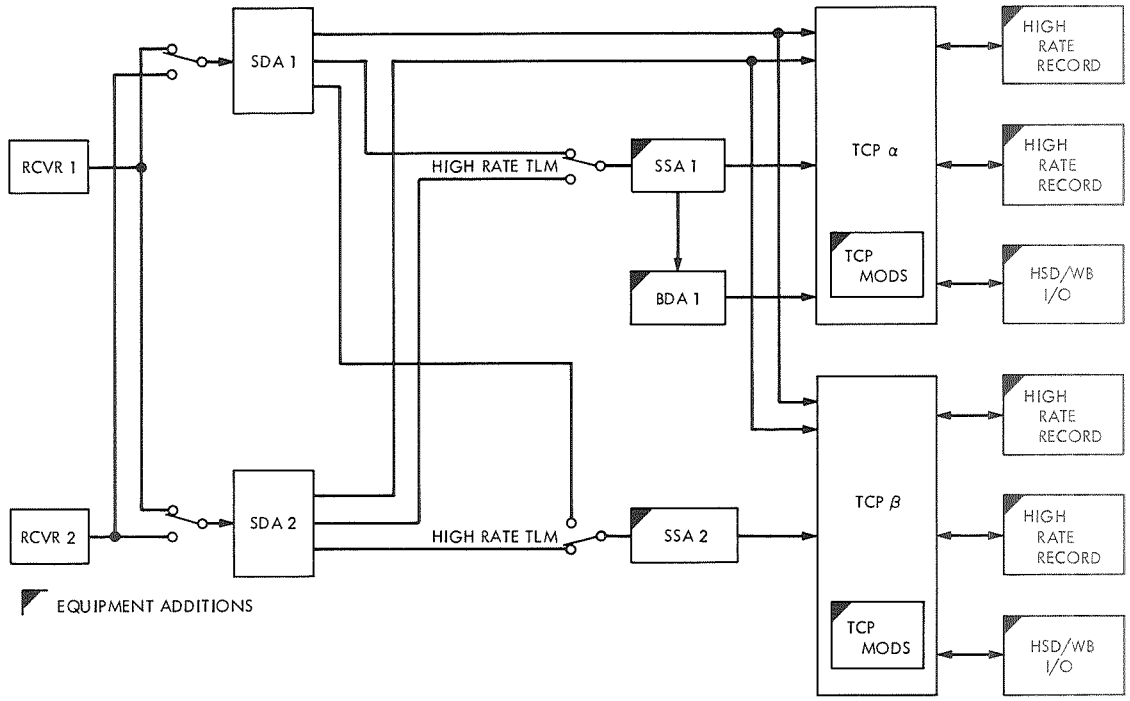

Fig. 2. MMT 1971 configuration signal flow diagram (DSS 71)

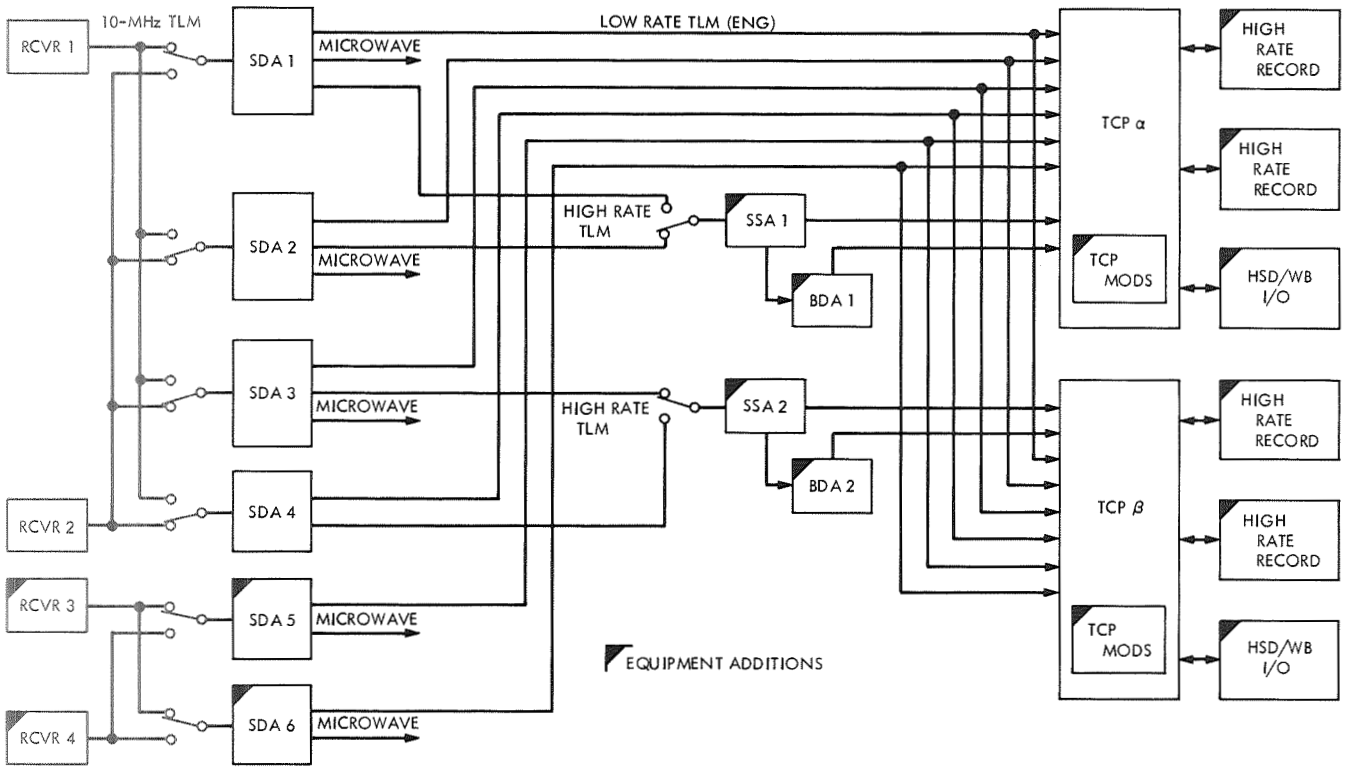

Fig. 3. MMT 1971 configuration signal flow diagram (DSS 14)

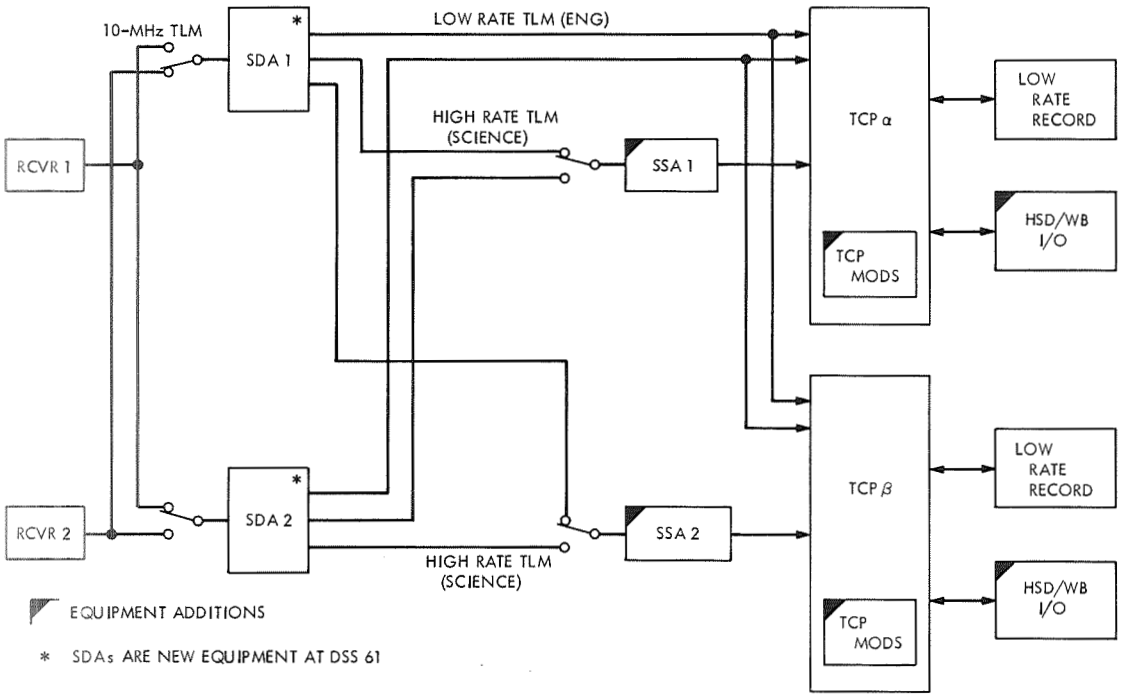

Fig. 4. MMT 1971 configuration signal flow diagram (DSSs 42, 51, and 61)

Multiple-Mission Command System

J. Wilcher
R. F. Systems Development Section
J. Woo
DSIF Digital Systems Development

The Multiple-Mission Command System (MMCS) Project was established in January 1969 to design, test, and install throughout the Deep Space Network (DSN) a command system capable of supporting all foreseeable spacecraft with a single command system. In order to provide support for the Mariner Mars 1971 (MM '71) Mission the equipment was required by early Fall of 1970. These objectives have all been met. All DSN stations considered prime for the MM '71 Mission have been implemented with the dual MMCS capability, including the PN sync units required for the MM '71 Mission. The DSN stations considered as backup stations for MM '71 have been implemented with dual MMCSs; however, only one PN sync unit per station was provided.

I. Introduction

The Multiple-Mission Command System (MMCS) Project was established in January 1969 to design, test, and install throughout the DSN a command system capable of supporting all foreseeable spacecraft with a single command system. In order to provide support for the *Mariner*-Mars 1971 (MM '71) Mission the equipment was required by early Fall of 1970. These objectives have all been met. All DSN stations considered prime for the MM '71 Mission have been implemented with the dual MMCS capability, including the PN Sync units required for the MM '71 Mission. The DSN stations considered as backup stations for MM '71 have been implemented with dual MMCSs, however, only one PN sync unit per station was provided.

II. System Verification Test

As an integral part of the MMCS implementation effort, system verification tests were conducted. These tests were designed to establish a means of evaluating the system's performance characteristics. The system was divided into three subsystem or assembly groups for individual evaluation and then combined for total system evaluation. These are as follows:

(1) Transmitter subsystem

(2) Exciter assembly

(3) Telemetry and command processor and command modulator assemblies

A. The Transmitter Subsystem

Performance measurements of the transmitter subsystem were made to evaluate the RF bandwidth, modulation distortion and modulation bandwidth. These measurements were made on both 10 and 20-kW transmitters.

B. Exciter Assembly

Performance measurements of the exciter assembly were made to evaluate the RF bandwidth, modulation

distortion, and modulation bandwidth. These exciter measurements are applicable to DSS 71 and CTA 21, which do not have transmitters.

C. TCP and Command Modulator Assemblies

The TCP and command modulator assemblies were evaluated using a special program referred to as the MMCS demonstration test program (Ref. 1). This program was designed to evaluate the operation of the TCP and command modulator assemblies in all of its various operational capabilities, i.e., bit rate, subcarrier frequencies, modulation index, synchronous or nonsynchronous symbol clock, subcarrier frequency verification, etc. The program also contains functions for verifying the system interface such as exciter status and confirmation loop check, transmitter status checks and system monitor and control interface checks.

All of the prime MM '71 deep space stations have been fully tested and have been transferred to DSIF operations. The MM '71 backup DSSs have been implemented and tested; however, they will not be transferred to DSIF operation until the Fall of 1971 due to extensive reconfiguration effort required at these DSSs.

III. Command Modulator Assembly (CMA)

The CMA implementation was completed in the DSIF with the DSS 14 installation in December 1970. Because of subsequent problems encountered during *Mariner* Mars '71 operational support testing, three engineering modifications have been made to the CMA. These modifications were required to: (1) generate the PSK-PN modulated output waveform independent of the phase relation between the subcarrier and twice subcarrier signals; (2) provide better interface on long circuits between the CMA and the exciter; and (3) improve command transmission reliability. The description of each modification is as follows:

A. PSK-PN Output Modification

Inverted PSK-PN modulated output waveform (data "1" waveform for data "0" or vice versa) could be generated in the CMA dependent on the relative phase adjustment between the fundamental subcarrier and twice subcarrier signals that drive the PN generator. The modification consisting of logic changes ensures that the pseudo-Manchester coder and decoder start at the proper state independent of the phase relation between the two subcarrier frequencies.

B. CMA-Exciter Interface Modification

Long and unterminated signal wires from the exciter caused intermittent false sampling in the CMA. Pull-up resistor and capacitor networks were installed in the Verification buffer to maintain the input lines at positive voltage whenever they are switched to open state.

C. Command Transmission Reliability Modification

Negative spikes (below ground level) resulting from ringing on long interassembly wiring in the CMA caused unwanted circuit response to occur. The modification, consisting of diodes clamped to ground and a capacitive filter, were installed in the data input lines of the command register to protect against spikes which carried them below ground. Additional diodes clamped to ground were installed in the parallel output (POT) buffer for the input lines from the TCP.

A TCP/CMA interface study is presently in progress in order to improve the input interface signal characteristics. Future changes are expected to result from this study.

Reference

1. Crow, R., et al., "DSIF Multiple-Mission Command System," in *The Deep Space Network*, Space Programs Summary 37-63, Vol. II, pp. 78-79. Jet Propulsion Laboratory, Pasadena, Calif., May 31, 1970.

Computer-Controllable Phase Shifter

R. C. Coffin
R. F. Systems Development Section

A voltage-variable phase shifter having a linear voltage-to-phase characteristic has been built and tested. The design uses a phase detector in a feedback loop configuration to linearize an RC phase shifter. The phase-shift characteristic is 72 degrees/volt operable over the range of 0 to 5 volts. Linearity is within ±1.5%. The design technique can be applied over frequencies extending from the audio range up to greater than 100 MHz.

In the era of Block IV pertormance specifications, it will be necessary to operate the ground stations by remote control. System configuration, failure analysis, and fault isolation will be controlled by computers. To facilitate automatic operation, it is first necessary to develop the capability to control certain functions remotely. One of the items to be automated is that of phase control. Several methods have been previously reported in Refs. 1 and 2.

Another approach to phase control is to build a nonlinear voltage-variable phase shifter and then linearize it by feedback. Figure 1 shows that the output of the nonlinear voltage-variable phase shifter is compared with its input in a phase detector. The error, which is the difference between the phase detector output and the control input, is then applied to the voltage-controlled phase shifter.

The implementation shown in Fig. 1 is incapable of operation over a full 360-deg range since the phase characteristic of the detector changes slope during that range. One of these slopes will place the loop in a positive feedback mode causing it to run away. By dividing the input/output frequency by two, it would be possible to achieve stable 360-deg operation; however, it is possible that under that configuration the phase characteristic might be slightly nonlinear due to end effects in the phase detector. Hence, it is recommended that division by at least four be used. Figure 2 shows the phase shifter utilizing this divide scheme.

It is possible to be in one of four regions of the phase detector characteristic since the divide chains are capable of starting up in different phases. In order to assure that the dividers are in the proper phase, it is necessary to monitor the feedback. The monitor circuitry compares the feedback voltage to preset limits and resynchronizes the dividers if out-of-range is detected. The monitor will guarantee proper phasing upon removal and reapplication of either dc or RF power.

A breadboard and a production prototype phase shifter have been built using the block diagram of Fig. 2. A buffer amplifier is used at the 10-MHz input and a limiting amplifier is incorporated as part of the voltage-variable phase shifter in order to restore losses. The voltage-

variable phase shifter is a transformer-coupled RC phase shifter with low-frequency PIN diodes serving as variable resistors.

Test results indicate that the phase shift versus control voltage deviates from a straight line (0 to +5 V = 360 deg) by less than ±1.5%. Maximum phase shift is greater than 430 deg. Output level versus phase is within ±0.8 dB and ±5% power supply variations change the output level by less than ±1 dB. Phase stability versus ±5% power supply variation is less than 1 deg. Phase stability measurements over ±10°C temperature range show that the phase characteristic remains within ±1.5%.

The phase shifter described above provides a linear phase versus control characteristic. However, the cost is evident in the size. The production prototype is built on three printed circuit boards. Two of the boards contain the voltage-variable phase shifter and its attendant amplifiers. The third board contains the divider chain, operational amplifiers, and monitor circuits. The entire circuit requires about 20 square inches of circuit board.

The primary advantages of this approach are its frequency capability and linearity. Linearity has proven to be very good (within 1.5%) and repeatable, unit to unit. The basic concept, that is, comparison of output and input in a phase detector, is applicable to any frequency. It is only necessary that a voltage-variable phase shifter and frequency dividers be built at that frequency. The upper frequency range is limited by the divider chain and is in the neighborhood of 150 MHz. The lower range, which can be extended into the audio frequencies, is limited by the design of reasonable size voltage-variable phase shifters.

References

1. Johns, C. E., "Digital Phase Shifter," in *The Deep Space Network,* Space Programs Summary 37-58, Vol. II, pp. 121–122. Jet Propulsion Laboratory, Pasadena, Calif., July 31, 1969.
2. Coffin, R. C., "Binary Digital Phase Shifter," in *The Deep Space Network,* Space Programs Summary 37-61, Vol. II, pp. 100–103. Jet Propulsion Laboratory, Pasadena, Calif., Jan. 31, 1970.

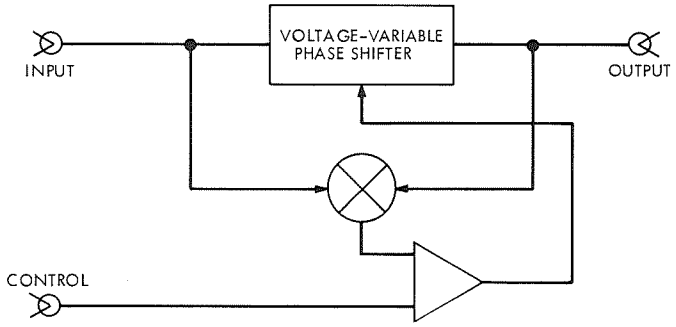

Fig. 1. Conceptual linear phase shifter

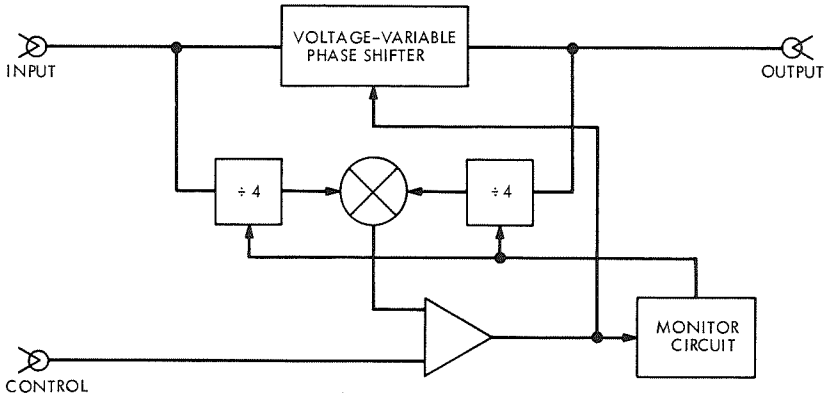

Fig. 2. Linear phase shifter

Data Decoder Assembly

C. R. Grauling
DSIF Digital Systems Development Section

Future deep space missions (e.g., Pioneer F/G) will be using convolutional coding. The present configuration of the Deep Space Network (DSN) is not suited to perform the decoding of this class of codes. This function (amongst others) will be performed by the Data Decoder Assembly which is scheduled for installation in the DSN in September 1971. This article presents a description of the Data Decoder Assembly and its implementation.

I. Introduction

The Data Decoder Assembly (DDA) is a new addition to the DSIF Telemetry and Command Subsystem scheduled for installation in the DSN in September 1971. The DDA will be capable of performing three mutually exclusive functions: sequential decoding of convolutionally encoded data, block decoding of 32/6 or 16/5 biorthogonal block coded data, and high-rate data formatting of coded or uncoded data for transmission on the Wideband Data Link with simultaneous recording of the data on magnetic tape. The sequential decoder function will be implemented at approximately 25,000 computations per second and will be useful at data rates of up to 2048 bps. The block decoding function will be used at the 26-m antenna sites only and will be capable of decoding at data rates of up to 2048 bps. The high-rate data formatting function is required at the 64-m antenna sites only and will be implemented at rates of up to 250 kbps.

This article presents a description of the implementation of the DDA. The major DDA component is a small microprogrammable digital computer. The discussion is in three parts. Each part is a description of the hardware, firmware, and software development, respectively.

II. DDA Hardware

The DDA consists of a single standard DSIF equipment rack. Each rack contains the following equipment:

(1) DDA Central Processing Unit (CPU)—Interdata Model 4 computer.

(2) Interface electronics assembly.

(3) Power supplies.

(4) HSDL/WBDL buffer (at 64-m antenna sites only).

Figure 1 is a block diagram of the DDA. The DDA Central Processing Unit and interface electronics assemblies are briefly described below.

A. DDA CPU

The DDA CPU is an Interdata Model 4 computer with the following optional equipment:

(1) Two high-speed direct memory channels (selector channels).

(2) Magnetic tape controller and selector channel (at 64-m antenna sites only).

(3) Sixteen-line interrupt module.

(4) Four 16-bit programmable input/output (I/O) channels.

The computer is microprogrammable and has a full instruction set which is an emulation of a subset of the IBM 360/20 instruction set. In addition there is a set of special DDA instructions which are used to implement functions in which computation speed is critical, such as the sequential decode function.

B. Interface Electronics Assembly

The interface electronics assembly consists of a set of functional subassemblies. Each functional subassembly consists of a single IC socket panel with wirewrap interconnections. Each socket panel contains from 100 to 150 sixteen-pin dual in-line package integrated circuits. The socket panels plug into a wirewrapped backplane assembly which accounts for all the interconnections between subassemblies and external equipment. Each functional subassembly is briefly described below.

1. FTS/DDA coupler. This subassembly provides a means by which the DDA CPU can obtain Greenwich Mean Time (GMT) from the Frequency and Timing System (FTS). GMT is always available in binary-coded decimal (BCD) format via this coupler. This subassembly also contains a millisecond counter and hundredths of a second counter. The millisecond counter clears at one-second intervals and is readable by the DDA CPU. The hundredths of a second counter automatically clears at midnight GMT and is both readable and loadable by the DDA CPU. This coupler also generates three interrupts synchronous with the 1-kpps, 100-pps, and 1-pps signals which are available from the FTS.

2. SSA/DDA coupler. This functional subassembly provides the interface necessary to allow symbols to be transferred directly into the DDA CPU core memory via a selector channel. Some data formatting is done in hardware in this coupler. This coupler provides the proper format for the following modes: uncoded, block coded, or convolutionally coded (rates 1/2, 1/3, or 1/4, frame synchronized or unsynchronized).

3. Decoded data buffer (DDB). This functional subassembly provides the hardware data formatting and the selector channel interface required for efficient transfer of data from the DDA CPU to the Telemetry and Command Processor (TCP). A single 16-bit control word allows the program to define DDA CPU core memory areas as sets of characters of 1, 5, 6, 8, or 16 bits, as well as define the number of characters to be packed in a 24-bit word and the number of trailing zeroes to be appended to each 24-bit word.

4. TCP/DDA coupler. This functional subassembly handles all communications between the TCP and DDA. It contains the circuitry required to decode the I/O controls generated by the XDS-920 in the TCP and perform the required input/output operations. Transfers of data from the TCP to the DDA are accomplished through the use of interrupts to the DDA CPU. The TCP can, at any time, issue a command, energize output M (EOM) instruction followed immediately by a parallel output transfer (POT instruction). The data is stored in a register in the coupler and the coupler generates one of three interrupts to the DDA CPU depending on which EOM had been issued. The interrupt processor in the DDA CPU then reads the data out of the register into the DDA CPU core memory.

The TCP/DDA coupler contains the hardware necessary to generate interrupts to the TCP. There are two interrupts which the DDA can generate. The generation of these interrupts is controlled via the interrupt status word (ISW), which is a 16-bit hardware register in the TCP/DDA coupler. The ISW is loadable by the DDA and readable by the TCP (via a dedicated command and parallel input sequence). Interrupts to the TCP are generally generated whenever the ISW is loaded by the DDA. The two most significant bits of the ISW are used to determine which of the two interrupts is to be generated. The remainder of the bits can be used as a message to the TCP concerning the interpretation of the newly generated interrupt. In this manner, it is possible for the two available interrupts to be used for multiple functions.

Data transfers from the DDA to the TCP are always via the DDB. The normal procedure is for the DDA CPU to issue a format command to the DDB, set up

the DDB selector channel and then load the ISW, thereby generating the proper interrupt to the TCP. The TCP response is to take the data as fast as it can via its parallel input channel. The TCP coupler monitors the TCP parallel input activity and controls a TCP busy flag which stops the selector channel whenever the DDB data registers are full and there is a word ready for transfer to the TCP.

5. Interrupt coupler. This subassembly provides the voltage level conversion circuitry for the 24-line parallel input bus and interrupts to the TCP and the interrupts associated with devices connected to the TCP emulator. This module also provides the acknowledge interrupt circuitry for interrupts generated by the FTS/DDA and TCP/DDA couplers to the DDA CPU. The DDA master clock is also located on this module.

6. TCP emulator (at 64-m antenna sites only). This functional subassembly is built on two circuit panels and provides four identical I/O channels which are electrically indistinguishable from the parallel input/parallel output (PIN/POT) channels of the XDS-920 computer used in the TCP. Special firmware is provided to operate the TCP emulator, providing emulation of the four XDS-920 parallel I/O instructions. The TCP emulator makes it possible to plug a Block Decoder Assembly (BDA), HSDL/WBDL, or Symbol Synchronizer Assembly (SSA) into the DDA without hardware modification.

III. DDA Firmware

The primary factor involved in the choice of the Interdata computer was the computational speed and flexibility available through microprogramming. A set of fifteen user-defined instructions has been built into the processor's read-only memory which allows the processor to perform relatively complex computations such as the sequential decode and tail correlation for frame synchronization acquisition at a rate which is approximately six times faster than the equivalent computation could be done using the standard instruction set. In addition to the extra instructions, the processor's interrupt-handling firmware has been modified to include the option of treating external interrupts on a priority basis. The special priority interrupt system firmware provides the queuing and servicing of interrupt processes in order of priority as defined by the interrupting device address. In this section this special firmware is briefly described.

A. TCP Autoload

This instruction is used to transfer an entire program from the TCP to the DDA. It is intended to be executed in the event of the occurrence of a program load interrupt from the TCP. Once execution of this instruction has started, the processor is put into a loop testing for the occurrence of program load interrupts. Each program load interrupt causes the processor to input a halfword (16 bits) from the TCP/DDA coupler. The first two halfwords are treated as beginning and ending addresses. Subsequent halfwords are stored in consecutive memory locations starting at the beginning address. The instruction terminates when a halfword is stored in the ending location. All other external interrupts which occur during the execution of this instruction are acknowledged but no action is taken.

B. Compute Tail Correlation

This instruction makes use of the so called "quick look" property of the class of convolutional codes currently being used to compute the likelihood that a given position in the received symbol stream is the end of a frame of coded data. Repeated execution of this instruction at all possible positions in the symbol stream is sufficient to find frame synchronization with arbitrarily high confidence.

C. Sequential Decode

This instruction implements the sequential decoding algorithm. It is necessary that there exists a properly formatted data buffer containing the received symbols and tail sequence associated with one spacecraft data frame. It is also necessary that the processor's general registers be loaded with all the parameters required by the instruction such as the location of metric tables, the impulse response, and the tail length. The execution time of this instruction is a variable depending upon the frame size and the details of the noisy received data. It is therefore necessary that this instruction be interruptable. This is accomplished by having the sequential decode firmware periodically test for the presence of an external interrupt. If an interrupt is detected, the firmware stores some of the processor microregisters in memory and does a premature exit with the location counter pointing to the *interrupt return* instruction. After the interrupting process has been completed, the *interrupt return* instruction is executed. *Interrupt return* is another user-defined instruction which restores the microregisters and transfers control back to the *sequential decode* instruction for continuation. Upon normal

completion of the *sequential decode* instruction, the location counter is incremented sufficiently to skip over the *interrupt return* instruction and the associated microregister storage area.

D. Conditionally Or Block

This instruction is used to load tail sequence into the received data buffer prior to the execution of *sequential decode*. It can also be used to add the comma-free vector into received data buffers for the block decode. The instruction performs a logical "exclusive or" of a programmable data mask into a buffer of up to 32 consecutive memory locations conditioned upon presence of ones in a 32-bit programmable register.

E. TCP Emulator Instruction

There is a set of four user-defined instructions which operate in conjunction with the TCP emulator hardware to completely emulate the PIN–POT I/O channel of the XDS-920 computer used in the TCP.

F. Halfword I/O Instructions

There is a set of four I/O instructions which are used to initiate data transfers over the 16-bit I/O channel between external devices and memory. These instructions are the counterparts to the standard I/O instructions which are 8-bit byte oriented.

IV. DDA Operational Software

Although the DDA has considerable special-purpose hardware and firmware to assist in performing the required functions, the primary control of the DDA is implemented in software. In this section, the operational program which implements the sequential decode function is discussed in order to illustrate the role that is played by software in the DDA. Figure 2 is the functional block diagram of the operational program which is used in the sequential decode mode. The various blocks (except the DDA Executive) shown in this figure may be thought of as subprograms. The system is implemented by having the DDA Executive Loop continuously checking for enabled subprograms and executing them when found. In general, subprograms may be enabled by interrupt processors or by the execution of other subprograms. The following is a brief description of each of the blocks.

A. Memory Fill

This subprogram is enabled by the occurrence of a *program load interrupt* and *initialization interrupt*. (These interrupts are generated by the TCP coupler, see *Section II-B-4*.)

B. Acquire Frame Synchronization

This subprogram is enabled under any of the following conditions: The whole system is initialized (such as at the beginning of a pass), the sequential decoder has declared itself out of synchronization due to excessive erasures, or the TCP has commanded that the sequential decoder go out of synchronization due to an anticipated data rate change. Once enabled, this subprogram acquires frame synchronization by repeated execution of the *compute tail correlation* instruction (see *Section III-B*) at all possible positions in the input system stream. The likelihood functions obtained in this fashion are retained and compared against a series of threshold values in order to find a likelihood value that implies a probability of synchronization which is sufficiently high to declare that synchronization has indeed been acquired.

C. Sequential Decode

This subprogram decodes a frame of convolutionally encoded data. It is enabled whenever frame synchronization has been acquired and a new frame of data properly formatted for sequential decoding has been loaded into core by the SSA coupler. This subprogram sets up the general registers and executes the *sequential decode* instruction. Normally, the *sequential decode* instruction is completable and upon completion this subprogram sends a message to the I-1 queue that a frame of decoded data is ready for transfer to the TCP. In the event that the *sequential decode* instruction is not completable (due to an excessively noisy frame of data), the *sequential decode* is artificially terminated and the *erasure* subroutine executed.

D. Erasure

This subroutine is executed when the *sequential decode* subprogram is unable to decode a frame in the allotted time. This subroutine sends a message to the I-2 queue that there is an erased frame ready for transfer to the TCP. If this subroutine is executed three consecutive times without a successful *sequential decode*, the decoder is declared out of synchronization and the *acquire synchronization* subprogram is enabled.

E. Memory Recall

This subprogram is enabled by the *memory recall interrupts* from the TCP. Recalled areas of DDA core are prepared for transmission over the I-2 interrupt lines.

F. I-1 Queue and I-2 Queue

These two subroutines control the transfer of data to the TCP by stacking I-1 and I-2 transfer requests. I-1 is reserved for decoded data; I-2 is used for all other transfers such as erasure data and special data requested by the TCP.

G. DDA Executive Loop

The flow chart of the DDA Executive Loop is shown in Fig. 3. Since all data transfers to the TCP must occur through the DDB, I-1 and I-2 transfers are mutually exclusive—priority being given to decoded data over the I-1 interrupt line. Each cycle of the Executive Loop begins with monitoring of the transfer queues and initiation of transfers when possible. Subprograms are then accessed on a priority basis and executed when enabled. When all enabled subprograms have been executed, the Executive Loop begins a new cycle.

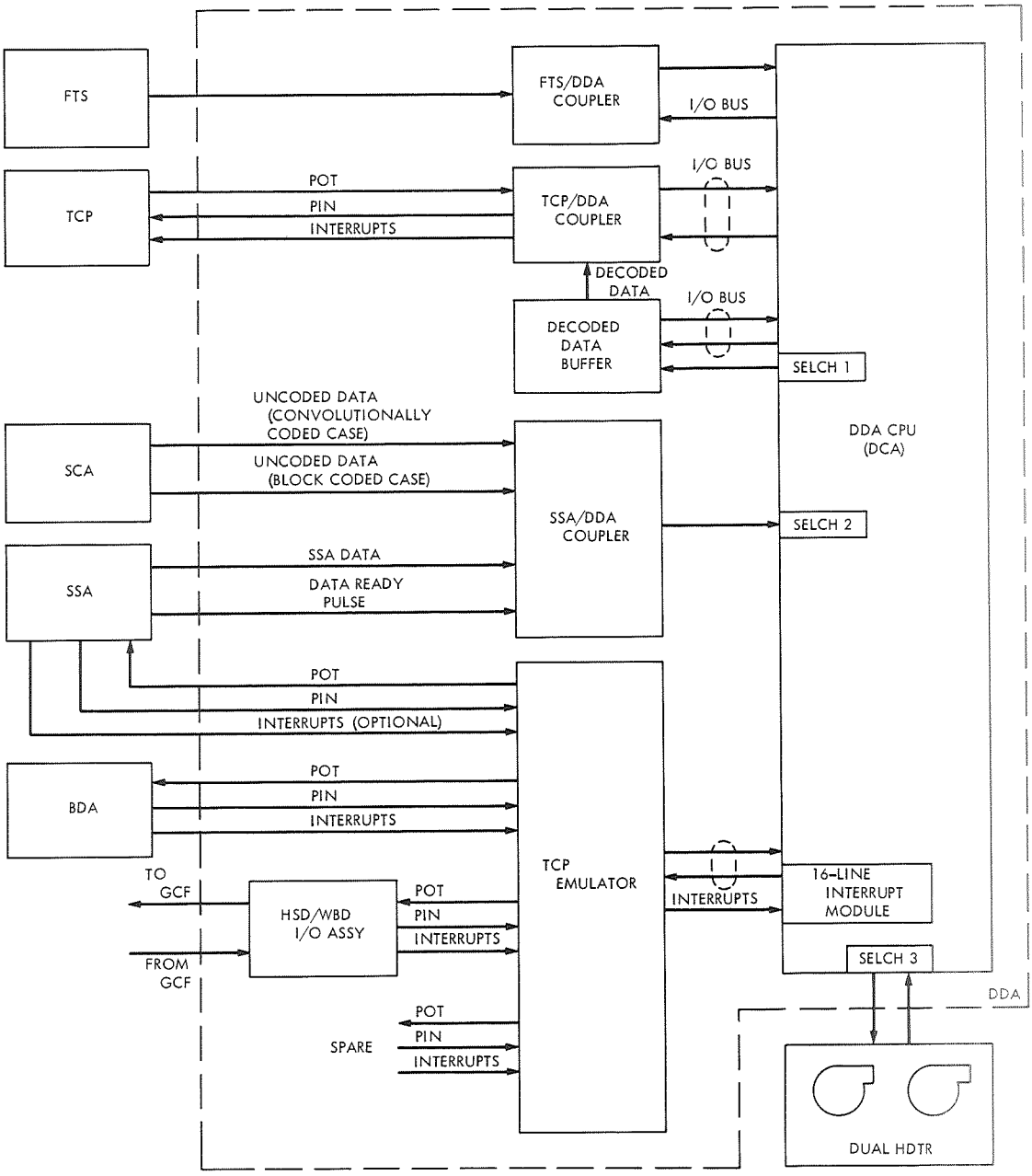

Fig. 1. Data Decoder Assembly block diagram

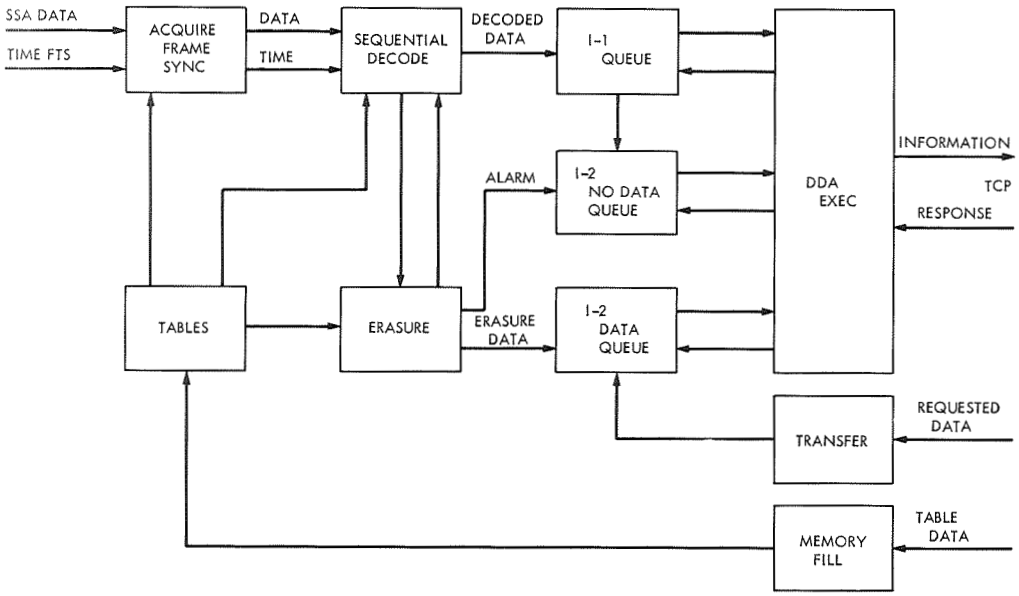

Fig. 2. DDA operational program functional block diagram

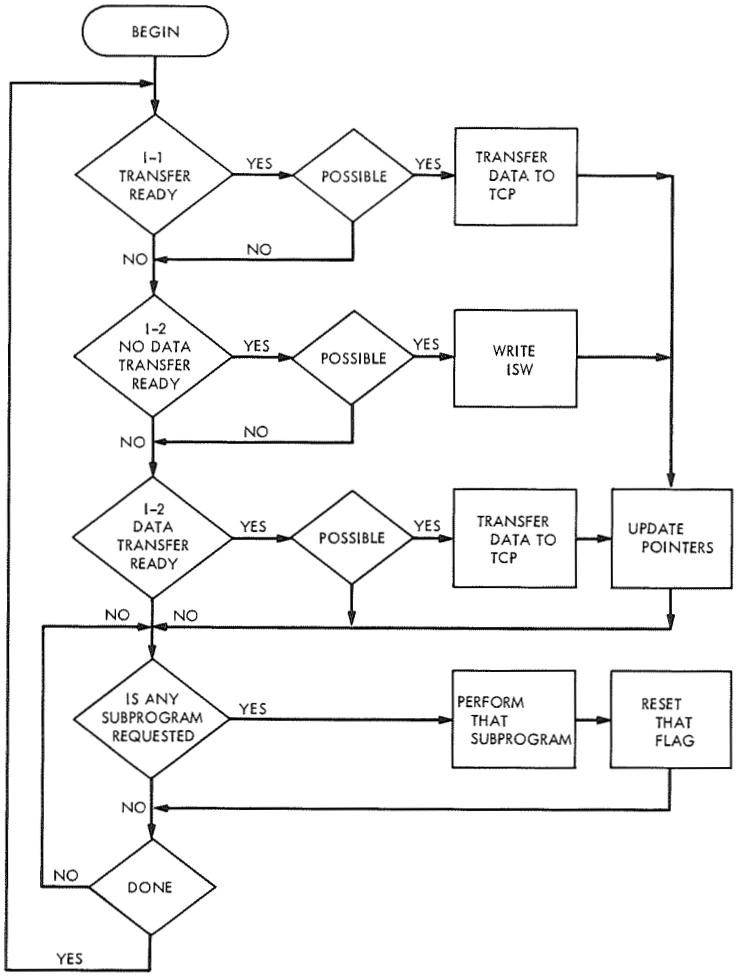

Fig. 3. DDA Executive Loop flow chart

Addendum

Referring to "MSFN/DSN Integration Program for the DSS 11 26-m Antenna Prototype Station," by R. Weber in *The Deep Space Network Progress Report*, Technical Report 32-1526, Vol. III, pp. 197–202, June 15, 1971, the following information is added:

The 5-MHz signals required for the subcarrier demodulator assemblies, which must be coherent with the receiver, will be provided by the MSFN timing system.

The Original Data Record (ODR) will be recorded on magnetic tape instead of the originally proposed APS-910 paper tape punch. This will permit the recording of a much higher tracking data sample rate, such as one sample per second, and therefore meet the *Pioneer F* requirements. The ODR data will be duplicates of the data being transmitted to the SFOF via the 4800-bps high-speed data lines. The magnetic tape units will consist of one new equipment rack, which will be added to the control rooms of each of the three integrated stations in the vicinity of the APS-910 computer.

The processing of the 29-point Antenna Pointing Predict message, as received on the high-speed data (HSD) lines, may be processed and used to drive the Antenna Position Processor (APP) simultaneously with the recording and high-speed data transmission of tracking data. However, it is not presently possible to receive the 29-point message cut a paper APP drive tape and verify the tape simultaneously with the recording and transmission of tracking data.

Operation of the DSN Command System From the Space Flight Operations Facility

W. G. Stinnett
DSN Engineering and Operations Office

Presented is a general description of the operation of the Deep Space Network (DSN) Command System from the Space Flight Operations Facility as configured for support of the Mariner Mars 1971 mission. Included are brief descriptions of functional capabilities along with the use of these capabilities by DSN and Flight Project personnel.

I. Introduction

The Space Flight Operations Facility (SFOF) Mark IIIA Command System has been developed at JPL to meet the requirements of the DSN and *Mariner* Mars 1971 Flight Project. Although full Mark IIIA requirements have not as yet been realized, operational experience has shown that one of the key design goals has been accomplished: the control of the use of the DSN Command System from the SFOF. This capability has led to, or will lead to, the following significant network operational improvements:

(1) Mission-independent procedures, thus minimum impact on network operational support for new flight projects.

(2) Minimum participation by Deep Space Station (DSS) personnel in the operation of the DSN Command System.

(3) High-speed data message control from the SFOF of the mission configuration and standards and limits utilized by the Telemetry and Command Processor (TCP) at the DSS.

(4) Direct entry and control of spacecraft commands into the DSN Command System by Flight Project personnel at the SFOF.

(5) Automatic verification, confirmation, and alarms from the DSS requiring minimal direct network personnel participation during spacecraft commanding.

This article discusses the Command System control that exists in the SFOF for use by DSN and Flight Project personnel. The material is presented in a sequence that is representative of the nominal support given for a DSS's track during which spacecraft commanding is to take place. The major items in the sequence are:

(1) SFOF Command System initialization.

(2) Pre-acquisition Command System operations.

(3) Flight project entry of command data.

II. Basic Software/Hardware Characteristics

The Command System software in the IBM 360-75 computer is organized in a manner that allows command system data to be sent to or accepted from a unique TCP at a DSS. Multiple streams (likewise multiple active TCPs) of data are possible if the software is initialized to do so. The discussion presented here will assume only one stream of data to and from a unique TCP.

Command system data are entered into the system via an IBM 2260 I/O device [cathode ray tube (CRT) with keyboard], a card reader, or from files of data generated by other software programs. Control of the use of these data in the system (e.g., transmission to a TCP) is normally done from the 2260 I/O device but can be done from a card reader.

Data can be displayed on the 2260 CRT, digital TV (DTV), line printers, or character printers. The type of data displayed on the 2260 CRT is generally administrative data. The data displayed on the other devices are formatted output and contain information concerning the contents of Command System high-speed data blocks.

III. SFOF Command System Initialization and Access Security

Before any high-speed data messages can be received from or sent to a TCP at a Deep Space Station, the Command System in the SFOF must be initialized. The Command System software in the SFOF is designed to work with multiple streams of data on a non-interactive basis. These independent processors (9 available) are each designed to work with a unique TCP in the network. Each requires initialization by the Computer Operations Chief prior to use. The parameters of initialization of an SFOF Command Processor are:

(1) Station and TCP (α, β, or γ) designation.

(2) Spacecraft number to be utilized in the high-speed data blocks.

(3) Flight project I/O device number allowed access to the software.

(4) Command Analysis Group I/O device number allowed access to the software.

The I/O devices mentioned above in (3) and (4) are the only devices capable of entering command data into the system. The flight project device is allowed entry of data concerning commands, command enable/disables, and recall data. The Command Analysis Group I/O device is allowed entry of data concerning configuration, standards and limits, test commands, and recall data.

After initialization by the Computer Operations Chief, the SFOF Command System is then made available to the Command Analysis Group for purposes of sending HSD messages to configure the TCP software and test the system end to end.

IV. Pre-acquisition Command System Operations

After the DSS countdown checkout and SFOF command processor initialization, the Command System is available for pre-acquisition checkout prior to flight project use. Included in this checkout are the following:

(1) Ensure good high-speed data link between the SFOF and the DSS.

(2) Send mission configuration messages to the TCP.

(3) Send command system standards and limits messages to the TCP.

(4) Exercise the system end to end with a test command.

(5) Ensure system is capable of supporting flight project command activity.

The DSN Command System Analysis Group, in coordination with members of the DSN Operations Control Team, inputs data into the SFOF Command System and initiates transmission to the DSS necessary for system control and checkout. During this pre-acquisition checkout, station personnel have no required operational function except to monitor the operation of station equipment. The system can be controlled entirely from the SFOF. Only in the instance of the discovery of a problem is there a requirement for direct intervention by DSS operations personnel.

The first item of checkout is to ensure a good HSDL to and from the DSS. A recall request configuration message is utilized for this purpose. Inherent within the design of the SFOF Command Processor is the ability to automatically retransmit messages if the verification message (message reflected back from the TCP) does not match what was transmitted from the SFOF. If a failure occurs in the verification process (i.e., the verification message is not received or does not match what was transmitted), the failure is isolated to a facility where immediate steps are taken to correct the problem.

The next operational item in the pre-acquisition checkout is to send the mission configuration and standards and limits data to the DSS. Existing at the DSS is multiple-mission hardware controlled by the software in the TCP. The parameters controlling this hardware are contained within the mission configuration and standards and limits messages. Although multiple-mission software presently does not exist for the TCP or at the SFOF, the operation of the system utilizing the *Mariner* Mars 1971 TCP operational program and the SFOF software has successfully demonstrated that control of the hardware at the DSS

can be accomplished from the SFOF. With the exception of entry of flight project commands, the entry of these data from the SFOF is perhaps the most powerful tool affecting Command System Network Operations. As soon as a Multiple-Mission Command System TCP Program is available, with the corresponding capability to generate all other supported project commands from the SFOF, the transmission of mission configuration and standards and limits data from the SFOF will affect network operations significantly. Network-wide, multiple-mission command procedures will be appropriate for support of all projects.

After the proper mission configuration and standards and limits data have been transmitted to the DSS, system operation is checked with the use of a test command. The system is configured exactly as for flight project support with the exception that the DSS RF output to the transmitter is inhibited. The test command is transmitted to the DSS and enabled. Proper verification and confirmation is monitored to ensure correct operation. After successful test command confirmation, the system is declared green for flight project use.

V. Flight Project Entry of Command Data

The direct entry of spacecraft commands into the DSN Command System by Flight Project personnel has proven to be an extremely efficient method of operation.

The automatic verification, confirmation, and alarming provided by the present system has led to "monitor only" operations by network personnel. All data concerning commands are entered by Flight Project personnel, with intervention by network operational personnel only upon the occurrence of a system problem. Perhaps the efficiency of this mode of operation is best described by a history of the Command System support of *Mariner IX* as of the date of writing of this article:

Total commands transmitted	599
Maximum commands transmitted during a station's track	481

The significance of the data above is that, on one occasion, 481 commands were transmitted to the spacecraft in less than 7 hours.

The Flight Project can enter commands from an IBM 2260 I/O device, a card reader, or from command data files generated either by card reader or by other software (COMGEN Program in the case of *Mariner* Mars 1971). Commands are transmitted to the DSS by specific operator instruction in the case of 2260 or card reader control. This mode is normally used during light command activity. If heavy command activity is scheduled, the normal mode of operation is by the use of command data files. A large file of commands can be "attached" to the Command System and automatic transmission to the DSS will occur based upon status messages received from the TCP. These messages inform the software in the SFOF when there is sufficient storage available in the TCP to accept more commands. Upon receipt of this message, the SFOF automatically transmits more commands to the TCP without operator intervention. The only operator instruction necessary is to initiate file transmission.

In addition to the transmission of command data to the DSS, the Flight Project has direct control of the command enabling process. Three modes of enabling are possible. At project option, commands can be enabled immediately (enable instruction is transmitted with the command data), automatically based upon a successful verify cycle, or manually by project operator specific instruction. The immediate enable mode is not normally used. This mode could be used in the case of a spacecraft emergency where a command is required immediately. The automatic enable mode is normally used during heavy command activity. The commands are transmitted to the DSS, and if the verification message matches what was transmitted, the SFOF Command System automatically constructs an enable message and sends it to the DSS without operator intervention. In the manual mode of enabling, the project command operator sends the commands to the DSS. When he is satisfied the commands are loaded properly in the TCP, he enters a specific instruction to enable the commands.

In addition to direct control of the command and enable messages transmitted to the DSS, the project can at any time send a message to the DSS to recall the commands from the TCP. In this manner, the project can know at all times what commands are loaded and their enable status.

VI. Future Plans

Operational planning is directed toward some future date at which time all network-supported projects will utilize the DSN Command System as described in this article. In order to accomplish this goal, software will have to be developed to accommodate all projects. It is hoped that by mid-1972, *Mariner* Mars 1971, *Pioneer F*, and *Pioneer VI–IX* missions will all be utilizing the DSN Multiple-Mission Command System. With the realization of these goals, the DSN Command System will be multiple mission in operations as well as functional capabilities.

Doppler Tracking System Mathematical Model

C. W. Bergman
DSIF Operations Section

The mathematical model that can be used to calculate the expected Deep Space Instrumentation Facility (DSIF) doppler tracking system phase noise σ_M is given by

$$\sigma_M = \sqrt{\sigma_R^2 + \sigma_A^2}$$

The rms phase noise σ_R is due to the receiver input noise and is a function of the received signal strength. The strong signal phase noise σ_A is characteristic of station configuration and for practical purposes is independent of signal strength. The value of σ_A is determined experimentally. The test results confirm the validity of the model.

I. Introduction

A model of the DSIF doppler tracking system has been developed. The purpose of the model is to predict the doppler system phase noise σ_M, which is measured with the Doppler System test. A block diagram of the system is shown in Fig. 1.

The results of this work show that the system rms phase noise σ_M can be accurately modeled by

$$\sigma_M = \sqrt{\sigma_R^2 + \sigma_A^2} \tag{1}$$

where σ_R is the rms loop phase noise due to received noise, and σ_A is the strong signal phase noise, which is dependent on station configuration.

II. Rms Loop Phase Noise

As given by Tausworthe (Ref. 1, p. 82)

$$\sigma_R^2 = \frac{\Gamma}{m\gamma^2}\left[\frac{1 + \left(\frac{a}{a_0}\right)\gamma}{1 + r_0} r_0\right] \tag{2}$$

In Fig. 2, rms loop phase noise σ_R is plotted as a function of m, the signal level in dB above threshold, for $\omega_{L0} = 12$, 48, and 152 Hz (ω_{L0} is the VCO loop filter bandwidth at threshold). As shown by Burt (Ref. 2), measured results agree closely with the theoretical calculation for $\sigma_R > 10$ deg. With increasing signal level, σ_R falls below the strong signal phase jitter σ_A (Ref. 3).

III. Strong Signal Phase Noise

At high S/N ratio, $m > 40$ dB, the receiver phase noise σ_R is small compared to other sources of noise in the system. The experimental results indicate that the total system noise can be obtained by taking the square root of the sum of the squares of the separate sources. Because the receiver VCO loop bandwidth varies with signal

strength, the strong signal phase noise also varies with bandwidth; however, in so far as the accuracy of Eq. (1) is concerned, the strong signal jitter can be assumed constant.

For the system doppler test there are four station configurations:

(1) Test translator (closed-loop test).

(2) Zero-delay device (closed-loop test).

(3) Test transmitter with common frequency standard.

(4) Test transmitter with separate frequency standard.

The station configuration can be altered by the selection of one of the three bandwidths.

Thus, the strong signal phase noise can be identified as

$$\sigma_A = \sigma_{A_{jk}}$$

where j indicates the system configuration and k indicates the VCO loop filter bandwidth used.

Almost every block in the diagram of Fig. 1 contributes to the system phase noise. An important use of the doppler tracking system model will be to permit comparison with measured data in isolating faulty component parts.

The identifiable sources of strong signal noise are given in Table 1.

IV. Test Results

Most of the testing to date has been done with the receiver test, which measures the doppler phase noise at the output of the 12.5-MHz phase detector (Point 1 in Fig. 1).

The relationship between the noise as measured by the receiver test, σ'_M, and the noise as measured by the system test, σ_M, is

$$\sigma_M = \sqrt{\sigma'^2_M + 1^2 + (3.6)^2 + 1.08} = \sqrt{\sigma'^2_M + 15.04}$$

The value of σ_A for the test translator configuration with $\omega_{LO} = 12$ Hz was measured and found to be 4.0 deg. The predicted values of

$$\sigma_M = \sqrt{\sigma_R^2 + \sigma_A^2}$$

are plotted in Fig. 5. Also plotted are the predicted value of

$$\sigma'_M = \sqrt{\sigma_R^2 + \sigma_A^2 - 15.04}$$

The measured values of the phase noise as a function of received signal strength above design threshold are also plotted and are seen to agree well with the predicted value of σ'_M.

References

1. Tausworthe, R. C., *Theory and Practical Design of Phase-Locked Receivers, Volume I*, Technical Report 32-819. Jet Propulsion Laboratory, Pasadena, Calif., Feb. 15, 1966.

2. Burt, R. W., "DSIF Systems Test Analysis and Verification," in *The Deep Space Network*, Space Programs Summary 37-56, Vol. II, pp. 131–134. Jet Propulsion Laboratory, Pasadena, Calif., Mar. 31, 1969.

3. Bunce, R. C., "Effect of VCO Noise on Phase-Lock Receiver Performance," in *The Deep Space Network*, Space Programs Summary 37-61, Vol. II, pp. 115–120. Jet Propulsion Laboratory, Pasadena, Calif., Jan. 31, 1970.

Table 1. Sources of strong signal noise

Contributor	Nominal phase noise deviation, deg	Comments
Rubidium standard, synthesizer, multipliers, and VCO	1.0	From the frequency standard curve in Fig. 3; the minimum noise from other sources is 4.3 deg. Due to cancellation of correlated noise at the output of multiplier B, the effective noise is 1 deg.
Doppler extractor	3.6	As measured
TDH:		
Digital noise	1.0	As measured
Quantization error	1.04	For values of $\sigma_M > 2.2$ this error is a constant. For $\sigma_M > 2.2$ the error is a function of the mean values of the phase as shown in Fig. 4.

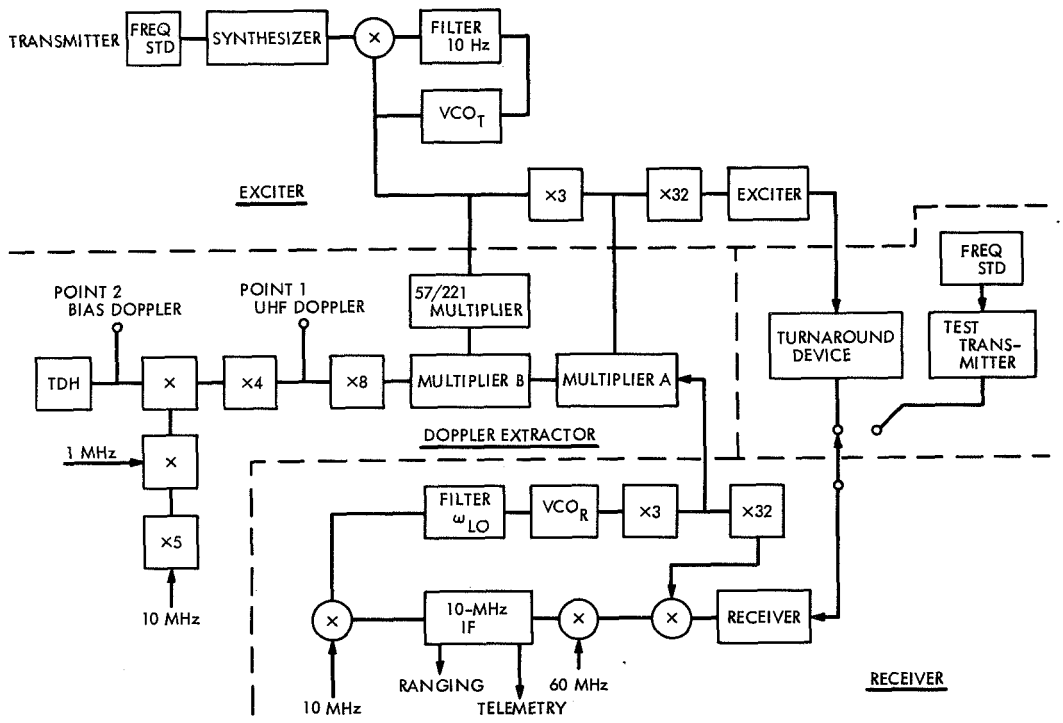

Fig. 1. Block diagram of doppler system

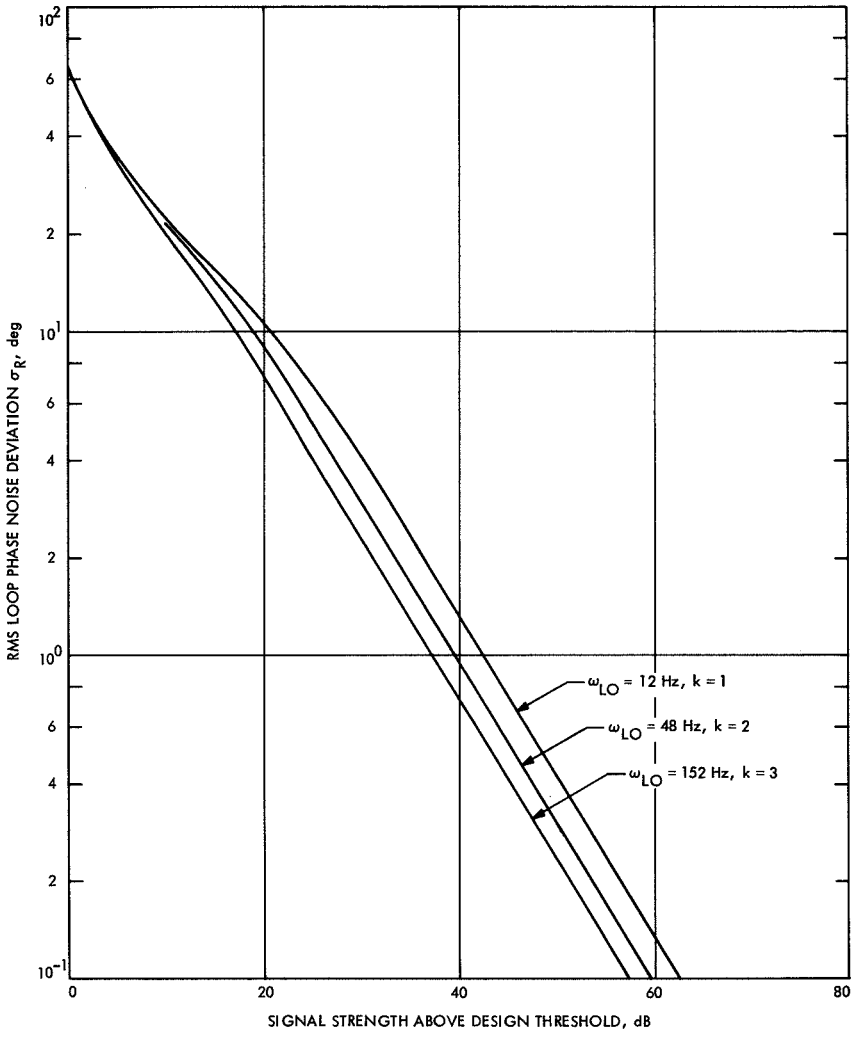

Fig. 2. Rms loop phase noise referenced to S-band vs signal strength

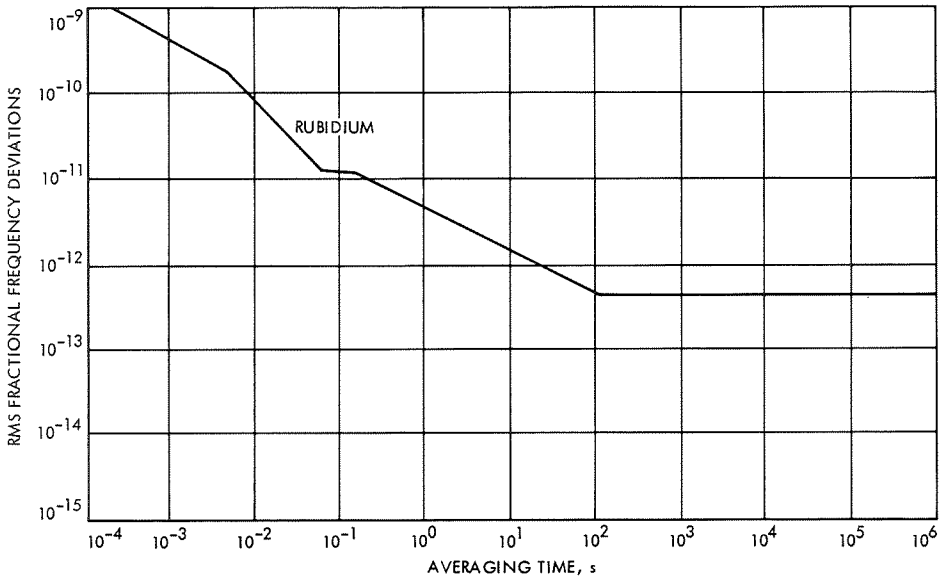

Fig. 3. Rubidium standard fractional frequency deviation

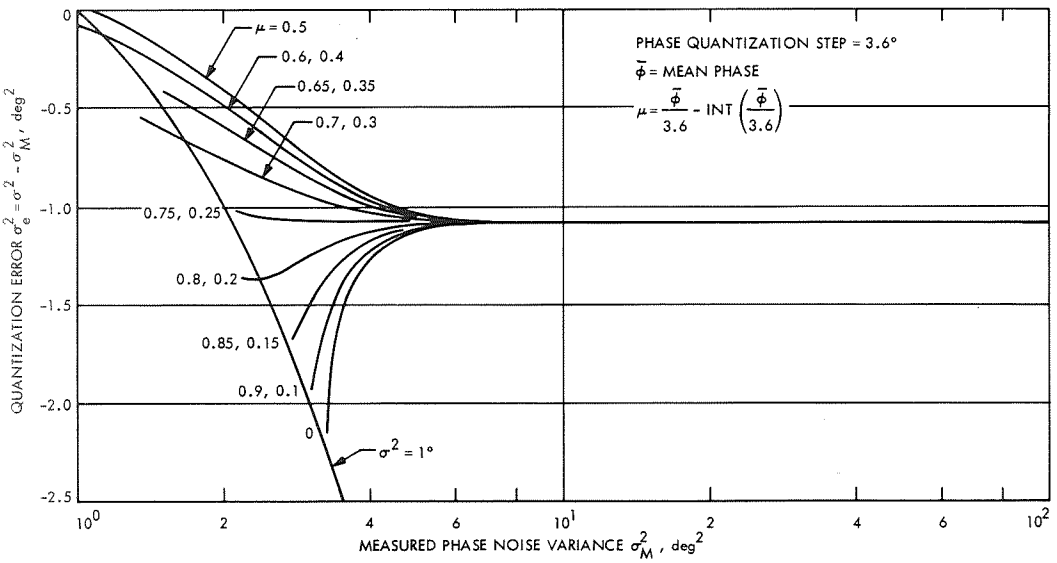

Fig. 4. Quantization error

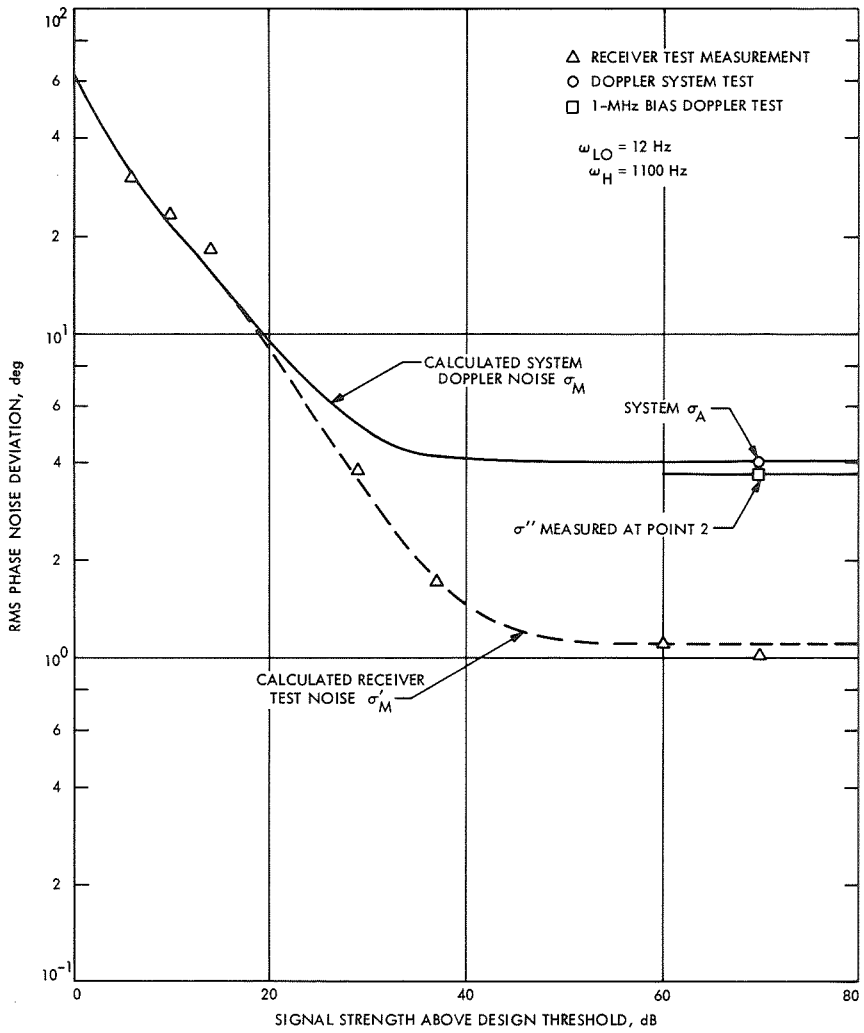

Fig. 5. System model

Numerical Evaluation of the Transient Response for a Third-Order Phase-Locked System

A. C. Johnson
DSIF Operations Section

A third-order phase-locked receiver is presently being investigated for possible use in tracking high doppler rates. This report presents additional data pertaining to the transient analysis of a model of a third-order phase-locked receiver.

Specifically, the instantaneous response of the system is calculated for an input phase function of the form

$$\theta(t) = \theta_o + \Omega_o t + \frac{1}{2}\Lambda_o t^2$$

The results presented may be compared with those of the usual second-order loop. It is hoped that this report will contribute some insight into the nature of the operation of third-order loops at least in the in-lock region.

I. Introduction

A third-order phase-locked receiver is presently being investigated for possible use in tracking high doppler rates. This report presents additional data pertaining to the transient analysis of a model of a third-order phase locked receiver presented in Ref. 1.

Specifically, the instantaneous response of the system is calculated for an input phase function of the form

$$\theta(t) = \theta_0 + \Omega_0 t + \frac{1}{2}\Lambda_0 t^2$$

where

θ_0 = initial phase offset
Ω_0 = initial frequency offset
Λ_0 = frequency rate, Hz/sec

The results presented may be compared with those of the usual second-order loop. It is hoped that this report will contribute some insight into the nature of the operation of third-order loops at least in the in-lock region.

II. Mathematical Model

A. Linear Transfer Function

From Ref. 1, a "realizable" open-loop filter transfer function for third-order phase-locked systems is of the form

$$F(s) = \frac{1 + \tau_2 s}{1 + \tau_1 s} + \frac{1}{(1 + \tau_1 s)(\delta + \tau_3 s)} \tag{1}$$

The definition of the parameters τ_1, τ_2, and τ_3 are given in Ref. 1. The resulting closed-loop transfer function $L(s)$

$$L(s) = \frac{rk(1+\delta) + r(1+\delta k)\tau_2 s + r(\tau_2 s)^2}{rk(1+\delta) + (r + r\delta k + \epsilon\delta k)\tau_2 s + (r + \epsilon + \delta k)(\tau_2 s)^2 + (\tau_2 s)^3} \tag{2}$$

where

$$r = AK\tau_2^2/\tau_1, \qquad AK \text{ is loop gain}$$
$$k = \tau_2/\tau_3$$
$$\epsilon = \tau_2/\tau_1$$

In terms of the closed-loop transfer function $L(s)$ there is the following relation between the input phase $\theta(t)$ and the phase error $\phi(t)$

$$\phi(s) = [1 - L(s)]\,\theta(s) \tag{3}$$

where

$$\theta(s) = \frac{\theta_0}{s} + \frac{\Omega_0}{s^2} + \frac{\Lambda_0}{s^3}$$

In general there will be non-zero initial conditions which can be expressed in the form: (Ref. 1)

$$U(s) = -\frac{K'}{s}\left[\frac{U_1}{1 + \tau_1 s} + \frac{U_2}{(1 + \tau_1 s)(\delta + \tau_3 s)} + \frac{U_3}{\delta + \tau_3 s}\right] \tag{4}$$

Here, K' is the gain from the output of the open loop filter $F(s)$, and the values of U_1, U_2, U_3 depend on initial capacitor voltages.

Thus the total phase error satisfies the relation:

$$\phi(s) = [1 - L(s)]\,(\theta(s) + U(s)) \tag{5}$$

B. Calculation of Loop Parameters

The loop parameters k and r must be calculated in terms of the parameters δ, and ϵ.

$$k = \left(\frac{2+\delta}{\delta^2}\right)\left\{1 - \left[1 - \frac{\delta^2}{(2+\delta)^2}\right]^{1/2}\right\} \approx \frac{1}{2(2+\delta)} \tag{6}$$

$$r = \frac{1}{(1+\delta)k}\left(\frac{V}{3}\right)^3 [1 + (1 - 3W/V^2)^{1/2}]^2 \times [1 - 2(1 - 3W/V^2)^{1/2}] \tag{7}$$

$$\left.\begin{aligned} W &= r + \delta k(r + \epsilon) \\ V &= r + \epsilon + \delta k \end{aligned}\right\} \tag{8}$$

The relation (7) expresses the condition that $L(s)$ has a pair of critically damped roots.

C. Calculation of Transient Response

The calculation of the transient response is done by implementing the Heaviside expansion formulas:

$$\sum p(a_n)/q'(a_n)\exp(a_n t) \tag{9}$$

for the case $q(s)$ has no repeated roots and

$$\sum_{r=0}^{n} (\psi^{(n-r)}(a)/[(n-r)!\,r!])\,t^r \exp(at) + H(t) \tag{10}$$

for the case when $q(s)$ contains $n+1$ repeated linear factors.

Here

$$\psi(s) = (s-a)^{n+1}\frac{p(s)}{q(s)} \tag{11}$$

The inverse Laplace transform is obtained for

$$[1 - L(s)]\,\theta_0/s, \quad [1 - L(s)]\,\Omega_0/s^2,$$
$$[1 - L(s)]\,\Lambda_0/s^3, \quad [1 - L(s)]\left(\frac{-K'U_1}{s(1+\tau_1 s)}\right),$$
$$[1 - L(s)]\left(\frac{-K'U_2}{s(1+\tau_1 s)(\delta + \tau_3 s)}\right)$$
$$\text{and } [1 - L(s)]\left(-\frac{K'U_3}{s(\delta + \tau_3 s)}\right) \tag{12}$$

Each of the above transforms is the quotient of polynomials $p(s)/q(s)$, where the degree of $q(s)$ is greater than the degree of $p(s)$. Also, it may be assumed that the leading coefficient of $q(s)$ is 1.

In case $q(s)$ has no repeated linear factors, the computation of the transient error, based on formula (9) is straightforward.

For the case when $q(s)$ has repeated linear factors,

$$q(s) = (s-a)^2 q_0(s) \tag{13}$$

where

$$q_0(a) \neq 0$$

Letting

$$\psi(s) = (s-a)^2 p(s)/q(s) \tag{14}$$

it is seen that

$$p(s)/q(s) = \frac{\psi'(a)}{s-a} + \frac{\psi(a)}{(s-a)^2} + h(s) \tag{15}$$

where

$$h(s) = \frac{p(s) - q_0(s)\left[\psi'(a)(s-a) + \psi(a)\right]}{(s-a)^2 q_0(s)} \tag{16}$$

is the sum of the partial fractions corresponding to the remaining factors of $q(s)$.

Since $|h(a)|$ is finite, one can write

$$p(s) - q_0(s)\left[\psi'(a)(s-a) + \psi(a)\right] = (s-a)^2 h_0(s) \tag{17}$$

Thus

$$h(s) = \frac{h_0(s)}{q_0(s)} \tag{18}$$

To find $h(s)$, one may equate the coefficients of like powers of s in Eq. (17). If $q_0(s)$ has repeated linear factors, the above procedure is applied to the rational function $h(s)$. This process may be continued until $p(s)/q(s)$ is decomposed into partial fractions. Once the partial fraction decomposition is completed, formulas (9) and (10) may be applied to obtain the inverse.

Thus the computational problem consists mainly of the numerical evaluation of the roots of $q(s)$, and in the determination of the numerical values of the polynomials $p(s_k)$ and $q_0'(s_k)$.

The JPL Library subroutine, POLZER, is used for the numerical evaluation of the roots s_k of $q(s)$. In every case considered, the roots were accurate within five decimal places. From a practical point of view, the errors made in evaluating the roots of $q(s)$ are insignificant, since the values of system parameters are seldom known to a high degree of accuracy.

The problem of implementing the general formula (10) on a digital computer appears to be quite difficult. Therefore, the evaluation of the transient response is limited to those cases where $q(s)$ has at most roots or order two.

III. Data Analysis

The data is presented in graphical form. The graphs display the response of the system to the inputs:

$$\frac{\theta(t)}{\Omega_0} = t \text{ (Figs. 1–5)}$$

and

$$\frac{\theta(t)}{\Lambda_0} = \frac{t^2}{2} \text{ (Figs. 6 and 7)}$$

for various values of the parameters ϵ and δ, and for zero initial conditions.

There are five curves per frame. These are numbered from 1 to 5 and corresponding parameters used to obtain the curve appear on the plot frame.

It is interesting to note that the maximum transient error is reasonably independent of the parameters ϵ and δ in the regions.

$$0 < \epsilon \leq 0.1, \qquad 0 \leq \delta \leq 0.1$$

As a practical example of the way these curves may be used, consider the case for the response to a frequency rate input when δ and ϵ are near zero, say $\delta = 0$ and $\epsilon = 0.001$. Then the peak response from Fig. 6 is

$$\frac{\phi_{ss}\omega_L^2}{\Lambda_0} = 1.22$$

Also, a reasonable assumption is that the maximum phase error for lock-on is 1 rad. If we also assume a DSIF receiver bandwidth of 10 Hz, then the maximum frequency rate is

$$\Lambda_{0_{max}} = 13.05 \text{ Hz/sec}$$

It is interesting to note that this will not meet the maximum one-way doppler rate expected at Jupiter encounter, which is 30 Hz/sec. However, for a bandwidth of 20 Hz the maximum frequency rate is approximately 52.6 Hz/sec.

Figure 8 is a plot of the transient response for the second-order loop where the input phase function is $\theta(t)/\Lambda_0 = t^2/2$. The response in this case is independent of the parameter δ and approaches a stable value of about 1.56 as $\epsilon \to 0$. For non-zero values of ϵ the steady-state response is unbounded.

References

1. Tausworthe, R. C., and Crow, R. B., "Practical Design of Third-Order Tracking Loops," Interim Report 900-450, April 27, 1971 (JPL internal document).
2. Tausworthe, R. C. "Theory and Practical Design of Phase-Locked Receivers," Technical Report 32-819, Jet Propulsion Laboratory, Pasadena, Calif., Feb. 15, 1966.
3. Churchill, R. V., *Operational Mathematics*. McGraw Hill Book Co., Inc., 1958.

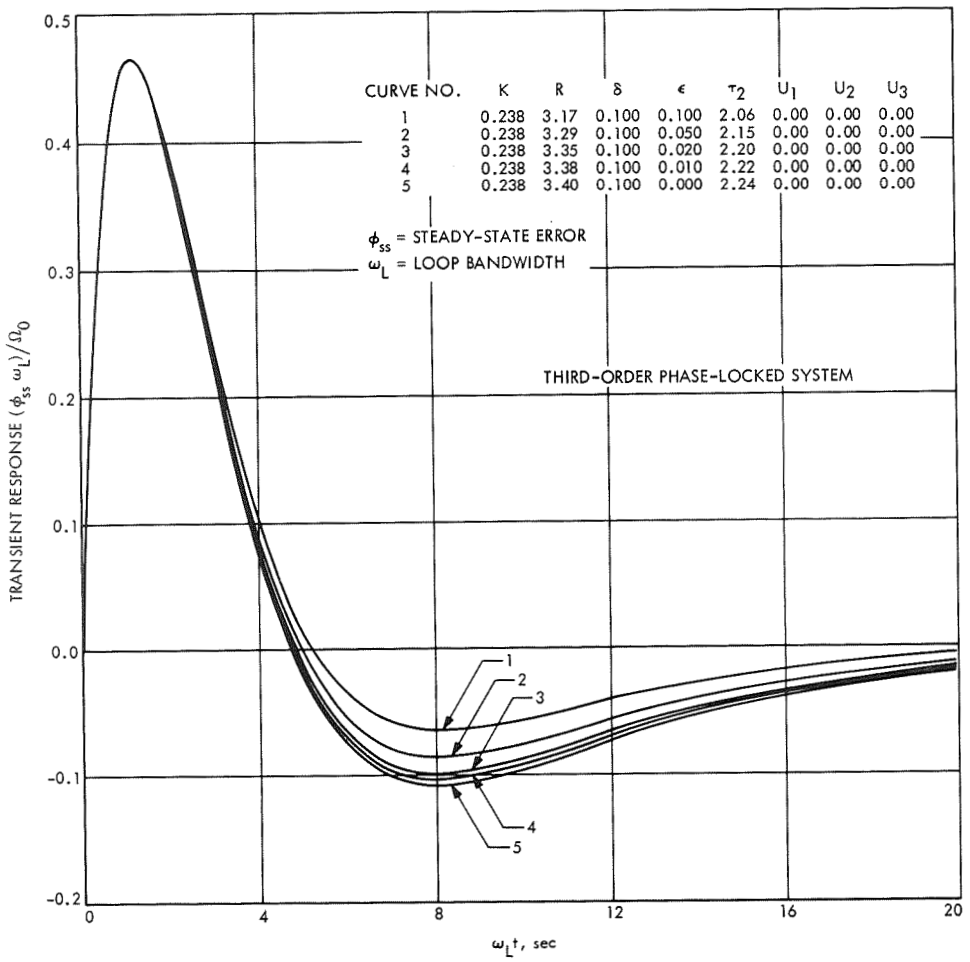

Fig. 1. Variable signal level, $\delta = 0.1$, $\epsilon = 0$ to 0.1 (third-order phase-locked system)

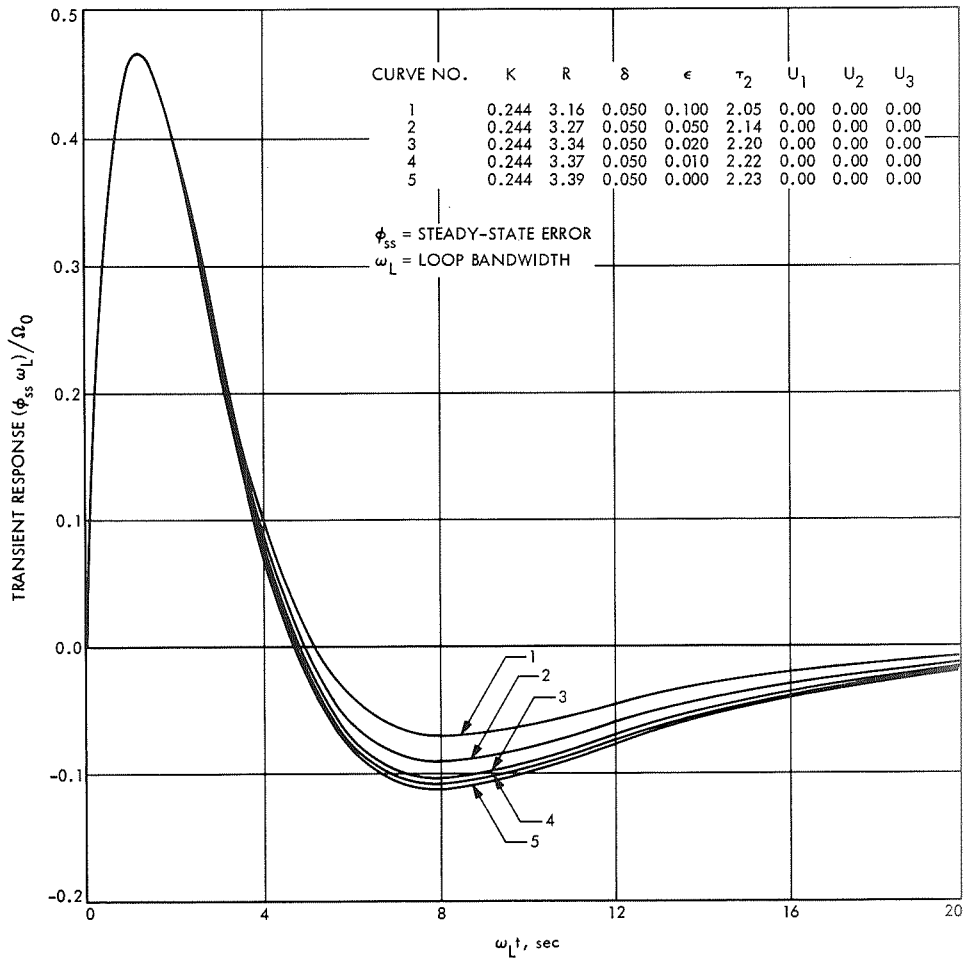

Fig. 2. Variable signal level $\delta = 0.05$, $\epsilon = 0$ to 0.1 (third-order phase-locked system)

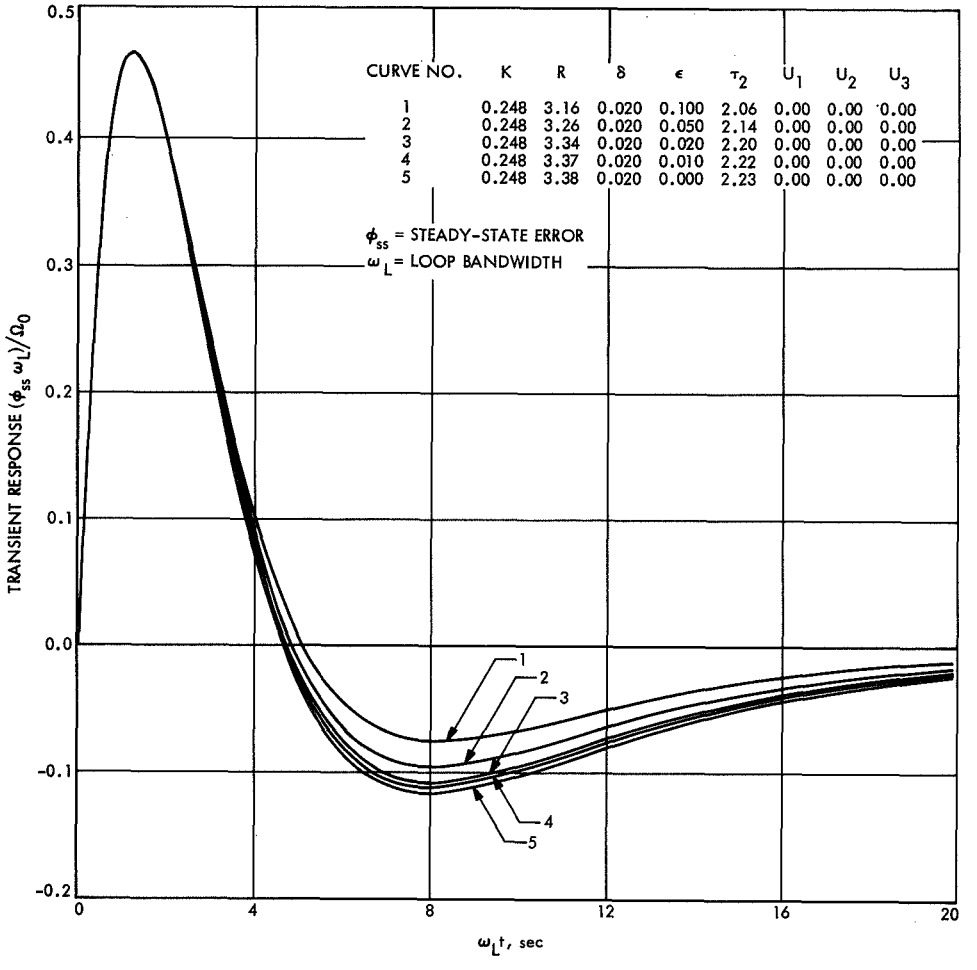

Fig. 3. Variable signal level $\delta = 0.02$, $\epsilon = 0$ to 0.1 (third-order phase-locked system)

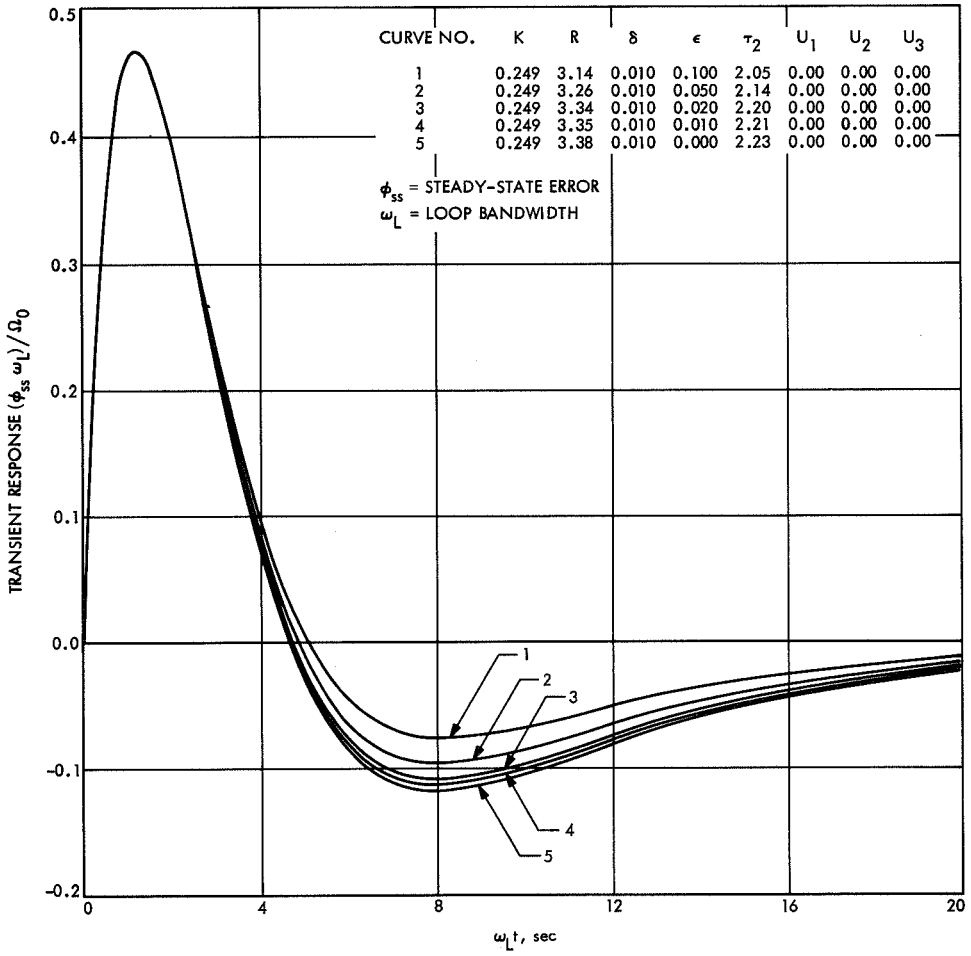

Fig. 4. Variable signal level, $\delta = 0.10$, $\epsilon = 0$ to 0.1 (third-order phase-locked system)

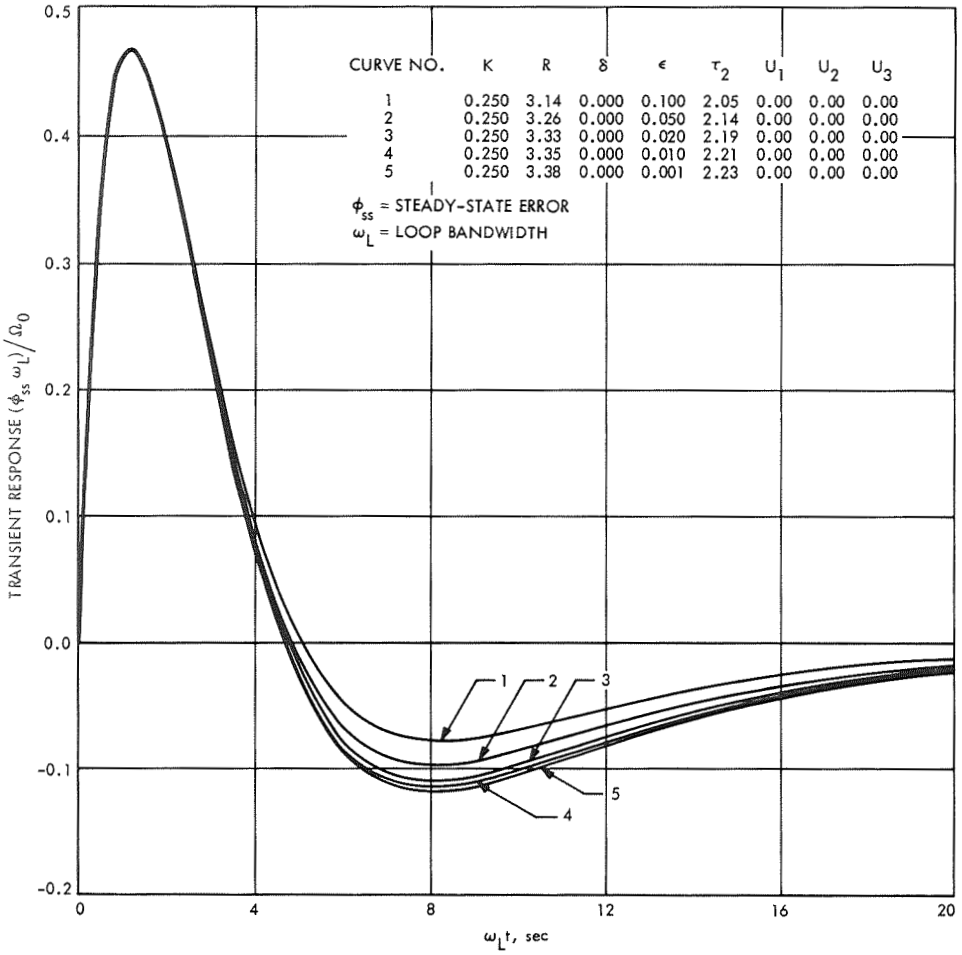

Fig. 5. Variable signal level, $\delta = 0$, $\epsilon = 0.001$ to 0.1, $\theta(t)/\Omega_0 = t$, $\theta(t)/\Lambda_0 = t^2/2$ (third-order phase-locked system)

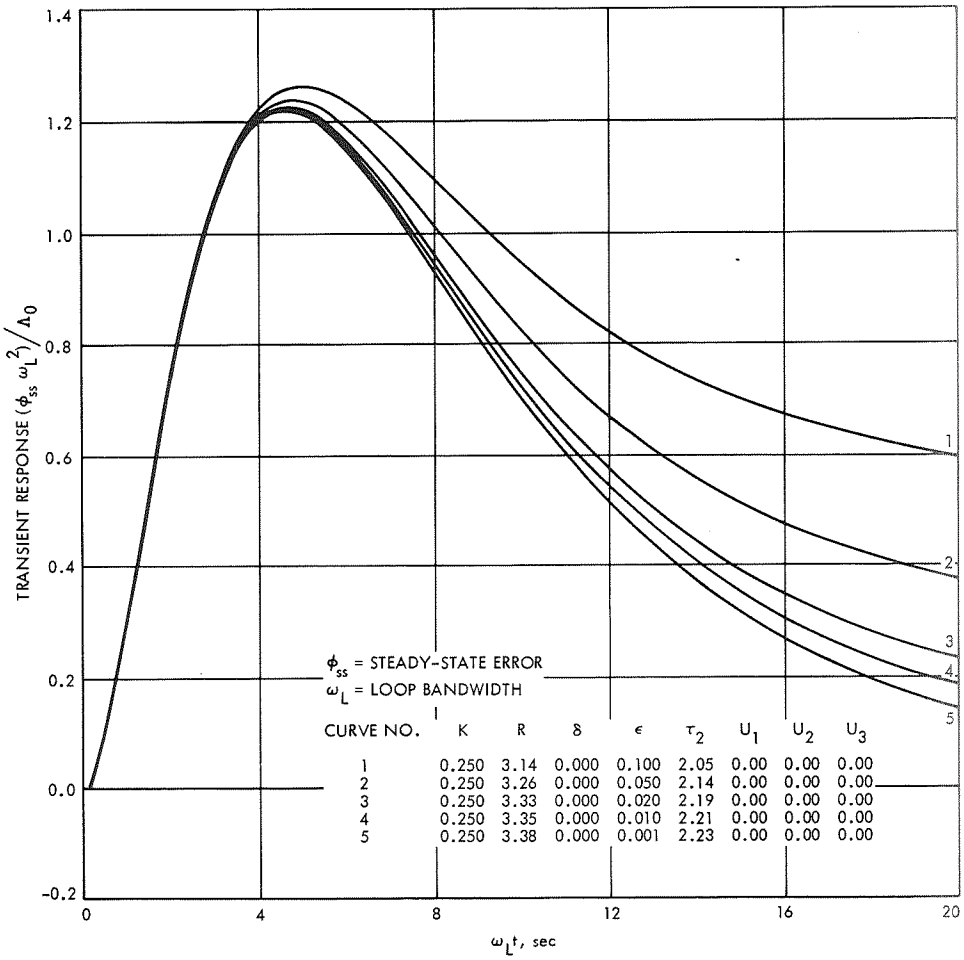

CURVE NO.	K	R	δ	ϵ	τ_2	U_1	U_2	U_3
1	0.250	3.14	0.000	0.100	2.05	0.00	0.00	0.00
2	0.250	3.26	0.000	0.050	2.14	0.00	0.00	0.00
3	0.250	3.33	0.000	0.020	2.19	0.00	0.00	0.00
4	0.250	3.35	0.000	0.010	2.21	0.00	0.00	0.00
5	0.250	3.38	0.000	0.001	2.23	0.00	0.00	0.00

Fig. 6. Variable signal level, $\delta = 0$, $\epsilon = 0.001$ to 0.1 (third-order phase-locked system)

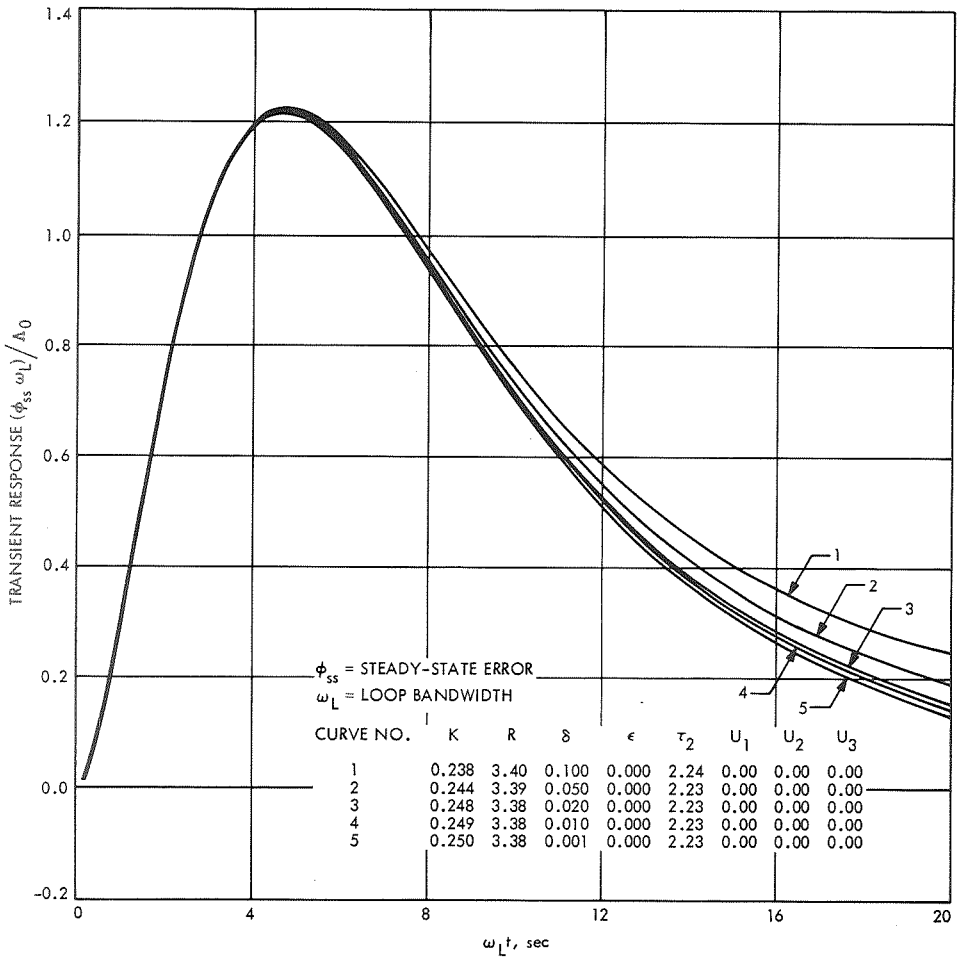

CURVE NO.	K	R	δ	ϵ	τ_2	U_1	U_2	U_3
1	0.238	3.40	0.100	0.000	2.24	0.00	0.00	0.00
2	0.244	3.39	0.050	0.000	2.23	0.00	0.00	0.00
3	0.248	3.38	0.020	0.000	2.23	0.00	0.00	0.00
4	0.249	3.38	0.010	0.000	2.23	0.00	0.00	0.00
5	0.250	3.38	0.001	0.000	2.23	0.00	0.00	0.00

Fig. 7. Variable signal level, $\delta = 0.001$ to 0.1, $\epsilon = 0$ (third-order phase-locked system)

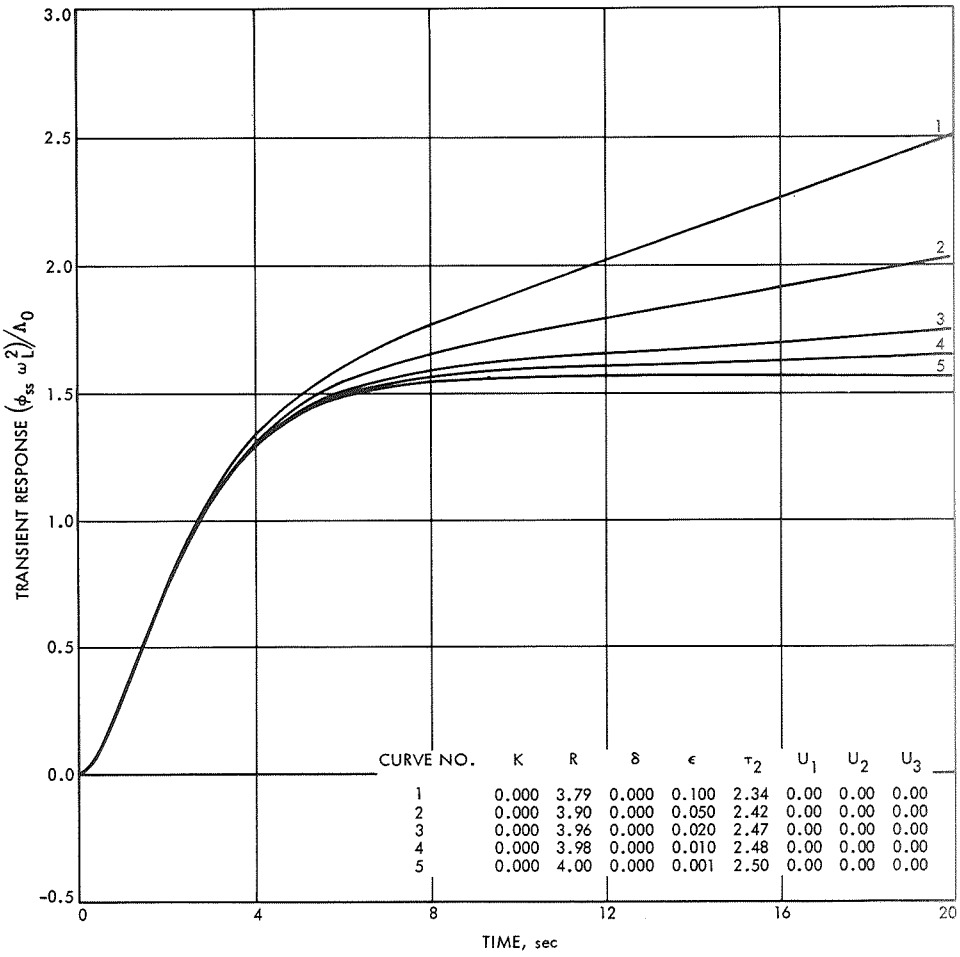

Fig. 8. Variable signal level, $\delta = 0$, $\epsilon = 0.001$ to 0.1 (second-order phase-locked system)

DSIF Operations Support of *Mariner* Mars 1971

D. W. Johnston
DSIF Operations Section

This article is an abbreviated description of DSIF Operations activities in preparation for, and up to and including, Mariner Mars 1971 launches H and I. New DSIF hardware is covered briefly, with rather more detailed coverage of the DSIF training, testing, operational documentation and performance aspects of the preparations.

I. Introduction

A direct result of the application of knowledge and experience accumulated by the DSIF during preparations for the now considerable number of past lunar and deep space missions has been the development of a logical standard pattern and sequence of events.

Basically, the major events in readying the DSIF for a mission are:

(1) Evaluation of new mission spacecraft parameters and possible requirements for new DSIF hardware (HW) and software (SW).

(2) Design, prototype fabrication and checkout of necessary additional new HW.

(3) Design of new SW.

(4) Procurement of production models of HW including spares, documentation, etc.

(5) Generation of engineering (mission independent) training program, initially for DSIF instructors, then DSS personnel.

(6) Generation of operations (mission dependent) training plan (DSN Test Plan, Vol. VI).

(7) Generation of operations (mission dependent) procedures (DSN Operations Plan, Vol. VII).

(8) Acceptance testing of SW programs.

(9) Implementation of any necessary mission independent DSS personnel training.

(10) Implementation of mission-dependent DSS personnel operational training (if possible with live spacecraft).

(11) Installation of HW at DSSs (per DSN Operations Plan, Vol. VI, DSIF Configuration Document).

(12) Delivery of SW to DSSs and implementation of HW and SW integration tests at DSSs (DSN Test Plan, Vol. VI).

(13) Implementation of DSS on-site training.

(14) Starting DSIF operational verification tests (OVTs).

(15) Supporting DSN system tests.

(16) Finalizing DSIF OVTs.

(17) Supporting DSN OVTs.

(18) Supporting MOS, OVTs and ORTs.

(19) Supporting launch and tracking.

Mariner Mars 1971 (MM-71) preparations followed this outline as closely as possible, but slippages in delivery of HW, SW, documentation, and in particular, loss of SFOF support, seriously restricted the early DSIF training, making numerous tradeoffs necessary.

II. New DSIF Hardware (HW) for MM-71 Era

The MM-71 mission design called for increased capabilities at the DSSs, the main requirements being to process four spacecraft subcarriers (one engineering and one science from each of two spacecraft) simultaneously, science up to 2 kbits/s at the 26-m stations, and 16.2 kbits/s at DSS 14, higher command activity, and repetitive occultation experiments.

These added requirements plus the continuing state-of-the-art improvements resulted in the following new equipment being installed prior to MM-71 launch:

(1) Open-loop receivers and peripheral equipment (at DSSs 14, 41, and 62).

(2) Additional SDAs (total of four at 12, 41, 62 and six at DSS 14).

(3) Command modulator assemblies (CMAs).

(4) New TCP HSDL buffers (for use with 4800 bps modems).

(5) Dual high-density digital recorders (DSSs 14, 71, and CTA 21).

(6) Dual low-density digital recorders (DSSs 12, 41, and 62).

(7) Symbol sync assemblies (SSAs).

(8) Block decoder assemblies (BDAs).

(9) Simulation conversion assemblies (SCAs).

(10) DSIF monitor system, Phase 1 (HW and SW).

(11) Updated station monitor console (SMC).

(12) Updated timing system (FTS II).

(13) Dual Block III masers.

The foregoing equipments were installed and, with the exception of the open-loop receivers, operational before launch. The open-loop receivers will be operational at the end of June 1971.

The various DSIF mission-independent software programs and the mission-dependent MM-71 software are described in "DSIF *Mariner* '71 Operational Program" by R. Chafin. Also the DSIF/S/C compatibility activities associated with MM-71 preparations are not covered in the article.

III. DSIF Training

A. Mission-Independent Training

Formal training for two engineers from each DSS was carried out during August 1970. This covered detailed theory of operation, calibration, maintenance and general operation of most of the equipments listed in Subsection II. After completion of the course the engineers returned to their respective stations with training packages and proceeded to instruct the station personnel on the operation and maintenance of the equipment in their respective areas of concern.

At this time the new equipment was delivered and installation started at the prime MM-71 stations.

B. Mission-Dependent Training

The mission dependent training took place at JPL and GDSCC during November and early December 1970. The trainees were: One Operations supervisor, one senior RF operator and two senior digital instrumentation operators from each of the MM-71 prime stations, i.e., DSSs 12, 14, 41, 51, 62, 71 and MSFN ACN, plus the DSIF elements of the DSN OCT, i.e., five assistant DSIF chiefs and five station controllers. Approximately six engineers from the DSIF Operations section also took part in the training to varying degrees.

1. Program objectives. The purpose of this training was to:

(1) Train operators in the use of MM-71 software and the recently updated hardware under realistic operational conditions.

(2) Familiarize operators with MM-71 spacecraft RF parameters.

(3) Check, verify and finalize MM-71 operational procedures with teams of DSS operators.

(4) Develop and exercise any special procedures required to work around spacecraft non-standard performance or spacecraft/DSIF design incompatibilities.

(6) Ensure immediate recognition and isolation of any inadvertent simulation-induced problems during DSIF/DSN/MOS tests.

(7) Familiarize members of the DSN operations organization, including the OCT, with pertinent aspects of the above.

2. Description of training program. The training covered by this section is outlined in Sections II, III and IV of Document 610-88, "DSN Test and Training Plan for *Mariner*-71 Project," Vol. VII of *DSIF Operations Test Procedures*. In general, the training consisted of lectures, classroom instruction, review of procedures, hands-on equipment familiarization, practice of procedures, observation, and tours of facilities.

A list of the speakers of the lecture portion of the program is contained in Table 1, which also lists their subjects. The classroom instruction, for operators only, consisted of familiarization with the SCA and TCP software programs, and was integrated with "hands-on" training on the computers. This phase was conducted at the Goldstone Network Training Support Facility and the DSS 12 control room, and lasted four days.

While the operators were at GDSCC, the supervisors were reviewing MM-71 documents. These were:

(1) 610-82, DSIF stations configuration

(2) 610-83, DSIF operating procedures

(3) 610-88, DSIF test and training plan

Tours of the Spacecraft Assembly Facility (SAF) and the Space Flight Operations Facility (SFOF) were conducted by G. Wade Earle and L. William Pellman, respectively.

Three days were utilized in performing station countdowns on the Multiple Mission Telemetry and Command Subsystems at DSS 12.

The final 12 days of training were conducted at the CTA 21. Both a live MM-71 spacecraft and the Simulation Center in the SFOF were used as data sources. The trainees operated station equipment in accordance with MM-71 Operating Procedures and DSIF Standard Operating Procedures and daily sequence of events. This phase was conducted on a team, or crew, basis; teams not involved in counting down the station or "tracking" periods observed activities at CTA 21 or in the SFOF.

3. Lecture series presentation. The series of lectures listed in Table 1 were presented at JPL, Pasadena. Lectures 1 through 13 were delivered at Von Karman Auditorium and were attended by all trainees. Lectures 14 through 15 were given at various locations in Buildings 126 and 230 and were attended by the Operations Supervisors only. Visual aids, namely slides, were used extensively.

4. Goldstone presentation. On Nov. 5, 1970 operator trainees attended classroom instruction on the SCA and TCP Software Programs. Each student received approximately three and one half hours on each program.

On Nov. 6 through Nov. 8, the following on-site training was held in the control room at DSS 12.

SCA. All individuals received 4 h of group training on the SCA mnemonic inputs. Eight hours were spent using the SCA as a data source for the TCP, with the students configuring the SCA, RCVR, SDAs, SSAs, BDAs and CMAs, as if in an actual countdown.

TCP. All individuals received 12 h training on the TCP/CMA software covering the telemetry and command portions of the program.

The major problem area was in the command portion of the software. The software and documentation was incorrect and certain interrupt patches were omitted.

For the Station Countdown 11 to 13 November 1970, all operator trainees plus the operation supervisor of the stations participated in the countdown tests. The group from each station had the opportunity to do each countdown twice for a total of 6 h actual hands-on practice. Included in the training was two hours theory on Y factor techniques.

SMC/CRT. The participating students were given an introduction to the CC-30 display system by video tape. Then a brief explanation was given as to how the monitor program will interface with the SMC/CRT, followed by a demonstration program from the DIS. In addition, convergence of the CC-30 color TV display was taught by hands-on training. The summary was presented by video tape.

5. CTA 21 presentation. Training was conducted at CTA 21 from Nov. 16 through Dec. 2, 1970 in three phases using equipment configurations as follows:

Nov. 16 through 21	CTA 21/Spacecraft at SAF/SFOF.
Nov. 23 through 25	CTA 21/Simcen/Spacecraft at SAF/SFOF OPS Control.
Nov. 30 through Dec. 2	CTA 21/Simcen/SFOF OPS Control; CTA 21/Simcen.

A final critique covering DSIF operator training for MM-71 was held on Dec. 3, 1970.

A typical sequence of events was used from Nov. 16 through Nov. 30. Minor modifications were made from time to time to facilitate changes in configuration. This sequence simulated a normal spacecraft pass with the following nominal schedule of activities:

0800–1100 PST	Station countdown
1100–1700 PST	Tracking
1700–1800 PST	Daily critique

As a result of the daily critiques, training activities during Dec. 1 and 2 concentrated on hands-on operation of the SCA only. Each team was allotted 2 h to operate the SCA in the stand-alone mode and as a data router in the Simcen long-loop mode. The trainees returned to their respective DSSs the second week in December 1970 and using the training packages provided, initiated the DSS on-site training programs. Two weeks were allocated to on-site training and the DSIF operational verification tests started on Jan. 1, 1970.

IV. DSIF Testing

Table 2 summarizes the number of operational tests supported by the various stations.

V. Operational Documentation

The main changes in the documentation for MM-71 were in the DSN Operations Plan, Vols. VII and VIII. Volume VII was subjected to a major revision which resulted in the basic document containing only DSIF MM-71 procedures for use on a day-by-day basis. This is supplemented by ten appendices covering rarely (or once only) used procedures e.g., MSFN ACN commanding, launch procedures etc. The second part of the document (addendum) is composed entirely of useful background information, e.g., spacecraft RF, Command, subsystem descriptions and parameters, etc.

The DSN Operations Plan, Vol. VIII basic content followed the MM-69 philosophy to a greater degree by containing only limited samples of launch predicts, and went into great detail on the initial acquisition study. The various documents were published as shown in Table 3.

VI. Operational Performance of New Equipment

The new equipment has performed very satisfactorily under operational conditions during OVTs, both launches, one trajectory correction maneuver and approximately 4 wk of tracking.

The main exception was the operation of the command system. In the early training and testing numerous command alarms and aborts were experienced. These were gradually eliminated by modifications (patches) to the DSIF TCP and SFOF 360/75 software programs and eventually reissues of both programs. However, approximately 6 wk prior to launch it became apparent that a "bit verify" alarm/abort problem still existed. This triggered an intensive 24-h/day trouble shooting exercise at GSDCC, CTA 21, and some of the overseas stations. The problem was isolated to a noise problem inherent in the TCP/CMA basic hardware design. A modification was hastily fabricated and personnel rushed to the prime MM-71 stations where it was installed and soak tests carried out prior to the ORT.

During the extensive soak tests a specific version of the bit verify abort problem (abort on first bit of first command in block) was observed on a random/periodic basis. This was isolated to a software induced hardware (timing) problem where an erroneous bit verify abort could occur because of the phase relationship between the DSS 1 PPS timing and the CMA CMD modulation frequency (random) coupled with the cumulative effect of the phase difference (periodic). A software program "fix" was generated. However, due to the lack of time to carry out extended checks on the fix before launch it was decided that any unknown side effect of the fix would be a greater risk than the known possibility of an erroneous command abort, and the fix was not incorporated for launch and midcourse. Both launches and the "I" midcourse correction were supported without any command problems.

After the midcourse correction a spacecraft CC&S update was carried out involving transmission of approximately 450 ground commands. These commands were planned to be sent continuously on 30-s centers, and in the early part of the exercise a total of 5-bit verify aborts occurred. These were noted as occurring approximately every 21 min, and simple arithmetic quickly tied this to the nominal subcarrier frequency over spacecraft actual frequency, which gives 1 1/1277, giving a coincident periodicity of 21 min, 17 sec. The commands were then continued with a break of 2 min every 20 min, thus avoiding the problem.

Phase four of the DSIF TCP operational program will incorporate a permanent fix for this problem together with other refinements.

Table 1. Lecture presentations

Lecture number	Speaker	Topic
1	R. K. Mallis	Introduction and Section 337 Organization
2	R. T. Hayes	Mission Operations
3	J. H. Duxbury	Spacecraft Systems
4	D. M. Scaff	Spacecraft Radio Subsystem
5	W. H. Chitty	Spacecraft Command Subsystem
6	C. E. Geuy	Spacecraft Telemetry Subsystems
7	I. L. Emig	Operator Training Schedule
8	J. R. Buckley	Station Countdown Philosophy
9	R. C. Chernoff	DSN/DSIF Monitor System
10	H. C. Thorman	SFOF Simulation Center
11	E. Garcia	Simulation Conversion Assembly
12	D. L. Gordon	DSN Operations Control Team
13	R. L. Chafin	DSIF Software Program Support
14	D. Nightingale	Introduction to Upgraded High Speed Data System
15	R. W. Burt	System COE Functions
16	R. B. Miller	SFOF Tracking System
17	W. H. Higa	Time Synchronization Systems
18	J. G. Leflang	Block III Masers
19	C. P. Wiggins	DSS Transmitters

Lectures 14 through 19 were attended by supervisors only.

Table 2. Operational tests

Tests	Station							
	ACN	12	14	41	51	62	71	Total
DSIF OVTs	4	13	12	12	11	10	4	66
MOS Launch I/cruise H	3	3		7	7	3	7	30
MOS Trajectory correction		1		5	5	1		12
MOS Trajectory correction 67-h test		—	—	—	—	—		
MOS Trajectory correction 85-h test		—	—	—	—	—		
MOS ORT	—	—	—	—	—	—	—	
DSN combined systems tests		6	1	3	3	3	2	18

Table 3. DSIF documentation

DSN Operations plan for MM-71			
Volume	**Title**	**Document number**	**Date**
Vol. VI	*DSIF Station Configuration*	610-82	10/9/70
		610-82; Rev. A	4/23/71
Vol. VII	*DSIF Operations Procedures*	610-83	11/1/70
		610-83; Rev. A	2/15/71
		610-83; Ad. 1	3/30/71
Vol. VIII	*DSIF Preflight Nominal Predictions*	610-84	4/20/71
DSN Test/Training Plan			
Vol. VI	*DSIF Engineering Test Procedures*		10/30/70
Vol. VII	*DSIF OPS Test Procedures*		8/15/70

DSIF *Mariner* Mars 1971 TCP Operational Program

R. L. Chafin
DSIF Operations Section

The Deep Space Instrumentation Facility (DSIF) Mariner Mars 1971 Telemetry and Command Processing (TCP) Operational Program provides the software necessary to support the Mariner Mars 1971 mission operations by processing all telemetry data from the spacecraft and providing a means to command the spacecraft from both the Space Flight Operations Facility and the station. The program is designed for use with the multiple-mission telemetry and multiple-mission command hardware. This article describes the organization, operation, and capabilities of this program.

I. Introduction

The DSIF *Mariner* Mars 1971 TCP Operational Program (Fig. 1) was developed to provide on-site processing of telemetry and command data for support of the *Mariner* Mars 1971 Project. It was designed to be used with the MMT and MMC hardware.

II. Program Description

The program is used in an XDS 920 computer with a 16,000-word core memory. The program was written with the objective of developing the telemetry and command sections separately. The telemetry and the command sections are combined in the same software package with an Executive. They were tested separately for functional integrity, then tested as a complete package for interference between sections.

A. Executive

The executive program provides the basic framework for the *Mariner* Mars 1971 operations program. It controls the execution of the TLM and the CMD subprograms and controls the I/O activity. It also controls those functions which are common to both the TLM and the CMD programs, such as the HSD and the magnetic tape output.

This program operates under a real-time environment, which generates interrupts to interface with the system hardware. These interrupts generate flags to indicate routines needing servicing. The executive program sequentially polls the TLM and CMD subprogram flags and executes those subprograms needing servicing.

The HSD blocks, which are generated in the TLM and CMD programs, are buffered by the executive and

output on the HSD lines. The HSD blocks are grouped in 5-block records and recorded on magnetic tape for the Original Data Record (ODR).

The executive controls the I/O typewriter typeins and typeouts. On typeins, the executive inputs the typein statement, tests the first character for the desired destination, (i.e., TLM, CMD, or EXC) and transfers the message to the appropriate program. Typeins starting with T go to the channel 1 telemetry, D go to the channel 2 telemetry, C go to command, B goes to both, and E goes to the executive. The TLM and CMD programs provide the typeout message to the executive, which, in turn, outputs them on the I/O typewriter.

B. Telemetry

The downlink transmitted by the spacecraft contains one or two telemetry data streams. During the cruise mission phase only one subcarrier is used, containing the engineering data. During the orbital mission phase a second subcarrier, containing the science data, is added. The station receiver locks up to the S-band carrier and provides the subcarriers to the SDA (Subcarrier Demodulator Assembly), one SDA to each subcarrier. The *Mariner* Mars 1971 TCP operations program processes each data stream separately. Channel 1 processes the engineering data and channel 2 processes the science data. The telemetry program frame syncs the engineering data and the low-rate science data and provides a TTY output as backup for the HSD output.

1. Channel 1. The channel 1 bit synchronizer consists of a combination of hardware and software. The integrated data stream from the SDA is sampled by the ADC (Analog to Digital Converter). The channel 1 subprogram makes an estimate of the bit transitions, calculates an error from the input data, and outputs a correction term to the numerical controlled oscillator. In terms of a phase-locked loop, the software provides the error detector and the filter; the numerical controlled oscillator is the VCO. The channel 1 telemetry program determines the logic value and the time of the incoming data and accumulates a digital data stream with appropriate time tags. The data is formatted into HSD blocks for outputting and recording. The analog data values are accumulated and processed to obtain an estimate of the SNR (signal-to-noise ratio).

2. Channel 2. The channel 2 bit synchronization is accomplished in the SSA (Symbol Synchronizer Assembly). For uncoded science telemetry, the data is input to the channel 2 program as a parallel digital number of 24 bits. For block-coded telemetry, that digital symbol data from the SSA is transferred to the BDA (Block Decoder Assembly) for decoding. The digital output from the BDA is input to the channel 2 program in a parallel 24-bit format. The channel 2 program formats the data into HSD blocks for outputting and recording. Data statistics are accumulated in the SSA and BDA. These statistics are input to the channel 2 program and are used to obtain estimates of the SNR for the telemetry stream.

3. Frame sync. Frame sync is obtained on the engineering data and the low-rate science data, using the PN bit sequence which is part of the *Mariner* Mars 1971 telemetry format. The engineering data stream is fully decommutated. The low-rate science is partially decommutated with pre-selected data parameters available for TTY output.

C. Command

The command program receives spacecraft commands from the SFOF by HSD, stores the commands, and outputs the commands to the CMA (Command Modulation Assembly). The CMA forms the command signal from the subcarrier frequency modulated by the command data and a PN sync signal.

1. Modulation index control. The command signal modulation index is controlled by the command program. The level of the command signal, which determines the modulation index, is controlled by a digital attenuator, and is set by the program.

2. Configuration control. The CMA configurations are stored in the configuration table. There is one configuration table entry for each mode. When a mode is entered, the appropriate configuration word is sent to the CMA. There it sets the relays, which generate the desired configuration. The configuration table can be modified by HSD input or by manual I/O input. The program provides an output of the contents of the configuration table upon either HSD or operator request.

3. Command stack. The stored commands are contained in the command stack. The program receives commands by either HSD input from the SFOF or by manual I/O entry. Commands are either *timed* commands or *priority* commands. Each new command is placed in the command stack following the preceding commands. *Priority* commands are output when they are

enabled. A series of enabled *priority* commands will be queued and output according to their entry into the command stack. Enabled *timed* commands will be output according to the transmission time associated with the command.

The program will provide a recall of the command stack upon request. The recall can be either by HSD or by manual I/O request. The recall response output, for an HSD request, is by HSD, for an I/O request it is by local RO display.

The status of the command stack is monitored and appropriate warning alarms are generated when the stack is near full, full, or contains commands which should be transmitted, but cannot be transmitted for some reason. When a particular command has been successfully transmitted, an HSD command confirmation message is output to the SFOF and the command is removed from the command stack.

4. System check. During the operation of the command program, the status of the station command system is continually checked. The parameters being checked are: transmitter ON, CMD modulation ON, correct exciter channel, and correct subcarrier frequency and bit rate. Discovery of any of these parameter outside their limits or in an incorrect state produces an alarm. The alarm message is sent to the SFOF by HSD and also displayed on the local RO display.

5. Commanding checks. During the time a command is being clocked out, the same system checks are being made. An anomalous system condition aborts the outgoing command. An abort HSD message is sent to the SFOF. The abort message contains the command that was attempted, the reason for the abort, and the bit on which the command was aborted.

The outgoing command signal is monitored by the command program. The subcarrier level and the PN sync level are checked each bit time. The outgoing command signal is demodulated and checked bit by bit against the command, which was intended to be sent. Any failure produces an abort.

6. Standard and limits tables. The limits of the parameters, which are checked during the system and commanding checks, are stored in the standards and limits tables. The table contains canned-in nominal limits. These limits can be modified by either HSD or manual I/O inputs. The contents of the table can be reviewed by means of a recall request. Again, the response to a recall request can be either HSD output or local RO output.

7. Incoming HSD message processing. The incoming HSD blocks are checked for a GCF error indication. They are also checked for proper station ID and spacecraft ID. If all checks are passed, the block is returned to the SFOF as a verification that the HSD block was received and the data in the block is routed to the proper destination. If the checks are not passed, an appropriate alarm is generated (placed in the verification message), which is sent to the SFOF. Rejection of the incoming HSD block by the command program is indicated by a specific bit in the alarm code included in the verification message. In this case, the verification message indicates that the original message was received by the command program, but was not acted upon because of an error in the format.

III. Operation

A. Initialization

There are a very large number of parameters required by the *Mariner* Mars 1971 operations program. In order to simplify the operation of the program, standard configurations and operating conditions were selected and canned into the program. A simplified initialization was designed for nominal operations. Capability of modifying the standard configuration is included in the design in order to accommodate nonstandard conditions. The nominal or standard telemetry initialization typeins are keyed to the different nominal mission phases:

Cruise	DCH/XX,Y,ZZ$	33⅓ bps engineering data
Orbital	DOL/XX,Y,ZZ$	8⅓ bps engineering data, 50 bps uncoded science data
	DOH/XX,Y,ZZ$	33⅓ bps engineering data, 50 bps uncoded science data
	DSD/XX,Y,ZZ$	8.1 kbps block coded spectral science data
	DTV/XX,Y,ZZ$	16.2 kbps block coded recorded science data

where

XX = the station number

Y = the TCP computer being used

ZZ = the spacecraft number

$ = the typein terminator

In the simplest configuration, the above typein is all that is required to initialize the telemetry program. For normal operations, one more typein is required to input the AGC calibration data for the AGC (voltage) to signal level (dBm) conversion. The telemetry program is started with the typein TRUN$. On starting, the telemetry program acquires the telemetry data streams and initiates the HSD output and the ODR recording.

The command program is initialized with the typein

CSS/XX,Y,ZZ$

This typein identifies the station number, computer, and spacecraft number to the command program.

The command signal modulation index is measured by station instrumentation and adjusted with a typein instruction. The command program is started with the typein CRUN$. The normal command operation is controlled remotely by HSD from the SFOF. Local manual control is available as a backup.

Nonstandard typeins are available to change the telemetry system configurations. For example, TS1/1,2,2$ modifies the channel 1 configuration to Receiver 1, SDA 2, computer B. Other telemetry bit rates are available, such as 1.0125, 2.025, 4.05, 8.1, 16.2 kbps, etc.; TB 2/10 is an example selecting 1.0125 kbps for telemetry channel 2. The bit loop SSA and BDA parameters, such as bandwidth, are canned in for each bit rate, but can be modified by nonstandard typeins.

Nominal configurations and parameters are canned in the program. Normal operation is to control the configurations and standard and limits parameters by HSD from the SFOF. However, nonstandard typeins are available to change these items at the station manually.

The HSD and ODR magnetic tape recording functions are normally enabled so that no operator action is required to initiate these functions. Typeins are available to control these activities. Each telemetry channel (i.e., 1 or 2) or command can be controlled separately or both together.

For example,

BHS/D$ disables all HSD output

CHS/D$ disables only command output

THS/D$ disables only channel 1 telemetry

DHS/D$ disables only channel 2 telemetry

The TTY output is not normally enabled. There is a complete set of typein statements that control the TTY output and the generation of headers.

B. Operation Modes

There are two telemetry modes, operating and initialization. The telemetry program processes the telemetry data during the operating mode. The processing is stopped during the initialization (or reinitialization) mode. During initialization typein statements are accepted to modify configurations, bit rates, etc. During the operating modes these input requests are ignored. The operating mode is initiated with a TRUN$ typein. Reinitialization is requested with typeins which stop the processing of the selected telemetry channel.

For example,

DIN/$ stops both telemetry channels

DIN1$ stops channel 1

DIN2$ stops channel 2

The command modes are more involved. They can be described as follows:

Calibrate 1. This mode is entered at the start of operations and is used to adjust the modulation index of the command signal.

Calibrate 2. This mode outputs parameters to the CMA. For example, going to CAL 2 mode allows a new subcarrier frequency to be sent to the CMA. Also, this mode is used when no commanding is anticipated, as when the station has no uplink.

IDLE 1. This is an idle mode where the spacecraft command loop is locked but no commanding can be accomplished. The system checks are made and alarms generated.

IDLE 2. This is the mode used when the station is in a commanding period but is between commands. System checks are made and alarms generated. The command system is ready to transmit commands.

Active. This is the mode used when a command is being transmitted. System check and command sig-

nal checks are made, and if any anomaly is detected, the command is aborted.

Abort. This mode is entered when a command is aborted. The PN sync code is inverted for 2 seconds to signal the spacecraft to inhibit that command, and 28 zeros are sent.

Figure 2 illustrates the mode sequence for the command program. The station brings the program to the CAL 1 mode and sets up the modulation index. After CRUN$ is entered by the station, the SFOF controls the mode by HSD. The command system is taken through CAL 2 and IDLE 1 and is ready for commanding. When a command is available for transmission, the program goes to active and transmits the command. The return is to IDLE 2 for a successfully completed command. The abort mode is entered directly from the active mode, upon detection of an anomaly. After the abort mode is completed, the program reverts to the mode specified in the abort return address. This will normally be IDLE 1. If IDLE 1 is the abort return mode, then no further commanding can be accomplished until action is taken to place the program in IDLE 2.

C. Manual Operation

The telemetry program is completely under manual station control. Normally the only action required is during initialization. In the operating mode the operation of the program is automatic.

The command program is normally operated remotely from the SFOF. In order to provide a backup capability in the event that communications are lost with the SFOF, a manual operating capability is included. The manual capability is normally locked out with a key-operated switch on the station manger's console. When manual operations is selected, the command program can be controlled locally. Commands can be entered into the command stack, enabled, and transmitted. The command system modes can be controlled by I/O typeins and commands can be aborted by operator initiative.

D. Performance Monitoring

The performance of the telemetry system is monitored with the estimated SNR produced by the program, the lock status information obtained from the receiver, SDA, bit loop, SSA and BDA, and from the received signal level obtained from the receiver AGC. This information is packed into the HSD blocks and is transmitted along with the telemetry data. The lock status information is also output with the TTY data.

The performance of the command system is monitored by the station personnel with a teleprinter (RO) output. The RO presents the significant command activity (such as commands entering the command stack and commands transmitted). Also the RO allows the operator visibility into the contents of the command stack, configuration cable, and the standards and limits table.

The previously described performance data, together with the telemetry and command program activity status, is sent to the station monitoring program in the digital instrumentation system (DIS) computer by means of a direct computer-to-computer link. The station monitor program displays the data on a CRT display for the station manager and sends the data to the SFOF as a part of the DSN Monitor System.

E. Inputs

The inputs to the telemetry program are the two telemetry data streams and the I/O initialization. The telemetry data streams are:

Channel 1 Engineering data, uncoded either 8⅓ or 33⅓ bps.

Channel 2 Science data, one of the following:

(a) Coded 50 bps.

(b) Block coded 1.0125, 2.025, 4.05, 8.1, 16.2 kbps. Recorded science, selected video, or spectral science.

The inputs to the command program are the I/O initialization, HSD messages from the SFOF, and manual operating I/O inputs. The HSD messages are:

Command	Contains up to 8 new commands.
Enable/disable	Enables or disables a command in the command stack.
Configuration	Modifies the configuration table.
Standards and limits	Modifies the standards and limits table.
Recall request	Requests recall of either the command stack, the configuration table, or the standards and limits table.

F. Outputs

The output of the telemetry program consists of HSD blocks. There are two telemetry formats. The engineering data and the low-rate science data HSD blocks contain 168 bits in each block. The higher-rate science data HSD

blocks contain 936 bits. The time to accumulate data from the spacecraft to fill up one HSD block is as follows:

Data rate, bps	Time to accumulate data, s	Bits per HSD block
8⅓	20.16	168
33⅓	5.04	168
50	3.36	168
1012.5	0.924	936
2025	0.462	936
4050	0.231	936
8100	0.1155	936
16200	0.05775	936

The HSD blocks consist of 1200 bits of header, data, overhead, and filler. The HSD operates at a rate of 4800 bps; therefore, a block is output every 0.25 s. From the above table it can be seen that only 2025-bps data and under can be sent by HSD. All higher data rates must use a wide-band (WB) line, which is only available between DSS 14 and the SFOF. The WB line operates at 50 kbps and is capable of transmitting a block every 0.024 s.

The output of the command program is the command data stream and the HSD messages, which report command activity to the SFOF. These messages are:

Confirm/abort — Reports the successful transmission of a command (confirm) or an unsuccessful transmission (abort).

Alarms — Detection of an anomalous system condition generates an alarm message containing a code indicating the cause of the alarm.

Recall response — A recall request will generate a message or series of messages in response. They will contain the contents of the command stack, the configuration table, or the standards and limits table as requested.

Verification — Every received HSD message is turned around and sent back as a verification that the block is received. Any alarms generated by the message or any outstanding alarms are added to the verification message.

All HSD blocks, both incoming and outgoing, are recorded on magnetic tape as an Original Data Record (ODR). All manual inputs are formatted into equivalent HSD records and also recorded on the ODR.

The backup TTY outputs data in three formats.

(1) 8⅓ or 33⅓ bps engineering data only.

(2) 50 bps science data only.

(3) 8⅓ and 50 bps data confined.

Only one TTY line is required for each of these data formats.

IV. Conclusion

The *Mariner* Mars 1971 TCP Operational Program provides the software necessary to support the *Mariner* Mars 1971 mission operations by processing all telemetry data from the spacecraft and providing a means to command the spacecraft from both the SFOF and the station.

Bibliography

Chafin, R. L., et al., "Mariner Mars 1971 TCP Operational Program," Document 610-141, Oct. 1, 1970 (JPL internal document).

Chafin, R. L., and Carter, R. D., "Software Requirements Document Mariner Mars 1971 TCP Operational Program," DSN Software Design Book DSW-2-6000-M71, Sept. 15, 1970 (JPL internal document).

Crow, R., et al., "DSIF Multiple Mission Command System," in *The Deep Space Network*, Space Programs Summary 37-63, Vol. II, pp. 77–94. Jet Propulsion Laboratory, Pasadena, Calif., May 31, 1970.

Frey, W., et al., "Multiple Mission Telemetry 1971 Configuration," in *The Deep Space Network*, Space Programs Summary 37-63, Vol. II, pp. 63–77. Jet Propulsion Laboratory, Pasadena, Calif., May 31, 1970.

Kinder, W. J., and Gatz, E. C., "Telemetry System," in *The Deep Space Network*, Space Programs Summary 37-58, Vol. II, pp. 3–11. Jet Propulsion Laboratory, Pasadena, Calif., July 31, 1969.

Kinder, W. J., "Multiple-Mission Command and Telemetry Systems High-Speed and Wide Band Data Formats," in *The Deep Space Network*, Space Programs Summary 37-62, Vol. II, pp. 3–5. Jet Propulsion Laboratory, Pasadena, Calif., Mar. 31, 1970.

Rakunas, R. R., and Schulze, A., "DSN Multiple-Mission Command System," in *The Deep Space Network Progress Report*, Technical Report 32-1526, Vol. III, pp. 4–6. Jet Propulsion Laboratory, Pasadena, Calif., June 15, 1971.

Wilcher, J. H., et al., "DSIF Multiple-Mission Command System," in *The Deep Space Network*, Space Programs Summary 37-59, Vol. II, pp. 119–139. Jet Propulsion Laboratory, Pasadena, Calif., Sept. 30, 1969.

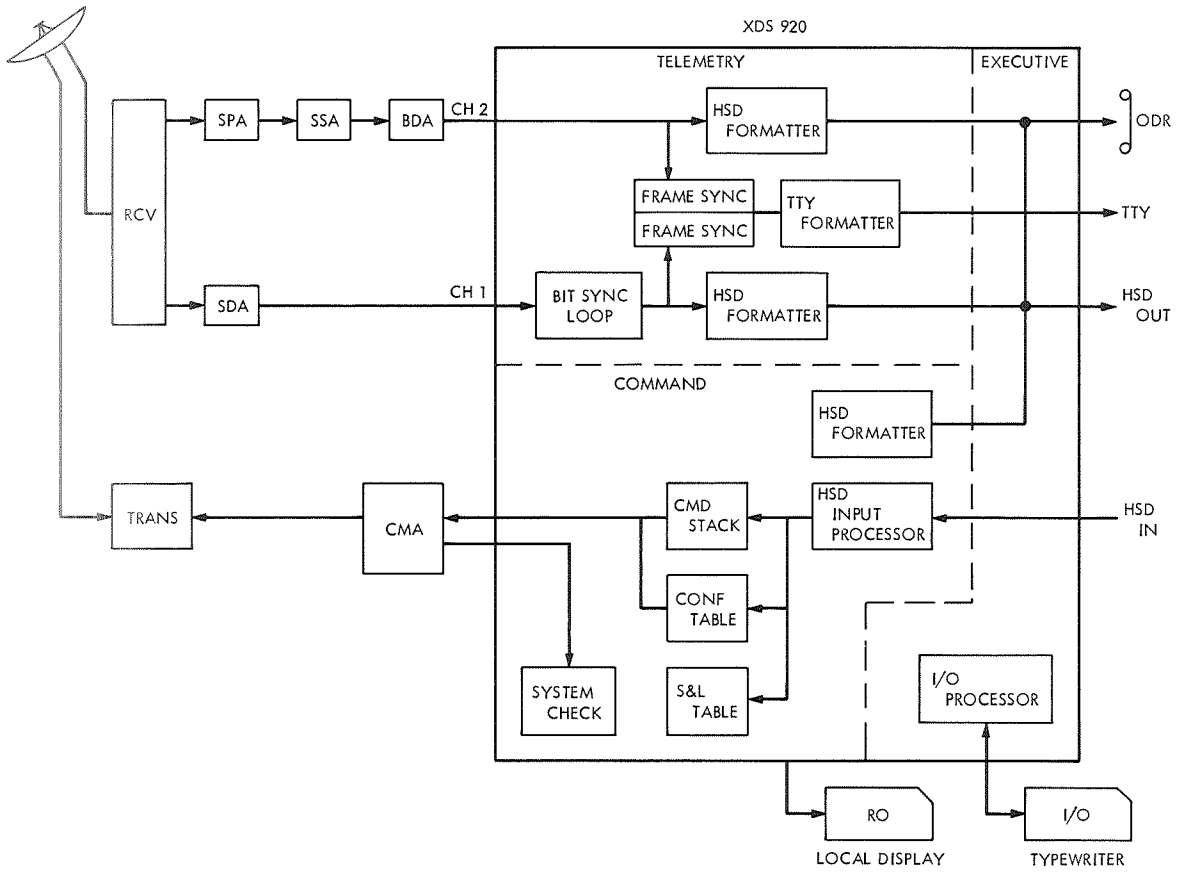

Fig. 1. *Mariner* Mars 1971 TCP Operational Program

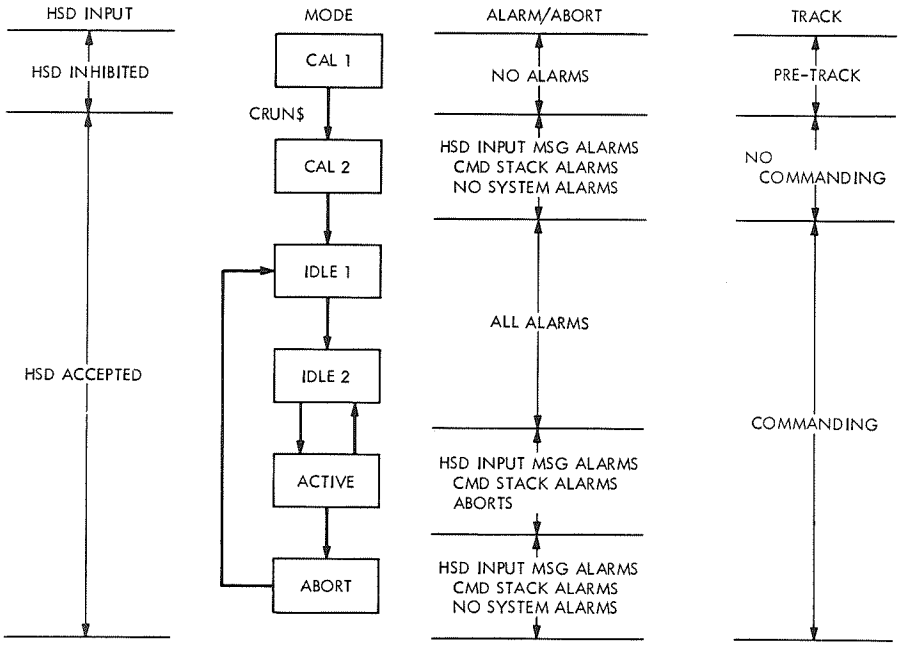

Fig. 2. *Mariner* Mars 1971 TCP Command Program

Bibliography

Anderson, J. D., *Determination of the Masses of the Moon and Venus and the Astronomical Unit from Radio Tracking Data of the Mariner II Spacecraft.* Technical Report 32-816. Jet Propulsion Laboratory, Pasadena, Calif., July 1, 1967.

Anderson, J. D., et al., "The Radius of Venus as Determined by Planetary Radar and Mariner V Radio Tracking Data," *J. Atmos. Sci.*, pp. 1171–1174, Sept. 25, 1968.

Berman, A. L., *Tracking System Data Analysis Report, Ranger VII Final Report,* Technical Report 32-719, Jet Propulsion Laboratory, Pasadena, Calif., June 1, 1965.

Berman, A. L., *ABTRAJ—On-Site Tracking Prediction Program for Planetary Spacecraft,* Technical Memorandum 33-391. Jet Propulsion Laboratory, Pasadena, Calif., Aug. 15, 1968.

Cain, D. L., and Hamilton, T. W., *Determination of Tracking Station Locations by Doppler and Range Measurements to an Earth Satellite,* Technical Report 32-534. Jet Propulsion Laboratory, Pasadena, Calif., Feb. 1, 1964.

Carey, C. N., and Sjogren, W. L., "Gravitational Inconsistency, in the Lunar Theory: Confirmation by Radio Tracking," *Science,* Vol. 160, pp. 875, 876, Apr.–June 1968.

Curkendall, D. W., and Stephenson, R. R., "Earthbased Tracking and Orbit Determination—Backbone of the Planetary Navigation System," *Astronaut. Aeronaut.,* Vol. 7, May 1970.

Curkendall, D. W., "Planetary Navigation: The New Challenges," *Astronaut. Aeronaut.,* Vol. 7, May 1970.

Efron, L., and Solloway, C. B., *Proceedings of the Conference on Scientific Applications of Radio and Radar Tracking in the Space Program,* Technical Report 32-1475. Jet Propulsion Laboratory, Pasadena, Calif., July 1970.

Flanagan, F. M., et al., *Deep Space Network Support of the Manned Space Flight Network for Apollo: 1962–1968,* Technical Memorandum 33-452, Vol. I. Jet Propulsion Laboratory, Pasadena, Calif., July 1970.

Flanagan, F. M., et al., *Deep Space Network Support of the Manned Space Flight Network for Apollo: 1969–1970,* Technical Memorandum 33-452, Vol. II. Jet Propulsion Laboratory, Pasadena, Calif., May 1, 1971.

Fjeldbo, G., and Eshleman, V. R., "Radio Occultation Measurements and Interpretations," in *The Atmospheres of Venus and Mars,* p. 225. Gordon and Breach, Science Publishers, Inc., New York, N. Y.

Goldstein, R. M., "Radar Time-of-Flight Measurements to Venus," *Astron. J.,* Vol. 73, No. 9, Aug. 1968.

Goldstein, R. M., and Rumsey, H., Jr., "A Radar Snapshot of Venus," *Science,* Vol. 169, Sept. 1970.

Gordon, H. J., et al., *The Mariner 6 and 7 Flight Paths and Their Determination From Tracking Data,* Technical Memorandum 33-469. Jet Propulsion Laboratory, Pasadena, Calif., Dec. 1, 1970.

Bibliography (contd)

Hamilton, T. W., et al., *The Ranger IV Flight Path and Its Determination From Tracking Data,* Technical Report 32-345. Jet Propulsion Laboratory, Pasadena, Calif., Sept. 15, 1962.

Kellermann, K. I., et al., "High Resolution Observations of Compact Radio Sources at 13 Centimeters," *Astrophys. J.*, Vol. 161, pp. 803–809, Sept. 1970.

Kliore, A., "Radio Occultation Measurements of the Atmospheres of Mars and Venus," in *The Atmospheres of Venus and Mars,* p. 205. Gordon and Breach Science Publishers, Inc., New York, N. Y.

Labrum, R. G., Wong, S. K., and Reynolds, G. W., *The Surveyor V, VI, and VII Flight Paths and Their Determination from Tracking Data,* Technical Report 32-1302. Jet Propulsion Laboratory, Pasadena, Calif., Dec. 1, 1968.

Lieske, J. H., and Null, G. W., "Icarus and the Determination of Astronomical Constants," *Astron. J.*, Vol. 74, No. 2, Mar. 1969.

Lorell, J., and Sjogren, W. L., *Lunar Orbiter Data Analysis,* Technical Report 32-1220. Jet Propulsion Laboratory, Pasadena, Calif., Nov. 15, 1967.

Lorell, J., *Lunar Orbiter Gravity Analysis,* Technical Report 32-1387. Jet Propulsion Laboratory, Pasadena, Calif., June 15, 1969.

Lorell, J., et al., "Celestial Mechanics Experiment for *Mariner,*" *Icarus,* Vol. 12, Jan. 1970.

McNeal, C. E., *Ranger V Tracking Systems Data Analysis Final Report,* Technical Report 32-702. Jet Propulsion Laboratory, Pasadena, Calif., Apr. 15, 1965.

Melbourne, W. G., et al., *Constants and Related Information for Astrodynamical Calculations,* Technical Report 32-1306. Jet Propulsion Laboratory, Pasadena, Calif., July 15, 1968.

Melbourne, W. G., "Planetary Ephemerides," *Astronaut. Aeronaut.*, Vol. 7, May 1970.

Miller, L., et al., *The Atlas–Centaur VI Flight Path and Its Determination from Tracking Data,* Technical Report 32-911. Jet Propulsion Laboratory, Pasadena, Calif., Apr. 15, 1966.

Mulhall, B. D., et al., *Tracking System Analytic Calibration Activities for the Mariner Mars 1969 Mission,* Technical Report 32-1499. Jet Propulsion Laboratory, Pasadena, Calif., Nov. 15, 1970.

Mulholland, J. D., and Sjogren, W. L., *Lunar Orbiter Ranging Data,* Technical Report 32-1087. Jet Propulsion Laboratory, Pasadena, Calif., Jan. 6, 1967.

Mulholland, J. D., *Proceedings of the Symposium on Observation, Analysis, and Space Research Applications of the Lunar Motion,* Technical Report 32-1386. Jet Propulsion Laboratory, Pasadena, Calif., Apr. 1969.

Muller, P. M., and Sjogren, W. L., *Consistency of Lunar Orbiter Residuals With Trajectory and Local Gravity Effects,* Technical Report 32-1307. Jet Propulsion Laboratory, Pasadena, Calif., Sept. 1, 1968.

Muller, P. M., and Sjogren, W. L., *Lunar Mass Concentrations,* Technical Report 32-1339. Jet Propulsion Laboratory, Pasadena, Calif., Aug. 16, 1968.

Bibliography (contd)

Null, G. W., Gordon, H. J., and Tito, D. A., *Mariner IV Flight Path and its Determination From Tracking Data,* Technical Report 32-1108. Jet Propulsion Laboratory, Pasadena, Calif., Aug. 1, 1967.

O'Neil, W. J., et al., *The Surveyor III and Surveyor IV Flight Paths and Their Determination From Tracking Data,* Technical Report 32-1292. Jet Propulsion Laboratory, Pasadena, Calif., Aug. 15, 1968.

Pease, G. E., et al., *The Mariner V Flight Path and Its Determination From Tracking Data,* Technical Report 32-1363. Jet Propulsion Laboratory, Pasadena, Calif., July 1, 1969.

Renzetti, N. A., *Tracking and Data Acquisition for Ranger Missions I–V,* Technical Memorandum 33-174. Jet Propulsion Laboratory, Pasadena, Calif., July 1, 1964.

Renzetti, N. A., *Tracking and Data Acquisition for Ranger Missions VI–IX,* Technical Memorandum 33-275. Jet Propulsion Laboratory, Pasadena, Calif., Sept. 15, 1966.

Renzetti, N. A., *Tracking and Data Acquisition Support for the Mariner Venus 1962 Mission,* Technical Memorandum 33-212. Jet Propulsion Laboratory, Pasadena, Calif., July 1, 1965.

Renzetti, N. A., *Tracking and Data Acquisition Report, Mariner Mars 1964 Mission: Near-Earth Trajectory Phase,* Technical Memorandum 33-239, Vol. I. Jet Propulsion Laboratory, Pasadena, Calif., Jan. 1, 1965.

Renzetti, N. A., *Tracking and Data Acquisition Report, Mariner Mars 1964 Mission: Cruise to Post-Encounter Phase,* Technical Memorandum 33-239, Vol. II. Jet Propulsion Laboratory, Pasadena, Calif., Oct. 1, 1967.

Renzetti, N. A., *Tracking and Data Acquisition Report, Mariner Mars 1964 Mission: Extended Mission,* Technical Memorandum 33-239, Vol. III. Jet Propulsion Laboratory, Pasadena, Calif., Dec. 1, 1968.

Renzetti, N. A., *Tracking and Data System Support for Surveyor: Missions I and II,* Technical Memorandum 33-301, Vol. I. Jet Propulsion Laboratory, Pasadena, Calif., July 15, 1969.

Renzetti, N. A., *Tracking and Data System Support for Surveyor: Missions III and IV,* Technical Memorandum 33-301, Vol. II. Jet Propulsion Laboratory, Pasadena, Calif., Sept. 1, 1969.

Renzetti, N. A., *Tracking and Data System Support for Surveyor: Mission V,* Technical Memorandum 33-301, Vol. III. Jet Propulsion Laboratory, Pasadena, Calif., Dec. 1, 1969.

Renzetti, N. A., *Tracking and Data System Support for Surveyor: Mission VI,* Technical Memorandum 33-301, Vol. IV. Jet Propulsion Laboratory, Pasadena, Calif., Dec. 1, 1969.

Renzetti, N. A., *Tracking and Data System Support for Surveyor: Mission VII,* Technical Memorandum 33-301, Vol. V. Jet Propulsion Laboratory, Pasadena, Calif., Dec. 1, 1969.

Bibliography (contd)

Renzetti, N. A., *Tracking and Data System Support for the Mariner Venus 67 Mission: Planning Phase Through Midcourse Maneuver,* Technical Memorandum 33-385, Vol. I. Jet Propulsion Laboratory, Pasadena, Calif., Sept. 1, 1969.

Renzetti, N. A., *Tracking and Data System Support for the Mariner Venus 67 Mission: Midcourse Maneuver Through End of Mission,* Technical Memorandum 33-385, Vol. II. Jet Propulsion Laboratory, Pasadena, Calif., Sept. 1, 1969.

Renzetti, N. A., *Tracking and Data System Support for the Pioneer Project. Pioneer VI. Prelaunch to End of Nominal Mission,* Technical Memorandum 33-426, Vol. I. Jet Propulsion Laboratory, Pasadena, Calif., Feb. 1, 1970.

Renzetti, N. A., *Tracking and Data System Support for the Pioneer Project. Pioneer VII. Prelaunch to End of Nominal Mission,* Technical Memorandum 33-426, Vol. II. Jet Propulsion Laboratory, Pasadena, Calif., Apr. 15, 1970.

Renzetti, N. A., *Tracking and Data System Support for the Pioneer Project. Pioneer VIII. Prelaunch Through May 1968,* Technical Memorandum 33-426, Vol. III. Jet Propulsion Laboratory, Pasadena, Calif., July 15, 1970.

Renzetti, N. A., *Tracking and Data System Support for the Pioneer Project. Pioneer IX. Prelaunch Through June 1969,* Technical Memorandum 33-426, Vol. IV. Jet Propulsion Laboratory, Pasadena, Calif., Nov. 15, 1970.

Renzetti, N. A., *Tracking and Data System Support for the Pioneer Project. Pioneer VI. Extended Mission: July 1, 1966–July 1, 1969,* Technical Memorandum 33-426, Vol. V. Jet Propulsion Laboratory, Pasadena, Calif., Feb. 1, 1971.

Renzetti, N. A., *Tracking and Data System Support for the Pioneer Project. Pioneer VII. Extended Mission: February 24, 1967–July 1, 1968,* Technical Memorandum 33-426, Vol. VI. Jet Propulsion Laboratory, Pasadena, Calif., Apr. 15, 1971.

Renzetti, N. A., *Tracking and Data System Support for the Pioneer Project. Pioneer VII. Extended Mission: July 1, 1968–July 1, 1969,* Technical Memorandum 33-426, Vol. VII. Jet Propulsion Laboratory, Pasadena, Calif., Apr. 15, 1971.

Renzetti, N. A., *Tracking and Data System Support for the Pioneer Project. Pioneer VIII. Extended Mission: June 1, 1968–July 1, 1969,* Technical Memorandum 33-426, Vol. VIII. Jet Propulsion Laboratory, Pasadena, Calif., May 1, 1971.

Renzetti, N. A., *Tracking and Data System Support for the Pioneer Project. Pioneers VI–IX. Extended Missions: July 1, 1969–July 1, 1970,* Technical Memorandum 33-426, Vol. IX. Jet Propulsion Laboratory, Pasadena, Calif., Aug. 15, 1971.

Sjogren, W. L., *The Ranger III Flight Path and Its Determination From Tracking Data,* Technical Report 32-563. Jet Propulsion Laboratory, Pasadena, Calif., Sept. 15, 1965.

Sjogren, W. L., et al., *Physical Constants as Determined From Radio Tracking of the Ranger Lunar Probes,* Technical Report 32-1057. Jet Propulsion Laboratory, Pasadena, Calif., Dec. 30, 1966.

Sjogren, W. L., et al., *The Ranger VI Flight Path and Its Determination From Tracking Data,* Technical Report 32-605. Jet Propulsion Laboratory, Pasadena, Calif., Dec. 15, 1964.

Bibliography (contd)

Sjogren, W. L., et al., *The Ranger V Flight Path and Its Determination From Tracking Data,* Technical Report 32-562. Jet Propulsion Laboratory, Pasadena, Calif., Dec. 6, 1963.

Sjogren, W. L., and Trask, D. W., *Physical Constants as Determined From Radio Tracking of the Ranger Lunar Probes,* Technical Report 32-1057. Jet Propulsion Laboratory, Pasadena, Calif., Dec. 30, 1966.

Sjogren, W. L., *Proceedings of the JPL Seminar on Uncertainties in the Lunar Ephemeris,* Technical Report 32-1247. Jet Propulsion Laboratory, Pasadena, Calif., May 1, 1968.

Stelzried, C. T., *A Faraday Rotation Measurement of a 13-cm Signal in the Solar Corona,* Technical Report 32-1401. Jet Propulsion Laboratory, Pasadena, Calif., July 15, 1970.

Stelzried, C. T., et al., "The Quasi-Stationary Coronal Magnetic Field and Electron Density as Determined From a Faraday Rotation Experiment," *Sol. Phys.*, Vol. 14, No. 2, pp. 440–456, Oct. 1970.

Thornton, J. H., Jr., *The Surveyor I and Surveyor II Flight Paths and Their Determination From Tracking Data,* Technical Report 32-1285. Jet Propulsion Laboratory, Pasadena, Calif., Aug. 1, 1968.

Vegos, C. J., et al., *The Ranger IX Flight Path and Its Determination From Tracking Data,* Technical Report 32-767. Jet Propulsion Laboratory, Pasadena, Calif., Nov. 1, 1968.

Winn, F. B., *Selenographic Location of Surveyor VI, Surveyor VI Mission Report: Part II. Science Results,* Technical Report 32-1262. Jet Propulsion Laboratory, Pasadena, Calif., Jan. 10, 1968.

Winn, F. B., "Post Landing Tracking Data Analysis," in *Surveyor VII Mission Report: Part II. Science Results,* Technical Report 32-1264. Jet Propulsion Laboratory, Pasadena, Calif., Mar. 15, 1968.

Winn, F. B., "Post Lunar Touchdown Tracking Data Analysis," in *Surveyor Project Final Report: Part II. Science Results,* Technical Report 32-1265. Jet Propulsion Laboratory, Pasadena, Calif., June 15, 1968.

Winn, F. B., *Surveyor Posttouchdown Analyses of Tracking Data,* NASA SP-184. National Aeronautics and Space Administration, Washington, D.C., p. 369.

Wollenhaupt, W. R., et al., *The Ranger VII Flight Path and Its Determination From Tracking Data,* Technical Report 32-694. Jet Propulsion Laboratory, Pasadena, Calif., Dec. 15, 1964.

NASA — JPL — Coml., L.A., Calif.